Joint Live Fire (JLF)
Final Report for Instrumentation for Local Accelerative Loading
22 JULY 2016

Jake Hawkins, CORVID Technologies
Robert Spink, Army Research Lab
Chris Monahan, Aberdeen Test Center
Anne Purtell, MCSC SIAT

DISTRIBUTION STATEMENT A: Approved for public release. Distribution is unlimited.

Joint Live Fire (JLF)
Final Report for Instrumentation
for Local Accelerative Loading

22 July 2016

PREPARED BY:

SPINK.ROBERT.J.1390636187
Digitally signed by SPINK.ROBERT.J.1390636187
DN: c=US, o=U.S. Government, ou=DoD, ou=PKI, ou=USA, cn=SPINK.ROBERT.J.1390636187
Date: 2016.07.25 08:37:34 -04'00'

ROBERT SPINK
BIOMEDICAL ENGINEER
ARMY RESEARCH LABORATORY

MONAHAN.CHRISTOPHER.B.1291493137
Digitally signed by MONAHAN.CHRISTOPHER.B.1291493137
DN: c=US, o=U.S. Government, ou=DoD, ou=PKI, ou=USA, cn=MONAHAN.CHRISTOPHER.B.1291493137
Date: 2016.07.25 07:19:40 -04'00'

CHRIS MONAHAN
ENGINEER
ABERDEEN TEST CENTER

PURTELL.ANNE.M.1366032025
Digitally signed by PURTELL.ANNE.M.1366032025
DN: c=US, o=U.S. Government, ou=DoD, ou=PKI, ou=USMC, cn=PURTELL.ANNE.M.1366032025
Date: 2016.07.22 11:41:35 -04'00'

ANNE PURTELL
USMC SURVIVABILITY LEAD
MARINE CORPS SYSTEMS COMMAND,
SYSTEMS ENGINEERING,
INTEROPERABILITY, ARCHITECTURE
AND TECHNOLOGY

Jake Hawkins
Digitally signed by Jake Hawkins
DN: cn=Jake Hawkins, o=Corvid Technologies, ou, email=jake.hawkins@corvidtec.com, c=US
Date: 2016.07.22 15:08:33 -04'00'

JAKE HAWKINS
COMPUTATIONAL ANALYST
CORVID TECHNOLOGIES

SERVICE LEAD:

CROCE.RAFFAELE.1031241029
Digitally signed by CROCE.RAFFAELE.1031241029
DN: c=US, o=U.S. Government, ou=DoD, ou=PKI, ou=USMC, cn=CROCE.RAFFAELE.1031241029
Date: 2016.07.29 08:19:55 -04'00'

RAFFAELE “RALPH” CROCE
LIVE FIRE DIVISION HEAD
MARINE CORPS OPERATIONAL TEST & EVALUATION ACTIVITY (MCOTEA)

APPROVED BY:

POLESNE.JOHN.T.1229281280
Digitally signed by POLESNE.JOHN.T.1229281280
DN: c=US, o=U.S. Government, ou=DoD, ou=PKI, ou=USA, cn=POLESNE.JOHN.T.1229281280
Date: 2016.08.11 08:49:10 -04'00'

JOHN T. POLESNE
JOINT LIVE FIRE TEST MANAGER
JLF ARMOR/ANTI-ARMOR GROUND
SYSTEMS

UGRINA.SANDRA.1041642226
Digitally signed by UGRINA.SANDRA.1041642226
DN: c=US, o=U.S. Government, ou=DoD, ou=PKI, ou=OSD, cn=UGRINA.SANDRA.1041642226
Date: 2016.08.17 10:51:45 -04'00'

DR. SANDRA UGRINA
DEPUTY DIRECTOR, OT&E/LFT&E

Table of Contents

Introduction 8
a. Background 9
b. Problem Statement 11
c. Prior Work 12
i. Resonance 12
ii. Base Strain Sensitivity 15
iii. DAQ and Signal Conditioning [5] 17
Test Objectives 21
Test Approach 21
a. Accelerometers and Gauges 21
i. Endevco 7270AM6 23
ii. ATC LOFFI 23
iii. ATC BOBKAT 24
iv. ATC Tiny BOB 24
v. ATC Mini BOB 25
vi. ATC AM6 Tall 25
vii. ATC Wheel Mount 26
viii. ATC Wave Spring with Base BOB 26
ix. ATC Spring Mount 27
x. Corvid Disk Mount 28
b. Phase I 29
c. Phase II 32
d. Phase III 36
Detailed Test Results 38
a. Test Conditions 38
i. Truth Data 38
ii. Data Matrices 42
b. Test Results 44
i. Phase I 44
ii. Phase II 53
iii. Phase III 57
c. Comparison with Pretest Prediction 60
d. Lessons Learned 65

i. Explosive Rig Testing 65
ii. Laboratory Testing 66
iii. Analysis Techniques 66
Summary of Findings 67
a. Summary of Results 67
i. Low Frequency Range (1 – 10 Hz) 67
ii. Medium Frequency Range (10 – 2,000 Hz) 71
iii. High Frequency Range (2,000 – 10,000 Hz) 76
b. Conclusions 81
c. Recommendations 82
d. Limitations on Data Use 83
e. Acknowledgements 84
Appendices 86
a. Appendix A – Smack Bar Test Results 86
b. Appendix B – Flyaway Test Results 127
c. Appendix C – Explosive Rig Test Results 141

List of Figures

Figure 1 – Vehicle Underbody Blast 9
Figure 2 – Evolution of the LOFFI [2] 10
Figure 3 – Exciting Resonance of Undamped Accelerometer 12
Figure 4 – Undamped Accelerometer Resonance 13
Figure 5 – FFT of Undamped Accelerometer Resonance 13
Figure 6 – Velocity Trace of Undamped Accelerometer Resonance during Test #1 14
Figure 7 – Velocity Trace of Undamped Accelerometer Resonance during Test #2 14
Figure 8 – Purpose of a Mechanical Filter 15
Figure 9 – Base Strain Sensitivity Setup 16
Figure 10 – Load Cell and Accelerometer Outputs from Base Strain Test 16
Figure 11 – Acceleration and Velocity of Accelerometer Subjected to Base Strain 17
Figure 12 – Aliased Signal in Successive Approximation ADC 18
Figure 13 – No Aliased Signal in Delta-Sigma ADC 19
Figure 14 – "Invisible Clipping" Graphic 20
Figure 15 – Isometric View of Endevco 7270AM6 [6] 23
Figure 16 – Isometric (a) and Section (b) Views of LOFFI 23
Figure 17 – Isometric (a) and Section (b) Views of BOBKAT 24
Figure 18 – Isometric (a) and Labelled (b) Views of Tiny BOB 24
Figure 19 – Isometric (a) and Section (b) Views of Mini BOB 25
Figure 20 – Exploded View of AM6 Tall 25
Figure 21 – Labelled Section (a) and Exploded (b) Views of Wheel Mount 26
Figure 22 – Isometric (a), Section (b), and Labelled Section (c) Views of Wave Spring with Base BOB 27
Figure 23 – Isometric (a) and Section (b) Views of Spring Mount 28
Figure 24 – Isometric (a) and Section (b) Views of Corvid Disk Mount 28
Figure 25 – TCU Smack Bar Machine 29
Figure 26 – TCU Smack Bar Machine with Programmer 30
Figure 27 – TCU Flyaway Machine 31
Figure 28 – Explosively-Driven Test Rig with Gauge Mount Locations 32
Figure 29 – Components of Floor Plate Assembly 33
Figure 30 – Lifting and Standing Components 33
Figure 31 – Steel Tower Mounted to Driver Plate of Explosively-Driven Test Rig 35
Figure 32 – Shot #7 Configuration for Explosively-Driven Test Rig 35
Figure 33 – ATC's Shaker Table Setup 37
Figure 34 – Polytec Tracking Filter used During Explosive Rig Testing 39
Figure 35 – Comparison of PDV, AM6 Tall, LDV, and Velodyne Displacements 41
Figure 36 – Example of Acceleration (a) and Velocity (b) Traces from Smack Bar Tests 45
Figure 37 – Average Peak Velocity (a) and Average Time-to-Peak Velocity (b) Data from all Smack Bar Tests 47
Figure 38 – Example of SRS (a) and SRS Percent Error (b) Plots from Smack Bar Tests 48
Figure 39 – Example of Acceleration (a) and Velocity (b) Traces from Flyaway Tests 49
Figure 40 – Average Peak Velocity (a) and Average Time-to-Peak Velocity (b) Data from all Flyaway Tests 51
Figure 41 – Example of SRS (a) and SRS Percent Error (b) Plots from Flyaway Tests 52

Figure 42 – Example of Acceleration (a) and Velocity (b) Traces from Explosive Rig Tests 53
Figure 43 – Average Peak Velocity (a) and Average Time-to-Peak Velocity (b) from all Explosive Rig Tests 56
Figure 44 – Example of SRS (a) and SRS Percent Error (b) Plots from Explosive Rig Tests 57
Figure 45 – Power Spectrum of Vertical Shaker Run #1 58
Figure 46 – Natural Frequencies of Mounting Plate #1 59
Figure 47 – Natural Frequencies of Mounting Plate #2 59
Figure 48 – Power Spectrum of Vertical Shaker Run #2 60
Figure 49 – Comparison of Velodyne Final Mesh Model (a) and Actual Rig (b) 61
Figure 50 – Comparison of Velodyne Model Soil Loading (a) and Actual Soil Loading (b) 62
Figure 51 – Numerical Accelerometers Used in Velodyne Simulations 62
Figure 52 – Comparison of Two Candidate Test Rig Simulated Results to Representative LFT&E Tactical Vehicle Floor Responses 63
Figure 53 – Comparison of Local Floor Plate Response in Prediction vs. Experiment 64
Figure 54 – Example of Endevco 226A (a), BOBKAT (b), Endevco 7270A (c), Endevco 7264D (d), and LOFFI (e) Velocity Traces 68
Figure 55 – Example of Endevco 226A (a), BOBKAT (b), Endevco 7270A (c), Endevco 7264D (d), and LOFFI (e) SRS Percent Error Plots 69
Figure 56 – Example of Endevco 7270AM6 (a) and Endevco 7280A (b) Velocity Traces and SRS Percent Error plots 71
Figure 57 – Example of Endevco 7270A (a), Endevco 7270AM6 (b), Endevco 7280A (c), Endevco 2262A (d), and LOFFI (e) Velocity Traces 73
Figure 58 – Example of Endevco 7270A (a), Endevco 7270AM6 (b), Endevco 7280A (c), Endevco 2262A (d), and LOFFI (e) SRS Percent Error Plots 74
Figure 59 – Example of BOBKAT (a) and LOFFI (b) SRS and SRS Percent Error Plots 76
Figure 60 – Acceleration Trace (a), Velocity Trace (b), SRS Plot (c), and SRS Percent Error Plot (d) Produced by Tiny BOB from Shot #4 78
Figure 61 – Acceleration Trace (a), Velocity Trace (b), SRS Plot (c), and SRS Percent Error Plot (d) Produced by Tiny BOB from Shot #5 79
Figure 62 – Acceleration Trace (a), Velocity Trace (b), SRS Plot (c), and SRS Percent Error Plot (d) produced by LOFFI from Shot #6 80

List of Tables

Table 1 – List of Accelerometers Analyzed 22
Table 2 – List of Gauges Analyzed..... 22
Table 3 – List of Accelerometers and Gauges Analyzed During Phase I..... 31
Table 4 – List of Gauges Analyzed During Phase II 36
Table 5 – List of Accelerometers and Gauges Tested During Phase III..... 37
Table 6 – Data Matrix for Smack Bar Testing..... 42
Table 7 – Data Matrix for Flyaway Testing..... 43
Table 8 – Data Matrix for Explosive Rig Testing..... 43
Table 9 – Data Matrix for Shaker Table Testing 44
Table 10 – Average End Velocity and Average Slope Values from Smack Bar Tests 46
Table 11 – Average End Velocity and Average Slope Values from Flyaway Tests 50
Table 12 – Average End Velocity and Average Slope Values from Explosive Rig Tests 54

Introduction

To properly compare blast effects on armored vehicles from test-to-test or test-to-simulation, appropriate instrumentation capable of surviving harsh mechanical loads without drift, biasing, or saturation is required. High fidelity computer modeling is increasingly being used to predict performance of blast test designs and results prior to full-scale testing. Correlating simulation to test data can aid in increasing confidence in the models to further inform test planning and interpret test results. However, it is difficult to collect consistently accurate data that can be compared across test-to-test and test-to-simulation with the current instrumentation used during testing. Recent advances in accelerometer design must be evaluated and, in lieu of acceptable performance, a new isolator system must be developed. A multi-axis input environment must be considered as few (if any) locations of interest within vehicles generate uniaxial loading.

This project is a joint undertaking of the MCSC Systems Engineering, Interoperability, Architecture and Technology (SIAT), the Army Research Laboratory (ARL), the Aberdeen Test Center (ATC), and CORVID Technologies. It leveraged past and current instrumentation projects underway within ARL, ATC, and USMC PEO-LS. Outcomes of this project support the tri-service Developmental Testing (DT) and Live Fire Test and Evaluation (LFT&E) community's efforts by improving instrumentation used by all services in Mine/Improvised Explosive Device (IED) testing. It enables the collection of consistent acceleration data which, in turn, will allow for accurate test and model evaluations. In addition, a test protocol was established so that new accelerometers and/or isolators developed for future use in LFT&E can be evaluated thoroughly against currently available technology.

Testing focused on available accelerometers and gauges as well as new concept gauges in an attempt to accurately capture acceleration content that spans three frequency ranges of interest: low (1 – 10 Hz), medium (10 – 2,000 Hz), and high (2,000 – 10,000 Hz). The low frequency range is analogous to bulk motion of vehicles during LFT&E, while the medium frequency range represents seat pan response and the high frequency range represents floor response. 10,000 Hz is the limit to the high frequency range since this has been shown to be the maximum frequency that can be transmitted through bone tissue under dynamic loading events via strain gauges.[1]

In Phase I, these instrumentation packages were tested using the TCU Flyaway and TCU Smack Bar apparatuses. These methods have known answers that can replicate the low and medium ranges, respectively, of the expected frequency spectrum of interest in LFT&E. Phase II of testing analyzed the gauges on an explosively-driven test rig. The test rig was designed to simulate a tactical vehicle floor during LFT&E and was intended to provide a realistic loading scenario with high frequency content for gauge evaluation. During Phase III, the best performing concepts were subject to constant power shaker table testing with frequencies varying between 10 Hz and 2,000 Hz.

Deliverables from this program included a Quick-Look Report, followed by a detailed test report that outlines recommended accelerometer and gauge configurations for use in future DT and LFT&E, including commercial and prototype configurations.

a. Background

The term "ballistic shock" is primarily associated with the shock experienced by armored combat vehicles when subjected to an enemy attack. Typical engagements of interest include Kinetic Energy (KE) projectiles, high explosive rockets, shaped charge projectiles, land mines, Explosively Formed Projectiles (EFPs) and Improvised Explosive Devices (IEDs). Live-fire, and other ground tests conducted with modern instrumentation, has proven the damage potential of ballistic shock. One of the primary interests in ballistic shock studies is to ensure that armored vehicles retain the ability to shoot, move, and communicate after a non-perforating projectile impact. Figure 1 illustrates a ballistic event on an armored tactical vehicle from a land mine.

Figure 1 – Vehicle Underbody Blast

The presence of high amplitude, high frequency shock (1 million G's at 1 MHz) in ballistic events makes it difficult to obtain accurate measurements at low frequencies (down to 1 Hz). Early measurements (< 1980) of ballistic events were confusing and inconsistent because of resonant ringing, baseline shift, and mechanical failure of the highest range (200,000 G's) accelerometers that were commercially available. Through time and many damaged sensors, it was learned that hard mounting accelerometers is not practical in a ballistic shock environment.

To overcome the problems experienced with the use of conventional accelerometers in this environment, nonstandard shock measurement techniques evolved. As shown in Figure 2, the first attempt at mitigating high frequency mechanical input to accelerometers was accomplished using an aluminum mounting block. Later methods used layers of dissimilar materials with varying mechanical impedances and geometries to alter the transmission and reflection of stress waves passing across them. To increase gauge displacement, effectively

lowering the mechanical input to the accelerometer, Duxseal (a heavy putty-like consistency sealing compound) was added as a damping material to the mount.

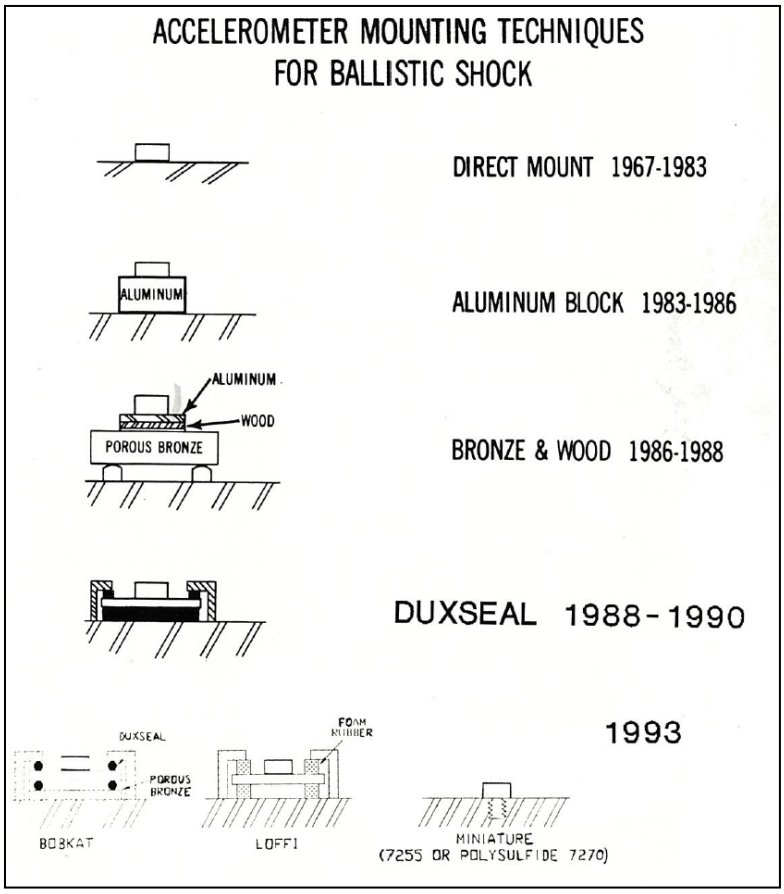

Figure 2 – Evolution of the LOFFI [2]

In the last revision of the mount, Duxseal was replaced with open cell foam. The resulting mechanical filter, dubbed the LOw Frequency Foam Isolated (or "LOFFI"), isolates a low level (2,000 G's) accelerometer from high frequency ballistic shock content (1 million G's at 1 MHz), while allowing more accurate measurement of the shock content below 200 Hz. Though there have been minor tweaks to the 1993 design, the LOFFI has been used in live-fire testing at ATC for nearly 20 years.

The US Army requirements for ballistic shock, US Navy requirements for shipboard shock, and US Air Force and NASA requirements for pyroshock now all require some sort of isolation to protect acceleration sensors from high frequency shock. Failure to protect sensors from these high frequency mechanical inputs leaves them susceptible to content above their resonant frequency which can cause physical damage to the sensor or data anomalies due to out of band energy effects in recording electronics.

b. Problem Statement

The purpose of this project is to evaluate legacy instrumentation along with recent advances in accelerometer design and isolation systems in order to identify those best suited for the unique conditions generated during ground vehicle LFT&E. To achieve this, each gauge was characterized with a variety of time domain and frequency domain characteristics. As previously stated, the frequency bandwidth of interest for this project spans 1 – 10,000 Hz. The lower end of this region was chosen as it encompasses the low frequencies associated with global body motion of a vehicle during LFT&E. The upper end of this region was chosen as it represents a conservative estimate of the highest frequency of floor displacements that can be transmitted through a combat boot and into the calcaneus during an underbody blast event.[1] Identifying the best gauge for specific data needs, such as hull response, local floor response, and seat input and response, is critical to successful testing and data analysis. *The goal is to enable the collection of consistent, accurate acceleration data across the frequency space pertinent to the assessment of vehicle response and injury to mounted occupants*. It is important to note that the 10,000 Hz frequency limit is not high enough to allow for conclusions to be drawn about electronics survivability during LFT&E.

The bandwidth of interest can be further divided into three general regions of particular interest to those assessing vehicle behaviors in underbody blast testing. These frequency regions roughly correspond to global body kinematics, seat response, and floor response. For the purposes of assigning gauge applicability in this report, global body kinematics were confined to 1 Hz to 10 Hz as this entails vehicle flight with a minimum duration of 100 ms. The bandwidth of seat response was considered to be superimposed upon global body kinematics and end at 2,000 Hz. This limit is based on the analysis of data taken from vehicles undergoing underbody blast tests as part of the LFT&E process. This data, taken with Endevco 7270A-20k accelerometers mounted to seat pans, show that 90% of the peak signal power dissipated by an average of 1,800 Hz. The bandwidth of floor response was also considered to be superimposed upon global body kinematic but encompasses the entire bandwidth of interest. Again, this region was limited by the ability of the boot and the foot to conduct floor oscillations into the skeleton.

Previous investigations of commercially available accelerometers have shown that accurately measuring the entire bandwidth of interest to the underbody blast community is problematic. Therefore, it is practical to divide the bandwidth of interest into distinct sections for the purposes of gauge evaluation. For this report, these divisions will follow the end points of the three regions described and correspond to global body kinematics, seat response, and floor response. They will henceforth be referred to as the low, medium, and high bandwidth regions and will span the following respective frequency ranges: 1 – 10 Hz; 10 – 2,000 Hz; 2,000 – 10,000 Hz.

c. Prior Work

As previously mentioned, accelerometers have been used in ballistic shock events since the 1960's, and since then, a great deal of research has been performed in order to better their performance under these harsh conditions. However, more recent research has highlighted the issues associated with accelerometers and the erroneous results they can produce under specific loading conditions. The following issues had to be considered before determining which accelerometers to analyze and the test procedures to use throughout this project.

i. Resonance

In an effort to capture high-rate, high-amplitude accelerative inputs to crew positions during vehicle LFT&E, the use of accelerometers capable of measuring up to 60,000 G's has become increasingly common. Typically these accelerometers are undamped and have high resonant frequencies with respect to the bandwidth of interest. As an example, an Endevco 7270A-20K accelerometer used in LFT&E has a specified resonant frequency of 400 kHz. Although the specified resonant frequency is very high, these accelerometers also have a large Q-factor, or amplification at resonance (up to 1000:1), because of lack of damping, that is easily excited by low-amplitude mechanical inputs containing frequencies at or above the resonant frequency.[3] To ensure linear response and minimize error, spectrum of the acceleration input must stay within the accelerometer's recommended bandwidth.[4]

Resonance of undamped accelerometers can be easily demonstrated by recording the accelerometer's response to a high frequency input with an oscilloscope. As shown in, Figure 3, an undamped accelerometer was placed on a fixed surface and lead from a #2 mechanical pencil was cracked against the case of the accelerometer behind the mounting hole away from direct contact with the sensing element.

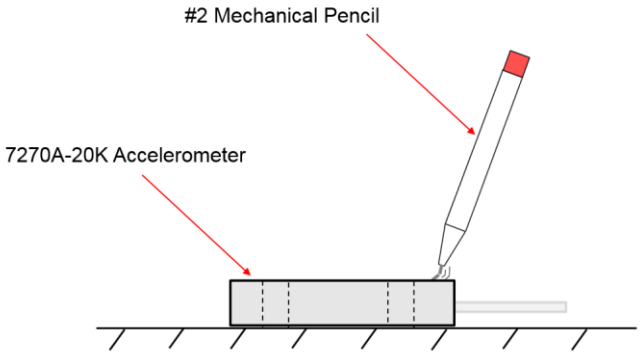

Figure 3 – Exciting Resonance of Undamped Accelerometer

The resulting output from the accelerometer excited by the lead pencil break, shown in Figure 4, is a lightly damped sinusoid with a peak value of approximately 12,000 G's. Noticeable in the trace are two distinct resonant frequencies resulting in a distinct beat

frequency. This is a result of the use of two seismic masses in the design of the accelerometer. An FFT of the resulting signal, shown in Figure 5, reveals the resonant frequencies of the seismic masses to be approximately 410,770 Hz and 430, 258 Hz, whose difference of approximately 19,500 Hz corresponds to the noticeable beat frequency in Figure 4.

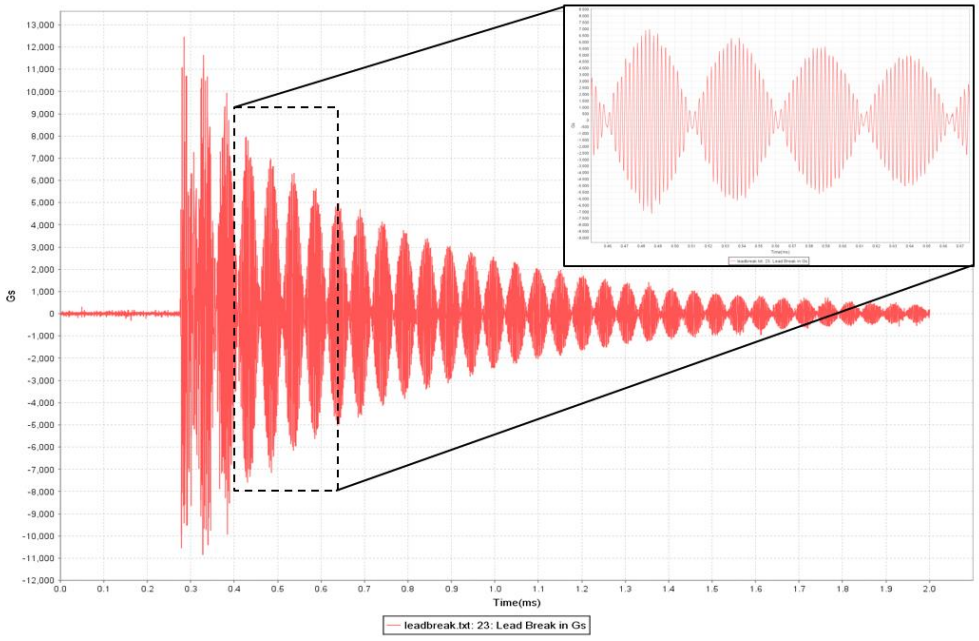

Figure 4 – Undamped Accelerometer Resonance

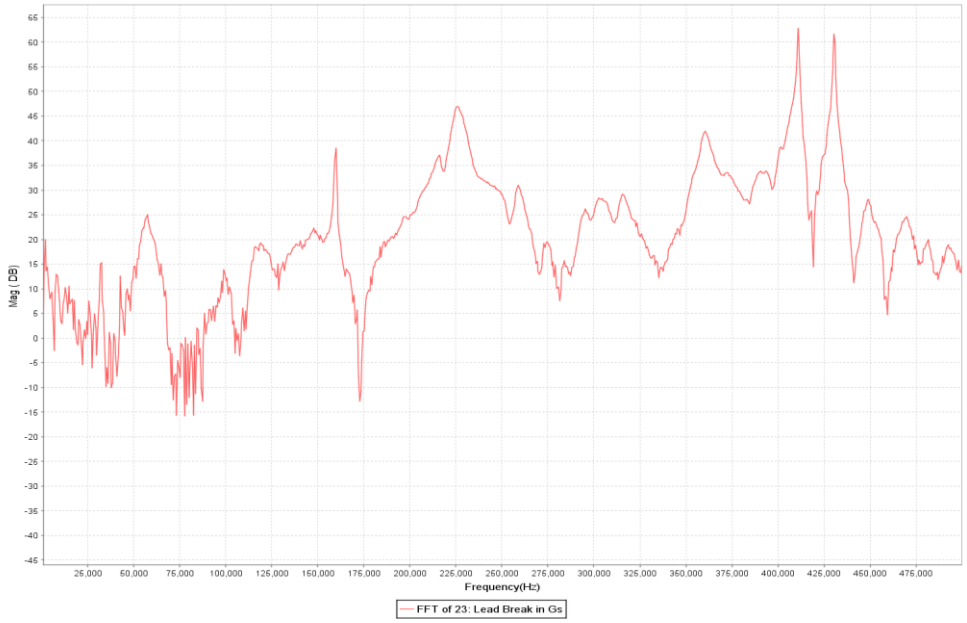

Figure 5 – FFT of Undamped Accelerometer Resonance

Integrating the acceleration trace shown in Figure 4 produces the velocity trace shown in Figure 6. Although the peak velocities are within reason, a slight positive drift from the x-axis occurs as positive error is accumulated during the numerical integration. This type of error is known as zero-shift error. Resonance induced zero-shift error changes from accelerometer to accelerometer with varying degrees of severity for any given test. Figure 7 shows that this zero-shift error was worse when this exact procedure was repeated for a second test.

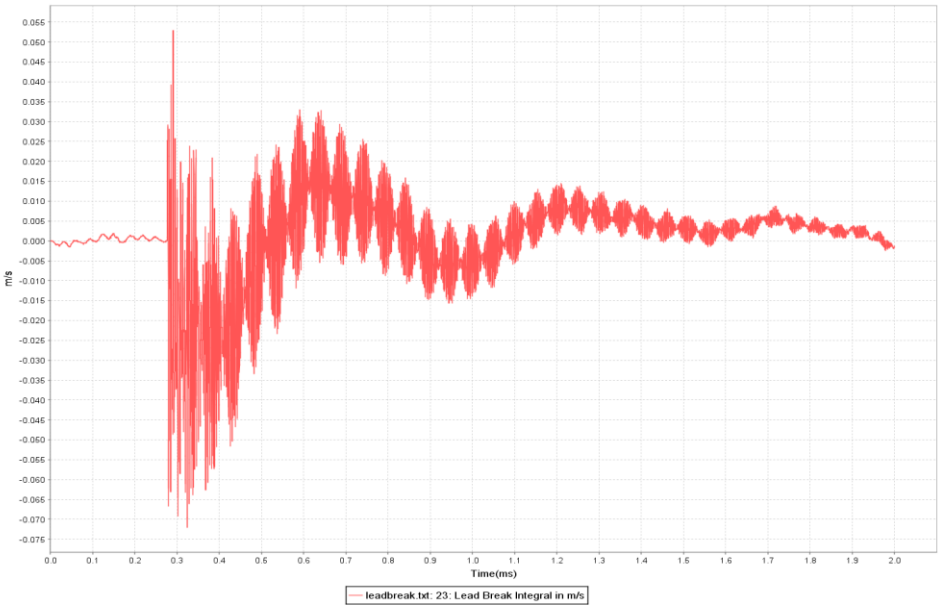

Figure 6 – Velocity Trace of Undamped Accelerometer Resonance during Test #1

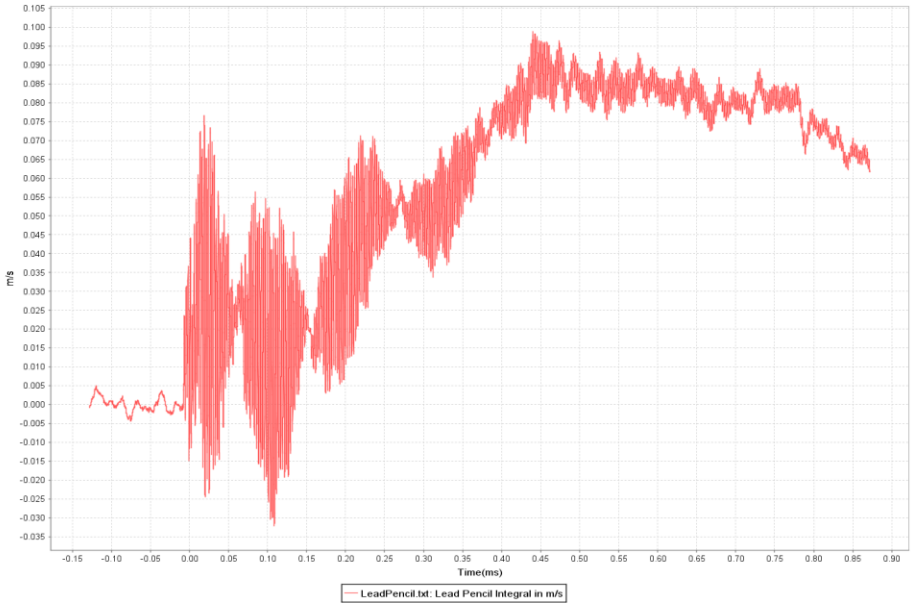

Figure 7 – Velocity Trace of Undamped Accelerometer Resonance during Test #2

In theory, if the resonant frequency were perfectly symmetric about the x-axis, this result would have little effect on the underlying true signal. However, one working theory is that there may often times be asymmetry to the resonant frequency of accelerometers (i.e. slightly more positive than negative or vice versa) allowing for error to accumulate during mathematical post-processing techniques such as integration. Often times, the result from an accelerometer at resonance is non-linear and non-repeatable.[4] One way to reduce resonance induced zero-shift error is to install a mechanical filter between the test subject and the accelerometer. As depicted in Figure 8, one of the main purposes of a mechanical filter is to protect the accelerometer from mechanical inputs that could excite its resonant frequency. Though the mechanical filter itself may have amplification at resonance, it should be designed so that its resonant frequency is above the bandwidth of interest but far enough below the accelerometer resonance to provide significant attenuation of mechanical input approaching accelerometer resonance.

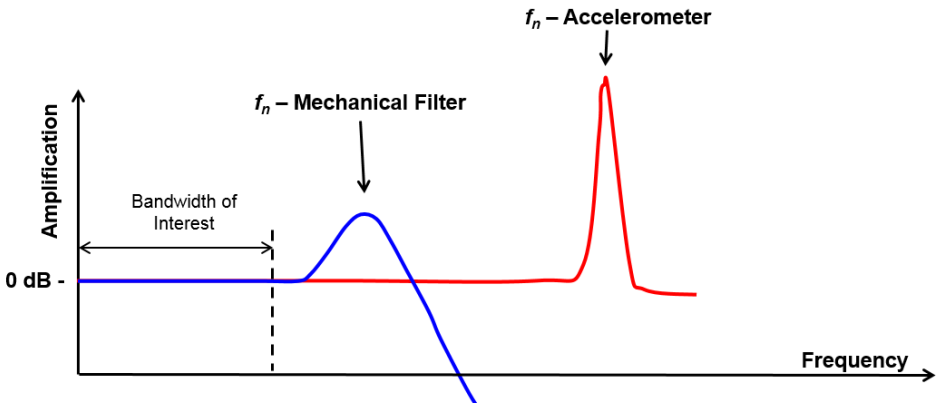

Figure 8 – Purpose of a Mechanical Filter

ii. *Base Strain Sensitivity*

Another suspected source of error resulting from the use of direct mount accelerometers is base strain. Base strain is caused when the base of the accelerometer experiences deformation due to an applied bending moment or torque. For example, an Endevco 7270A-20K is specified by the manufacturer to have a base strain sensitivity of less than 0.5 mV at 250 microstrain. With a specified sensitivity of 10 µV/G, that equates to an approximate output of 50 G's. To demonstrate this concept, an Endevco 7270A-20K was attached to a test beam measuring 4" x ½" x 36" and loaded via an Instron machine, as shown in Figure 9.

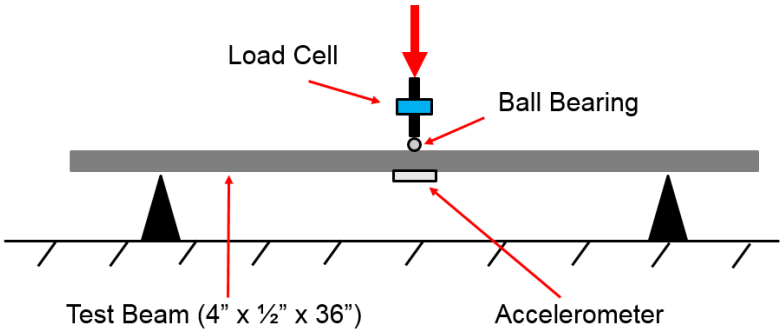

Figure 9 – Base Strain Sensitivity Setup

A load of approximately 1,200 lbs was applied, and the outputs from a reference load cell and the accelerometer were recorded. The estimated strain value at the location of the accelerometer under these conditions was determined to be approximately 330 microstrain. At the specified base strain sensitivity, that would result in an estimated accelerometer output of approximately 67 G's. The measured output of the reference load cell and accelerometer are shown in red and blue, respectively, in Figure 10.

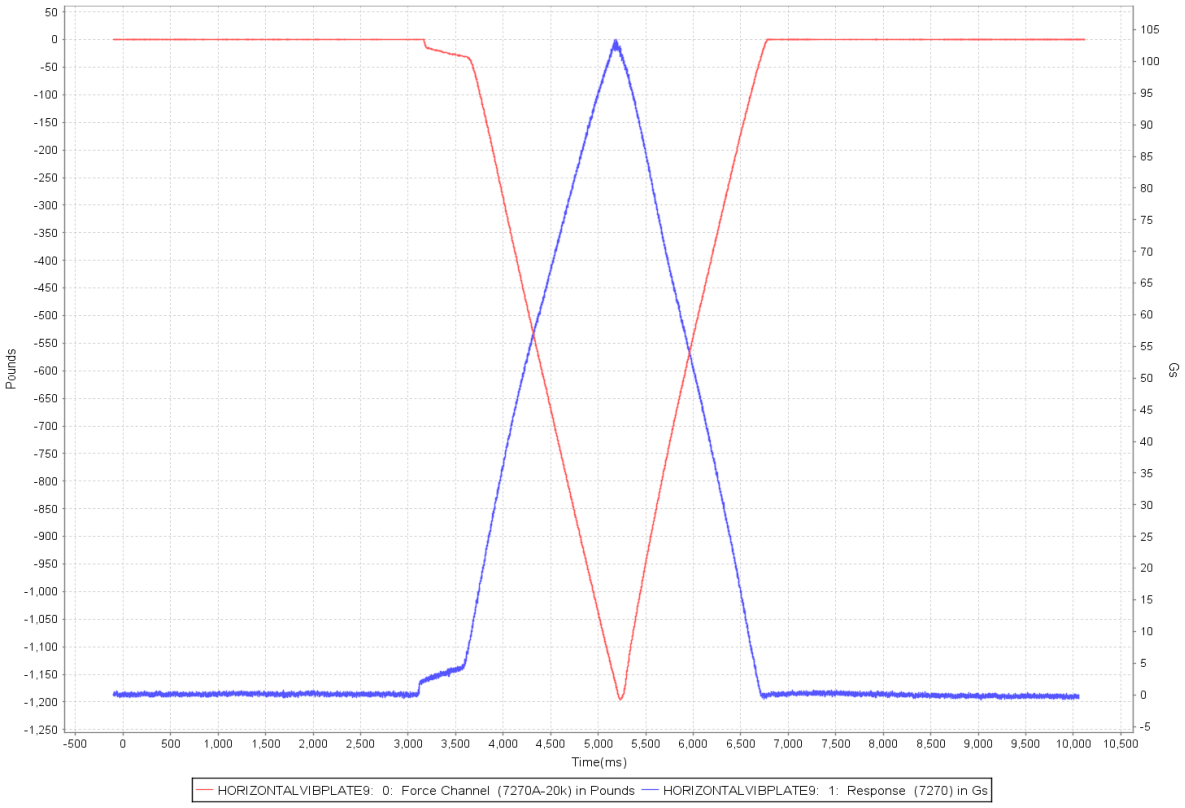

Figure 10 – Load Cell and Accelerometer Outputs from Base Strain Test

As the figure shows, the output of the accelerometer is proportional to the load applied to the bar. At a peak load of approximately 1,200 lbs the accelerometer had an output of approximately 105 G's, which in line with the predicted output of 67 G's. The unwanted

deformation at the base of the accelerometer produces a temporary zero-shift in the measured acceleration. Integrating the output of an accelerometer experiencing base strain demonstrates the potential for error in velocity estimation that could occur when trying to analyze dynamic events where high base strains are present. The resulting velocity and acceleration traces are plotted in Figure 11. The indicated velocity of the event was approximately 1,750 m/s which would have indicated an approximate displacement 2,500 m, which is obviously incorrect.

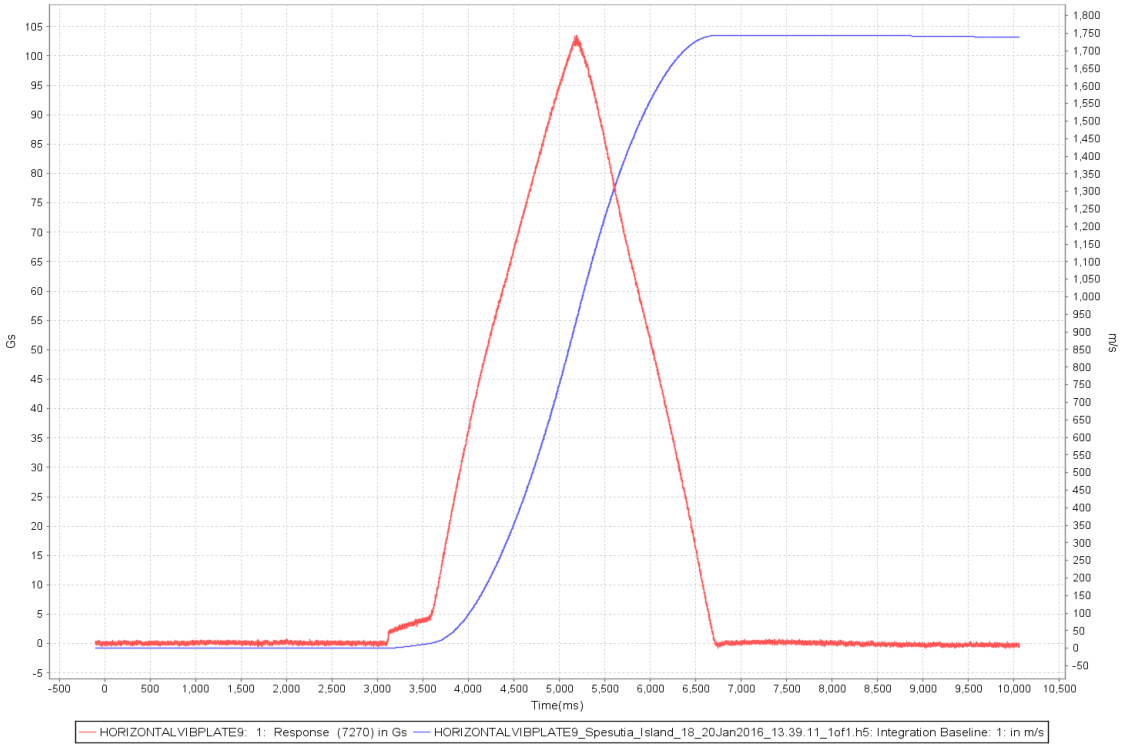

Figure 11 – Acceleration and Velocity of Accelerometer Subjected to Base Strain

One way to reduced base strain induced zero-shift error is to avoid using direct mounted accelerometers. Once again, the use of a mechanical filter between the test subject and the accelerometer can help attenuate the base strain without erroneously influencing the output of the accelerometer.

iii. DAQ and Signal Conditioning [5]

The DAQ system and signal conditioner are two more possible sources of error that can produce erroneous results when using accelerometers during LFT&E. As previously stated, high frequency signals that approach the resonance of an accelerometer can non-linearly affect the accelerometer's output, but more importantly, any frequencies higher than the sampling rate can produce incorrect results as well. This is known as "aliasing." Aliasing is caused when a signal with content above the Nyquist frequency is present in the sampled dataset, regardless if this high frequency content is authentic or caused by accelerometer resonance. This means the

higher frequency data will fold over to a frequency below the Nyquist frequency and cause distortion in the energy band of interest, i.e., out of band energy

For example, an FFT was performed on manufactured signals digitized with two separate analog-to-digital converters (ADC) with different operational characteristics. The first ADC used was a Successive Approximation ADC (SA-ADC) on which the Nyquist fold-over was successfully demonstrated. The second ADC used was a Sigma-Delta ADC (SD-ADC) on which the Nyquist fold-over was not present.

The frequency of an aliased signal can be determined by the equation below:

$$F_a = |R * N - F_s|$$

where F_a is the aliased frequency, F_s is the signal frequency, R is the sample rate, and N is the integer number of the sample rate closest to input signal frequency.

To demonstrate the fold-over effect on a SA-ADC, a sinusoid was generated with a signal frequency of 13.5 kHz and digitized via the SA-ADC with a sample rate 10 kHz. According to the theorem, the fold over frequency should occur at 3.5 kHz. As shown in the Figure 12, the blue trace is an FFT of the 13.5 kHz input signal digitized at the appropriate sampling rate. The aliased signal represented by the red trace in the FFT shows significant content at the 3.5 kHz predicted fold over frequency even though the system was digitizing at 10 kHz, as a result of "true aliasing."

The same input parameters were then used on a SD-ADC and the resulting FFT can be seen in Figure 13. This plot shows that an aliased signal does not appear at the predicted 3.5 kHz frequency. This is because the SD-ADC consists of an oversampling modulator followed by a digital decimation filter that filters the aliased signal from the band.

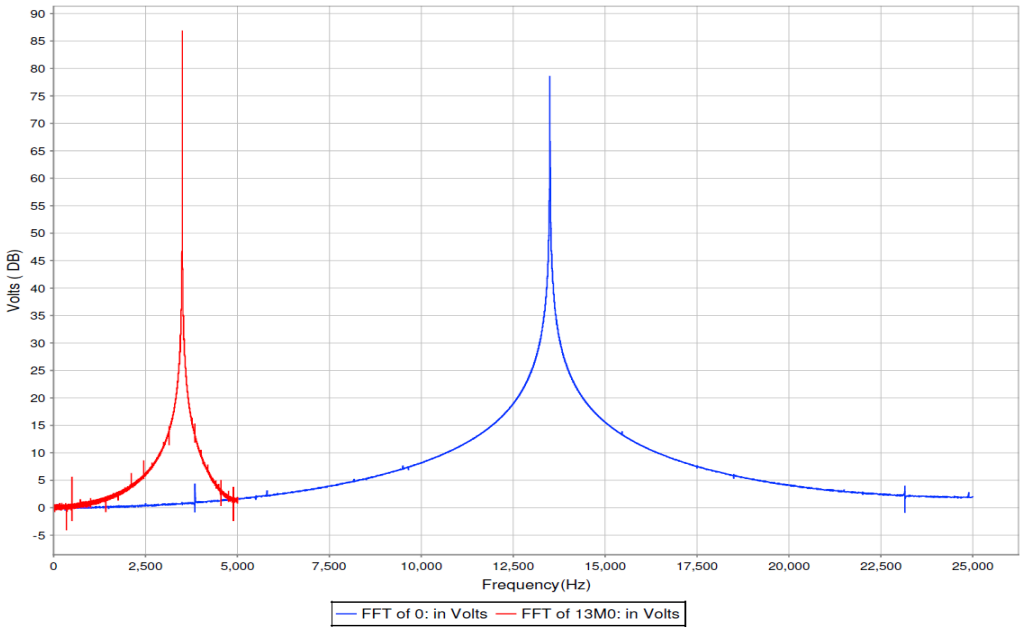

Figure 12 – Aliased Signal in Successive Approximation ADC

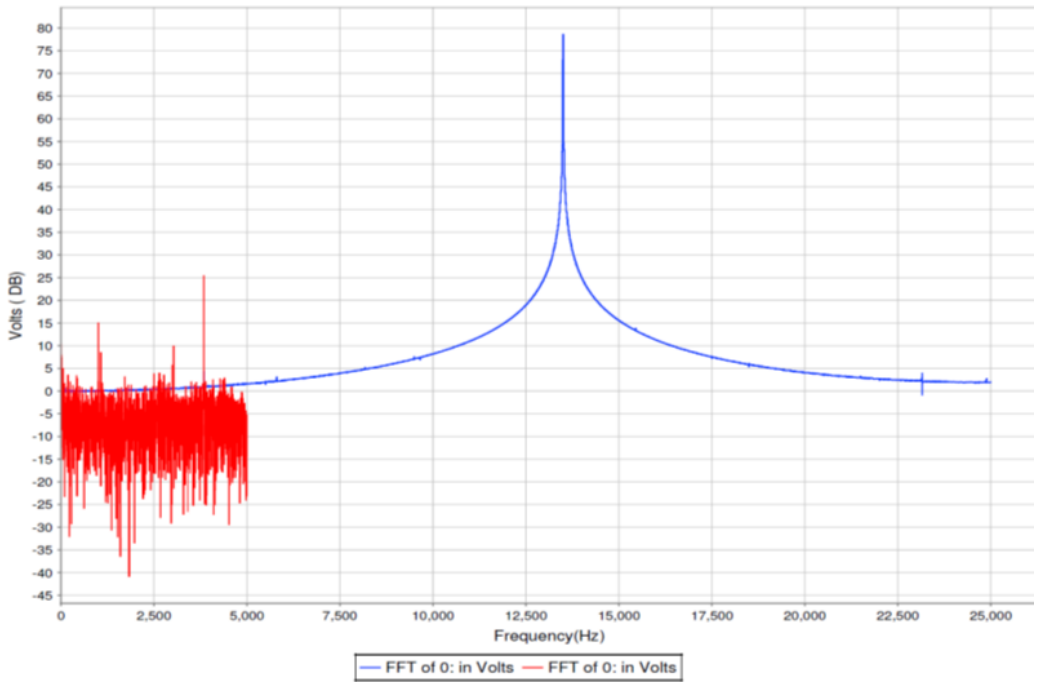

Figure 13 – No Aliased Signal in Delta-Sigma ADC

A second form of DAQ error that can be caused by accelerometer resonance is an internal DAQ clipping of the signal that is "invisible" to the instrumentation operator. As represented in Figure 14, the output at resonance of an undamped accelerometer combined with the true input signal enters the DAQ as a combined analog signal and is amplified and clipped by the pre-filter gain stage. The clipped signal is then filtered by the analog filter which removes the obviously clipped signal and is sent to a post-filter gain before entering the ADC. The clipped signal cannot be detected after it has been digitized and can cause severe distortion to digitized signal. In most cases the digitized signal is reduced by this effect, but in some cases this can cause an amplified signal.

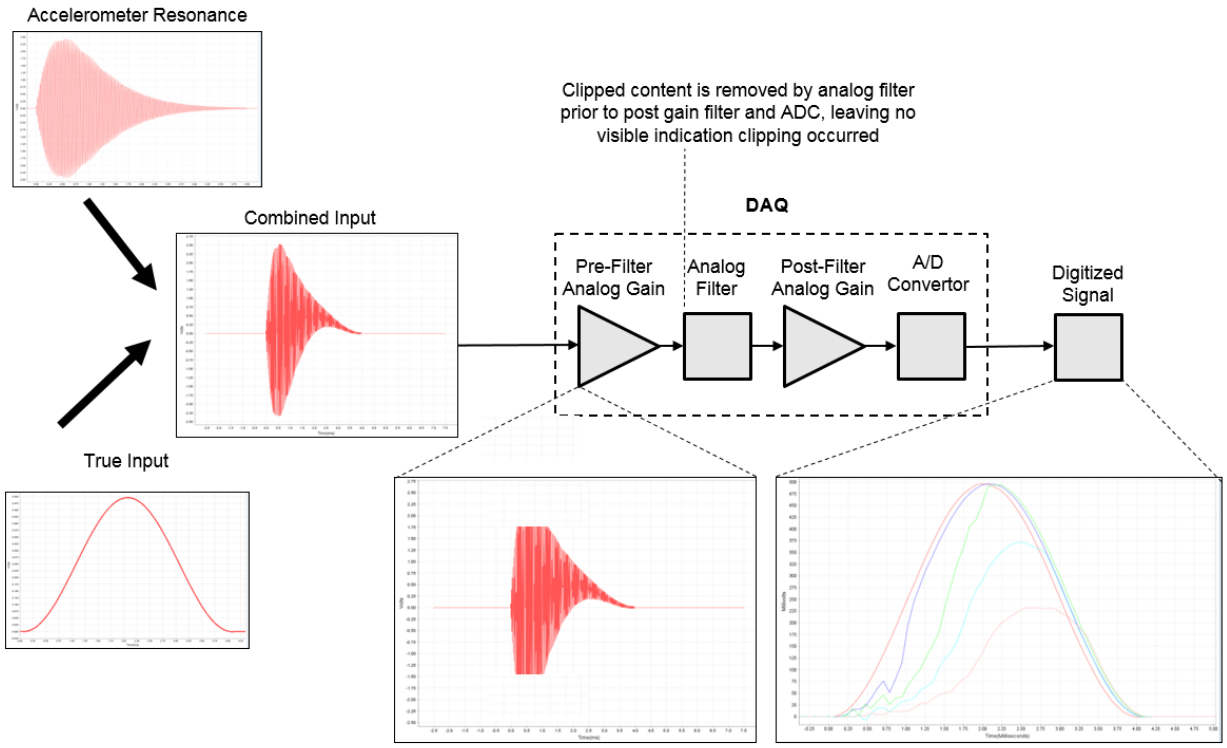

Figure 14 – "Invisible Clipping" Graphic

The research presented above helped determine which accelerometers were tested during this project and establish the test procedure used to characterize them. The issue of accelerometer resonance and base strain can both be solved with the use of a mechanical filter between the test subject and the accelerometer. But care must be taken when using mechanical filters. As physical objects, their components and assemblies are also capable of resonating. Furthermore, they may attenuate frequencies in a non-linear or non-repeatable manner. Carefully selected filter materials and designed filter assemblies have the ability to allow the frequencies of interest to pass with acceptably low and predictable attenuation or amplification while ameliorating the problems of base strain and resonance. For the remainder of this report, the term "accelerometer" will refer to direct mount accelerometers, and "gauge" will be used to describe accelerometer packages that have built in mechanical filters.

To help avoid aliasing, this project employed the use of a DAQ system featuring a SD-ADC and an anti-aliasing filter with a cutoff frequency ten times below the sampling frequency of each data source. As shown in Figure 13, the combination of an oversampling modulator followed by a digital decimation filter allows for data to be collected within the band of interest without experiencing aliasing. Furthermore, to prevent any "invisible clipping" from happening, several precautionary measures were taken. The first was to provide an ample head room to ensure internal clipping of the combined signal would not occur by setting the gain values to provide a peak measuring window approximately fifty times higher than the expected peak value. The second preventative step was to ensure that pre-filter gain was not used if possible. With the absence of pre-filter gain, the combined signal entering the DAQ will not clip the first

stage amplifier if it is within the measuring window and will not be disguised upon application of the analog filter. It should also be noted that this phenomenon can only occur in extreme circumstances. For all intents and purposes, a majority of the high frequency oscillations present in undamped accelerometer resonance are above 400 kHz and a majority of that is attenuated by the long run of data cables (~200') that connect the accelerometer to the DAQ.

The research above also provides further justification for the project by emphasizing the need for an established accelerometer and gauge test protocol. These issues must be considered and accounted for during testing in order to keep the evaluation process accurate and consistent.

Test Objectives

The objective of this project is to characterize commercially available accelerometers and gauges, in addition to prototype gauges, using controlled and consistent testing. To achieve this objective, a method to quantify the time domain and frequency domain accuracy had to be established. The goal is to have an accelerometer or gauge, whether commercial or prototype, that provides consistent and accurate data for use in test-to-test and test-to-simulation comparisons for each previously defined frequency range (low, medium, and high). The specific objectives of each phase of testing are listed below:

- Phase I
  - Evaluate existing commercially available accelerometers and gauges for:
    - Low frequency, ballistic trajectory accuracy (ATC Flyaway)
    - Medium frequency content accuracy (TCU Smack Bar)
  - Establish performance baselines for evaluation of accelerometer and gauge capabilities
- Phase II
  - Evaluate existing commercially available and concept gauges for:
    - Explosive DT and LFT&E -like environment (Explosive Rig)
      - High frequency, high G performance
      - Low frequency, ballistic trajectory accuracy
  - Establish performance baselines for evaluation of gauge performance
- Phase III
  - Evaluate best performing commercially available and concept gauges for:
    - Constant power on-axis accuracy (vertical): 10 – 2,000 Hz (Shaker Table)
    - Constant power off-axis accuracy (horizontal): 10 – 2,000 Hz (Shaker Table)
  - Establish performance baselines for evaluation of gauge performance and off-axis sensitivity

Test Approach

a. Accelerometers and Gauges

All phases of this project analyzed a variety of accelerometers and gauges. In summary, Table 1 displays the accelerometers that were used throughout this project and their relevant manufacturer provided specifications. It is important to note that the specifications for the

Endevco 7280A are ITAR controlled and have been withheld from this report; however, these specifications can be obtained through Endevco after proper verification. Some of the accelerometers listed in Table 1 were also used as the sensing devices in the gauges that were analyzed. Table 2 lists the name of each gauge, its internal accelerometer, and its overall mass. Following Table 2 is a brief description of each gauge with an explanation of the concept behind their design.

Table 1 – List of Accelerometers Analyzed

Accelerometer	Damping	Linear Range [G's]	Sensitivity [mV/G]	Mass [g]
Endevco 2262A	Critically Damped	2,000	0.25	28
Endevco 7264D	Undamped	2,000	0.20	1
Endevco 7270A	Undamped	20,000	0.01	1.5
Endevco 7280A	Underdamped	-	-	1.4

Table 2 – List of Gauges Analyzed

Gauge	Accelerometer	Mass [g]
Endevco 7270AM6	Endevco 7270A	8.4
LOFFI	Endevco 2262A	89.6
BOBKAT	Endevco 7270A	99.8
Tiny BOB	Endevco 7270A	17.2
Mini BOB	Endevco 7270A	117.4
AM6 Tall	Endevco 7270A	13.5
Wheel Mount	Endevco 7270A	70.1
Wave Spring	Endevco 7264D	175.7
Base BOB	Endevco 7270A	41.6
Spring Mount	Endevco 2262A	174.8
Corvid Disk Mount	PCB 3991	71.5

i. *Endevco 7270AM6*

The Endevco 7270AM6 is a commercially available mechanically filtered gauge that was developed by Sandia National Laboratories. According to the manufacturers, "the mechanical isolator consists of an aluminum housing lined with two layers of elastomer filter that cushions the model 7270A piezoresistive accelerometer."[6] The Endevco 7270AM6 used for this particular project had linear range limit of 60,000 G's. An example of this gauge can be seen in Figure 15.

Figure 15 – Isometric View of Endevco 7270AM6 [6]

ii. *ATC LOFFI*

The LOFFI is a mechanically filtered gauge that houses an Endevco 2262A accelerometer and can be mounted to the standard ATC LOFFI mount ring. The LOFFI consists of an aluminum gauge plate that the accelerometer is bolted to. The gauge plate is sandwiched between two ½" thick EPDM foam rubber pads. The whole assembly is mounted to the LOFFI mount ring through the LOFFI top ring with three bolts. The screws have a rubber isolator around them to prevent impact with the gauge plate. Figure 16 displays an isometric and section view of the LOFFI.

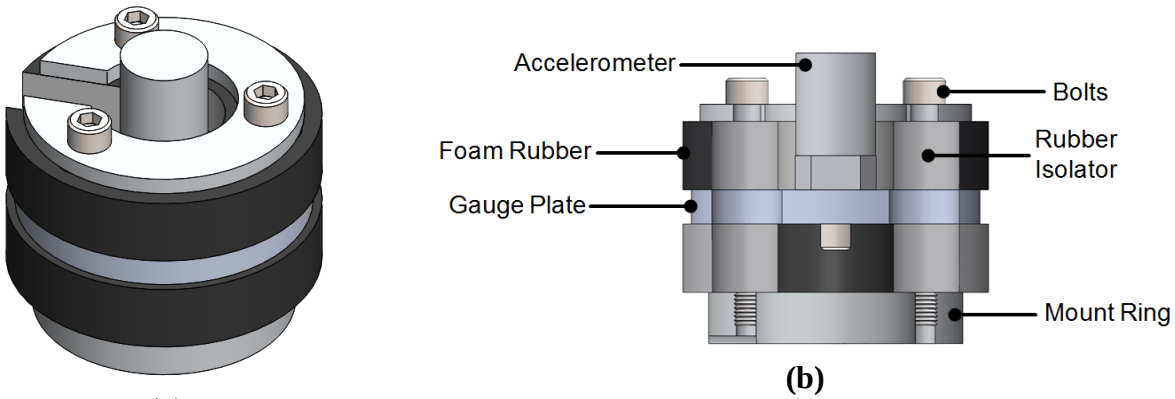

Figure 16 – Isometric (a) and Section (b) Views of LOFFI

iii. *ATC BOBKAT*

The BOBKAT is a mechanically filtered gauge that uses an Endevco 7270A accelerometer. The BOBKAT is intended to be mounted on the standard ATC LOFFI mount ring. The accelerometer is attached to the BOBKAT Star, which is sandwiched between to 0.5" layers of ISODamp. The whole assembly is bolted through the super spider clamp with three bolts that go into the standard LOFFI mount ring. An isometric and labelled section view of the BOBKAT can be seen in Figure 17.

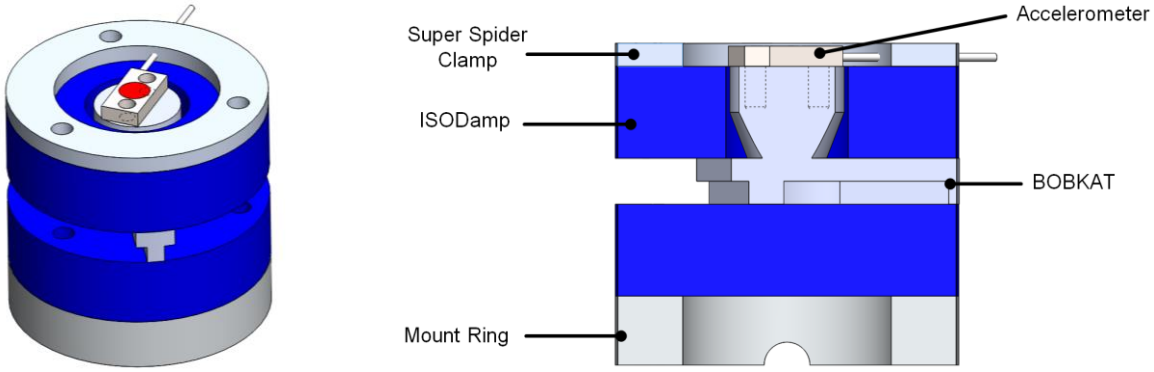

(a) **(b)**

Figure 17 – Isometric (a) and Section (b) Views of BOBKAT

iv. *ATC Tiny BOB*

The Tiny BOB is a miniaturized version of the standard ATC BOBKAT. The Tiny BOB is a mechanically filtered gauge that houses an Endevco 7270A accelerometer. This gauge consists of the 7270A with a spacer over the sensing element, sandwiched between two thin pieces of ISODamp. The ISODamp pads act as the mechanical filter within the gauge. This setup requires the accelerometer to have a spacer on the topside of the accelerometer to prevent undue stress on the sensing element of the accelerometer. The upper housing, lower housing, and the accelerometer spacer are all made out of aluminum. An isometric and labelled view of the Tiny BOB can be seen in Figure 18.

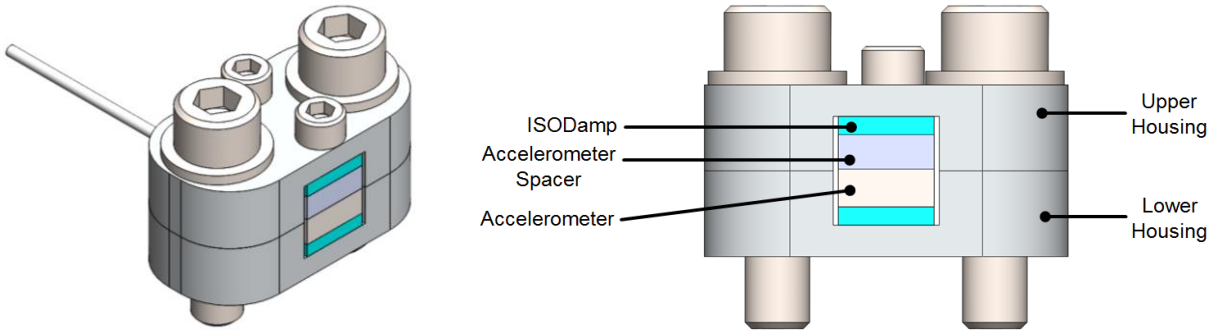

(a) **(b)**

Figure 18 – Isometric (a) and Labelled (b) Views of Tiny BOB

v. *ATC Mini BOB*

The Mini BOB is mechanically filtered gauge that houses an Endevco 7270A accelerometer. This gauge is almost identidical to the Tiny BOB, with the only difference being the form factor. This design allows the Mini BOB to be mounted to the typical LOFFI ring, and allows for the LOFFI to be mounted on top. This reduces the overall foot print that is consumed. The upper and lower housings and the spacer are made out of alumimum. Figure 19 shows an isometric view and a labelled section view of the Mini BOB.

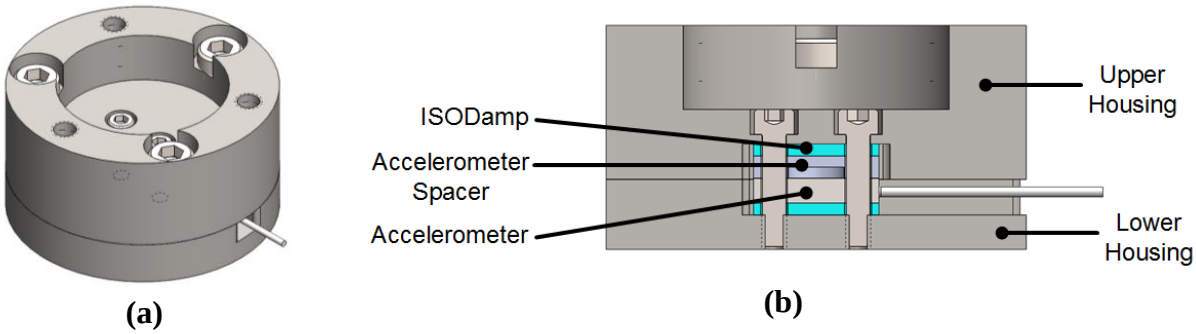

Figure 19 – Isometric (a) and Section (b) Views of Mini BOB

vi. *ATC AM6 Tall*

The AM6 Tall is very similar to the Tiny BOB and Mini BOB, with similar construction, but the AM6 Tall has a different form factor. This form factor is derived from the Endevco 7270AM6 gauge. The intention of this mount was to offer similar mechanical filtering but greater displacement. The mount also offers the user a different way to mount the gauge to the test item. An exploded view of this gauge can be seen in Figure 20.

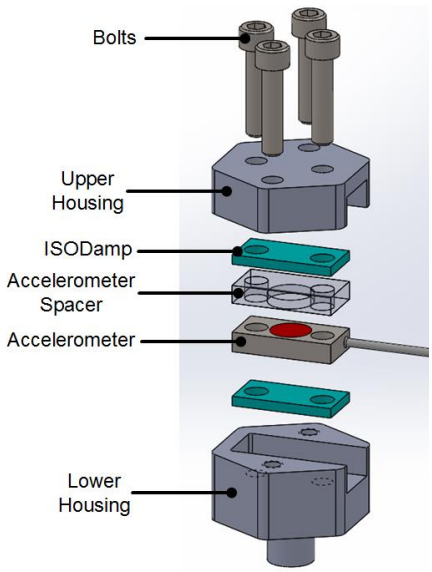

Figure 20 – Exploded View of AM6 Tall

vii. *ATC Wheel Mount*

The Wheel Mount is a mechanically filtered gauge that houses an Endevco 7270A accelerometer. The intended design was to have the "wheel spring" made out of copper. The tested configuration was made out of aluminum. This gauge has a "wheel spring" on the top and bottom of the accelerometer housing. It also has internal magnets that are intended to produce Eddy current damping; however, they were not used for this particular project. The Wheel Mount can be mounted directly to the standard LOFFI mount ring. Figure 21 shows a labelled section view and an exploded view of the Wheel Mount.

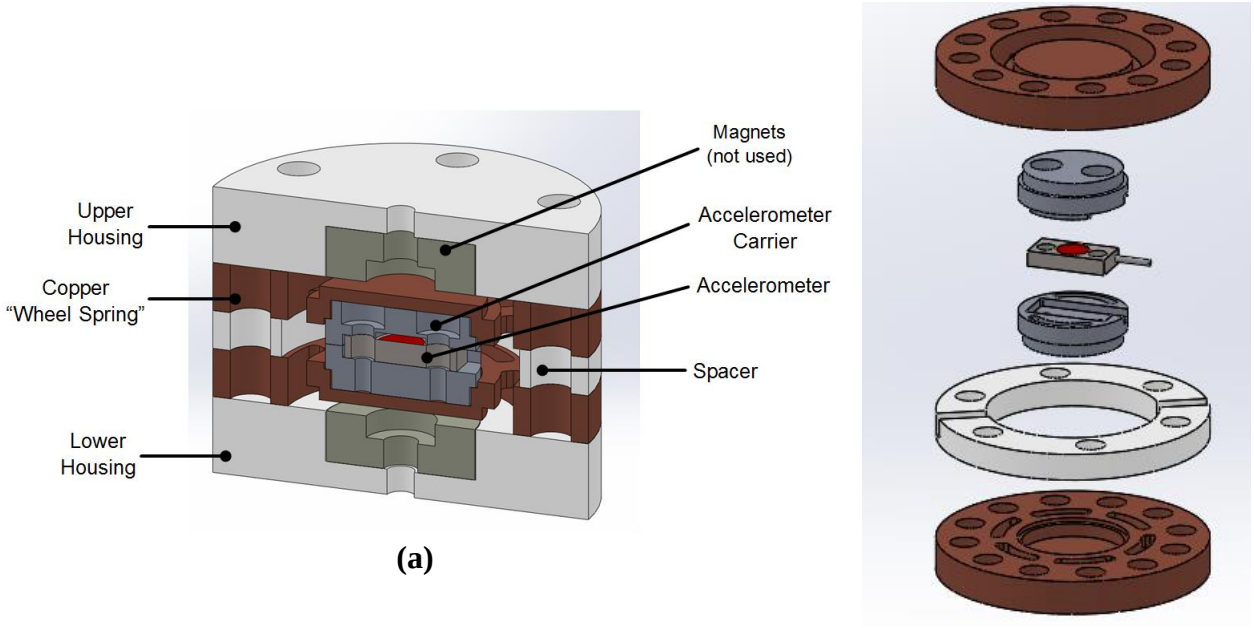

Figure 21 – Labelled Section (a) and Exploded (b) Views of Wheel Mount

viii. *ATC Wave Spring with Base BOB*

The combination of these concept gauges is an example of collocated gauges. Individually, the Wave Spring is a mechanically filtered gauge that houses an Endevco 7264D accelerometer. The housing is made from aluminum, and the accelerometer carrier is made from ABS plastic. The accelerometer carrier is suspended by two wave springs, one on the top and bottom of the accelerometer carrier. The accelerometer carrier uses two O-rings to help keep the carrier centered in the housing and to reduce high frequency input from the side walls of the carrier. Mounted beneath the Wave Sprint is the Base BOB, which is very similar to the Tiny BOB and Mini BOB. The only difference is the form factor change to allow for the mounting of the Wave Spring on top. Views of this collocated gauge can be found in Figure 22.

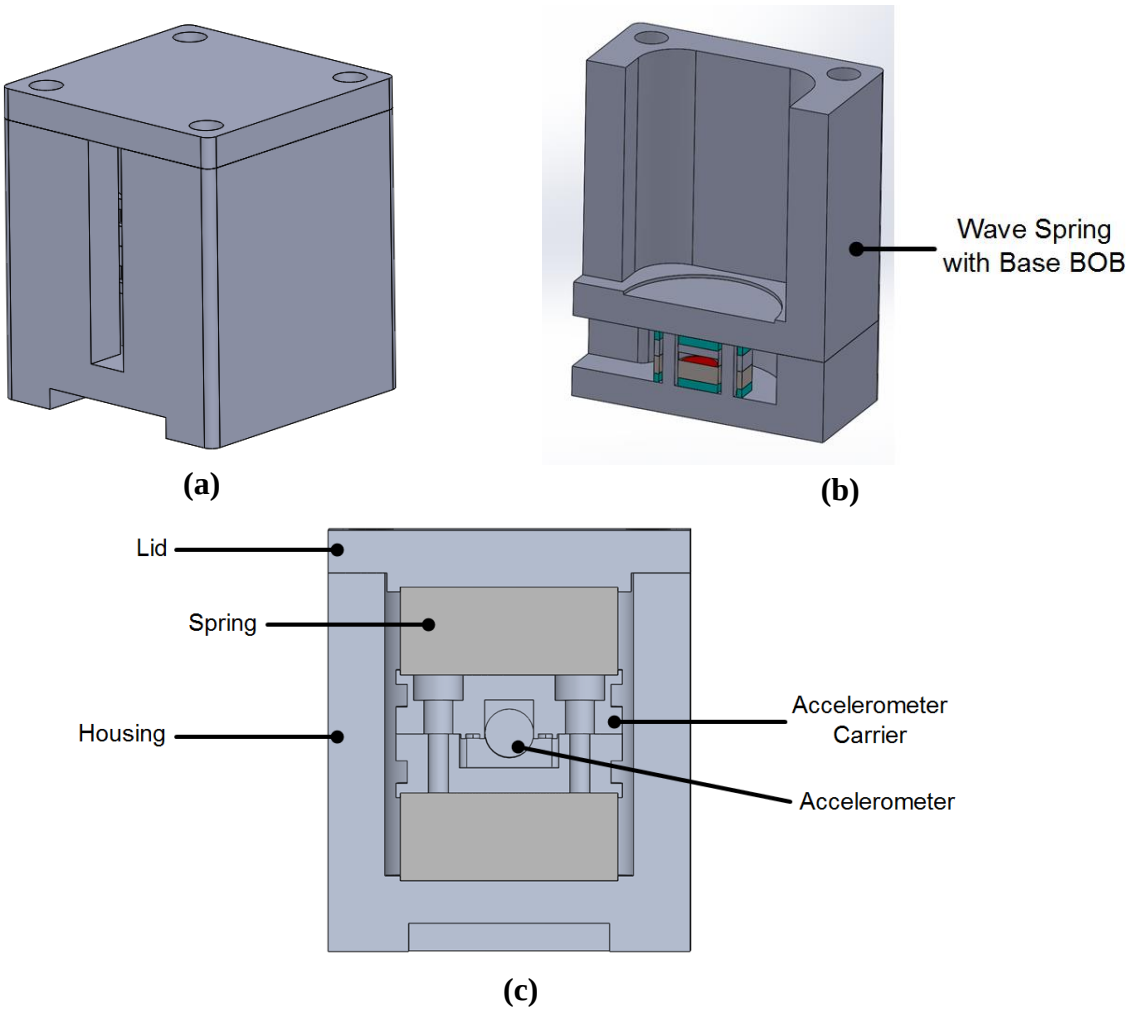

Figure 22 – Isometric (a), Section (b), and Labelled Section (c) Views of Wave Spring with Base BOB

ix. *ATC Spring Mount*

The Spring Mount is also a mechanically filtered gauge that houses an Endevco 2262A accelerometer and can be mounted on the standard LOFFI mount ring. This gauge has two coil springs that sit on the top and bottom of the accelerometer carrier. The intended housing and carrier are intended to be made out of aluminum, but were tested using a 3D printed ABS plastic outer housing. An isometric view of the gauge can be seen in Figure 23 (a), but the section view in Figure 23 (b) shows how the gauge is assembled.

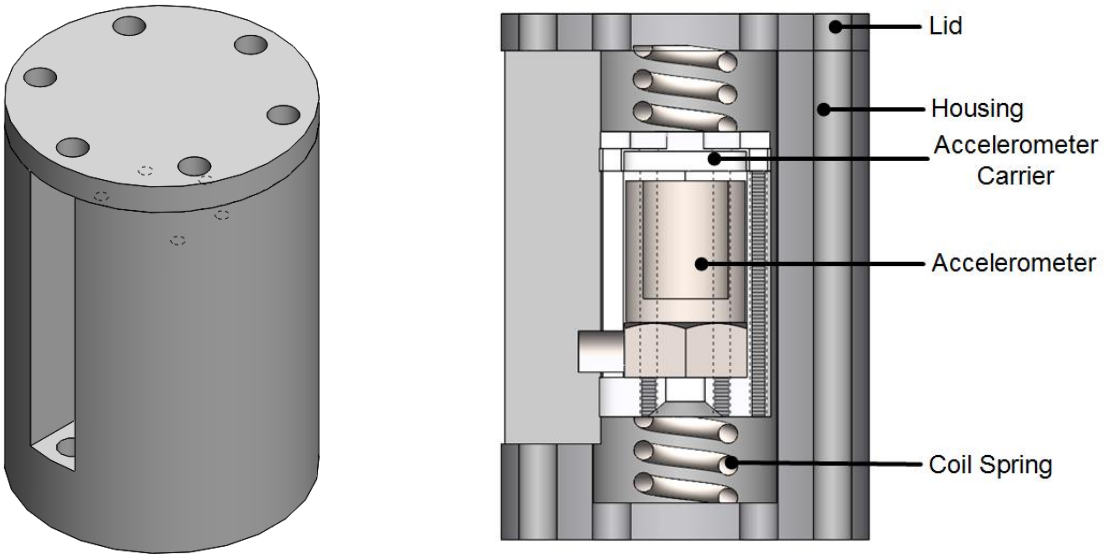

Figure 23 – Isometric (a) and Section (b) Views of Spring Mount

x. *Corvid Disk Mount*

The Corvid Disk Mount is a gauge that houses a PCB 3991 accelerometer and can be mounted using a standard LOFFI mount ring, as can be seen in Figure 24. Also shown in Figure 24 is a section view that better illustrates the design behind the gauge. The accelerometer is attached to the bottom disk with a pod of polyurethane, and the bottom disk is sandwiched between the top ring and the mount ring with six bolts. Both the bottom disk and top ring are composed of polycarbonate and were 3-D printed due to their complex geometry. When assembled, these components create internal cavities that were filled with silicone prior to testing. This silicone helps damp the unwanted high frequency content while maintaining continuity throughout the gauge.

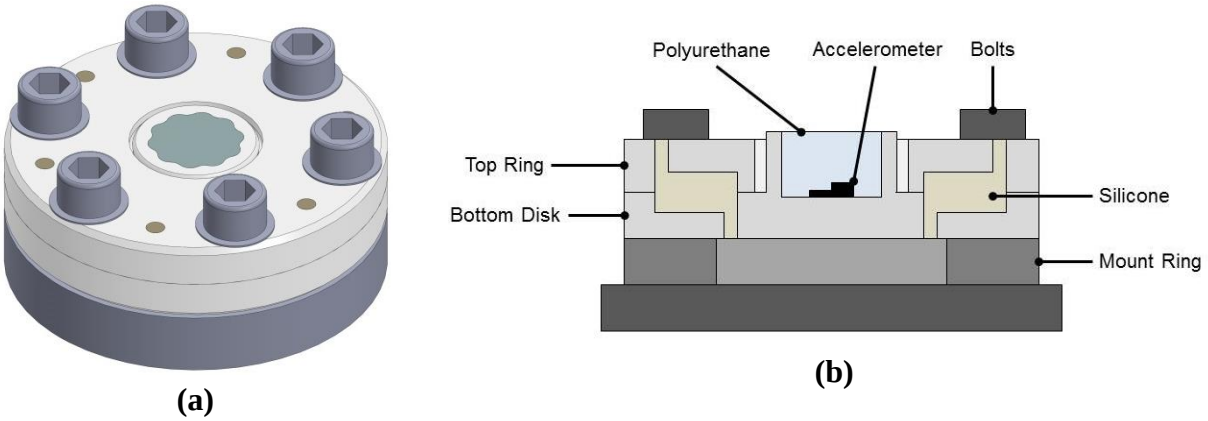

Figure 24 – Isometric (a) and Section (b) Views of Corvid Disk Mount

b. Phase I

During Phase I, the TCU Smack Bar machine was used to analyze the medium frequency content performance of the accelerometers and gauges of interest. Designed by Texas Christian University (TCU) and shown below in Figure 25, the system consists primarily of a compressed air gun and a flat steel bar fixed on either end to spring steel and base supports. A steel slug is launched from the compressed air gun and impacts the underside of the 36" long, ½" thick steel bar below the device under test. The resulting metal-on-metal contact is measured by both the device under test and a non-contact laser Doppler vibrometer (LDV) isolated from the test fixture (fixed to the ceiling).

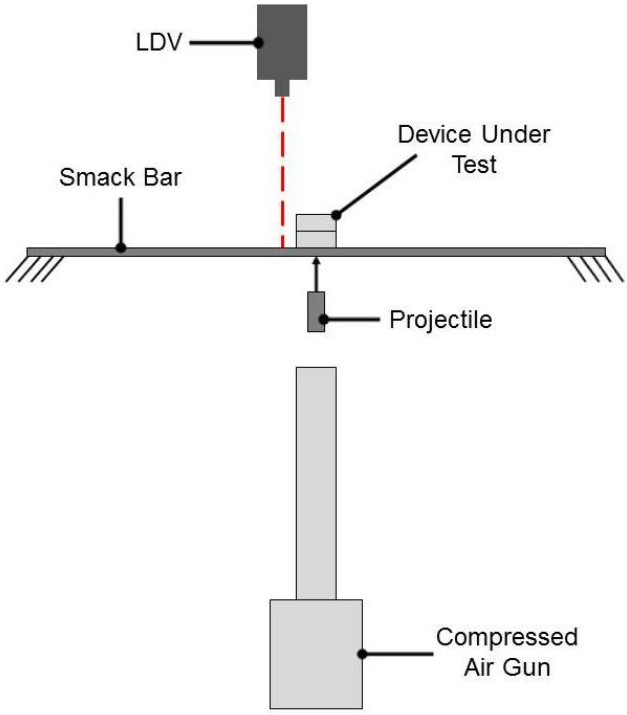

Figure 25 – TCU Smack Bar Machine

The system was originally designed to test objects weighing up to one pound and produce a shock level that fits within the envelope specified in the ballistic shock limits of MIL STD 810F Method 522.

Typically a 1" long flat-nose projectile has been used for testing; however, during some initial testing it was discovered that the metal-on-metal impacts on the smack bar were too severe for direct mount accelerometer testing and produced content outside of the medium frequency range. Therefore a "programmer" was added to the underside of the test bar. After testing several materials, the combination of two 0.01" thick pieces of duct tape was found to consistently yield an input which stressed the upper limits of the accelerometers without causing failure. The 1" flat projectile was also replaced by the 3" rounded projectile. This new configuration can be seen in Figure 26.

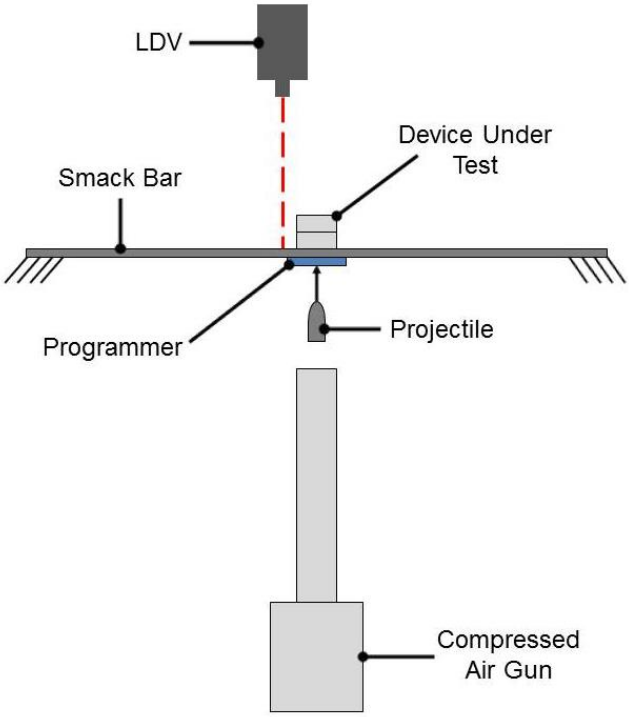

Figure 26 – TCU Smack Bar Machine with Programmer

Also during Phase I, the TCU Smack Bar machine was outfitted with the Flyaway attachment and used to analyze the low frequency performance and ballistic trajectory accuracy of the accelerometers and gauges of interest. The Flyaway attachment was designed by ATC to test for low frequency accuracy and can be seen in Figure 27. The setup is similar to the Smack Bar machine with the exception that the impacted surface (called the flyaway disc) and the device under test are unconstrained in the vertical direction and are free to travel after impact. Total free vertical travel is limited to 30", but this provides enough time to measure the response of the device during freefall. Additionally, a ½" thick layer of ISODamp was placed on the bottom of the flyaway disk specifically to eliminate high-frequency mechanical input so that only the low-frequency response of the device under test could be measured.

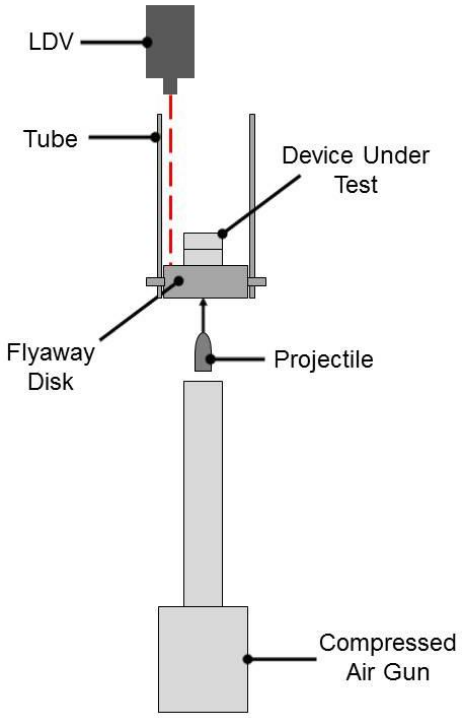

Figure 27 – TCU Flyaway Machine

Throughout Phase I, the gauges shown in Table 3 were analyzed at a variety of air gun pressures. For the Smack Bar tests, the pressure varied between 8 psi and 70 psi, depending on the linear range of the accelerometers and gauges. For example, the Endevco 2262A was only able to reach an air gun pressure of 12 psi before reaching its linear range limit of 2,000 G's. For the Flyaway tests, the air gun pressure remained a constant 20 psi for all accelerometers and gauges. Additionally, each test at a specified pressure was repeated several times to ensure accuracy. Throughout Phase I, all accelerometers and gauges were operated with a sampling rate of 1 MHz.

Table 3 – List of Accelerometers and Gauges Analyzed During Phase I

Accelerometer/Gauge	Smack Bar	Flyaway
Endevco 2262A	✓	✓
Endevco 7270A	✓	✓
Endevco 7270AM6	✓	✓
Endevco 7280A	✓	✓
Endevco 7264D		✓
BOBKAT	✓	✓
LOFFI	✓	✓

c. Phase II

During Phase II, the explosively-driven test rig was used to simultaneously analyze both the high frequency, high acceleration performance of the gauges as well as the low frequency, ballistic trajectory accuracy. The purpose of this rig was to provide a standardized and consistent method of explosively testing gauges by simulating the behavior of a typical walk-on floor in a tactical vehicle during LFT&E. This was intended to be the most authentic test in the protocol and introduced many of the "real world" complications of explosive testing environments for this type of instrumentation. As this test had the highest test-to-test variability, the rig was designed to accommodate multiple gauges in symmetric locations for intra-test comparisons. Gauge performance on this platform is the most indicative of performance in vehicles undergoing live-fire testing.

The explosively-driven test rig was designed to analyze up to 16 gauges simultaneously. Due to the severity of the acceleration produced by the test rig, no direct mount accelerometers were tested during this phase of the project. A schematic of the test rig can be seen in Figure 28, with black markers indicating the position of the between-supports gauge location with an outer radius of 14" and blue markers representing the on-support gauge locations with an inner radius of 10". The test rig is composed of five major components: legs, a driver plate, supports, a floor plate, and angle brackets (not visible in Figure 28). These components are assembled using welds, M12 fasteners, and hitch pins. The driver plate has an outer diameter of 6', a thickness of 8", and is composed of RHA. It is one of the HME-C Working Group's rigid heave plates that was created to assess impulse from soil compositions and preparation conditions.

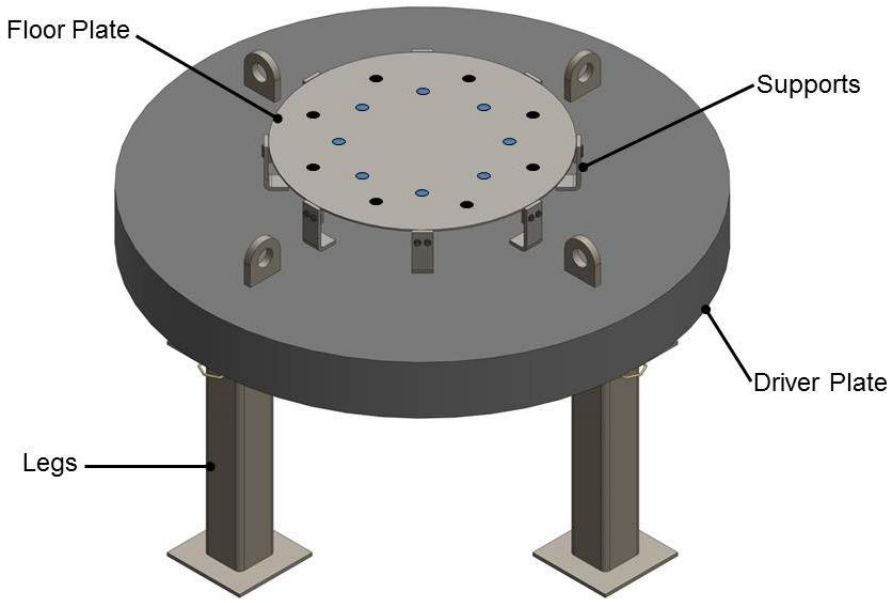

Figure 28 – Explosively-Driven Test Rig with Gauge Mount Locations

Welded to the driver plate are eight supports composed of 1018 mild steel, which can be seen in Figure 29 along with the angle bracket and the floor plate. The angle bracket is

commercially available steel angle and the top plate is cut from high-hard steel. The angle brackets are fastened to the supports, and the floor plate is welded to each angle bracket. The floor plate has an outer diameter of 3’ and is ¼” thick. Also welded to the driver plate are four lifting eyes and four leg inserts, as shown in Figure 30.

The four legs can be connected to the leg inserts with hitch pins to give the driver plate a specified standoff of 30”, a height that is also common to the HME-C test program. These hitch pins are present during assembly to provide stability but are removed before detonation. The entire assembly weighs 9,640 lbs. The floor plate and angle bracket assembly are replaced after each test to aid in test preparation and prevent potential plastic deformation from altering the performance from shot-to-shot.

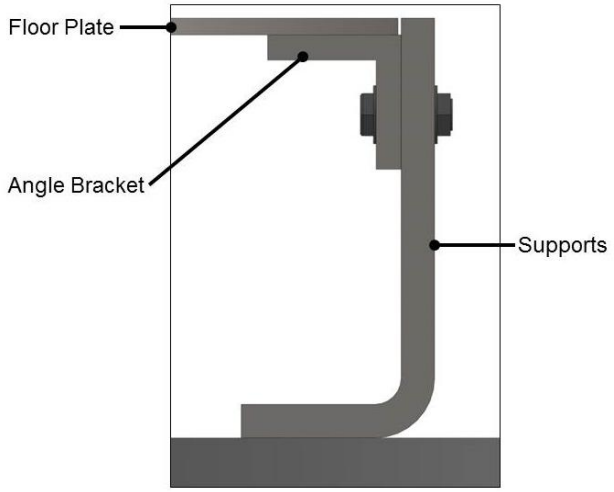

Figure 29 – Components of Floor Plate Assembly

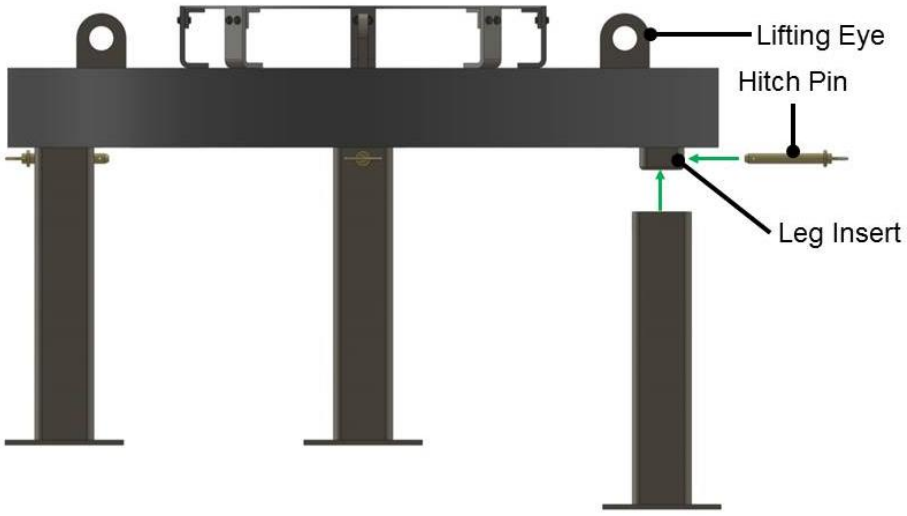

Figure 30 – Lifting and Standing Components

During testing, gauges are mounted on any of the 16 symmetric locations on the floor plate provided by the symmetric support spacing around the circumference. As previously mentioned, these locations are varied to be on a support at an inner radius of 10" or between supports at an outer radius of 14". This allows for a wide range of inputs for each of the gauges being investigated. One of the locations on the outer radius was dedicated to the LDV as a method of collecting "truth" data. Then, the entire assembly is placed over a buried explosive charge before the hitch pins are removed. This allows the assembly to be simply supported with a specified standoff between the charge and the driver plate. The initial shock of the blast is absorbed by the driver plate and transferred through the supports and connections to the floor plate to load the gauges. This impulsive loading is similar to that of a tactical vehicle floor, where the hull absorbs the initial loading and transfers the energy to the floor of the vehicle through bolted or welded joints.

The design of the explosively-driven test rig allows for the mounted gauges to experience similar peak accelerations and shock frequencies as those experienced by instrumentation on the walk-on floors of tactical vehicles during LFT&E. As previously mentioned, the angle brackets and floor plate may experience plastic deformation and were therefore designed to be replaced after each shot, but the explosive charge mass was kept below that which would have induced plastic deformation in the driver plate and floor support legs so that they may be reused.

The explosively-driven test rig was designed through iterative computational physics simulations. This process allowed for the effect of variables such as charge type, charge size, overburden, standoff, component material, and geometry to be determined and optimized to generate the input loading profile of interest as compared to typical LFT&E measurements.

For Phase II, there were a total of seven explosively-driven test rig shots. The first shot was a "check out" shot with only 10 lbs of C-4 and a 4" overburden. However, shots two through four were full-charge shots that featured 20 lbs of C-4 with a 4" overburden. The next two shots, five and six, had 20 lbs of C-4 and a 4" overburden as well, but they also featured a 3" diameter steel tower between the driver plate and floor plate. It was initially desired for the Explosive Rig tests to produce acceleration content that forces the gauges to approach their linear range limit, even though they contain built in mechanical filters. However, Shots #2, #3, and #4 were not severe enough to produce this type of content; therefore, the steel tower was installed between the driver plate and floor plate as a source of a metal-to-metal impact. However, even with this impact, the acceleration content produced by the explosively-driven test rig appeared unchanged. For data processing purposes, Shot #2 through Shot #6 were all considered to be identical. This steel tower can be seen between the driver plate and floor plate in Figure 31.

Figure 31 – Steel Tower Mounted to Driver Plate of Explosively-Driven Test Rig

Since the steel tower was not able to change the acceleration content produced by the explosively-driven test rig, a second approach was used in an attempt to produce severe content. For the final shot, Shot #7, a small charge of C-4 was placed under a 3" diameter and 1" thick steel puck on the driver plate as seen in Figure 32. This small amount of C-4 was detonated to launch the steel puck into the floor plate and produce the severe acceleration content without the use of a buried charge. However, detonation of this C-4 produced some unintended negative consequences by severing the wires of the gauges mounted on the floor plate. Data from this shot was rendered useless and removed from the analysis, but more information about this shot can be found in the *Lessons Learned* section.

Figure 32 – Shot #7 Configuration for Explosively-Driven Test Rig

There were a total of 18 different gauges tested on the explosively-driven test rig; however, some were multiples of the same gauge and some gauges did not produce coherent results. Therefore, only 11 gauges were analyzed in the data processing and analysis stages of this project. All gauges had a sampling rate of 1 MHz for Phase II. A list of these gauges can be seen in Table 4.

Table 4 – List of Gauges Analyzed During Phase II

Gauge	Shot 1	Shot 2	Shot 3	Shot 4	Shot 5	Shot 6
Endevco 7270AM6	✓	✓	✓	✓	✓	✓
LOFFI	✓	✓	✓	✓	✓	✓
BOBKAT	✓	✓	✓	✓	✓	✓
Tiny BOB	✓	✓	✓	✓	✓	✓
Mini BOB	✓	✓	✓	✓	✓	✓
AM6 Tall	✓	✓	✓	✓	✓	✓
Wheel Mount	✓	✓	✓	✓	✓	
Wave Spring	✓	✓	✓	✓	✓	✓
Base BOB	✓	✓	✓	✓	✓	✓
Spring Mount	✓	✓	✓	✓	✓	✓
Corvid Disk Mount					✓	✓

d. Phase III

During Phase III, Shaker Table testing was used to perform on-axis and off-axis vibration analyses on the gauges of interest. ATC's shaker table is capable of producing constant power vibrations with simultaneous frequencies ranging from 10 – 2,000 Hz. All gauges that were analyzed during this phase were tested simultaneously to ensure commonality and minimize total test schedule and cost. Two tests were conducted on the shaker table to assess both vertical and horizontal mounting configurations. Figure 33 shows the setup of the vertical Shaker Table test.

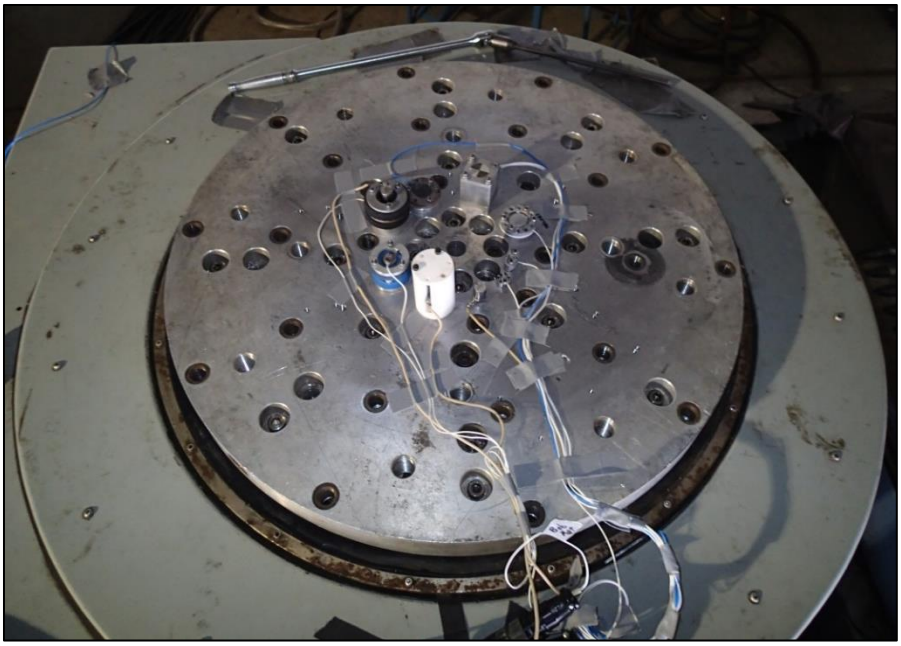

Figure 33 – ATC's Shaker Table Setup

For this phase of the project, only the best performing gauges were tested, but the shaker table also featured a reference accelerometer that is intended to produce the objective truth results. However, as this project shows, the output of an accelerometer is not always accurate. Table 5 lists each of the gauges that were analyzed using ATC's shaker table, including the reference accelerometer. For Phase III, the sampling rate for the gauges of interest varied among 50 kHz, 100 kHz, 200 kHz, and 400 kHz in an attempt to analyze the sampling rate's influence on the measured results.

Table 5 – List of Accelerometers and Gauges Tested During Phase III

Accelerometer/Gauge
Endevco 2262A (Plate Reference)
Endevco 7270AM6
LOFFI
BOBKAT
Tiny BOB
Mini BOB
Wheel Mount
Wave Spring
Base BOB
Corvid Disk Mount

Detailed Test Results

a. Test Conditions

i. Truth Data

In order to accurately evaluate the gauges during each phase of the project, the measured results needed to be compared to "truth" data. However, each test conducted during the project utilized a different source of truth data, and each source of truth data had its own limitations in accuracy. The following section outlines the sources of truth data for this project and any accuracy issues associated with them.

1. Laser Doppler Vibrometer (LDV)

LDV is an instrument that uses a laser beam to take non-contact velocity measurements of a surface. Since this device is the most versatile, it was used as a source of truth data for the Smack Bar, Flyaway, and Explosive Rig tests. The laser beam is aimed at a surface location of interest and the vibration amplitude and frequency are extracted from the Doppler shift of the reflected beam frequency due to the motion of the surface. The output is a voltage measurement that is directly proportional to the velocity component along the direction of the laser beam. For this particular project, a Polytec OFV-505 Vibrometer Head and a Polytec OFV-5000 controller were used to obtain this data with a maximum range of 20 m/s. As previously mentioned, this device can be used in live-fire field testing, such as Explosive Rig testing, but it is best suited for use in laboratory environments, such as Smack Bar or Flyaway testing. Throughout the entire project, its sampling frequency was 1 MHz, which results in a Nyquist frequency of 500 kHz. For the Explosive Rig, due to the nature of the test, only approximately 75 ms of the LDV data is considered useful. After 75 ms, the laser gets obstructed from the dirt and debris and is no longer able to record a valid measurement.

One issue with LDV is that dropouts can occur when the laser beam does not shine directly on the reflective surface. Intended to improve the signal-to-noise ratio of the input signal of the sensor head, a tracking filter was used during Explosive Rig testing only. The filter bridges brief dropouts, which always occur due to the speckle nature of the light scattered back from the object. Brief dropouts are significantly increased when the system is used in a non-laboratory explosive test due to the amount of dirt and debris that can cross the laser beam. A "fast mode" tracking filter was selected for use during Explosive Rig testing. The response of the tracking filter is shown below in Figure 34.

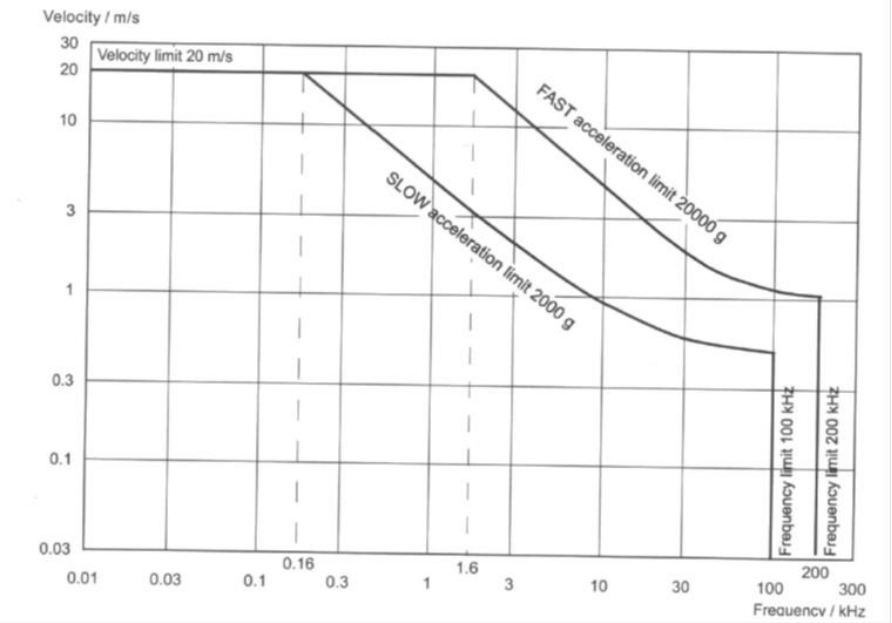

Figure 34 – Polytec Tracking Filter used During Explosive Rig Testing

2. Stereo Digital Image Correlation (SDIC)

SDIC is another source of truth data that was used during the Explosive Rig tests. Vic-3D software was used to track the movement of the floor plate via digital image correlation analysis. Prior to the shot, two high-speed cameras were placed at a 30-45 degree angle from one another facing the test area and were calibrated using a calibration board specific to Vic-3D. Also, before detonation, the floor plate of the rig was painted with a high contrast speckle pattern. Once detonation occurs, Vic-3D has the ability to track movement by measuring the motion and deformation of the speckled area in the videos. This allows the user to gather displacement and velocity data, as well as material deformation and strain, at a frequency of 10 kHz. SDIC has the lowest sampling frequency of all the sources of data, but its Nyquist frequency of 5 kHz still spans the low and medium frequency ranges of interest and is well within the high frequency range.

SDIC is largely limited by the clarity of the speckle pattern in the shot; the individual speckles need to be large enough to be distinct, but small enough to achieve a sufficient density and randomness in the pattern. Additionally, obstructions such as dust and debris during the shot can obscure the pattern and prevent analysis in the covered area. There is also a time when areas of the images are distorted from the density gradient produced by the air shock passing over the floor plate. The system also depends on the cameras remaining stationary after calibration; any movement of the cameras or camera shake during a blast event will invalidate any data recorded during or after the movement, as well as requiring the cameras to be recalibrated before the next shot. For this particular project, the SDIC truth data is only considered useful for the first 15 ms before the shockwave reaches the camera stands and causes the cameras to shake. Also, for this project, there were issues with camera synchronization. For the results to be accurate and

meaningful, the frame capture of the cameras must be perfectly synchronized; however, during the data processing stage, it was determined that the two videos used for Shot #5 were off by about 1.5 ms, or 15 frames. This issue was fixed for Shot #5 by removing 15 frames from one of the two videos and rerunning the displacement calculations. SDIC data was gathered on Shots #2, #5, and #6, but limited access to the videos used for data calculations lead to Shot #5 being the only example of trustworthy SDIC data.

3. Photon Doppler Velocimeter (PDV)

PDV is a source of truth data that uses the Doppler shift of reflected light to estimate a velocity of a moving reflector. The physics behind the data acquisition process are similar to those of LDV, but due to the instrumentation requirements, PDV was only used as a source of truth data for the Explosive Rig tests. The equation relating the velocity is shown below:

$$f = f_0 \frac{2|u|}{c}$$

where f is the measured beat frequency, f_0 is the original frequency of the laser (c/1550.045*10^{-9}), c is the speed of light, and u is the velocity of the moving reflector. The measured beat frequency, f, is extracted from the voltage vs. time trace recorded on the oscilloscope by computing a time-wise short-time-Fourier-transform using SIRHEN, a Sandia National Laboratory developed computer program. This data is portrayed using a spectrogram, which relates velocity (or frequency) of the moving reflector vs. time vs. spectral density at a given velocity (or frequency). Because in this test the moving object is known to not fail, a singular velocity vs. time profile can be extracted from the three-dimensional data using a fitting routine (robust or Gaussian based). This velocity vs. time data can then be integrated into distance or its derivative can be used to relate acceleration. Typically, PDV can have an extremely high sampling frequency of up to 2 GHz, but for this particular project, the sampling frequency was reduced to 200 kHz. This produces a Nyquist frequency of 100 kHz that is still well above the high frequency range of interest.

One major issue with the PDV data is that there is no knowledge of the vector coordinates of u, just its magnitude. This translates to the diagnostic not knowing if the moving reflector is moving towards or away from the PDV probe. There are some common rules-of-thumb as to how one can tell if the velocity should be positive or negative:

1. If it is a known oscillating system, each time the velocity crosses zero
2. If the slope of the velocity is constant as the velocity crosses zero

However, one can be fooled by scenarios such as if a shock reaches the free surface immediately when the velocity reaches zero. This data can be analyzed in coherence with the accelerometer data which shows general positive/negative directions to inform the more precisely PDV measured velocities.

It is important to note that the optics used to record the PDV data were mounted on the driver plate. This means that the velocity data that was collected represents the relative velocity

between the driver plate and the floor plate, unlike the LDV and SDIC data which represent absolute velocity. For example, Figure 35 shows the displacement calculated from the PDV data compared to the AM6 Tall, LDV, and Velodyne displacements. As can be seen, the PDV displacement begins to diverge from the AM6 Tall, LDV, and Velodyne displacements at around 4.5 ms. This is expected since the PDV data represents relative displacement and the other displacements are absolute. To avoid this issue, the all PDV data was truncated after 4 ms when compared to other sources of data.

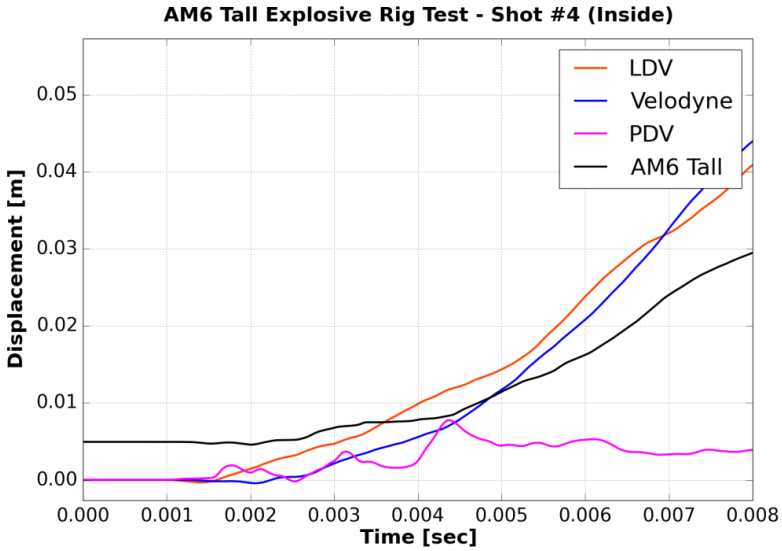

Figure 35 – Comparison of PDV, AM6 Tall, LDV, and Velodyne Displacements

4. Velodyne

Velodyne is a commercial multi-physics, multi-numerics finite element solver developed by Corvid Technologies that is capable of simulating high strain rate and detonation events. As previously mentioned, Velodyne was employed to design the explosively-driven test rig and provide predictive results. Velodyne has the ability to incorporate numerical accelerometers, which record the three-dimensional acceleration of a single point on the model and output data at a 1 MHz frequency. The simulations performed for this particular project contained numerical accelerometers at identical locations to the gauges welded on the rig (the on-support location at an inner radius and the between-supports location at an outer radius). Due to its predictive nature, Velodyne is not necessarily a source of truth data; however, the results produced by the simulations are extremely comparable. Therefore, the Velodyne results were included in the final results produced for the Explosive Rig tests. More information about the Velodyne simulation and the data produced by it can be found in the *Comparison with Pretest Prediction* section.

ii. Data Matrices

As outlined in the *Test Approach* section, there were a variety of accelerometers and gauges analyzed using four different tests (Smack Bar, Flyaway, Explosive Rig, and Shaker Table) with multiple test strengths; therefore, Table 6, Table 7, Table 8, and Table 9 were created to specify which accelerometers and gauges were tested under which conditions and the number of times the tests were repeated. For example, Table 6 lists all the sources of data that were recorded during the Smack Bar tests. This table shows that the 7270A was tested at 10 psi three times, 20 psi three times, and 30 psi three times. It also shows that LDV data was collected for every Smack Bar test that was recorded. However, Table 7 shows that during the Flyaway tests, every gauge was tested multiple times with an air gun pressure of 20 psi. But for the LOFFI tests, LDV data was not recorded since the LOFFI obstructed the LDV's view of the flyaway disk.

Table 8 is a similar list that displays the data collected for the Explosive Rig tests. For this particular project, there were a total of seven Explosive Rig tests, but there was an obvious error with the data collected from Shot #2, and as previously mentioned, Shot #7 was faulty; therefore, the data from Shot #2 and Shot #7 were removed from the analysis as outliers. Also, SDIC data was originally collected for Shots #2, #5, and #6, but the frame synchronization issue was only resolved for Shot #5. Furthermore, since the Velodyne data comes from the finite element method, which is deterministic rather than stochastic, repeating the simulation multiple times will not be beneficial as it will produce the exact same result every time; therefore, there is only one set of Velodyne data that contains both the on-support location and the between-supports location accelerations. Table 8 also lists the locations of the source of data.

Unfortunately, performance issues were encountered during both on-axis and off-axis Shaker Table testing. Phase III of the *Test Results* section describes these issues in more detail, but the list shown in Table 9 is still representative of the data gathered during this phase.

Table 6 – Data Matrix for Smack Bar Testing

Source	**Air Gun Pressure [psi]**							
	8	**10**	**12**	**20**	**30**	**50**	**60**	**70**
7270A	-	3	-	3	3	-	-	-
7280A	-	5	-	1	3	1	1	1
2262A	3	-	3	-	-	-	-	-
7270AM6	-	4	-	3	1	3	-	-
BOBKAT	-	3	-	-	3	3	-	1
LOFFI	-	3	-	-	3	3	-	3
LDV	3	18	3	10	10	10	1	5

Table 7 – Data Matrix for Flyaway Testing

Source	Air Gun Pressure [psi]
	20
7270A	3
7280A	3
2262A	3
7270AM6	3
7264D	2
BOBKAT	3
LOFFI	2
LDV	17

Table 8 – Data Matrix for Explosive Rig Testing

Source	Location	Shot Strength [lb. of C-4]	
		10	20
Endevco 7270AM6	On-Support	1	4
LOFFI	Between-Supports	1	4
BOBKAT	Between-Supports	1	4
Tiny BOB	Between-Supports	1	4
Mini BOB	Between-Supports	1	4
AM6 Tall	On-Support	1	4
Wheel Mount	Between-Supports	1	3
Wave Spring	Between-Supports	1	4
Base BOB	Between-Supports	1	4
Spring Mount	On-Support	1	4
Corvid Disk Mount	Between-Supports	-	2
LDV	Between-Supports	1	4
Velodyne	Both	-	1
SDIC	Both	-	1
PDV	Between-Supports	-	2

Table 9 – Data Matrix for Shaker Table Testing

Source	Direction	
	On-Axis	**Off-Axis**
Endevco 2262A (Plate Reference)	4	4
Endevco 7270AM6	4	4
LOFFI	4	4
BOBKAT	4	4
Tiny BOB	4	4
Mini BOB	4	4
Wheel Mount	4	4
Wave Spring	4	4
Base BOB	4	4
Corvid Disk Mount	4	4

b. Test Results

As previously stated, the overall goal of this project is to evaluate each gauge by characterizing their time domain and frequency domain performance properties under a variety of loading conditions. The time domain performance properties include their acceleration and velocity traces as well as their peak velocity, time-to-peak velocity, average end velocity, and average velocity slope. The frequency domain performance properties include a shock response spectrum (SRS) and shock response spectrum percent error when compared to truth data. To produce the SRS plots, a maximum spectrum SRS was performed with a damping ratio of 0.05 and 400 points ranging between 1 – 10,000 Hz. Since numerous gauges were analyzed using a variety of tests, the full set of the acceleration, velocity, SRS, and SRS percent error plots have been placed in the *Appendix*; however, the following section walks through an example of the test results that were produced for each phase of the project and explains how they can be interpreted.

i. Phase I

1. Smack Bar Tests

The first two plots that were produced from the data gathered during the Smack Bar Tests were the acceleration and velocity traces, as seen in Figure 36.

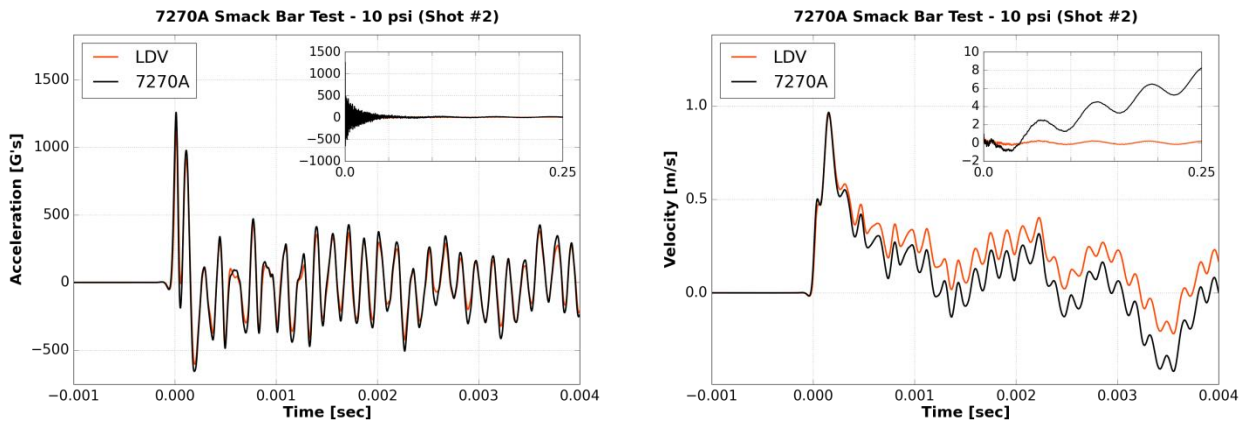

(a) **(b)**

Figure 36 – Example of Acceleration (a) and Velocity (b) Traces from Smack Bar Tests

These specific acceleration and velocity data traces come from the direct mounted Endevco 7270A accelerometer with an air gun pressure of 10 psi, but the responses of all accelerometers and gauges for all Smack Bar tests were plotted in a similar manner. To create these plots, a low-pass 4th order Butterworth filter with a cutoff frequency of 10,000 Hz was first applied to the acceleration, and then the filtered acceleration was integrated to get the velocity trace. Both graphs show the accelerometers response plotted on top of the LDV response over the first 4 ms post-trigger, with the full 0.25 second traces plotted in the top right corner. The main 4 ms traces allow for evaluation of the early-time response of the accelerometer with differences in peak velocity and time-to-peak velocity easily visible. The full 0.25 second plots help visualize how susceptible the accelerometer is to velocity drift from this particular input. For the direct mounted accelerometers, base strain induced zero-shift error is expected, but it is also probable that resonance induced zero-shift error is present in most Smack Bar test results. There is a significant amount of high frequency energy produced when the metal slug impacts the metal bar. This mechanical input is easily capable of exciting accelerometer resonance, but the DAQ was configured to capture content in the frequency range of 0 – 100 kHz, below the resonant frequencies of many of the accelerometers tested.

To help quantify susceptibility to drift, the average velocity and velocity slope over the last 100 ms were calculated for each Smack Bar test. The absolute values of these results were then averaged together for each accelerometer and gauge to produce the average end velocity and average slope values shown in Table 10.

Table 10 – Average End Velocity and Average Slope Values from Smack Bar Tests

Source	Average End Velocity [m/s]	Average Slope [m/s^2]
Endevco 7270A	11.03	42.73
Endevco 7280A	14.36	64.9
Endevco 2262A	0.07	0.84
Endevco 7270AM6	1.23	6.13
BOBKAT	5.8	34.45
LOFFI	0.03	0.35

Ideally, both the average end velocity and average slope should be as close to zero as possible. The average end velocity quantifies the late-time offset error, and the average slope quantifies the average zero-shift error; however, combined, the two values quantify the total error associated with the late-time response of each accelerometer and gauge. This value was only calculated over the last 100 ms in order to exclude the data created during the event.

The next set of results that were created for the Smack Bar tests, were the peak velocity and time-to-peak velocity values. These calculations were performed using an algorithm that analyzes the filtered velocity trace and determines the peak velocity and time-to-peak velocity after the impact event occurs.[7] Figure 37 displays this data in histogram style graphs.

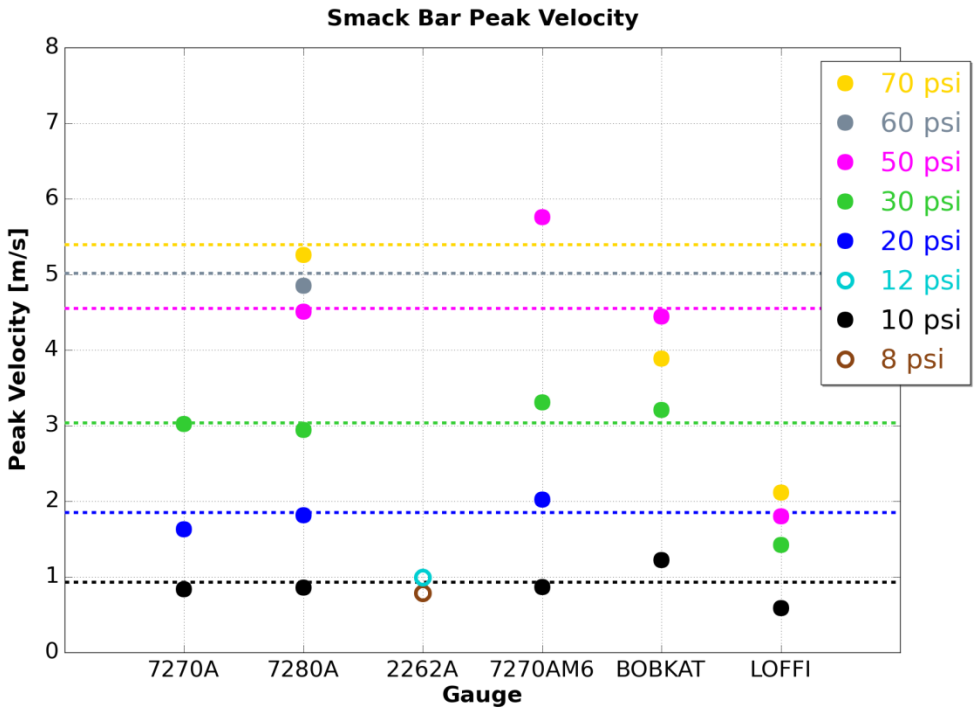

(a)

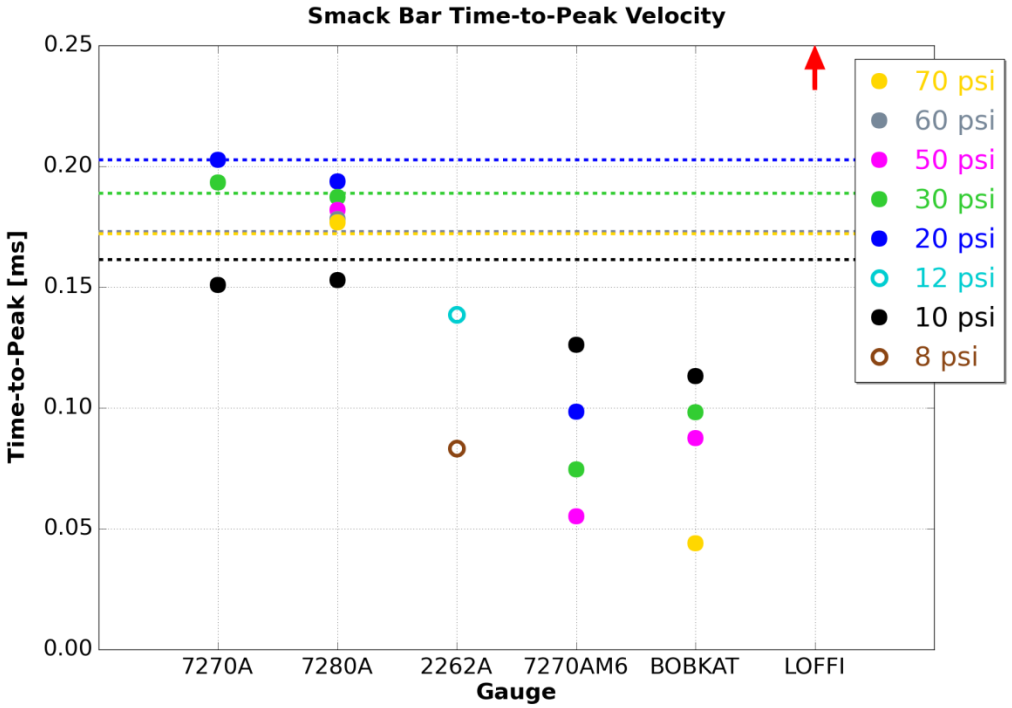

(b)

Figure 37 – Average Peak Velocity (a) and Average Time-to-Peak Velocity (b) Data from all Smack Bar Tests

Figure 37 displays the average peak velocity and average time-to-peak velocity values for all Smack Bar tests. Each accelerometer and gauge that was analyzed is listed on the abscissa, and each air gun pressure has its own color. Since each shot was repeated multiple times, the average response of that particular accelerometer or gauge is shown. For example, the Endevco 7270A was tested at 10 psi three different times, and the average peak velocity for all three of these shots is about 1 m/s, as shown in Figure 37 (a). The dotted lines on the plots represent the average response of the LDV over all shots at that specific pressure value. Since the LDV is an accurate source of truth data for the Smack Bar tests, an accurate accelerometer or gauge will have responses close to the dotted line that represents the corresponding shot strength. It should be noted that mass considerations were not taken into account when comparing the population average for peak velocity and time-to-peak velocity values. The variance in mass between accelerometers likely resulted in different peak velocities in some scenarios.

It should also be noted that while all results were filtered with a 10 kHz low-pass filter, not all of the accelerometers and gauges tested were capable of responding at that frequency. For instance, the LOFFI has a very slow time-to-peak as the mechanical response of the filter assembly is less than 100 Hz and is being compared to LDV data that has an upper frequency content limit of 500 kHz. Ultimately, these calculations are one of many values that could be used to quantify early-time response accuracy; however, these are the preferred calculations

since they provide an objective approach to characterizing each accelerometer and gauge. The red arrow in Figure 37 (b) indicates that the LOFFI average time-to-peak velocity values are well outside of the range of the plot. While all other accelerometers and gauges had time-to-peak velocity values below 0.25 ms, the LOFFI's average time-to-peak values for 10, 30, 50, and 70 psi were all above 1 ms; therefore, the red arrow was used to indicate the relative inaccuracy of the LOFFI's early-time response while still maintaining a reasonable ordinate range. Also, the hollow circles used for the 8 psi and 12 psi markers indicate that there is no corresponding LDV average peak velocity and average time-to-peak velocity values for those pressures. This is due to the laser dropout that occurred during those specific shots. If the laser dropout is severe enough, the algorithm that calculates peak velocity and time-to-peak velocity values returns zero values for both calculations. Since these pressure levels were only used to test the Endevco 2262A, there are no supporting tests that provide corresponding LDV peak velocity and time-to-peak velocity values. Also, it is important to note that the dotted line that represents the average LDV time-to-peak velocity for 50 psi tests is present, it is just not visible as it is located directly behind the 60 psi and 70 psi LDV lines.

The last set of results that were produced from the Smack Bar test data were the SRS and the corresponding SRS percent error when compared to the LDV truth data. An example of these plots can be seen in Figure 38.

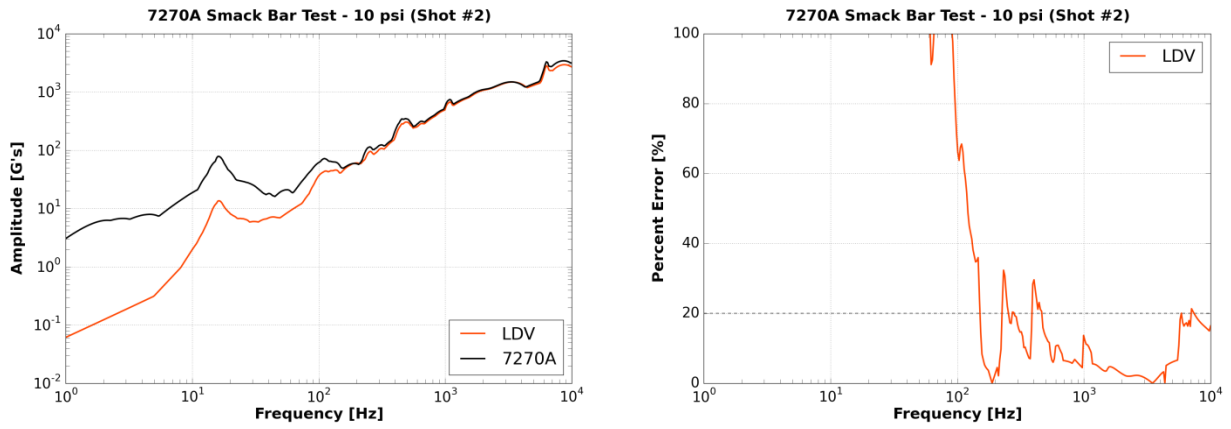

(a) **(b)**

Figure 38 – Example of SRS (a) and SRS Percent Error (b) Plots from Smack Bar Tests

Once again, the SRS and SRS percent error results in Figure 38 come from the directly mounted Endevco 7270A accelerometer with an air gun pressure of 10 psi, but the frequency domain response for all accelerometers and gauges from all Smack Bar tests are plotted in a similar manner. Figure 38 (a) shows the frequency domain comparison between the accelerometer and the LDV ranging from 1 – 10,000 Hz. This data was obtained by performing an SRS analysis on the 10,000 Hz filtered acceleration data shown in Figure 36 (a).

Then, these SRS traces were numerically compared by finding the percent error between them with respect to the LDV data as the truth data, as shown in Figure 38 (b). As previously mentioned, the assumption that the LDV is considered truth data is relatively accurate since the

Smack Bar Tests were conducted in a laboratory environment and peak test velocities were well within the operating limits of the LDV. The SRS percent error plot also features an error bar at 20%. This value is the quantitative threshold used to distinguish between accurate and inaccurate responses. These particular plots featured in Figure 38 show that the Endevco 7270A did not accurately capture content below 150 Hz for the Smack Bar test. This is often a sign that the accelerometer is susceptible to zero-shift error, which is also supported by the high average end velocity and average slope values listed in Table 10. It is important to note that the same information can be inferred from both plots, but the ordinate of the SRS plot is logarithmic. This means that large differences between two traces may not be easily visible at higher amplitudes; therefore, the SRS percent error plot is used to quantify these differences since it has a linear ordinate.

While Figure 37 displays the full set of average peak velocity and average time-to-peak velocity value and Table 10 displays the full set of average end velocity and average slope values from the Smack Bar tests, Figure 36 and Figure 38 represent just a single example of a particular pressure level for a particular accelerometer. As previously mentioned, the full set of these plots can be seen in *Appendix A*.

2. Flyaway Tests

Once again, the first two plots that were produced from the data gathered during the Flyaway tests are the acceleration and velocity traces, as shown in Figure 39.

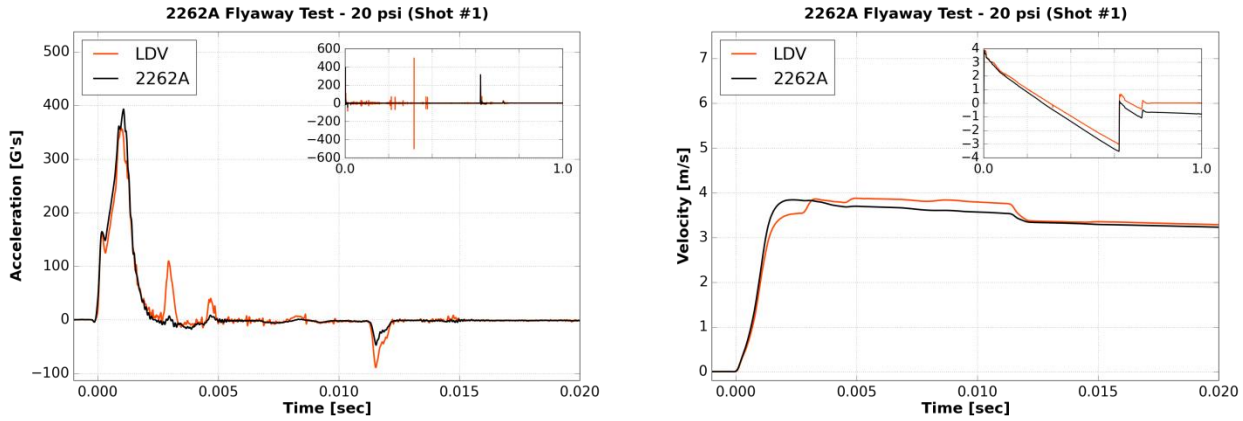

(a) **(b)**

Figure 39 – Example of Acceleration (a) and Velocity (b) Traces from Flyaway Tests

These specific acceleration and velocity traces were produced by the direct mounted Endevco 2262A accelerometer with an air gun pressure of 20 psi. However, the responses of all accelerometers and gauges during all Flyaway tests were plotted in a similar manner. Similarly to the Smack Bar tests, a low-pass 4th order Butterworth filter with a cutoff frequency of 10,000 Hz was first applied to the acceleration data to produce the traces shown in (a). Then this data was integrated to produce the velocity traces in (b). Both graphs show the accelerometer's

response plotted on top of the LDV response over the first 20 ms post-trigger, with the full 1 second traces plotted in the top right corner. Once again, the main 20 ms trace allows for evaluation of the early-time response of the accelerometer and visualization of the peak velocity and time-to-peak velocity. The full 1 second plots shown in the top right corner display the late-time response of the accelerometer during and after the low frequency, ballistic trajectory event. It is in these corner plots where zero-shift error and the resulting velocity drift will be visible. However, the nature of the Flyaway test implies that both the resonance and base strain induced zero-shift errors should be relatively small when compared to the Smack Bar test results.

In an attempt to quantify these reduced zero-shift errors, the second set of results that were calculated using the Flyaway data are the average end velocity and average slope values, as shown in Table 11.

Table 11 – Average End Velocity and Average Slope Values from Flyaway Tests

Source	Average End Velocity [m/s]	Average Slope [m/s^2]
Endevco 7270A	1.38	1.56
Endevco 7280A	42.96	41.87
Endevco 2262A	0.81	0.62
Endevco 7270AM6	24.18	25.49
Endevco 7264D	1.5	1.48
BOBKAT	0.92	0.7
LOFFI	0.27	0.2

Once again, using the data over the last 100 ms, the average velocity and velocity slope of each Flyaway test was calculated. Then, their absolute values were averaged together to produce the average end velocity and average slope for each accelerometer and gauge tested. By only using the last 100 ms of the velocity trace, the calculations are void of the event data and only indicate the late-time performance of each gauge. Similarly to the Smack Bar tests, an ideal accelerometer or gauge would have an average end velocity and average slope of zero as it returns to its initial resting position. It is important to note that these values must be interpreted collectively to provide a complete quantification of the late-time error of the accelerometer or gauge.

Also using the velocity traces, the next set of results that were produced for the Flyaway tests were the peak velocity and time-to-peak velocity values. These calculations were performed using the same algorithm used for the Smack Bar tests. The average results from all of these calculations can be seen in Figure 40.

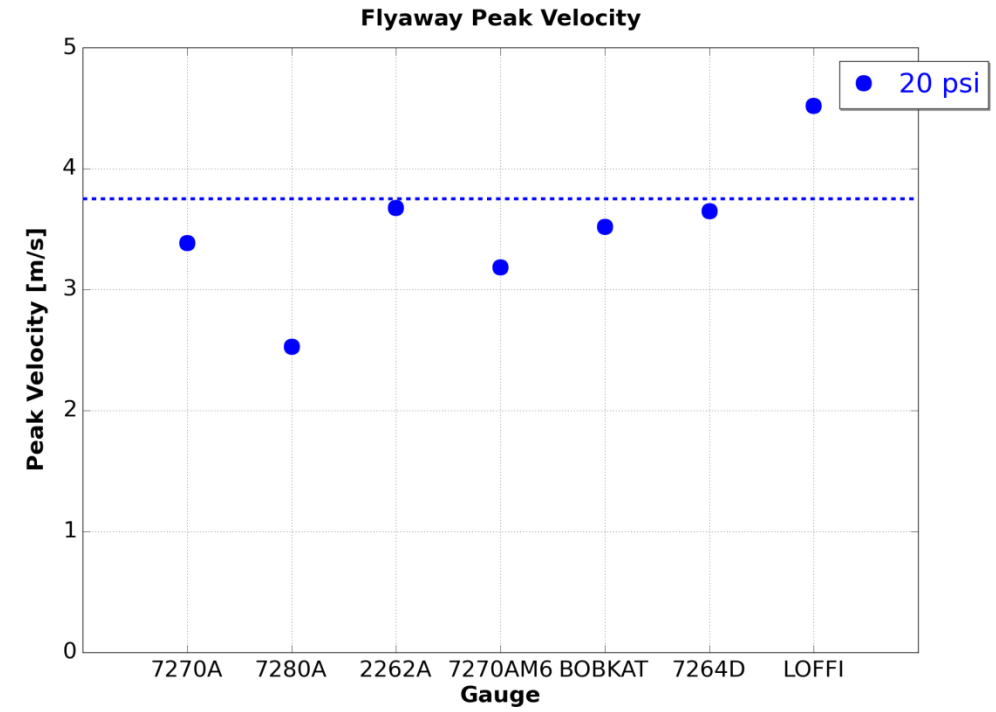

(a)

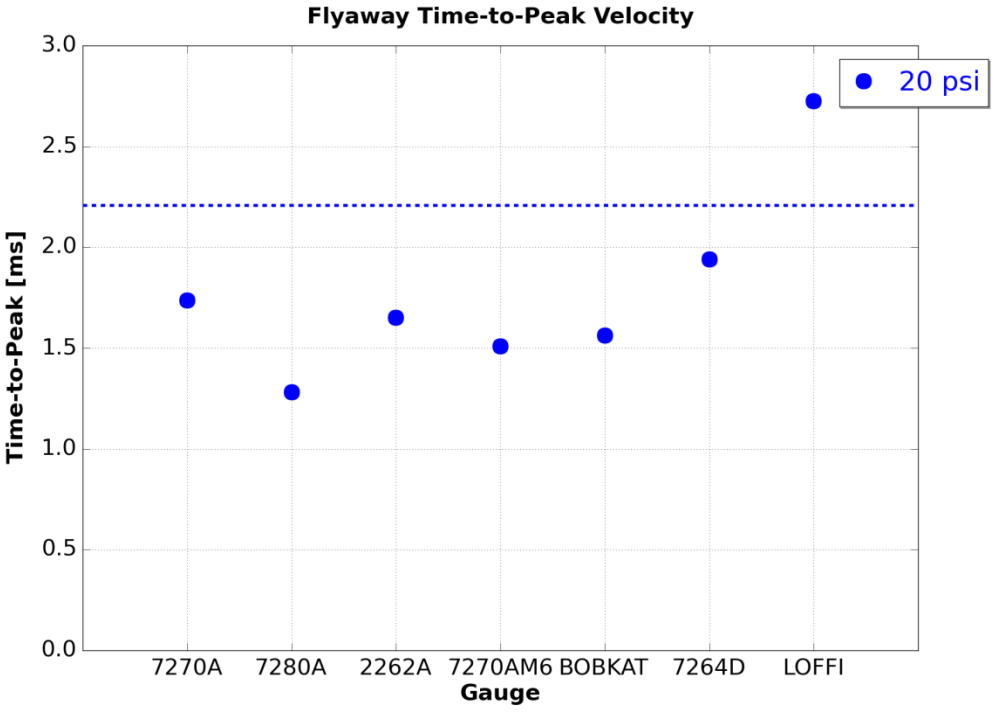

(b)

Figure 40 – Average Peak Velocity (a) and Average Time-to-Peak Velocity (b) Data from all Flyaway Tests

Figure 40 displays the average peak velocity and average time-to-peak velocity for all Flyaway tests. Similarly to the peak velocity and time-to-peak velocity plots shown for the Smack Bar tests, each accelerometer and gauge that was analyzed is on the abscissa, but the only air gun pressure that was tested for the Flyaway tests was 20 psi. Once again, the dotted lines shown on the plots represent the average response of the LDV over all the shots. The closer an average value is to the dotted line, the more accurately it was able to capture the early-time content of the Flyaway test since the LDV is considered an accurate source of truth data for this particular test. It should be noted that mass considerations were not taken into account when determining the population average for peak velocity and time-to-peak velocity values. Though the mass of the flyaway disk remained constant test-to-test, the variance in mass between accelerometers and gauges likely resulted in different LDV peak velocities in some scenarios. It should also be noted that while all results were filtered with a 10 kHz low-pass filter, not all of the accelerometers and gauge assemblies tested were capable of responding at that frequency. In this instance, the peak velocity and time-to-peak velocity values of the BOBKAT are closer to the population average as the Flyaway test produced a slower rise time input, closer to the mechanical response of the BOBKAT. Whereas in Figure 37 (b), the rise time of the input was much faster than the response rate of the BOBKAT causing the time-to-peak velocity values to be lower than direct mounted gauges. This indicates that the peak velocity and time-to-peak velocity values are simply indicators of early-time response accuracy, and the results are not completely rigid.

Once again, the last set of results that were produced from the data obtained during the Flyaway tests were the SRS and the corresponding SRS percent error plots. These can be seen in Figure 41.

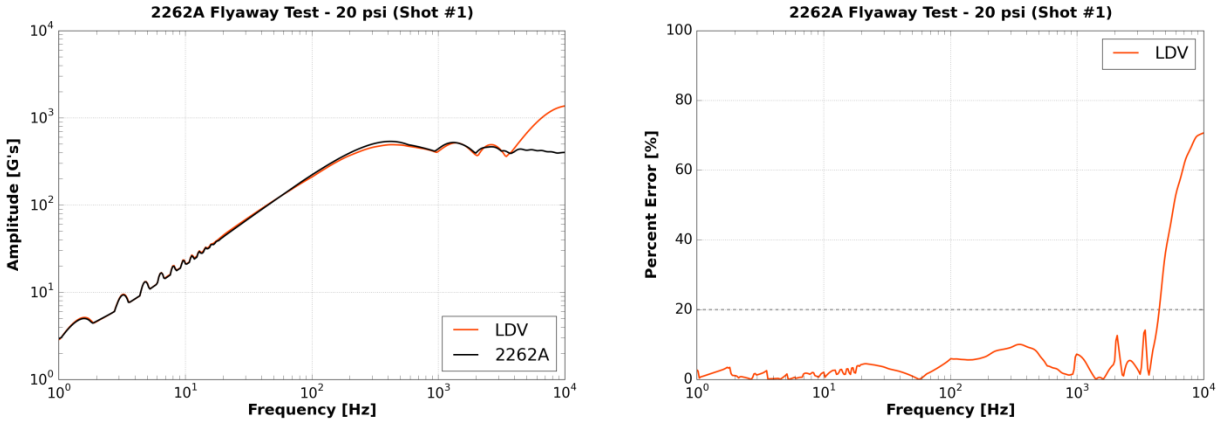

(a) **(b)**

Figure 41 – Example of SRS (a) and SRS Percent Error (b) Plots from Flyaway Tests

The SRS and SRS percent error plots shown in Figure 41 also come from the direct mounted Endevco 2262A accelerometer with an air gun pressure of 20 psi, but the frequency domain response of all accelerometers and gauges for all Flyaway tests were plotted in a similar manner. The SRS plot compares the frequency domain response of the gauge to the LDV from 1

– 10,000 Hz, and was created by performing an SRS analysis on the 10,000 Hz filtered acceleration data. These SRS traces were then numerically compared by finding the percent error between the two to create the percent error plot shown in Figure 41 (b). Similarly to the Smack Bar tests, the LDV is considered a reliable source of truth data for the Flyaway tests since it occurs in a laboratory environment. Although instances of dropout were present, see corner plot of Figure 39 (a), the rise and peak velocities were accurately captured. Once again, the SRS percent error plot also features a 20% error bar that illustrates the difference between accurate and inaccurate responses. These particular plots show that the Endevco 2262A accurately captured all but the extremely high frequency content (> 4,000 Hz) present in the Flyaway test.

Similarly to the Smack Bar results, Figure 40 displays the complete set of average peak velocity and average time-to-peak velocity values, and Table 11 displays the complete set of average end velocity and average slope values from the Flyaway tests, but Figure 39 and Figure 41 only display the response of a single accelerometer during a single shot. The full set of these time domain and frequency domain responses for all Flyaway tests can be found in *Appendix B.*

ii. Phase II

Phase II of this project consisted solely of the Explosive Rig tests; however, the data processing for this phase was similar to the processing performed in Phase I. The first results that were produced were the acceleration and velocity traces. An example of these traces can be seen in Figure 42.

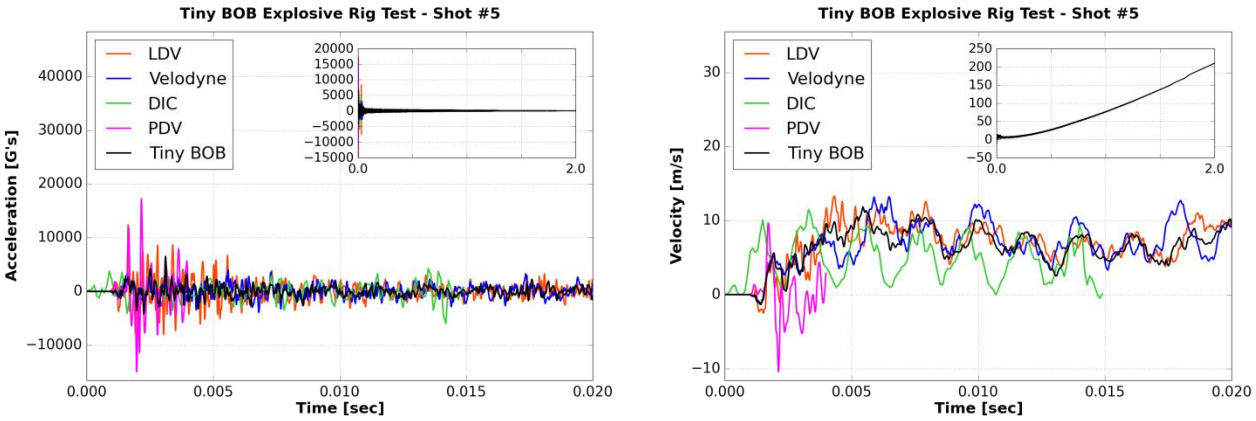

(a) **(b)**

Figure 42 – Example of Acceleration (a) and Velocity (b) Traces from Explosive Rig Tests

The plots shown in Figure 42 come from the Tiny Bob during Shot #5, but the acceleration and velocity traces from all gauges for all Explosive Rig tests are presented in the *Appendix* similarly. Unlike the Smack Bar tests or Flyaway tests, the Explosive Rig tests have four possible sources of truth data, as seen in Figure 42. As shown in the full data matrix in Table 8, all shots had LDV data, four had relevant Velodyne data, two had PDV data, and one had DIC data. It is important to note that the LDV data is only directly comparable to gauges

that were mounted at the between-supports locations since this is where the laser was aimed at; however, it was still compared to the on-support gauges since experimental truth data for this particular test was relatively limited. This discrepancy has been noted in the result plots of all on-support gauges for consideration during evaluation of the results. For all acceleration traces shown in (a) except for the DIC data, a low-pass 4th order Butterworth filter with a cutoff frequency of 10,000 Hz was applied. This is due to the DIC data being recorded at a frequency of 10,000 Hz; therefore, no content above 5,000 Hz was recorded. Then, these filtered acceleration traces were integrated to produce the velocity traces shown in (b). Both graphs show the gauge's response compared to the different types of truth data over the first 20 ms. For acceleration and velocity plots from Shot #1, the corner plots span 1.5 seconds since only 10 lbs of C-4 was used, but the corner plots from all other shots span 2 seconds. However, it may be difficult to see the LDV, Velodyne, DIC, and PDV data in the corner plots since they were plotted behind the gauge data and end at 75 ms, 40 ms, 15 ms, and 4 ms, respectively. Similarly to the previously presented acceleration and velocity plots, the initial 20 ms allows for the visualization of the early-time response of the gauge, and the full corner plots display the late-time response. Since the purpose of the Explosive Rig tests was to stress the gauges and determine how effective their mechanical filters are, it is a definite possibility that both resonance and base strain induced zero-shift errors are present in the collected gauge data.

The next set of performance parameters that were calculated to characterize the late-time response of the gauges during the Explosive Rig tests are the average end velocity and average slope values, as shown in Table 12.

Table 12 – Average End Velocity and Average Slope Values from Explosive Rig Tests

Source	Average End Velocity [m/s]	Average Slope [m/s^2]
Endevco 7270AM6	293.07	66.93
Wave Spring	8.69	3.18
Base BOB	12.51	6.51
Wheel Mount	129.34	66.21
AM6 Tall	150.26	83.64
BOBKAT	71.32	24.08
Mini BOB	78.12	43.16
LOFFI	3.99	7.49
Spring Mount	409.65	19.79
Tiny BOB	153.28	133.77
Corvid Disk Mount	186.68	75.43

To obtain these values, the average velocity and velocity slope over the last 100 ms were calculated. Then the absolute value of these calculations were averaged together to produce the

average end velocity and average slope values for each gauge. For the Explosive Rig tests, the last 100 ms is void of the data produced by the initial loading and projectile motion, including slam down, and instead contains data that solely indicate the gauge's late-time performance. It is important to note that the average end velocity and average slope calculations for the Wheel Mount exclude the data from Shot #5 since it is apparent that this test damaged the gauge and produced erroneous results; however, the plots from this shot are still included in the *Appendix* as proof. Once again, an ideal gauge will have an average end velocity and average slope value of zero as the test rig returns to a resting state in the small crater produced by the buried charge. However, it is important to consider both of these values when deciding on late-time response accuracy since only using one of the two values could provide a false representation of performance.

Similarly to the Smack Bar and Flyaway tests, the velocity plots were then used to calculate the peak velocity and time-to-peak velocity values for each gauge at each shot strength. The average of these calculated results can be found in Figure 43.

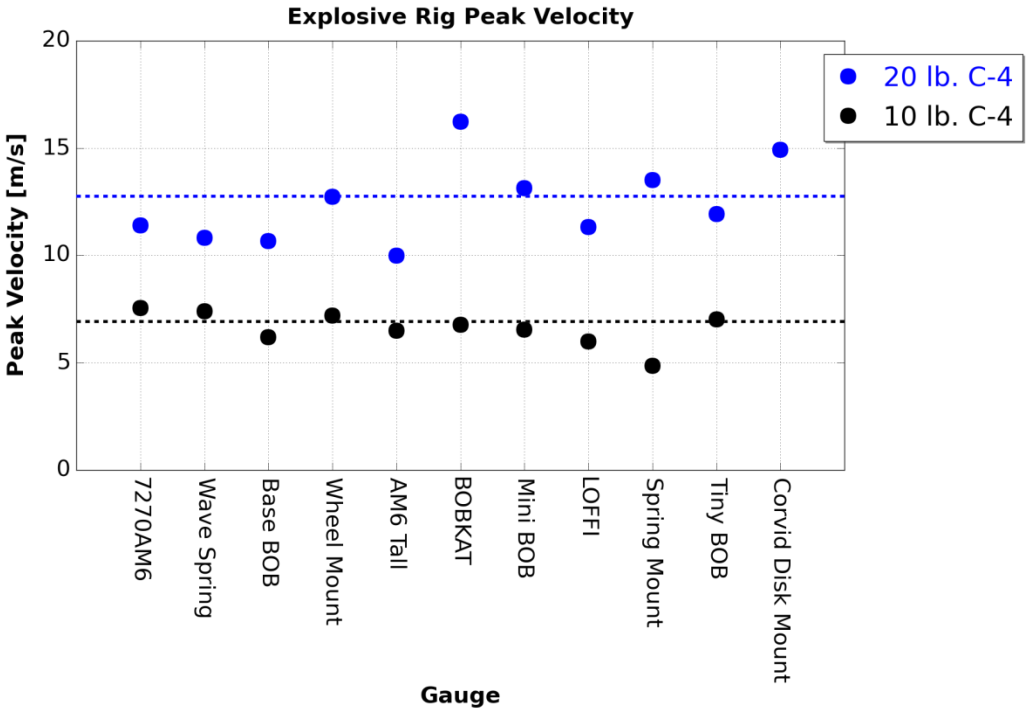

(a)

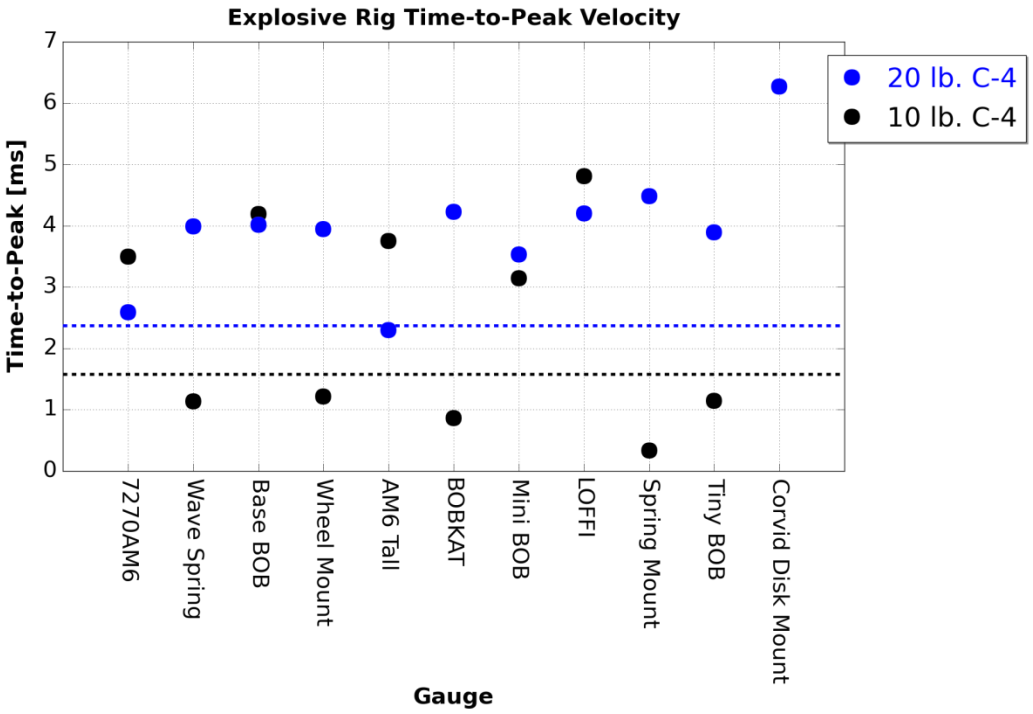

(b)

Figure 43 – Average Peak Velocity (a) and Average Time-to-Peak Velocity (b) from all Explosive Rig Tests

Figure 43 displays the average peak velocity and time-to-peak velocity values for all Explosive Rig tests. Similarly to the previous peak velocity and time-to-peak velocity graphs, each gauge that was analyzed is on the abscissa, and each charge size has its own color. Since the 20 lb. of C-4 shot was repeated multiple times, the average response of that particular gauge is shown. Once again, the dotted lines on the plots represent the average response of the LDV over all shots at that specific charge size. LDV was the only source of truth data included in the peak velocity and time-to-peak velocity plots since it was the only reliable source of experimental and non-predictive truth data. It is important to remember that the LDV was limited by the velocity tracking filter shown in Figure 34 and may not accurately represent the response of the test rig to 10,000 Hz. The tracking filter was necessary to eliminate significant amounts of dropout due to dust and debris interfering with light reflection back to the sensor head. The tracking filter is limited to 20,000 G's of acceleration and can reduce peak velocities at higher frequencies. Similarly, mechanical filters on some of the gauges may limit them from capturing content over the full frequency range of interest. Ultimately, this could produce inaccurate results when compared to the LDV data that was only limited by the tracking filter. Therefore, the results produced by the peak velocity and time-to-peak velocity plots must be considered indicators of early-time performance and not definitive results.

Similarly to the Smack Bar and Flyaway tests, the last set of results that were produced from the Explosive Rig tests were the SRS and the SRS percent error plots, examples of which can be seen in Figure 44.

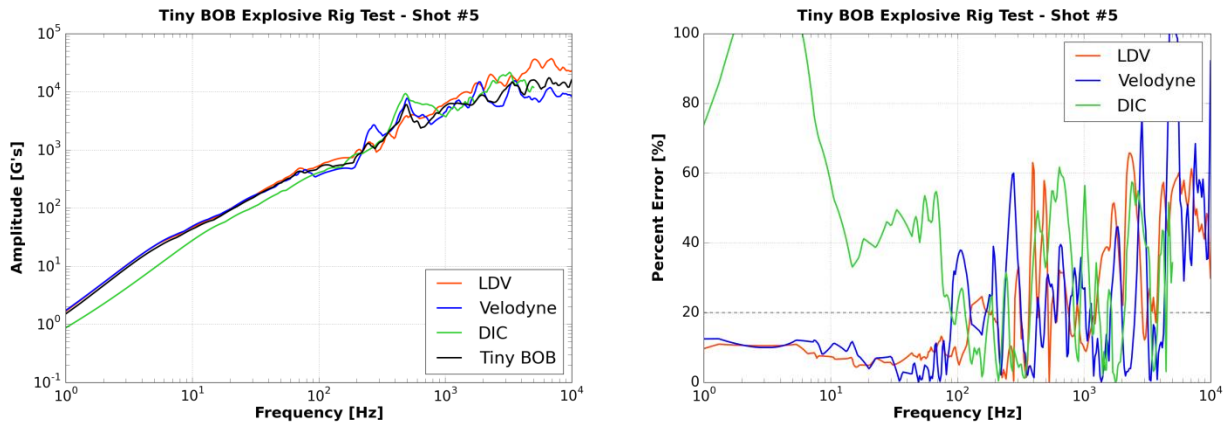

(a) **(b)**

Figure 44 – Example of SRS (a) and SRS Percent Error (b) Plots from Explosive Rig Tests

The SRS and SRS percent error plots shown in Figure 44 also come from the Tiny BOB during Shot #5, but these plots are indicative of the frequency domain response plots produced for all gauges during all Explosive Rig tests. Similarly to the previous SRS plots, the plot shown in (a) compares the frequency domain response of the gauge to the results produced by various types of truth data from 1 – 10,000 Hz. However, the DIC data was collected at a frequency of 10,000 Hz; therefore, its SRS plot can only reach its Nyquist frequency of 5,000 Hz. These SRS traces were created by performing an SRS analysis on the 10,000 Hz filtered acceleration data shown in Figure 42 (a). They were then numerically compared by calculating the percent error between the gauge trace and each truth data trace, as shown in (b). This plot also has a 20% error bar that helps distinguish the difference between accurate and inaccurate responses and allows for a comparison among all the different types of truth data gathered for this particular shot. It is important to note that the PDV data was not included in the frequency domain analysis due to its short duration and limited number of data points.

As was the case previously, Figure 43 shows the complete set of average peak velocity and average time-to-peak values, and Table 12 shows the average end velocity and average slope for all gauges during the Explosive Rig tests. However, Figure 42 and Figure 44 only display the behavior of a single gauge during a single shot. The full set of acceleration, velocity, SRS, and SRS percent error plots can be found in *Appendix C*.

iii. Phase III

As indicated in the *Test Approach* section, Phase III was to consist of on-axis and off-axis Shaker Table testing at constant power with frequencies simultaneously ranging from 10 – 2,000 Hz. To ensure commonality and minimize total test schedule and cost, all gauges were tested

simultaneously. During the first iteration of shaker testing, all the gauges of interest were mounted to a 12" square, ½" thick aluminum plate. This plate was then secured to the shaker table via four ½" diameter bolts located at the corners. With this configuration, the output from the reference accelerometer and the gauges of interest were recorded while performing an on-axis and off-axis vibration analysis. After reviewing the results, it was apparent that the power produced was not constant over the 10 – 2,000 Hz range as expected. As shown in Figure 45, the amplitude of the response measured by the reference accelerometer had significant power above the input value around 750 Hz and 1,370 Hz.

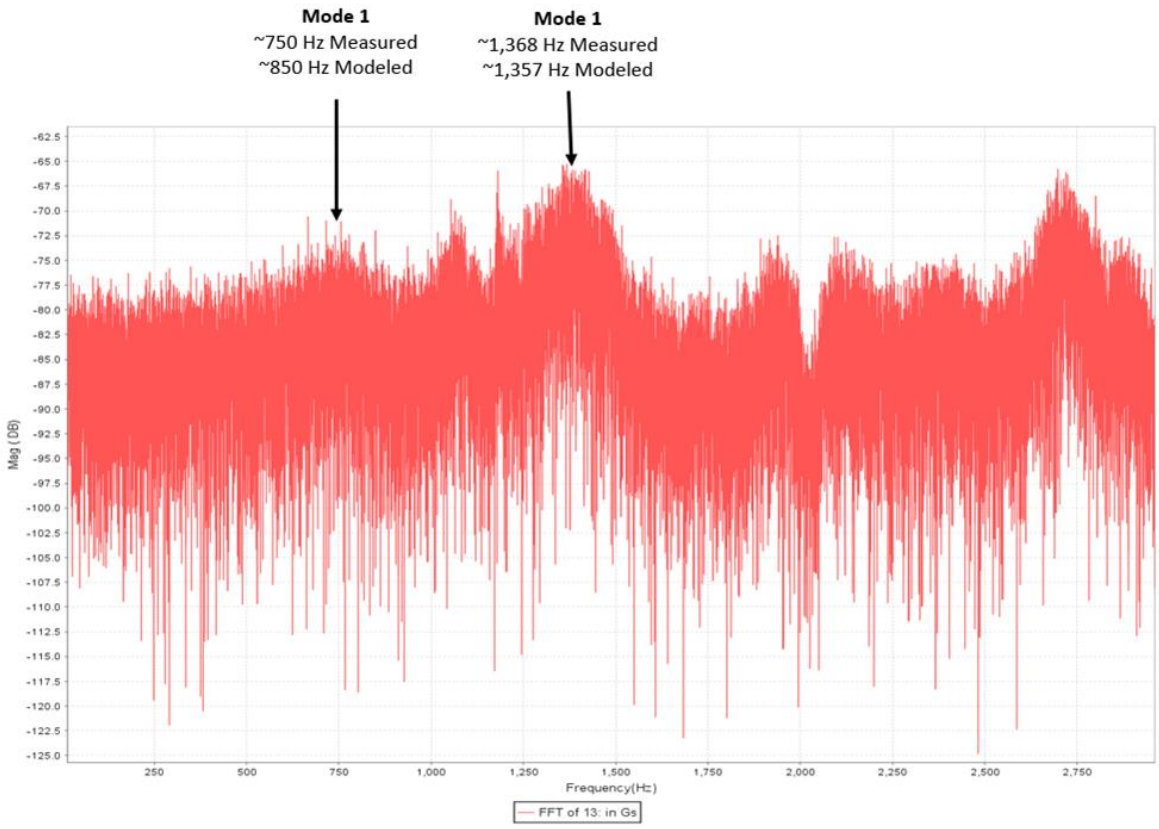

Figure 45 – Power Spectrum of Vertical Shaker Run #1

It was suspected that the increased amplitude at these frequencies was attributed to resonance of the square plate to which all gauges were mounted. To test this theory, a SolidWorks frequency simulation was conducted to determine the approximate natural frequencies of the square mounting plate. As shown in Figure 46, the first and third fundamental frequencies of this plate were estimated at 850 and 1,357 Hz, respectively, confirming the source of the content shown in Figure 45.

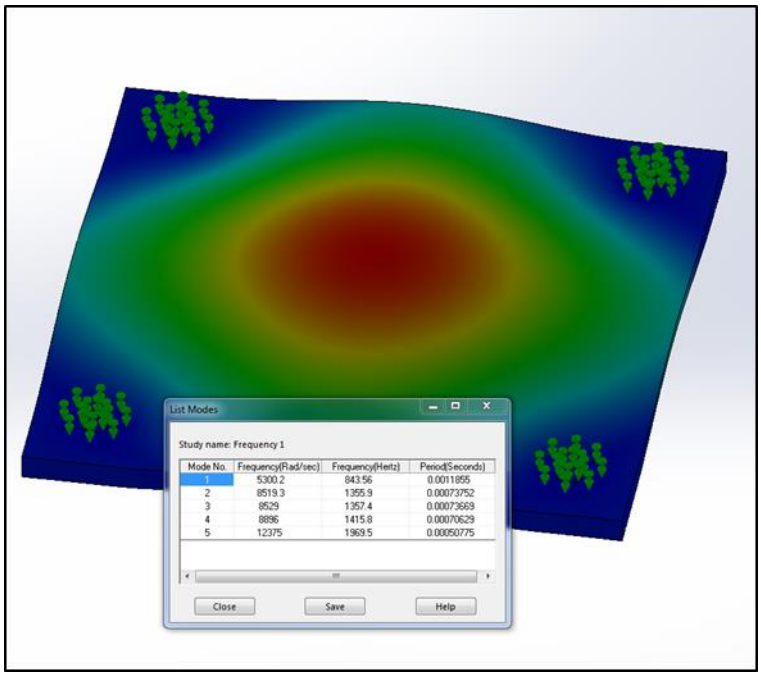

Figure 46 – Natural Frequencies of Mounting Plate #1

As a result, gauges were then mounted to a substantially thicker plate as shown in Figure 33. The second mounting plate measured 28.5" in diameter with a 2" thickness and was secured to the shaker table with 24 ½" diameter bolts. Before shaker testing was conducted, the plate was modeled to determine its fundamental frequencies under the mounting conditions. As shown in Figure 47, the lowest fundamental frequency was estimated to be 2,179 Hz, above the 2,000 Hz upper limit of the table.

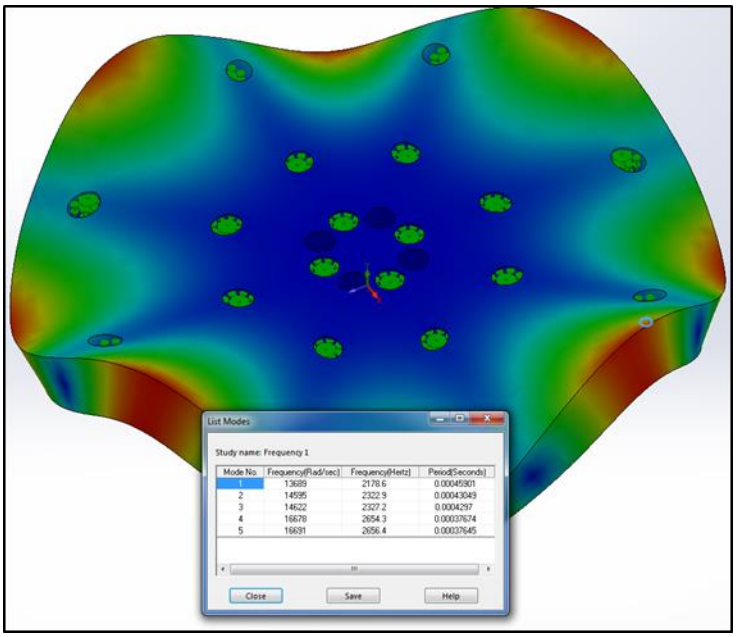

Figure 47 – Natural Frequencies of Mounting Plate #2

After the second on-axis vibration analysis was completed, the results were analyzed to determine whether the reference accelerometer located on the mounting plate showed constant power from 10 – 2,000 Hz. As can be seen in Figure 48, once again the power spectrum was not constant across the frequency band of interest. It is suspected that a separate accelerometer, used in the shaker table control system as feedback to vary input, may have been malfunctioning and causing the table to produce a non-flat spectrum. Ultimately, due to time and budgetary restrictions, further Shaker Table tests were not possible and the results gathered were not analyzed as they did not provide useful information above 400 Hz.

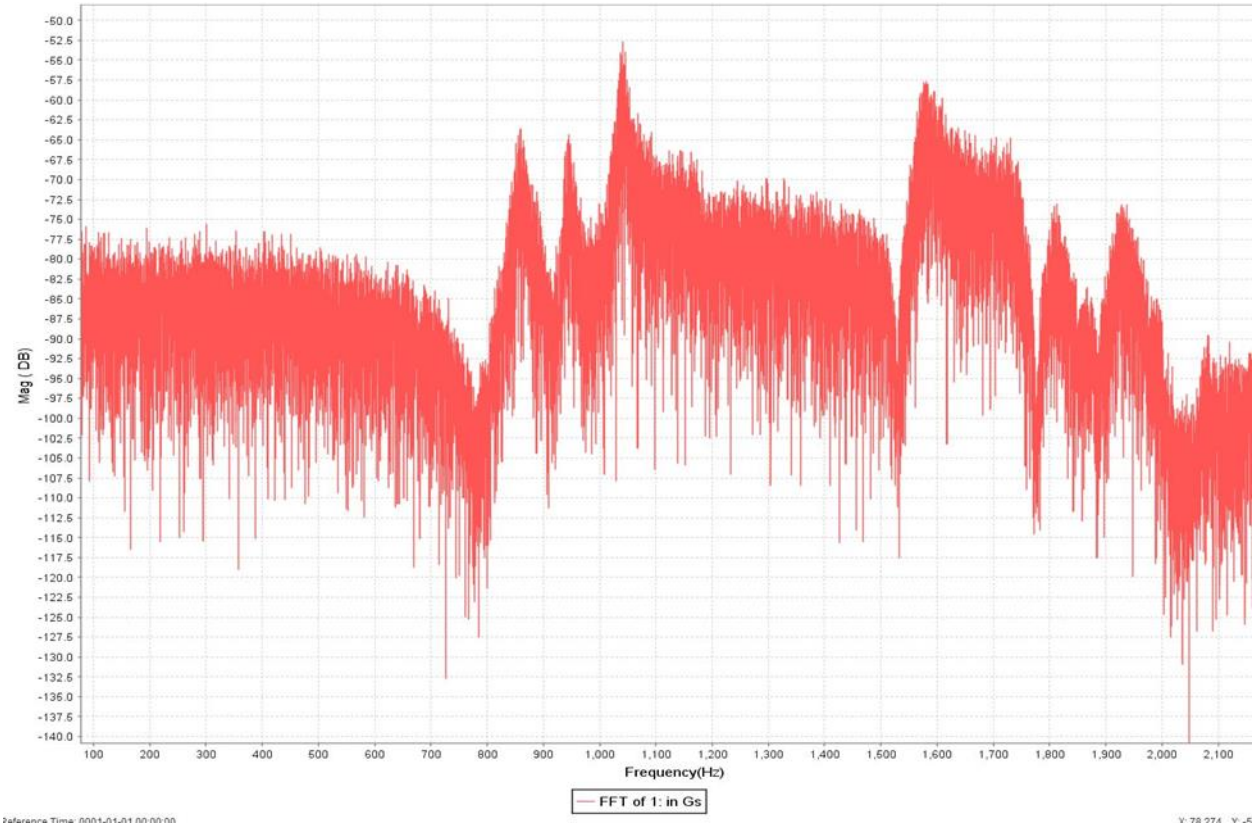

Figure 48 – Power Spectrum of Vertical Shaker Run #2

c. Comparison with Pretest Prediction

As mentioned earlier, pre-test predictions and explosively-driven test rig design and development analysis were performed in Velodyne™. Velodyne is a commercially available multi-physics software package for computational solid, fluid, and structural mechanics. Each of the solvers is based in first principles physics which, when combined, make up Corvid's High-Fidelity Computational Physics (HFCP) approach to solving complex, high-rate, large-strain scenarios. Velodyne's features include a:

- robust, energy conserving, automatic contact solver
- Smooth Particle Hydrodynamics (SPH) solver to recapture eroded element mass and

momentum in a coupled continuum approach

- coupled adaptive mesh refinement (AMR) based Eulerian fluid dynamics solver for fluid-structure interaction simulation
- heat transfer solver for thermo-mechanical interaction.

This package of solvers is built into a highly scalable framework allowing for efficient parallel processing hundreds to thousands of processors in a distributed memory environment. These features enable Velodyne (within a single software package) to run full-scale, end-to-end modeling for blast and impact conditions at mesh and time step fidelities required to capture the necessary physics involved in ground vehicle underbody blast survivability events.

For this particular project, Velodyne was used to design the explosively-driven test rig. A comparison of the final mesh model and the actual rig prior to detonation can be seen in Figure 49.

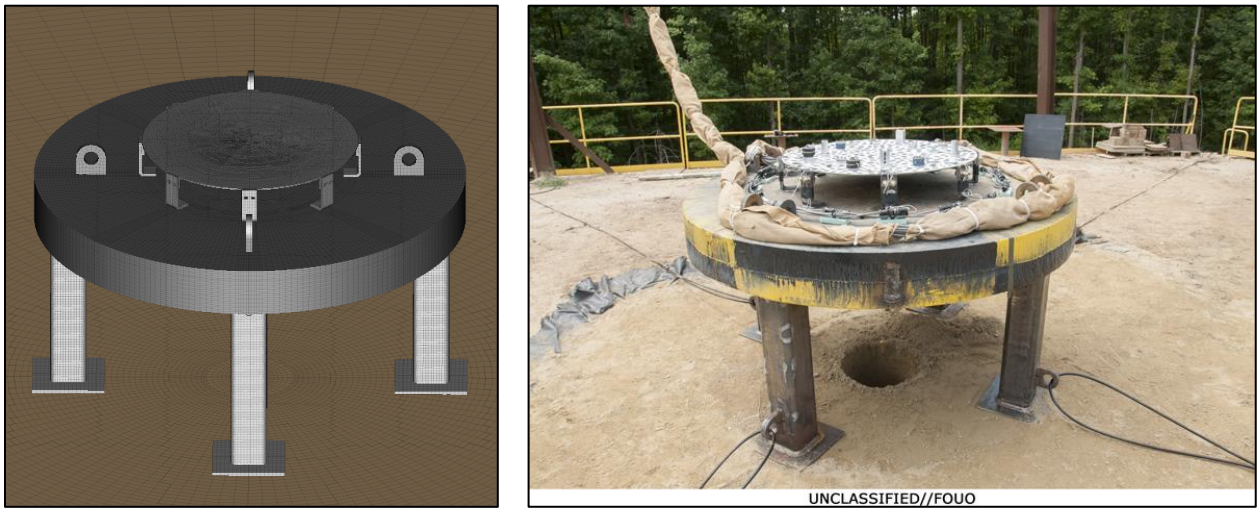

(a) **(b)**

Figure 49 – Comparison of Velodyne Final Mesh Model (a) and Actual Rig (b)

Iterative simulations were performed by adjusting charge type, charge size, amount of soil overburden, rig materials, and rig geometry until the numerically measured acceleration amplitudes and dominant frequencies approximated those typically measured in LFT&E of tactical vehicle floors. The benefit of using Velodyne over other commercially available finite element solvers is its ability to accurately predict blast loading as established through successful pre-test predictions for full vehicle system DT and LFT&E events. For this particular project, Velodyne has the ability to model the detonation of the buried C-4 charge and transfer that energy to the test rig through the resulting shock wave and soil loading. Figure 50 compares the soil loading of the Velodyne model and the soil loading captured by the high speed camera during a shot with 20 lb. of C-4.

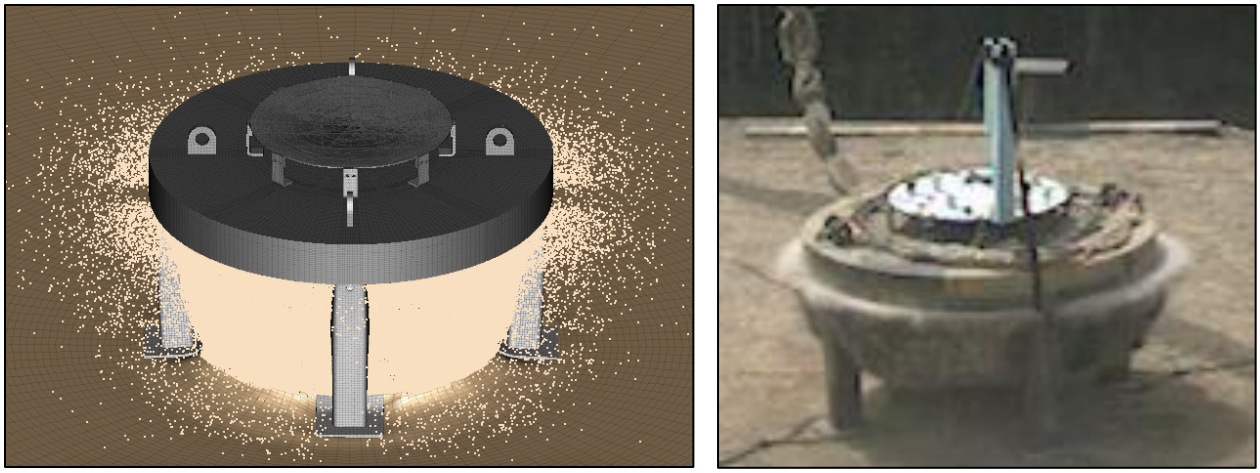

(a) **(b)**

Figure 50 – Comparison of Velodyne Model Soil Loading (a) and Actual Soil Loading (b)

To collect data from the Velodyne simulations, numerical accelerometers were added to the meshed model in various locations. These numerical accelerometers use the results from the HFCP simulation to output the three-dimensional acceleration experienced at specified points on the rig. A layout of the numerical accelerometers used in the simulations can be seen in Figure 51.

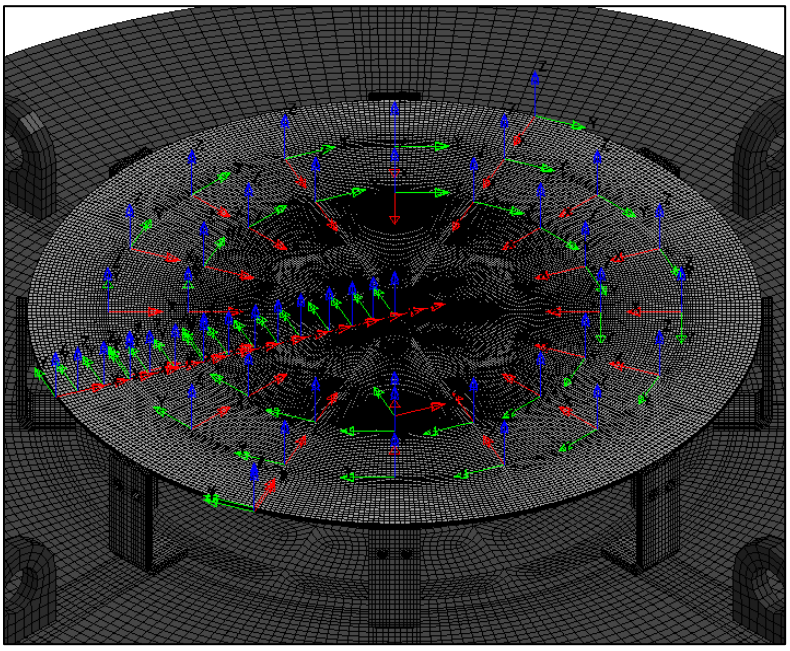

Figure 51 – Numerical Accelerometers Used in Velodyne Simulations

By arranging multiple numerical accelerometers throughout the floor plate, the optimal position for the gauges under test could be determined. Based on the simulation results, it was determined that there were two positions on the floor plate that produce acceleration amplitudes and frequencies similar to those experienced during LFT&E of tactical wheeled vehicle floors.

An illustration of this comparison is shown in Figure 52, where the 6’ design displayed in green is the final version of the rig. These positions are at the on-support locations at an inner radius of 10” and at the between-support locations at an outer radius of 14”. Since the rig is symmetric with eight supports, this results in a total of 16 gauges that can be tested simultaneously. Note in the figure, there is amplification of LOFFI floor data approaching 200 Hz that is not seen in the AM6 response though these gauges were located in close proximity of each other. Early data from this effort and prior experience informed the decision not to focus on that mode as it is a characteristic of the LOFFI mount rather than the floor intended to be mimicked.

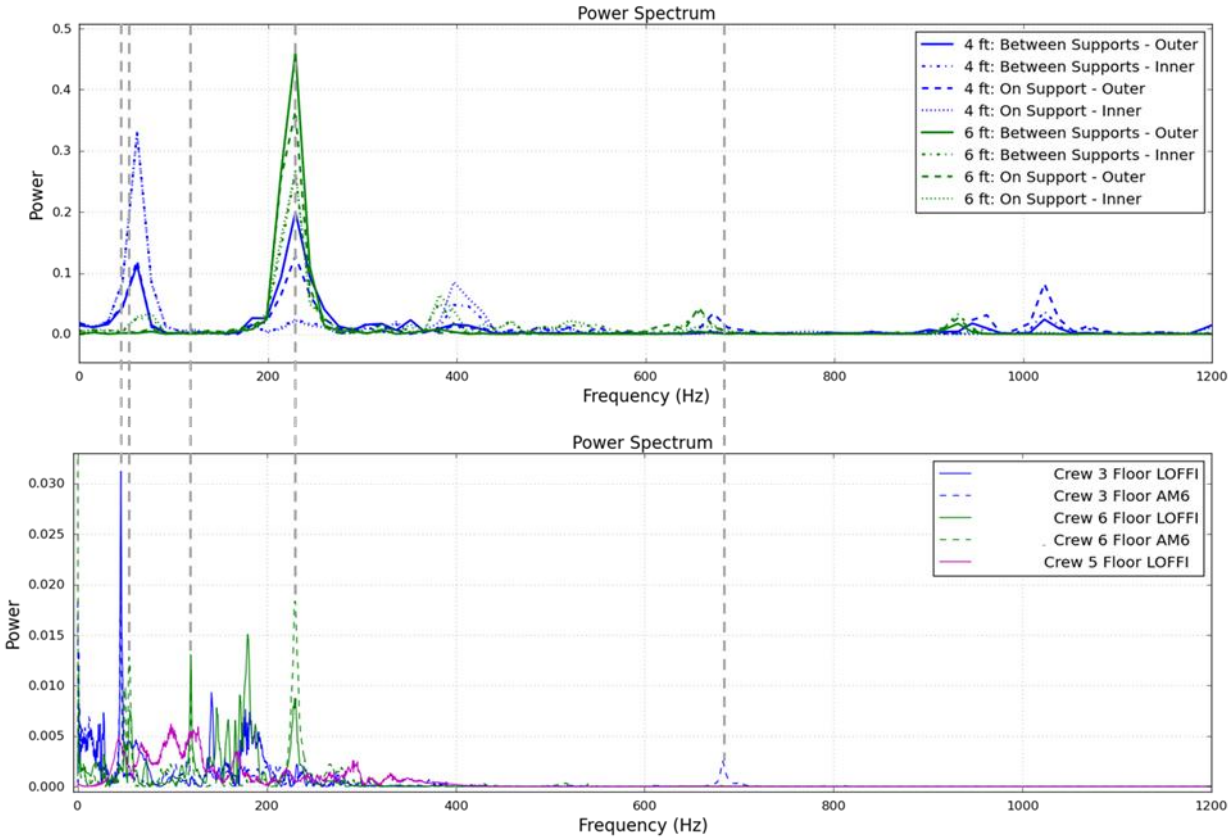

Figure 52 – Comparison of Two Candidate Test Rig Simulated Results to Representative LFT&E Tactical Vehicle Floor Responses

A comparison between the final Velodyne simulation and Shot #5 is shown in Figure 53. In (a) the time history of the local velocity is compared showing similarities to both LDV and Tiny BOB velocity profiles, timing, and frequency content, though the numerical simulation presents high amplitude oscillations later throughout the event due to the lack of damping modes that exist in the physical response. This is typical for FE methods when artificial damping is not applied. Overall, the SRS response of the traces in (b) confirm that the model captured the key responses such as frequencies the floor plate amplified around 250 Hz and 400 Hz, likely the primary modes of vibration for the structure. The better alignment between Tiny BOB and

Velodyne results supports the concerns with the LDV tracking filter influence on some medium and high frequency bands.

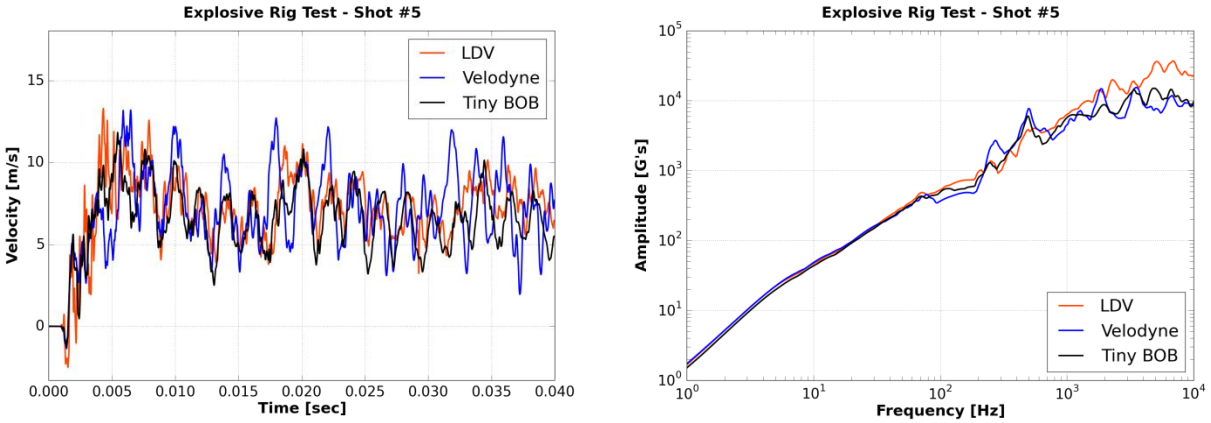

(a) **(b)**

Figure 53 – Comparison of Local Floor Plate Response in Prediction vs. Experiment

Despite the accuracy of Velodyne, it is still considered a predictive tool rather than a direct measurement of the experimental result. There are some differences between the HFCP model and the actual explosively-driven rig that may cause some discrepancies in the results. The most influential source of discrepancy between the Velodyne results and the experimental results is likely the composition and compaction of the soil. The Velodyne model uses HME-C developed Engineered Soil at a compaction level below the standard Roadbed most similarly to what has been used within the WIAMan program on the Accelerative Loading Fixture. This soil condition was the objective of the test team, but no hard metrics were mandated for test setup to expedite testing within the limited range time and budget available. Additionally, the crew at ATC's Grenade Range used instrumentation to assess soil conditions at the surface, but it is impossible to eliminate all variability for large-scale, outdoor experimental tests such as these.

Furthermore, the HFCP model does not feature the actual gauges and their wiring mounted to the rig. The masses of the gauges and wiring may be considered insignificant when compared to the mass of the entire test rig, but their influence may affect the measurements recorded by the numerical accelerometers. Most importantly, Velodyne uses the finite element method which features its own uncertainties and ranges of error. This is due to the fact that the finite element method uses numerical methods to approximate the solution of a system of partial differential equations that have no known analytical solution. As previously mentioned, the predictive nature of Velodyne keeps it from being a source of experimental truth data, but these results can be seen on all the acceleration, velocity, SRS, and SRS percent error plots produced for the Explosive Rig tests as collecting truth data on this test configuration with high confidence was challenging.

d. Lessons Learned

i. Explosive Rig Testing

Overall, Explosive Rig testing of the gauges presented was successful; however, in hind sight, several adjustments could have been made to achieve optimal test conditions and results. The first of such adjustments would have been to the reference or "truth data" sources. In the laboratory, the LDV produced accurate results and proved to be an excellent source for comparison to truth for devices under test. When the LDV was moved from an indoor laboratory setting to the live-fire range for Explosive Rig testing, several obstacles hindered its performance. Brief signal dropouts are inherent in the LDV system when dirt, dust, or debris pass through the laser beam and interfere with the reflectivity of the beam back to the sensor head. As a result, a high velocity tracking filter (built into the Polytec velocity decoder) was used to bridge brief dropouts anticipated in Explosive Rig testing. Unfortunately, it was not realized until after testing that the tracking filter is acceleration limited to 20,000 G's with a frequency response of only 200,000 Hz. Although the frequency response range is well above the area of interest, it is possible that there were localized accelerations at or above the acceleration limit on the test rig that may have been attenuated by the filter. In future testing, the tracking filter should be excluded from the LDV and all data should be post processed to remove signal drop out such that peak acceleration values are retained.

Secondly, among LDV, SDIC, and PDV, there was no truth data source that extended the full duration of the Explosive Rig test event. All three systems are impacted by either the shock front or the soil ejection and can only record meaningful results for the duration of the unobstructed view of the test rig. For example, the total flight duration of the Explosive Rig was approximately 1.5 seconds, yet the longest meaningful truth data record was approximately 75 ms, or only 5 percent of the total event. While the peak accelerations and velocities occurred within this timeframe, there is some interest in the bulk motion throughout the duration of the event which was not recorded via a reliable truth measurement. In future testing, more work should be done to include a truth data source that accurately measures the bulk motion of the test rig for the full duration of the event in order to make a comparison to the low frequency regime of gauges designed to capture such information.

In the second phase of Explosive Rig testing, a steel tower was welded to the driver plate to impact the floor plate and provide high frequency, metal-on-metal acceleration content in an attempt to further stress the upper limits of the devices under test. While it was observed that the impactor did indeed contact the floor plate, it did not produce the desired metal-on-metal acceleration content that is characteristic to many underbody blast events conducted during live-fire testing. In a field expedient effort to produce a higher level of ballistic shock, the welded impactor was removed and cut down to a 1" thick, 3" diameter steel puck. The puck was then placed atop a small charge of C-4 between the thick driver plate and simulated floor plate and detonated, effectively creating an explosively driven impactor to excite a high level of ballistic shock on the floor plate. Unfortunately, provisions made to secure and protect instrumentation

lines that connect the gauges to the data acquisition system were not sufficient, and all lines were severed immediately upon detonation of the secondary projectile. While post-shot observations of the floor plate showed that the secondary projectile had the desired effect, there was no usable data from the event, and many test items were destroyed. Though the technique of a secondary projectile may be effective, further work needs to be done to characterize the resulting impact on the floor plate and better provisions would need to be in place to ensure the survival of instrumentation lines should this be pursued in future testing.

ii. Laboratory Testing

A majority of the initial phases of the project included laboratory testing of selected accelerometers on the Smack Bar and Flyaway apparatuses from which several lessons were learned. After Flyaway testing had already begun, it was learned that the apparatus was not sized to accommodate all of the test items with a corresponding truth data measurement. As a result, the LOFFI was tested on the Flyaway apparatus without a source of truth data and later compared to LDV measurements made during Flyaway testing of the BOBKAT. Though each gauge had an identical input from the compressed air gun, the mass of each was slightly different, and one cannot confidently conclude the truth measurements from BOBKAT testing would match those from LOFFI testing. Should future Flyaway testing occur, the apparatus should be sized to accommodate all test items such that a truth measurement can be made. In addition, all testing, either Smack Bar or Flyaway, should begin at a common input and end at the upper limits of the particular device under test.

iii. Analysis Techniques

Consensus should be made on the best practices for analyzing data collected during the testing described in this report. Recall that the analysis of acceleration data included the application of a 10,000 Hz low-pass filter regardless of the frequency domain of interest. That is to say that a low frequency designated accelerometer (1 – 10 Hz) was post-processed at 10,000 Hz and compared to the truth data at the same bandwidth. However, several of the gauges tested, including the LOFFI, BOBKAT and Endevco 2262A, have a frequency response less than 10,000 Hz. On the other hand, the LDV has the ability to record frequency content up to 500 kHz before post-processing. As a result, gauges like the LOFFI, whose frequency response is limited to less than 100 Hz by its mechanical filter, were compared to a truth data with a much faster frequency response. In future testing, low and medium frequency accelerometers and gauges should be compared to truth data that has been post-processed to match the frequency response of the corresponding instrumentation.

Summary of Findings

a. Summary of Results

The overall goal of this project was to characterize each of the accelerometers and gauges tested by documenting their time domain and frequency domain performance properties and to provide instrumentation recommendations for data collection that falls within the three frequency ranges of interest: low (1 – 10 Hz), medium (10 – 2,000 Hz), and high (2,000 – 10,000 Hz). A combination of the number of accelerometers and gauges that were analyzed and the number of tests that were performed produced hundreds of plots that can be seen in full in the *Appendix*, but the following sections serve to summarize the results from those tests and highlight the best performing gauges for the three frequency ranges of interest.

i. Low Frequency Range (1 – 10 Hz)

The only test that was performed that produced dominantly low frequency content was the Flyaway. Its damped projectile impact and the resulting freefall produced a majority of low amplitude and low frequency acceleration, unlike the Smack Bar and Explosive Rig tests.

Figure 40 (a) suggests that the accelerometers that produce the most accurate peak velocity values for the Flyaway tests are the Endevco 2262A and the Endevco 7264D. However, the Endevco 7270A and its mechanically filtered counterpart, the BOBKAT, were also relatively accurate in measuring peak velocity. Conversely, all accelerometers and gauges had difficulty measuring accurate time-to-peak velocity values, as seen in Figure 40 (b). The accelerometer that measured the most accurate value for this parameter is the Endevco 7264D with the Endevco 7270A, Endevco 2262A, and the BOBKAT closely behind. The instrumentation that measured the most inaccurate peak velocity and time-to-peak velocity values for this particular test are the Endevco 7270AM6, Endevco 7280A, and LOFFI. It should be noted that because of size limitations, truth data could not be simultaneously collected on the Flyaway with the LOFFI.

However, Table 11 suggests that the most accurate late-time responses were produced by the LOFFI, Endevco 2262A, and BOBKAT. This is likely because the LOFFI and BOBKAT are both mechanically filtered, and the Endevco 2262A is critically damped with a high sensitivity value. On the other hand, the most inaccurate late-time responses were produced by the Endevco 7270AM6 and the Endevco 7280A. These late-time performance errors are likely due to the fact that these instruments have lowest sensitivity values of all the accelerometers used. This low sensitivity makes it difficult to distinguish the low frequency, low amplitude content from the noise produced by the accelerometers.

Further distinction among the best performing gauges can be seen the full acceleration and velocity traces as well as the SRS and SRS percent error plots shown in *Appendix B*; however, the most telling of these plots have been reproduced in Figure 54 and Figure 55. These two figures compare the velocity traces and corresponding SRS percent error plots, respectively, of the Endevco 2262A, BOBKAT, Endevco 7270A, Endevco 7264D, and LOFFI.

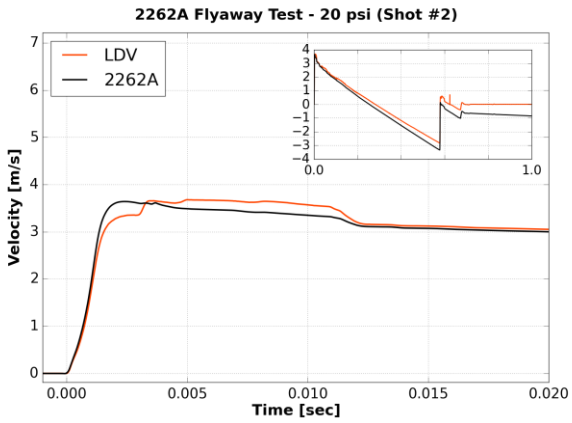

(a)

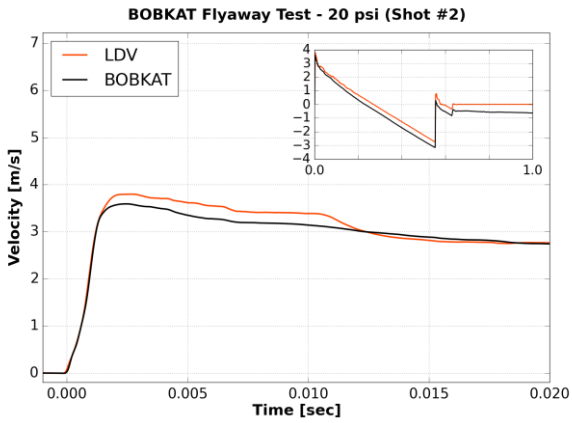

(b)

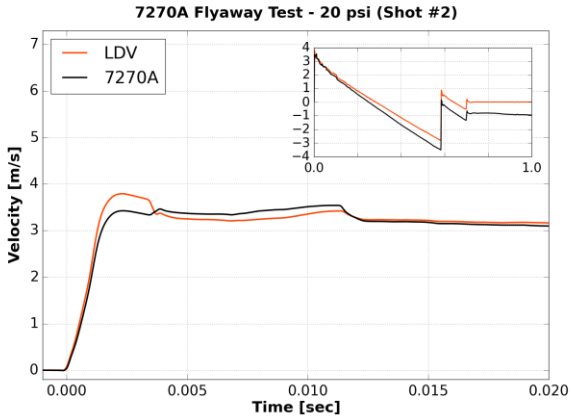

(c)

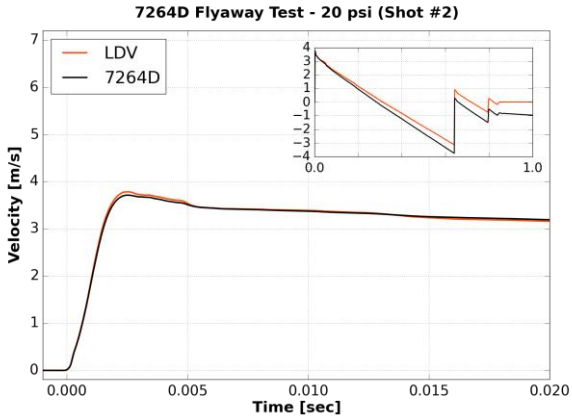

(d)

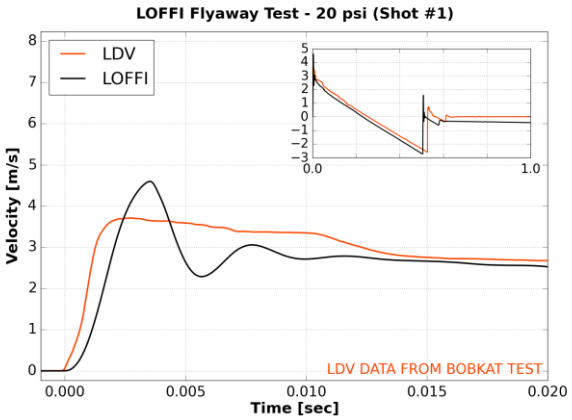

(e)

Figure 54 – Example of Endevco 226A (a), BOBKAT (b), Endevco 7270A (c), Endevco 7264D (d), and LOFFI (e) Velocity Traces

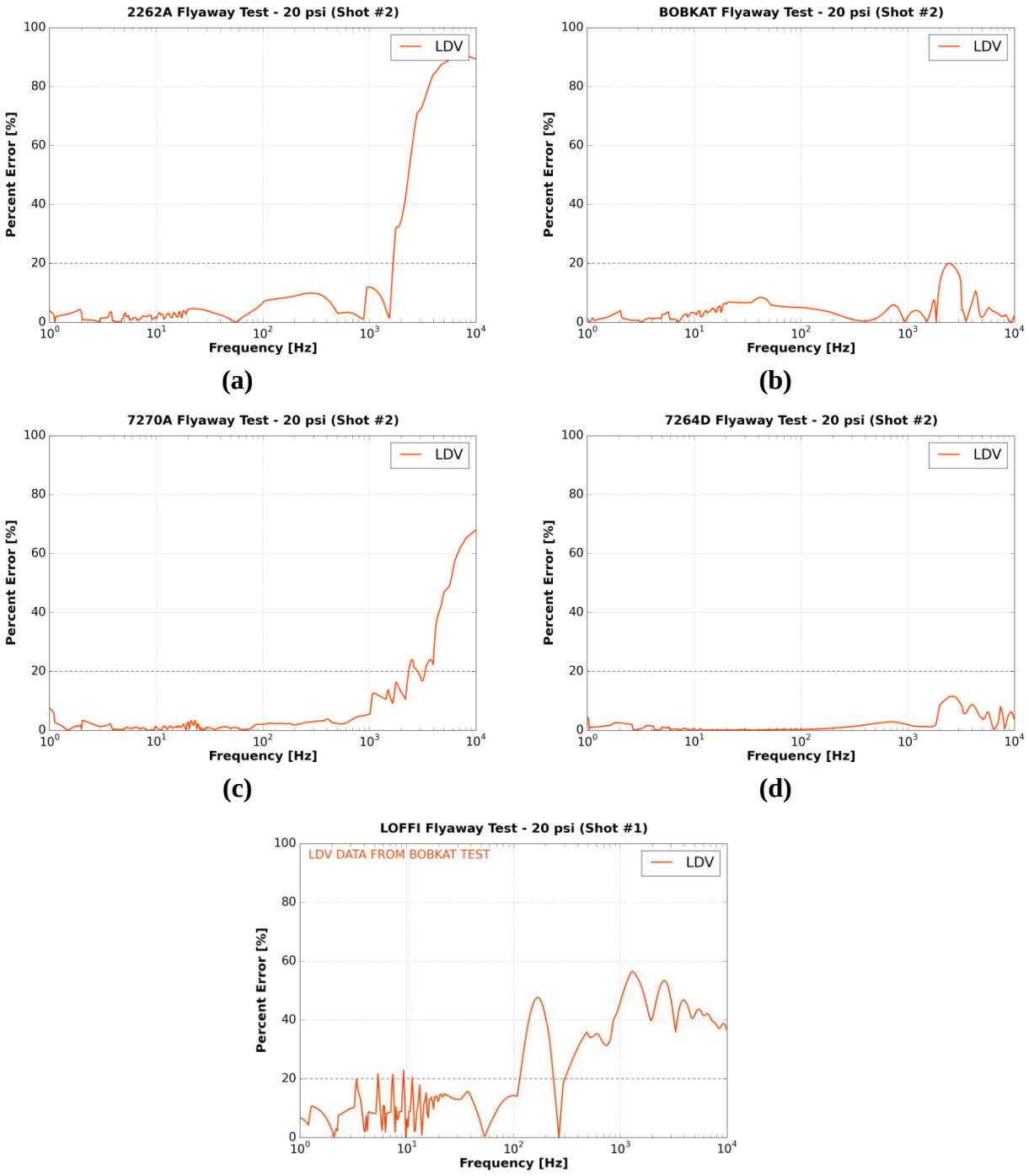

Figure 55 – Example of Endevco 226A (a), BOBKAT (b), Endevco 7270A (c), Endevco 7264D (d), and LOFFI (e) SRS Percent Error Plots

Figure 54 and Figure 55 only represent examples of the results that were produced from the Flyaway tests, but they are indicative of the overall performance of these accelerometers and gauges. The large 20 ms plots in Figure 54 display their ability to capture early-time responses of this low frequency content, but the corner plots visualize their late-time response accuracy and

correspond to the values presented in Table 11. It is important to note that since no LDV data was gathered during the LOFFI Flyaway tests due to the laser's obstructed view, the results from the LOFFI were compared to the LDV results from a BOBKAT test since they have similar mass properties. This discrepancy has been noted in plots produced for the LOFFI. The plots in Figure 54 show that all of the accelerometers and gauges produced relatively accurate late-time responses with minimal velocity drift, but the Endevco 7264D was the only device that could accurately capture the early-time response of the Flyaway test. Similarly, Figure 55 shows that all accelerometers and gauges produced accurate SRS results over the low frequency range of interest. However, even though minimal high frequency content was produced by the Flyaway test, the Endevco 7264D stands out as the most accurate accelerometer or gauge for any frequency range of interest when subject to this acceleration content. Based on these findings, it is suggested that the Endevco 7264D be used to measure low frequency content in the range of 1 – 10 Hz, but its low linear range of 2,000 G's must be considered for each particular application.

However, special consideration must be given to the LOFFI if it is desired to solely capture bulk motion of an object subject to content similar to that produced during the Flyaway tests. Figure 54 shows that the LOFFI is not able to accurately measure the early-time response of the test, and Figure 55 illustrates how it cannot accurately capture any acceleration content above 100 Hz; however, the average end velocity and average slope values shown in Table 11 prove that it is the gauge best suited for measuring late-time response and accurately tracking bulk motion of the Flyaway test.

Conversely, the most inaccurate Flyway test results were produced by the Endevco 7270AM6 and the Endevco 7280A. These accelerometers produced the most inaccurate peak velocity and time-to-peak velocity values as well as the most significant drift in the late-time velocity plots, as seen in Figure 56. These significant drifts propagated into the SRS percent error plots to produce the highest errors in the 1 – 10 Hz frequency range, which can also be seen in Figure 56. As previously mentioned, this is likely due to their low sensitivity values that make it difficult to distinguish low frequency content from noise in the acceleration trace.

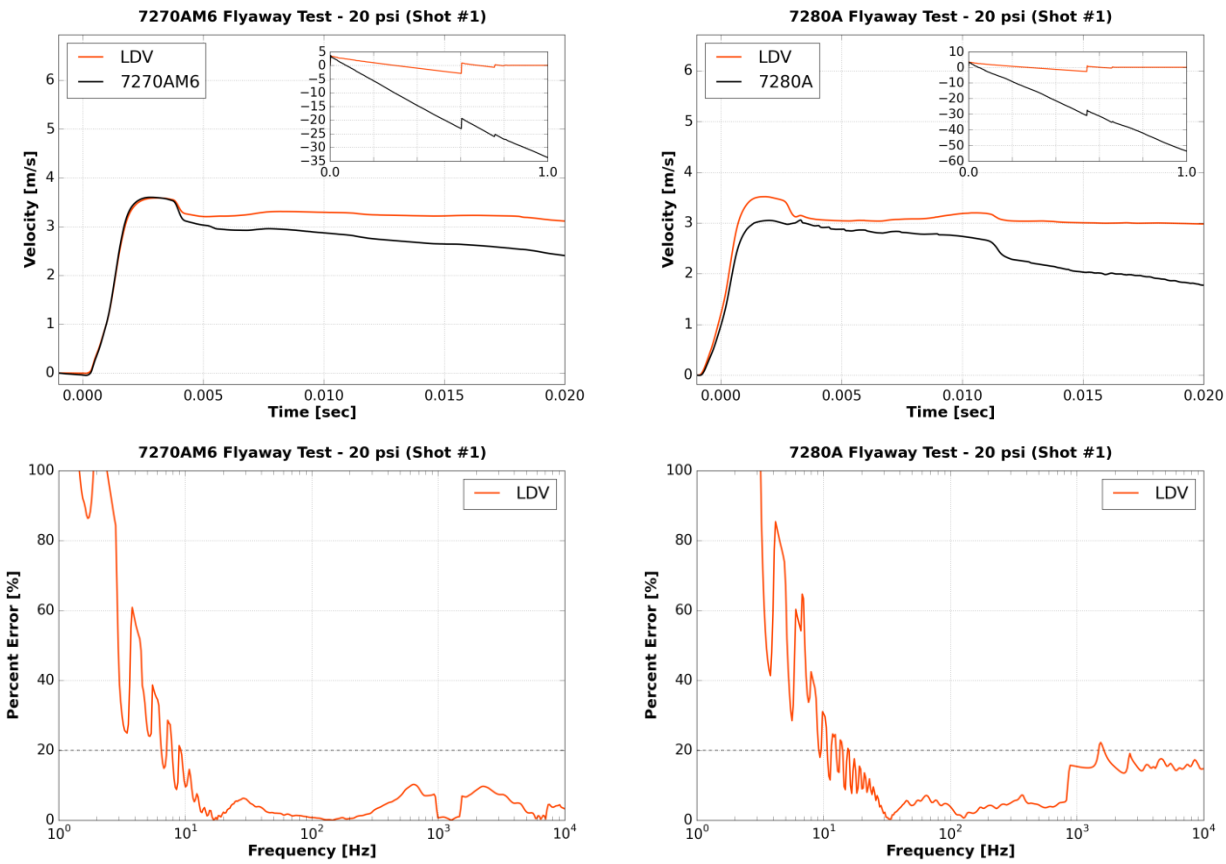

(a) **(b)**

Figure 56 – Example of Endevco 7270AM6 (a) and Endevco 7280A (b) Velocity Traces and SRS Percent Error plots

ii. *<u>Medium Frequency Range (10 – 2,000 Hz)</u>*

Since there were issues with the Shaker Table, the only test that reliably produced a majority of medium frequency content was the Smack Bar. Its projectile impact was slightly damped with the use of a programmer, but the bar's fixed ends localized the vibrations to the center of the bar and kept the accelerometers and gauges from experiencing freefall.

The peak velocity and time-to-peak velocity plots in Figure 37 show that the devices with the best early-time velocity response are the Endevco 7280A and the Endevco 7270A. The peak velocity and time-to-peak velocity values measured by these accelerometers are relatively close to the corresponding values measured by the LDV. The other accelerometer that measured these values relatively accurately is the Endevco 2262A. However, it is important to note that this accelerometer was only tested at 8 psi and 12 psi due to its low linear range limit, as previously explained. Even though laser dropout made calculating the LDV peak velocity and time-to-peak velocity values at these pressures impossible, the resulting values measured by the Endevco 2262A seem to lie where expected. The Endevco 7270AM6 measured relatively accurate peak velocity values, but its time-to-peak velocity values seem to be consistently low, which is likely due to the fact that it is mechanically filtered. Similarly, the two gauges that measured the most

inaccurate peak velocity and time-to-peak values are the BOBKAT and LOFFI; however, this is to be expected since the mechanical filters used in these gauges have a roll-off frequency within this medium frequency range of interest.

Conversely, the average end velocity and average slope values in Table 10 show that the instrumentation that measured the most accurate late-time response are the LOFFI and the direct mount Endevco 2262A. Since the accelerometer within the LOFFI is the Endevco 2262A, this once again shows that a mechanically filtered gauge and/or a damped accelerometer is better suited for measuring the bulk motion of an object. The instrumentation that measured the most inaccurate average end velocity and average slope values are the Endevco 7270A and the Endevco 7280A. Once again, this is likely due to the fact that these gauges have relatively low sensitivity values when compared to the Endevco 2262A.

The acceleration, velocity, SRS, and SRS percent error plots used to characterize these gauges are all presented in the *Appendix*, but Figure 57 and Figure 58 provide examples of the velocity traces and the corresponding SRS percent error plots, respectively, for the Endevco 7270A, Endevco 7270AM6, Endevco 7280A, Endevco 2262A, and LOFFI.

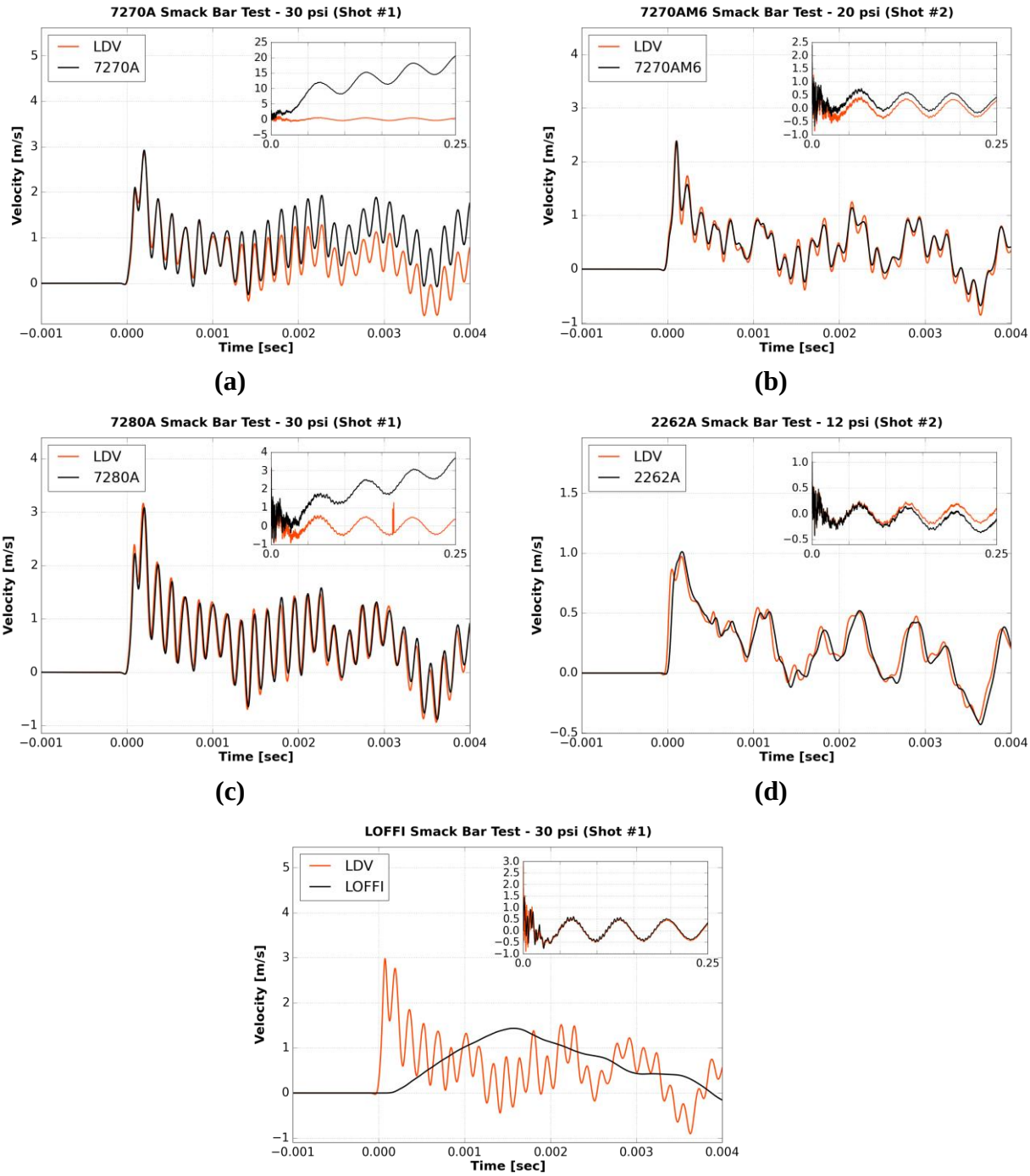

Figure 57 – Example of Endevco 7270A (a), Endevco 7270AM6 (b), Endevco 7280A (c), Endevco 2262A (d), and LOFFI (e) Velocity Traces

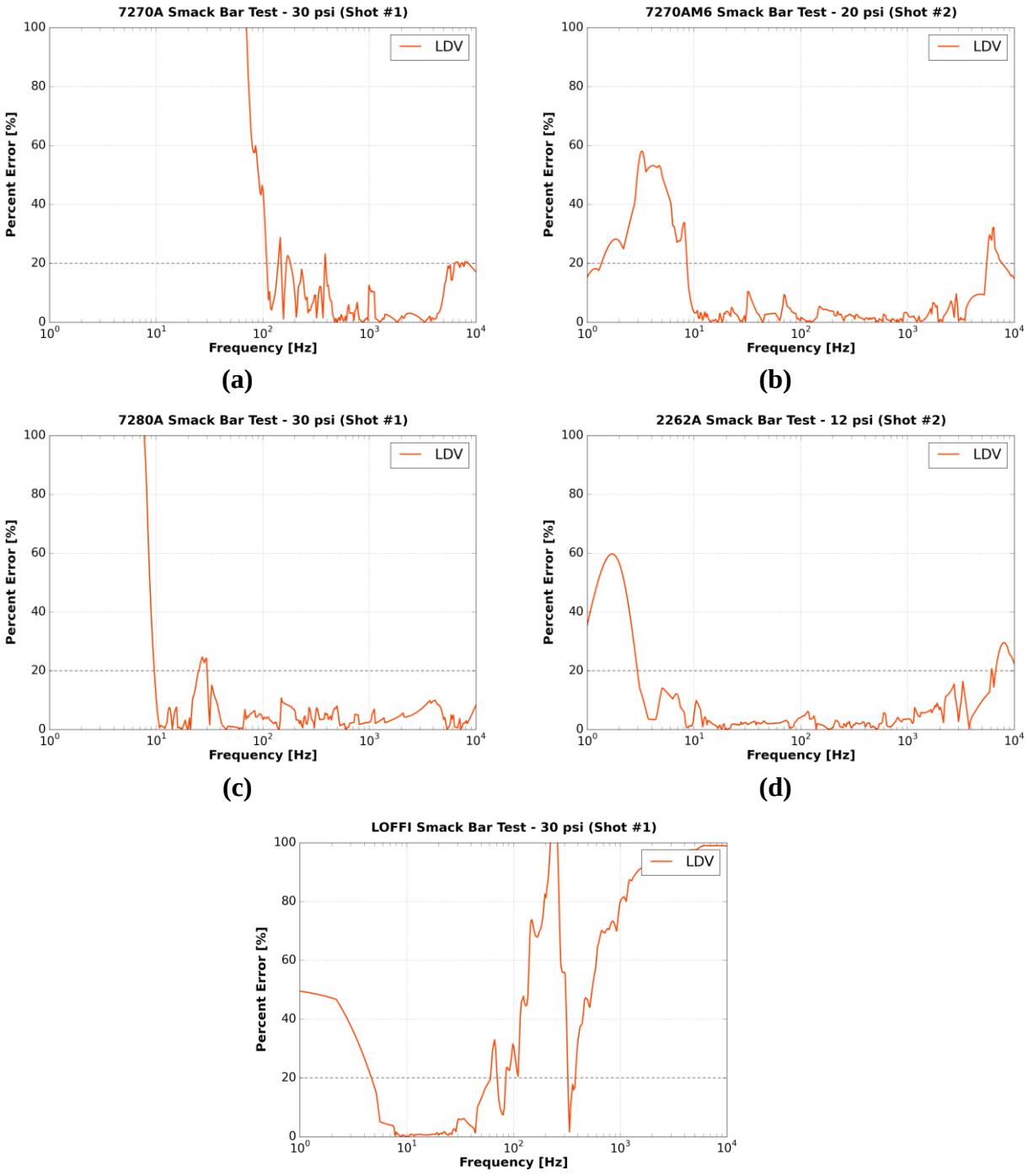

Figure 58 – Example of Endevco 7270A (a), Endevco 7270AM6 (b), Endevco 7280A (c), Endevco 2262A (d), and LOFFI (e) SRS Percent Error Plots

The plots shown in Figure 57 and Figure 58 highlight several key characteristics about the top performing accelerometers and gauges. Once again, these plots are just examples of the results produced by them during the Smack Bar testing, but they represent the overall performance of each accelerometer and gauge. The corner plots displayed in Figure 57 show

that the Endevco 7270A and Endevco 7280A experienced the worst velocity drift while the Endevco 7270AM6 and Endevco 2262A experienced minimal velocity drift. However, more importantly, the corner plots in Figure 57 and the values in Table 10 show that the LOFFI is the most consistent and accurate at measuring late-time response. On the other hand, Figure 57 (e) also shows how inaccurate the LOFFI is at capturing early-time responses that occur faster than 100 Hz.

Figure 58 shows that of these gauges, the LOFFI and the Endevco 7270A have the worst frequency domain accuracy. The SRS percent error plot for the LOFFI corroborates that it cannot accurately capture content above 100 Hz, and the Endevco 7270A's SRS percent error plot shows that it cannot accurately capture any content below 100 Hz when subject to this medium range frequency content. However, the frequency domain accuracies for the other three gauges are all relatively similar. The Endevco 7270AM6, Endevco 7280A, and the Endevco 2262A seem to have accurate frequency ranges of 10 – 5,000 Hz, 10 – 10,000 Hz, and 3 – 6,000 Hz, respectively, for the Smack Bar tests. The accurate frequency domain for all three of these accelerometers span the medium frequency range of interest, but the time domain results seem to suggest that the Endevco 7280A is the best suited for capturing the response of medium range frequency content. The Endevco 7280A may have one of the more inaccurate late-time responses, but it has one of the most accurate early-time responses, and it produced one of the most accurate SRS plots. More importantly, the internal damping and low sensitivity value of the Endevco 7280A allow it to be subject to higher accelerations than the competitor accelerometers. However, it should be noted that a case can be made for using the Endevco 2262A over the Endevco 7280A to measure this type of content as it also produced accurate measurements, but one must be careful not to exceed its linear range of 2,000 G's.

As previously stated, the BOBKAT and LOFFI measured the most inaccurate peak velocity and time-to-peak velocity values most likely due to their mechanical filters. The specific value of the roll-off frequency for these gauges can be identified from their SRS and SRS percent error plots, examples of which have been reprinted in Figure 59 from the *Appendix*.

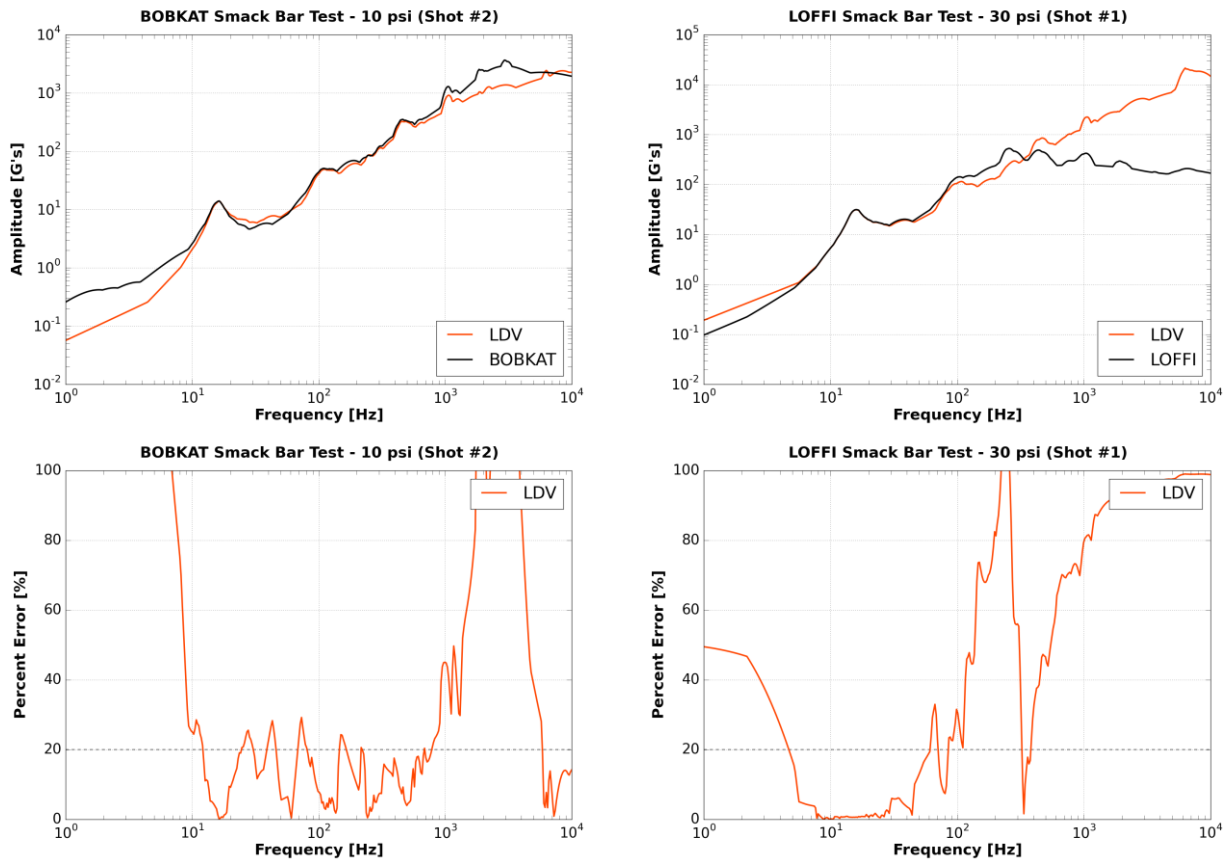

(a) **(b)**

Figure 59 – Example of BOBKAT (a) and LOFFI (b) SRS and SRS Percent Error Plots

The SRS plot in Figure 59 (a) shows that the BOBKAT tends to amplify any content above 1,000 Hz and subsequently filters any content beyond 3,000 Hz. This implies that the gauge produces erroneous results for any content beyond 1,000 Hz even though its roll-off frequency appears to be 3,000 Hz. Similarly, the SRS plot in Figure 59 (b) shows that the LOFFI amplifies any content above 100 Hz and filters any remaining content beyond 300 Hz. Overall, these parameters show that the BOBKAT and LOFFI should not be trusted to accurately measure content within the frequency range of 10 – 2,000 Hz; however, it is important note the late-time accuracy of the LOFFI. As previously mentioned, the recommended gauge for the medium frequency range content, the Endevco 7280A, has poor late-time performance. To combat this, it is suggested to collocate an Endevco 7280A and a LOFFI when measuring content similar to that produced by the Smack Bar. This will allow user to gather the early-time and frequency responses from the Endevco 7280A and use the LOFFI to obtain the late-time response produced by bulk motion.

iii. <u>High Frequency Range (2,000 – 10,000 Hz)</u>

The harsh conditions and high accelerations produced by the Explosive Rig made it the test best suited to produce content in the high frequency range of interest. As previously

described, it is the most applicable test in the protocol since it introduces many of the "real world" complications associated with using this type of instrumentation in LFT&E. The explosion and soil loading produce dominant content in the high frequency range of interest, but the subsequent projectile motion of the rig simultaneously provides a source of low frequency content.

The peak velocity and time-to-peak velocity plots in Figure 43 highlight the early-time performance of all the gauges compared to the LDV when subject to this explosive content. More specifically, Figure 43 (a) shows that all gauges measured relatively accurate peak velocity values with a charge size of 10 lbs, but a charge size of 20 lbs produce more diverse results. Overall, the gauges that measured the most accurate peak velocity values are the Wheel Mount, Mini BOB, and Tiny BOB. However, Figure 43 (b) shows that the measured time-to-peak velocity values are extremely varied across each gauge and each shot size when compared to the LDV results. Nevertheless, the gauges with the most accurate time-to-peak velocity values are the Wheel Mount, Tiny BOB, and Wave Spring.

Despite the large number of gauges analyzed during the Explosive Rig testing, the data in the peak velocity and time-to-peak velocity plots does not clearly separate the best and worst performing gauges from the others; therefore, final gauge recommendation conclusions must be based on acceleration and velocity traces as well as SRS and SRS percent error plots. As previously mentioned, the full set of these data plots can be seen in the *Appendix*, but Figure 60 and Figure 61 provide examples from the best performing gauge – the Tiny BOB.

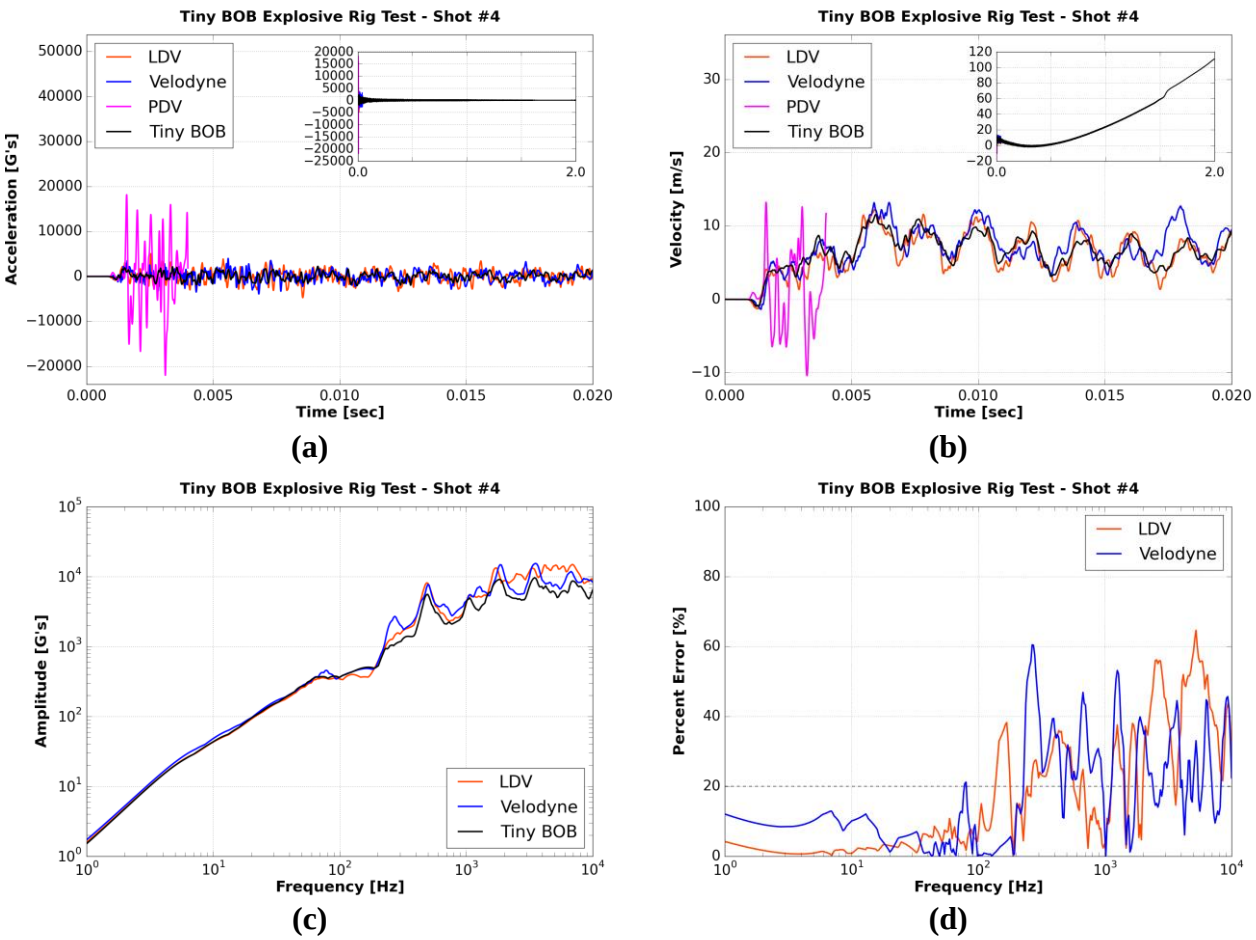

Figure 60 – Acceleration Trace (a), Velocity Trace (b), SRS Plot (c), and SRS Percent Error Plot (d) Produced by Tiny BOB from Shot #4

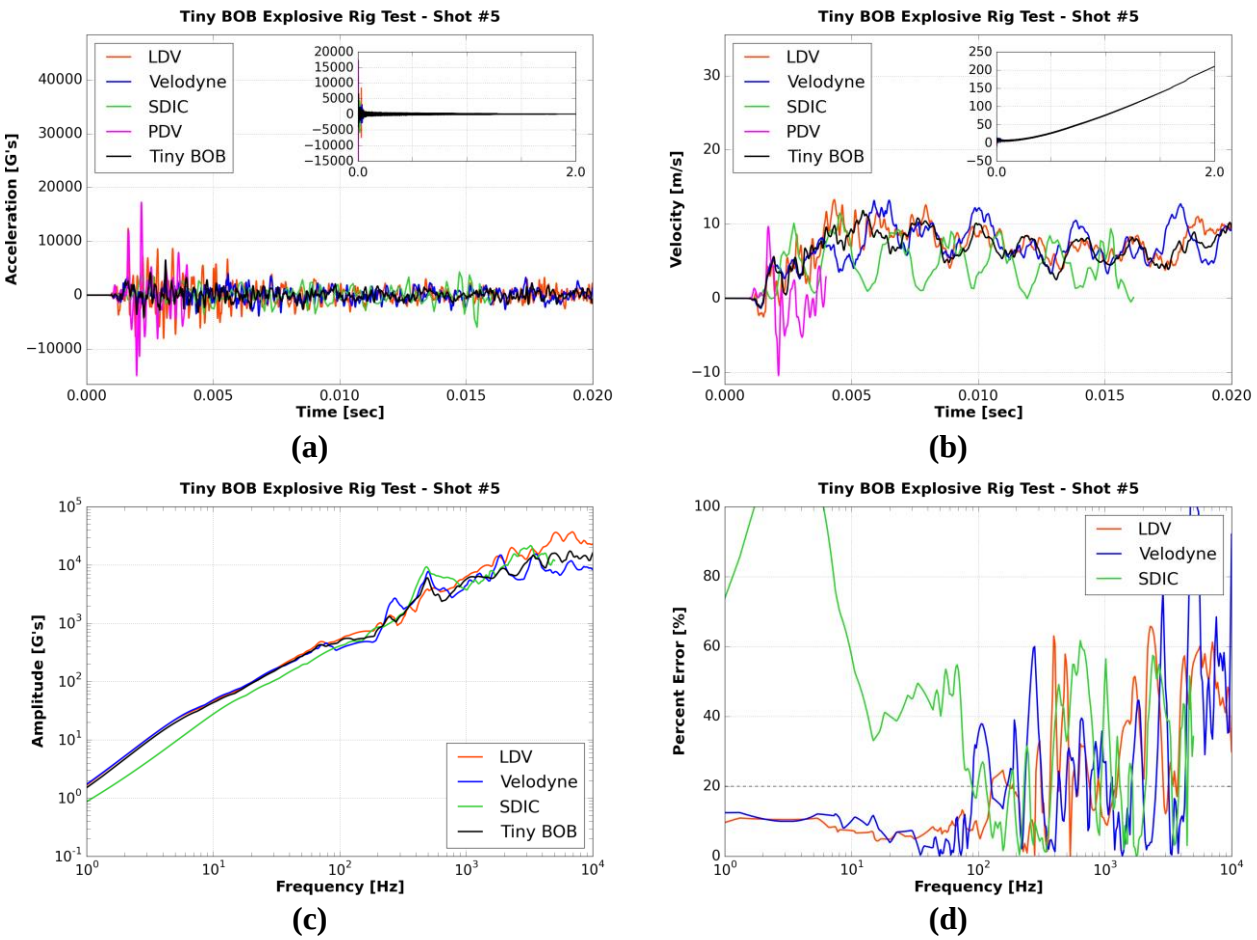

Figure 61 – Acceleration Trace (a), Velocity Trace (b), SRS Plot (c), and SRS Percent Error Plot (d) Produced by Tiny BOB from Shot #5

Compared to the other gauges, the Tiny BOB seemed to have the best overall performance for the Explosive Rig tests. Its peak velocity and time-to-peak velocity results were not the most accurate, but it performed relatively well when compared to a majority of the gauges. However, the Tiny BOB distinguished itself from the other gauges by producing consistently accurate velocity traces and SRS plots, as shown in both Figure 60 and Figure 61. For these plots, it is important to establish which source of "truth" data is the most trustworthy. Figure 61 (b) shows the velocity traces of all three sources of Explosive Rig truth data along with Velodyne and Tiny BOB velocity traces on a single plot. The LDV, Velodyne, and Tiny BOB traces seem to match relatively well with corresponding peaks and valleys throughout the early-time response; however, the SDIC and PDV traces seem to conflict with these traces as well as with each other. The source of this discrepancy is not definitively known, but the findings from this comparison are not just limited to this specific gauge or shot. This same trend can be found throughout all the plots produced from the Explosive Rig test data. For the SDIC, it is possible that these differences are caused by unresolved timing issues or shock wave distortion on a pixel size scale. The source of the PDV discrepancy could be its subjective data processing method or the fact that it measures relative velocity and is being compared to absolute velocities.

Regardless, the entire set of Explosive Rig plots shown in the *Appendix* seem to suggest that the LDV is the most accurate source of truth data for this particular test.

Overall, the Tiny BOB was the only gauge that was able to consistently replicate the early-time response of the LDV and Velodyne, as can be seen in both Figure 60 and Figure 61. While the SRS percent error of the Tiny BOB is not consistently below 20% for frequencies higher than 100 Hz, it was still the most accurate at capturing the frequency content in the high frequency range of interest.

However, one negative aspect of the Tiny BOB is that it is susceptible to velocity drift, as visible in the corner plots of Figure 60 (b) and Figure 61 (b). For an undamped, minimally sensitive accelerometer, such as the Endevco 7270A in the Tiny BOB, two seconds is a relatively long time to collect data from a high frequency explosive event. If it is desired to capture the bulk motion of an item that is subject to high frequency content, the results suggest the use of a LOFFI. To prove this recommendation, the results produced by the LOFFI during Shot #6 have been reproduced in Figure 62.

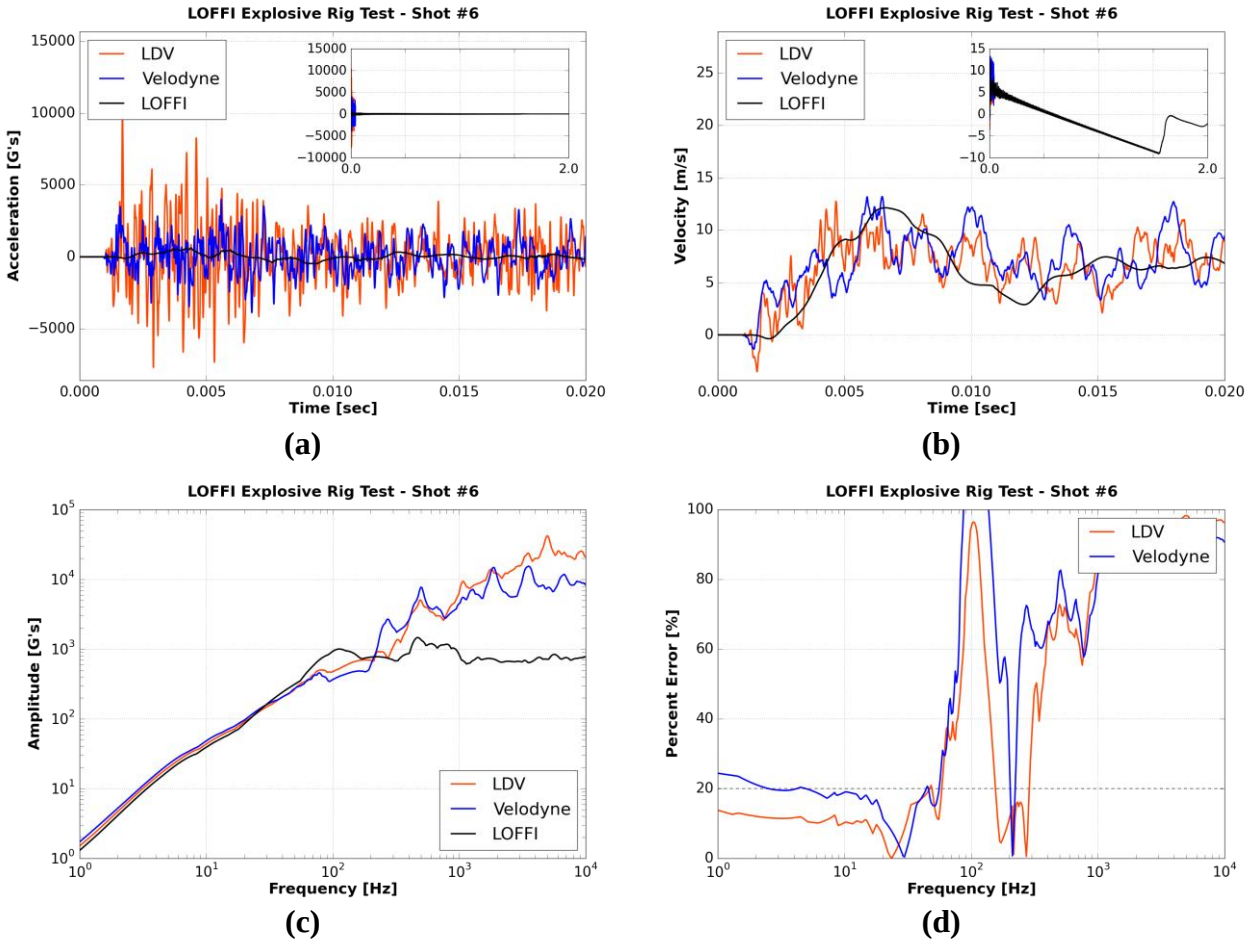

Figure 62 – Acceleration Trace (a), Velocity Trace (b), SRS Plot (c), and SRS Percent Error Plot (d) produced by LOFFI from Shot #6

The early-time response of the LOFFI shown in Figure 62 (a) and (b) emphasis how influential the LOFFI's mechanical filter is on the measured output. The effect from this filter can also be seen in the amplification and roll-off present in the gauge's SRS plot (c). However, the corner velocity plot displayed in (b) and the values listed in Table 12 show how the LOFFI can measure bulk motion of items over long durations with relative accuracy. There is still a marginal amount of drift present in the late-time velocity plot, but the combination of the critically damped, highly sensitive Endevco 2262A accelerometer and the heavily influential mechanical filter make it the best choice for measuring bulk motion of objects subject to high frequency and high amplitude acceleration content. However, Figure 62 emphasizes that in this type of environment, the results from the LOFFI cannot necessarily be considered accurate beyond a frequency of 60 Hz. An ideal instrumentation layout to measure high frequency content would be to collocate a Tiny BOB to capture the early-time and high frequency response and a LOFFI to accurately capture the bulk motion.

b. Conclusions

The tests performed during this project allowed for the characterization of accelerometers and gauges and highlighted which instrumentation is the most accurate at capturing time and frequency content throughout the three frequency ranges that correspond to the global body kinematics (low frequency), seat response (medium frequency), and floor response (high frequency) of a tactical vehicle during LFT&E. The Flyaway test helped determine that for low frequency inputs, the Endevco 7264D measures the most accurate early-time response with the best peak velocity and time-to-peak velocity values, but it also produces accurate late-time results with minimal velocity drift. Furthermore, it produced the most accurate SRS plot with percent errors less than 20% across all three frequency ranges of interest. However, careful consideration must be taken to not exceed the accelerometer's linear limit of 2,000 G's.

The results from the Smack Bar tests suggest that several of the direct mount accelerometers can accurately capture the content in the medium frequency range of 10 – 2,000 Hz, but the Endevco 7280A had the most accurate and consistent overall performance. The other accelerometers that performed well in this frequency range are the Endevco 7270A and the Endevco 2262A, but they are limited by their linear range limits. Compared to these two accelerometers, the internal damping of the Endevco 7280A allows it to survive medium frequency range content with much higher acceleration amplitudes.

Finally, for the high frequency range content, the Explosive Rig test determined that the Tiny BOB is the most accurate at measuring the overall time domain and frequency domain responses. Compared to the other gauges tested, the Tiny BOB was the most accurate at producing early-time acceleration and velocity traces. This accuracy propagated to the SRS plots with comparatively low percent error in the high frequency range of interest. However, one disadvantage of the Tiny BOB is its inaccuracy at measuring the late-time response of objects in explosive environments.

However, it is important to note that throughout all three frequency ranges, it was determined that the LOFFI is the gauge best suited for measuring the low frequency associated with bulk motion. It produced more accurate late-time responses with lower average end velocity and average slope values than all three recommended gauges over their respective frequency ranges. This is likely due to a combination of the gauge's heavily influential mechanical filter that filters at around 100 Hz and the fact that its internal accelerometer is a critically damped with a high sensitivity value.

In addition to providing recommended accelerometers and gauges for the three frequency ranges, this project also established a test protocol to evaluate future accelerometers and gauges. The Smack Bar, Flyaway, Explosive Rig, and Shaker Table tests can all be consistently repeated to provide a comparison between future accelerometer development and the current accelerometer standards. Furthermore, the results show that there is still room for improvement in the accuracy of the time domain and frequency domain responses across all three frequency ranges.

c. Recommendations

Since this project was aimed at improving the accuracy of experimental data gathered during live-fire testing, it is recommended that the results presented be incorporated into the tri-service DT and LFT&E community's efforts. By integrating the gauges suggested, accurate acceleration data can be gathered and used for more effective test-to-test and test-to-simulation comparisons. Ultimately, this will produce vehicles that are better protected from the dangers produced by ballistic shock.

However, it is also recommended that the efforts from this project be extended to resolve any testing issues that became apparent. Most notably, the performance issues discovered during Shaker Table testing limited the suggested test protocol to three tests: Smack Bar, Flyaway, and Explosive Rig. To complete the test protocol and increase accelerometer recommendation confidence, it would be beneficial to eliminate the uncertainty associated with the Shaker Table test results and include them in the device evaluation process. Furthermore, the various pressures used for the Smack Bar tests do not easily allow for direct accelerometer-to-accelerometer comparisons at constant pressure levels. If repeated, it would be recommended to establish a minimum pressure level to test each accelerometer or gauge and to incrementally increase the pressure level by a constant value until the limit of each device is reached. This will improve accelerometer recommendation confidence by allowing for uniform and direct instrumentation comparisons. Likewise, it is recommended to reinvestigate the Explosive Rig test setup since the desired high amplitude accelerations were not achieved with the steel tower or puck. Ideally, it would be beneficial to incorporate a secondary impact between a projectile and the floor plate after detonation in order to produce the high frequency, high amplitude content from metal-to-metal contact and replicate a blast projectile impacting the bottom of a tactical vehicle floor. Furthermore, to narrow the scope of the future project, it is recommended

to remove the following concept gauges from the gauges of interest due to their initial poor performance: Wheel Mount, AM6 Tall, and Corvid Disk Mount.

It is recommended that accelerometer and gauge research and development be continually supported. As the results show, there is still room for improvement in both the time domain and frequency domain responses. Most notably, the high frequency acceleration produced by the explosively-driven rig showed that this is still the most difficult content to accurately capture; therefore, the tri-service DT and LFT&E community would greatly benefit by providing continual support for new accelerometer and gauge developments.

d. Limitations on Data Use

It is important to stress that the choice in instrumentation is ultimately subject to the user's discretion. The results presented for this project provide general characterization of the accelerometers and gauges of interest, but the number of repeat tests performed is not high enough to establish a meaningful statistical confidence level. In the end, users should perform research and consider the application before finalizing instrumentation decisions.

It is also important to note that the explosively-driven test rig was able to produce the anticipated high frequency content, but it was not able to produce the acceleration amplitudes that were desired. Ideally, the Explosive Rig tests would have stressed the gauges to approach the linear range limit of the internal accelerometers, but the impact between the floor plate and the steel tower was not severe enough. Because of this, the gauge recommendation for the high frequency range is currently limited to live-fire tests that produce acceleration amplitudes of 10,000 G's or less (based on the average value measured by the LDV). However, the recommended future work of creating a secondary impact between a projectile and the floor plate after detonation would achieve the goal of increasing the applied acceleration amplitude and approaching the stress limits of each gauge's internal accelerometer.

Other limitations on the data stem directly from its acquisition parameters and post processing. For example, the peak velocity and time-to-peak velocity values for the LDV were calculated from acceleration data that was filtered at 10,000 Hz; however, some of the gauges do not have the ability to measure content with frequencies that high due to their mechanical filter. This means that performing a comparison of peak velocity and time-to-peak velocity values between the LDV and the mechanically filter gauges is not exactly equivalent. Performing a direct and valid comparison would require the LDV data to be filtered at each individual gauge's roll-off frequency, but this roll-off frequency cannot be determined without performing a full data analysis. Even then, deciding the roll-off frequency for each gauge would be a subjective process. Therefore, it was decided to use the objective approach of filtering all LDV data at 10,000 Hz and consider the peak velocity and time-to-peak velocity comparison simply a characterization of each gauge. Another limitation on the data was the fact that the accuracy of the truth data used for the Explosive Rig tests is questionable. It was shown that of the three types of experimental truth data that were recorded, the LDV appeared to be the most accurate. However, the soil ejection that occurred during the Explosive Rig test meant that a tracking filter

was required to prevent laser dropout. Ultimately, this filter increased the reliability of the LDV, but it could have negatively affected the accuracy of the acceleration data gathered.

e. Acknowledgements

The authors would like to acknowledge the contributions of organizations beyond the direct JLF provided funding for this project.

- HME-C Program: Rigid heave test rig provided for "piggy-backing" on for implementation of the explosively-driven test rig
- Aberdeen Test Center: Accelerometers and R&D mounts provided for evaluation purposes
- WIAMan Engineering Office: Accelerometers provided for evaluation purposes
- USMC Autocell: HFCP support and accelerometers and R&D mount provided for evaluation

References

[1] W. N. Hardy, J. H. Bolte IV, K. A. Danelson “TASK 4.2 JUMP START: Whole-Body Blast-Induced Accelerative Loading, Structure Interaction, and Mechanical Response of PMHS and Hybrid III ATD,” US Army Research Laboratory, August 2013

[2] W. S. Walton “Special Study of the Improvement and Validation of Transducers (Ballistic Shock Measurement),” US Army Combat Systems Test Activity, October 1993

[3] R. D. Sill, “Development of a Damped Piezoresistive MEMS High Shock Sensor,” PCB Piezotronics Inc., February 18, 2016

[4] A. S. Chu, “Problems in High-Shock Measurement,” Endevco Corporation

[5] W. S. Walton, B. T. Hepner, C. B. Monahan, “Ideas for Addressing ‘Out of Band Energy’ in Ballistic Shock Measurements,” Shock and Vibration Symposium, November 2011

[6] “Model 7270AM6 Piezoresistive accelerometer,” Endevco, February 17, 2016 https://www.endevco.com/product/prodpdf/7270AM6.pdf

[7] R. J. Spink, “A Simple Method for Processing Measurements of Vehicle Response to Underbody Blast during Live Fire Test and Evaluation,” US Army Research Laboratory, August 2014

Appendices

a. Appendix A – Smack Bar Test Results

i. Endevco 7270A

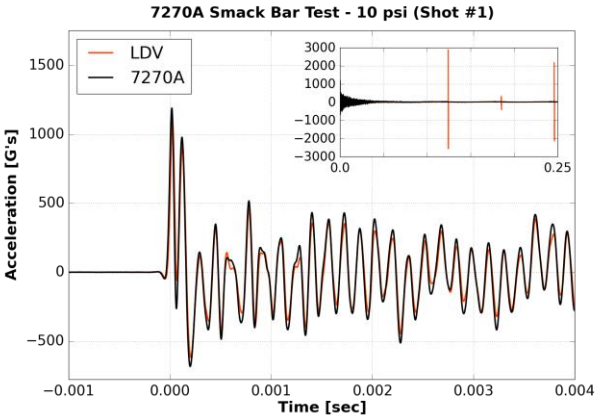

(a)

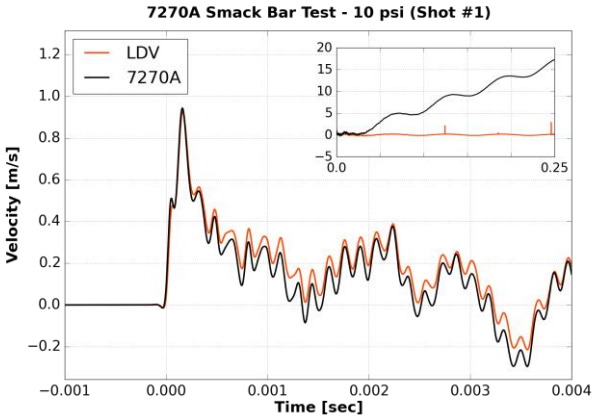

(b)

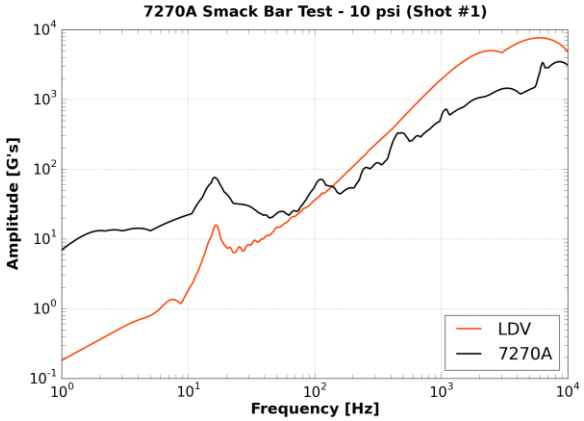

(c)

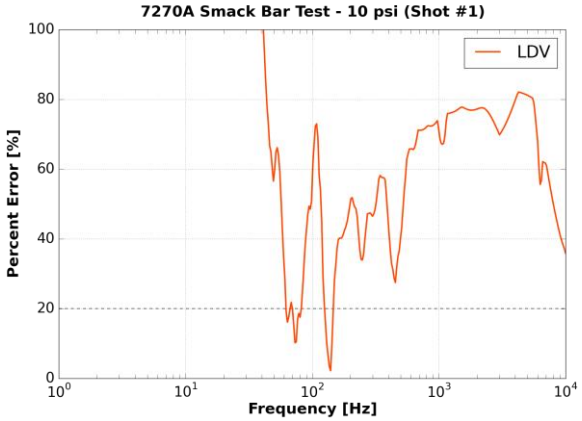

(d)

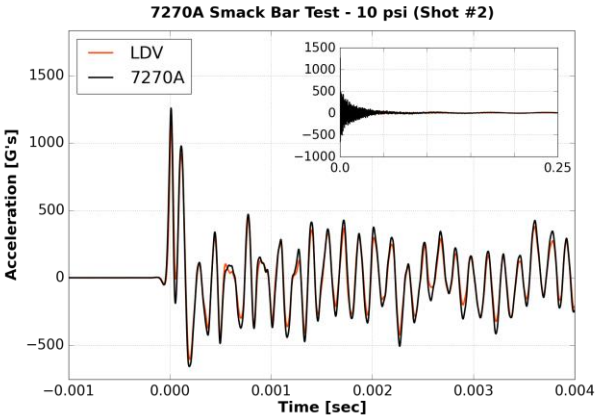

(a)

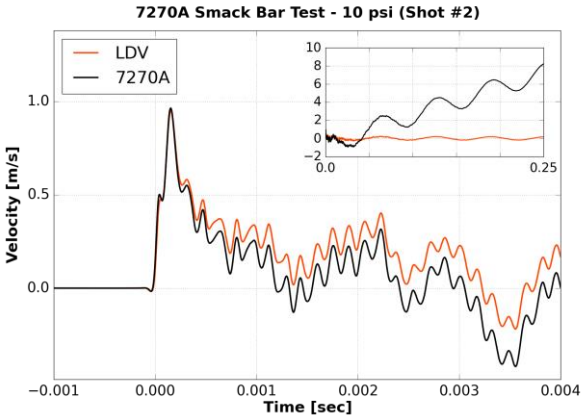

(b)

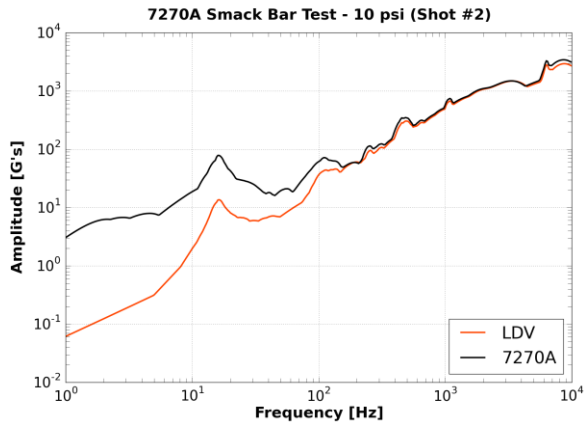
7270A Smack Bar Test - 10 psi (Shot #2)
Amplitude [G's]
Frequency [Hz]
LDV
7270A

(c)

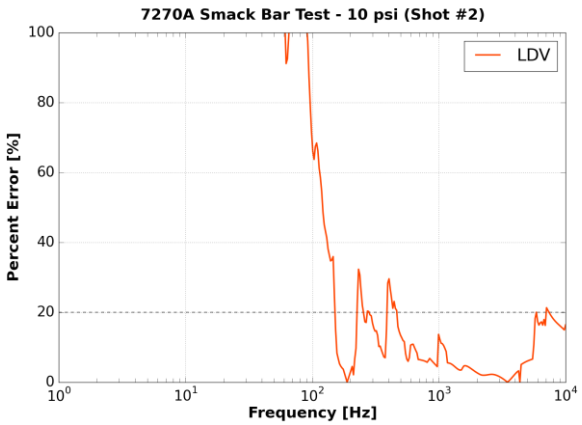
7270A Smack Bar Test - 10 psi (Shot #2)
Percent Error [%]
Frequency [Hz]
LDV

(d)

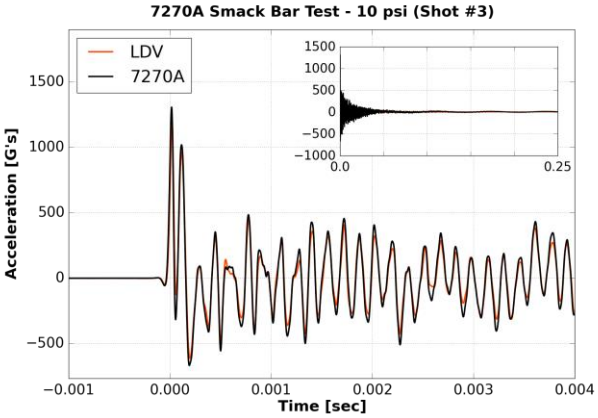
7270A Smack Bar Test - 10 psi (Shot #3)
Acceleration [G's]
Time [sec]
LDV
7270A

(a)

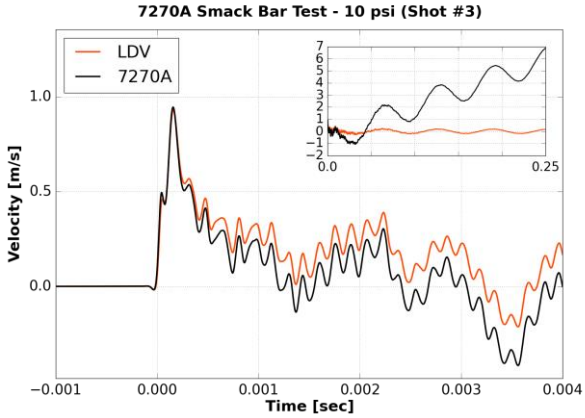
7270A Smack Bar Test - 10 psi (Shot #3)
Velocity [m/s]
Time [sec]
LDV
7270A

(b)

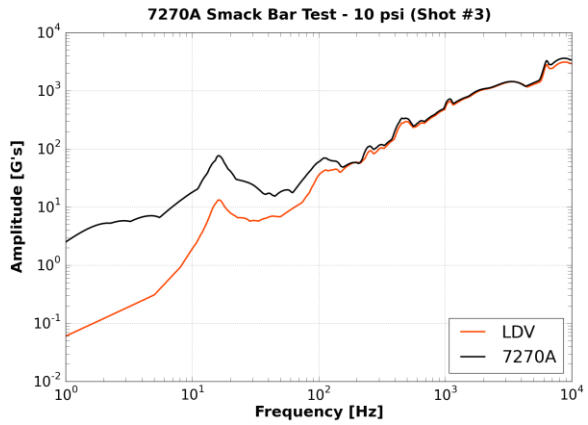
7270A Smack Bar Test - 10 psi (Shot #3)
Amplitude [G's]
Frequency [Hz]
LDV
7270A

(c)

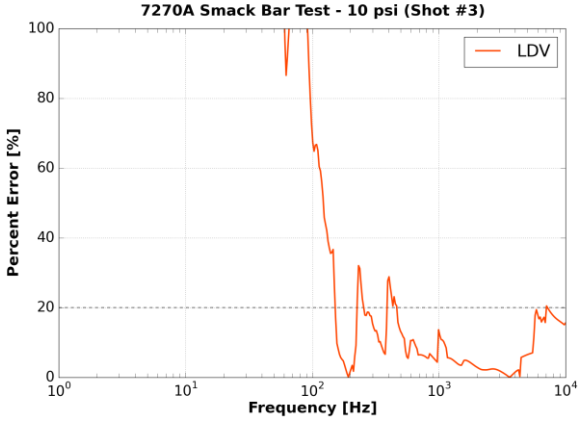
7270A Smack Bar Test - 10 psi (Shot #3)
Percent Error [%]
Frequency [Hz]
LDV

(d)

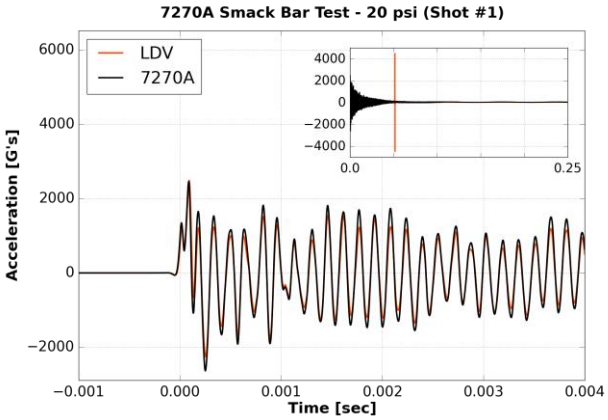
7270A Smack Bar Test - 20 psi (Shot #1)
LDV
7270A
Acceleration [G's]
Time [sec]

(a)

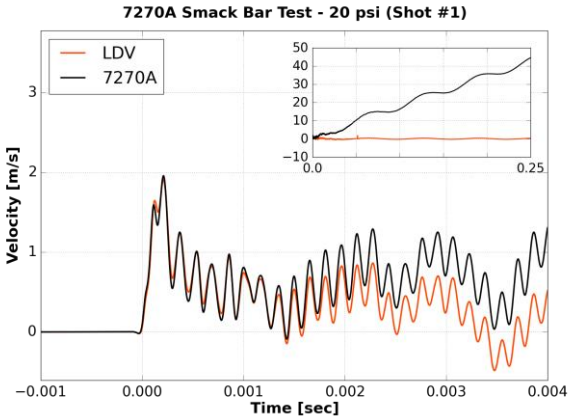
7270A Smack Bar Test - 20 psi (Shot #1)
LDV
7270A
Velocity [m/s]
Time [sec]

(b)

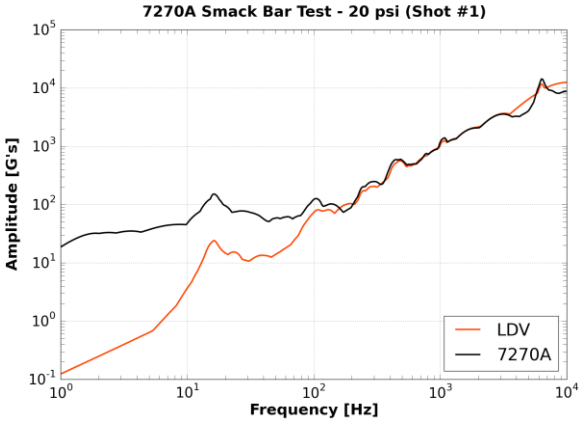
7270A Smack Bar Test - 20 psi (Shot #1)
LDV
7270A
Amplitude [G's]
Frequency [Hz]

(c)

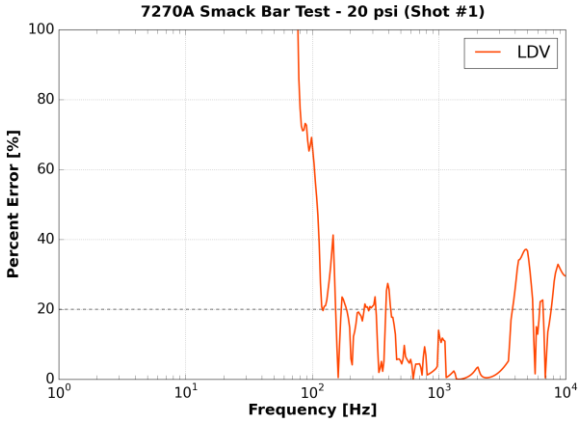
7270A Smack Bar Test - 20 psi (Shot #1)
LDV
Percent Error [%]
Frequency [Hz]

(d)

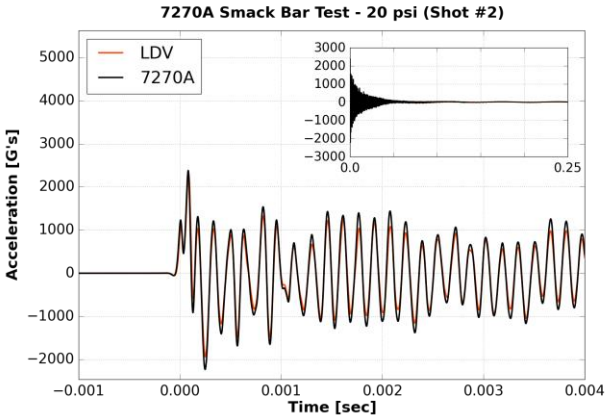
7270A Smack Bar Test - 20 psi (Shot #2)
LDV
7270A
Acceleration [G's]
Time [sec]

(a)

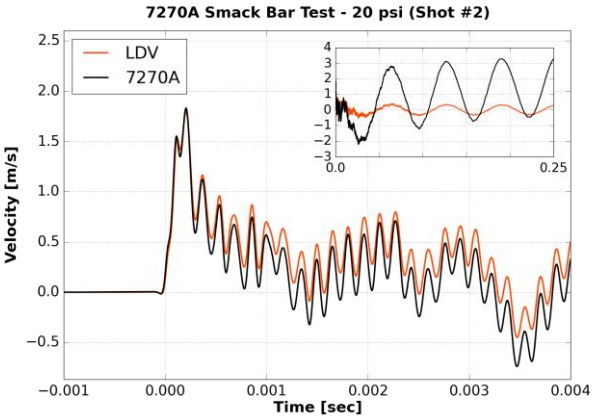
7270A Smack Bar Test - 20 psi (Shot #2)
LDV
7270A
Velocity [m/s]
Time [sec]

(b)

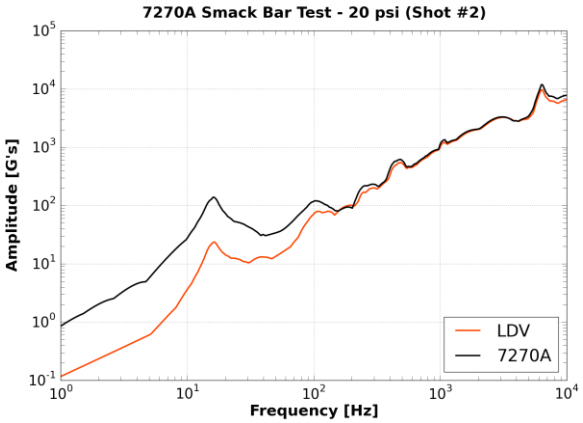
7270A Smack Bar Test - 20 psi (Shot #2)
Amplitude [G's]
Frequency [Hz]
LDV
7270A

(c)

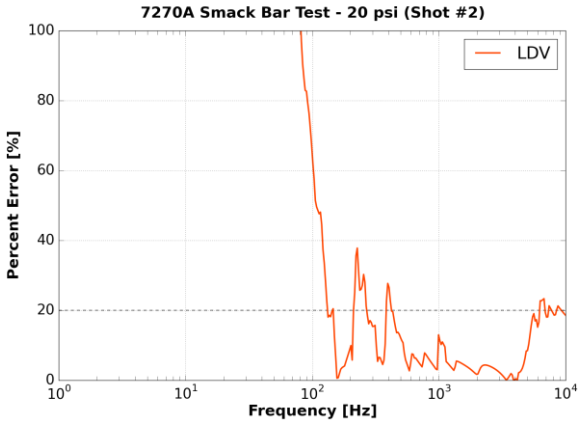
7270A Smack Bar Test - 20 psi (Shot #2)
Percent Error [%]
Frequency [Hz]
LDV

(d)

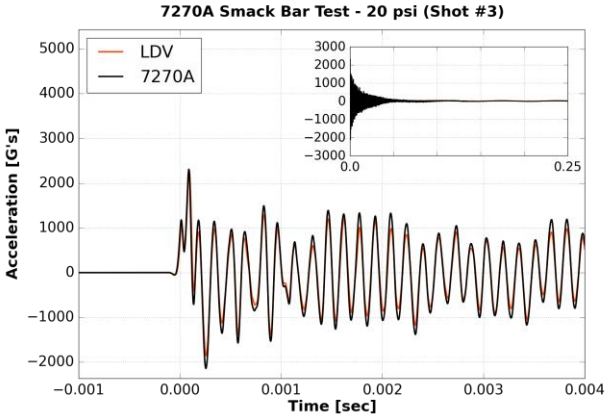
7270A Smack Bar Test - 20 psi (Shot #3)
Acceleration [G's]
Time [sec]
LDV
7270A

(a)

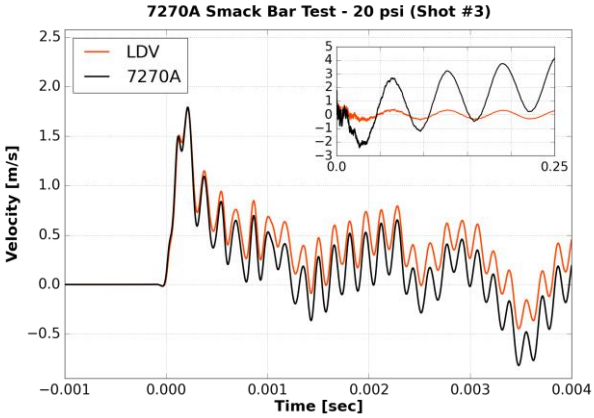
7270A Smack Bar Test - 20 psi (Shot #3)
Velocity [m/s]
Time [sec]
LDV
7270A

(b)

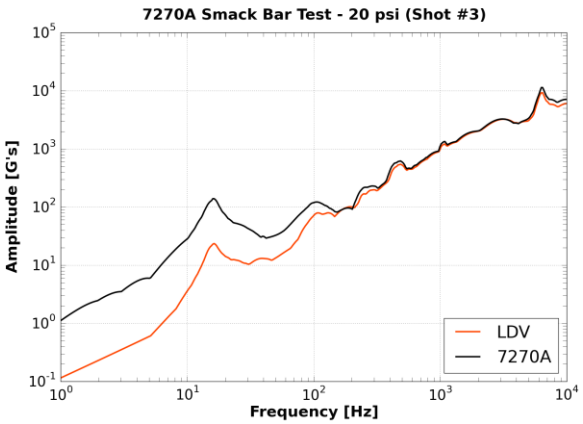
7270A Smack Bar Test - 20 psi (Shot #3)
Amplitude [G's]
Frequency [Hz]
LDV
7270A

(c)

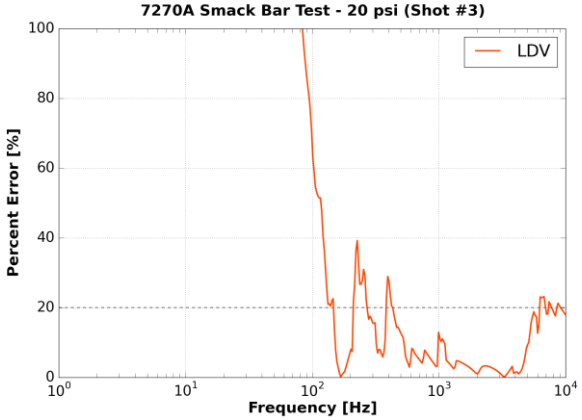
7270A Smack Bar Test - 20 psi (Shot #3)
Percent Error [%]
Frequency [Hz]
LDV

(d)

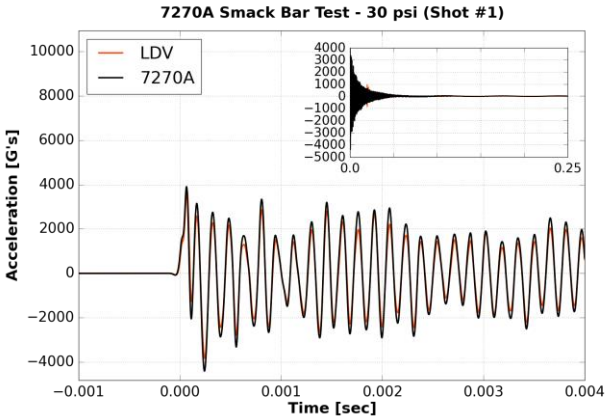
7270A Smack Bar Test - 30 psi (Shot #1)
LDV
7270A
Acceleration [G's]
Time [sec]

(a)

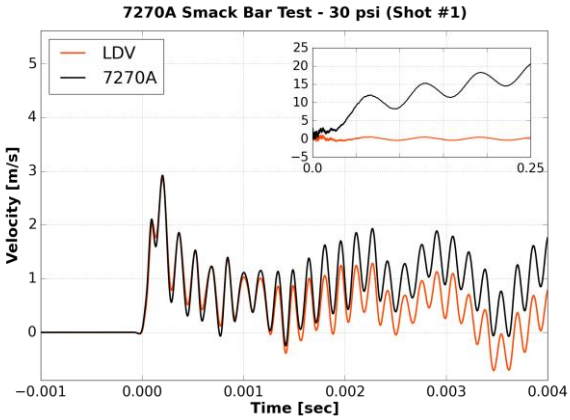
7270A Smack Bar Test - 30 psi (Shot #1)
LDV
7270A
Velocity [m/s]
Time [sec]

(b)

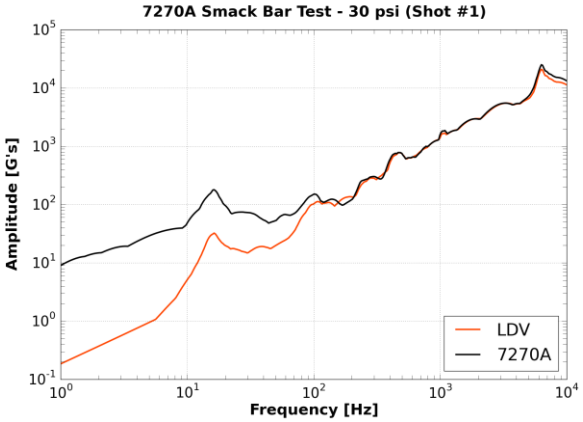
7270A Smack Bar Test - 30 psi (Shot #1)
LDV
7270A
Amplitude [G's]
Frequency [Hz]

(c)

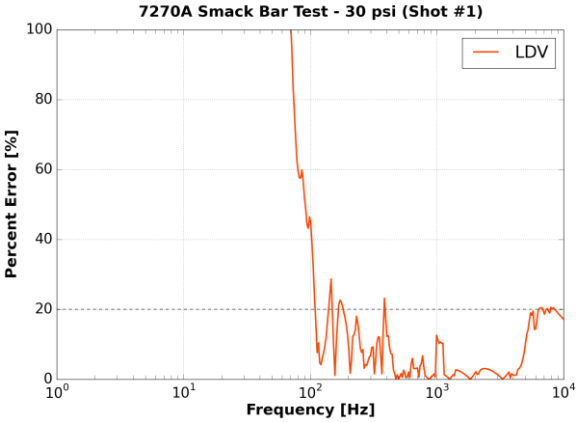
7270A Smack Bar Test - 30 psi (Shot #1)
LDV
Percent Error [%]
Frequency [Hz]

(d)

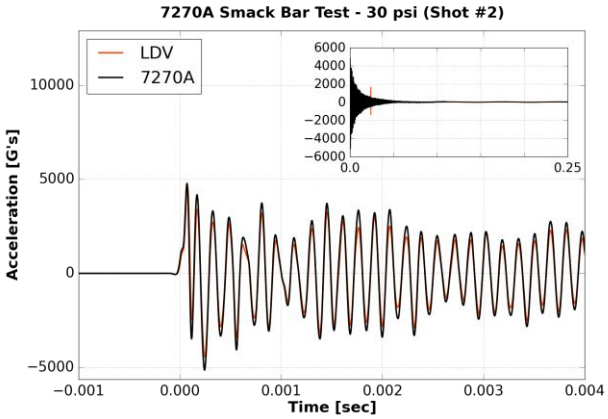
7270A Smack Bar Test - 30 psi (Shot #2)
LDV
7270A
Acceleration [G's]
Time [sec]

(a)

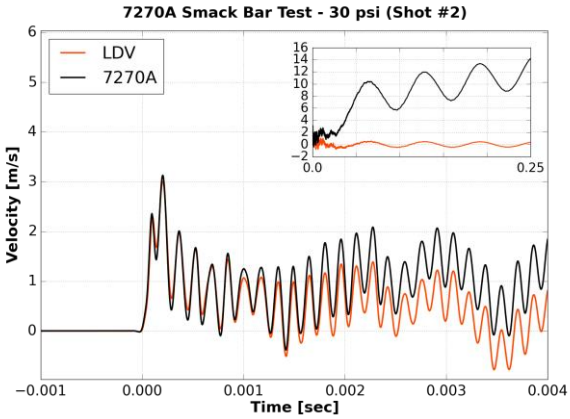
7270A Smack Bar Test - 30 psi (Shot #2)
LDV
7270A
Velocity [m/s]
Time [sec]

(b)

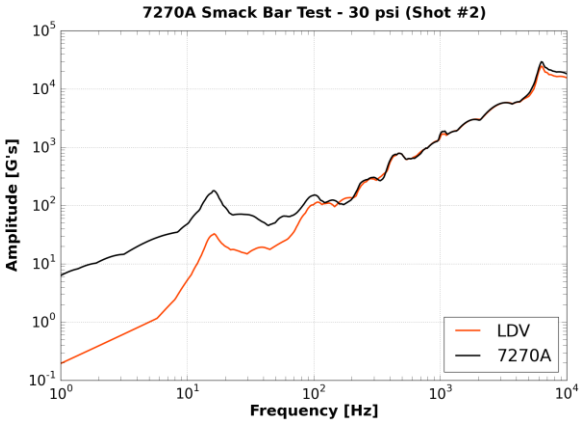
7270A Smack Bar Test - 30 psi (Shot #2)
Amplitude [G's]
Frequency [Hz]
LDV
7270A

(c)

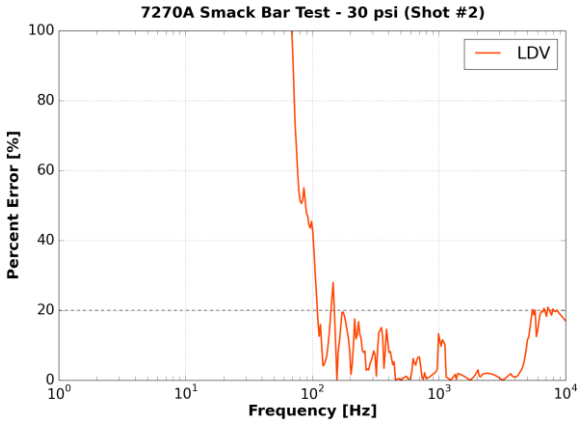
7270A Smack Bar Test - 30 psi (Shot #2)
Percent Error [%]
Frequency [Hz]
LDV

(d)

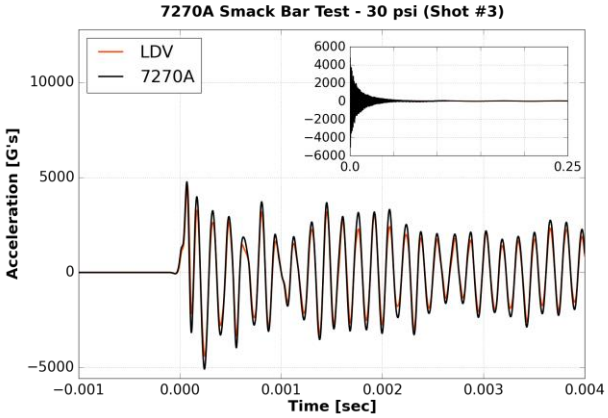
7270A Smack Bar Test - 30 psi (Shot #3)
Acceleration [G's]
Time [sec]
LDV
7270A

(a)

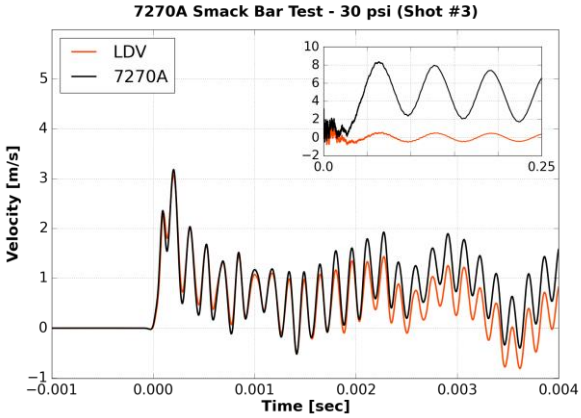
7270A Smack Bar Test - 30 psi (Shot #3)
Velocity [m/s]
Time [sec]
LDV
7270A

(b)

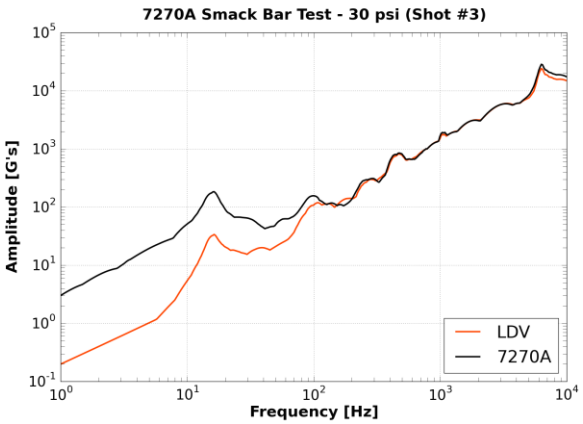
7270A Smack Bar Test - 30 psi (Shot #3)
Amplitude [G's]
Frequency [Hz]
LDV
7270A

(c)

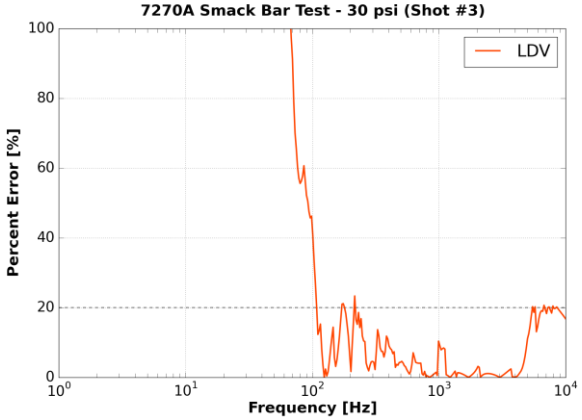
7270A Smack Bar Test - 30 psi (Shot #3)
Percent Error [%]
Frequency [Hz]
LDV

(d)

ii. Endevco 7280A

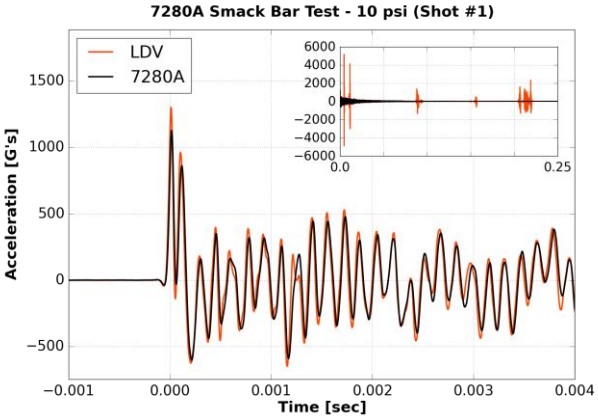

(a)

(b)

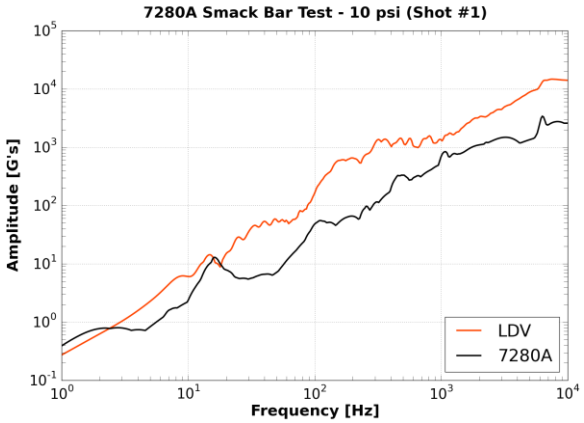

(c)

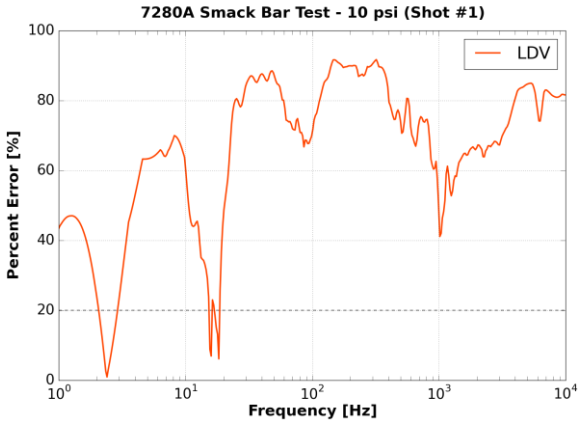

(d)

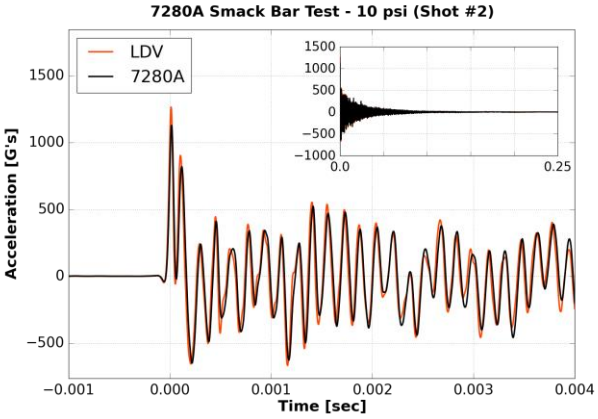

(a)

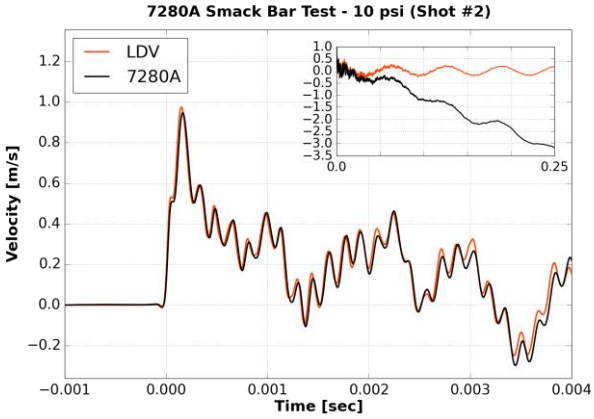

(b)

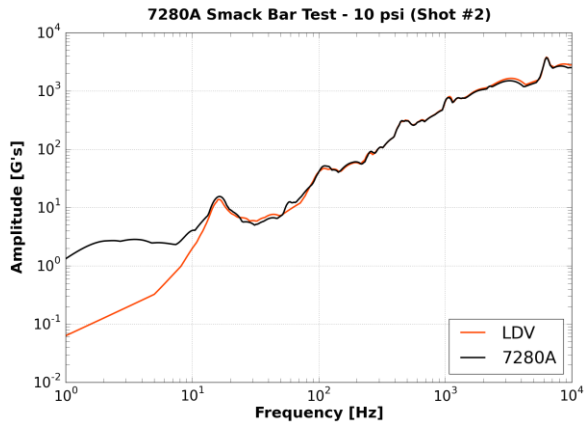
7280A Smack Bar Test - 10 psi (Shot #2)
Amplitude [G's]
Frequency [Hz]
LDV
7280A

(c)

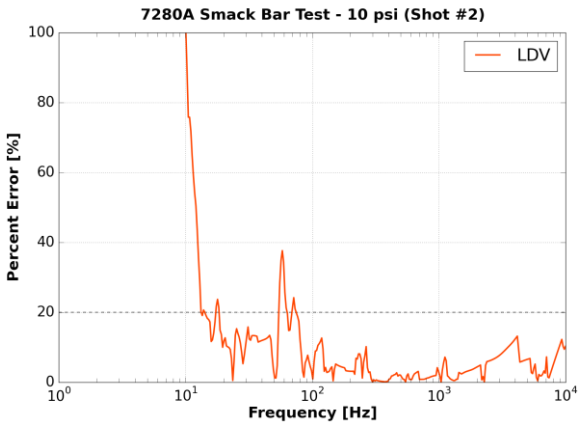
7280A Smack Bar Test - 10 psi (Shot #2)
Percent Error [%]
Frequency [Hz]
LDV

(d)

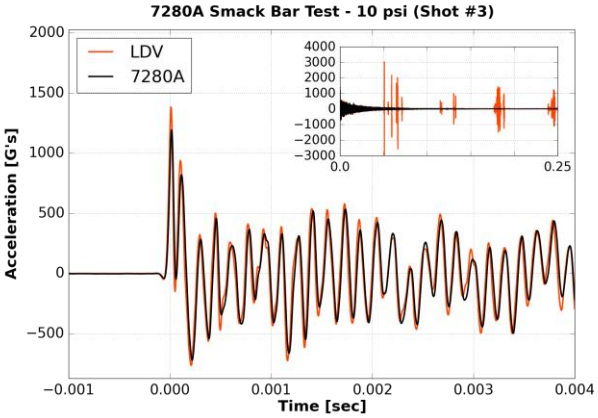
7280A Smack Bar Test - 10 psi (Shot #3)
Acceleration [G's]
Time [sec]
LDV
7280A

(a)

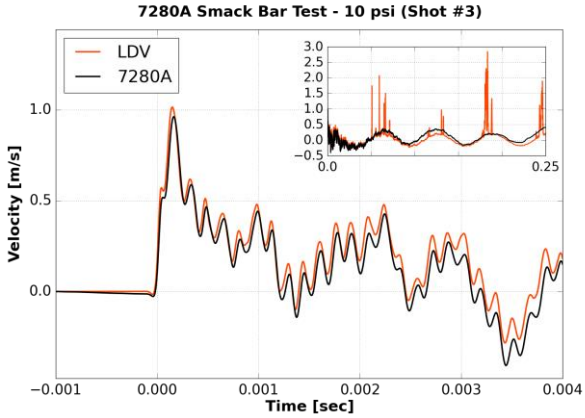
7280A Smack Bar Test - 10 psi (Shot #3)
Velocity [m/s]
Time [sec]
LDV
7280A

(b)

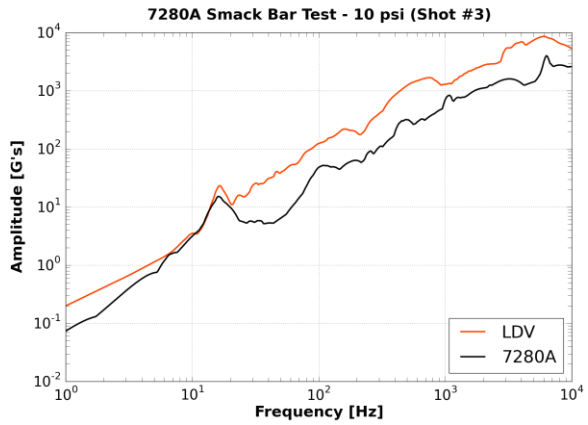
7280A Smack Bar Test - 10 psi (Shot #3)
Amplitude [G's]
Frequency [Hz]
LDV
7280A

(c)

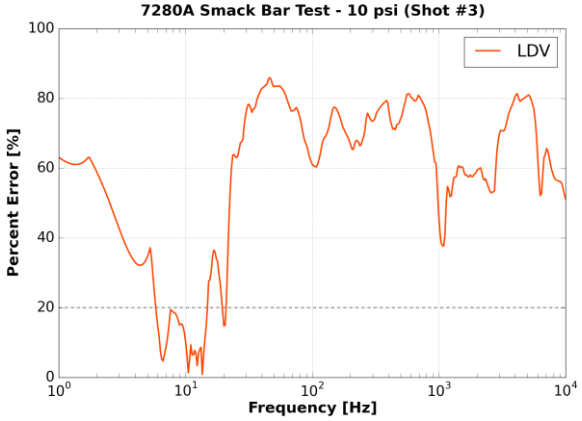
7280A Smack Bar Test - 10 psi (Shot #3)
Percent Error [%]
Frequency [Hz]
LDV

(d)

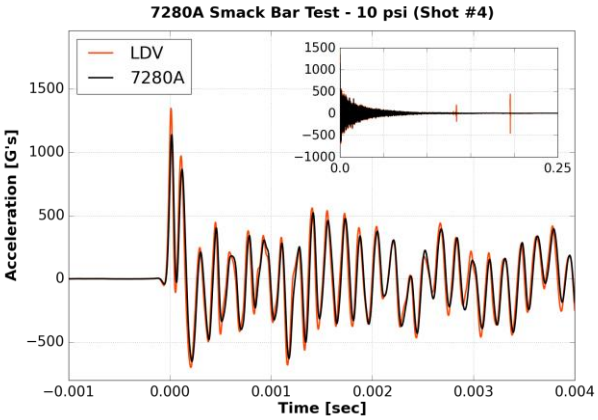
7280A Smack Bar Test - 10 psi (Shot #4)
LDV
7280A
Acceleration [G's]
Time [sec]

(a)

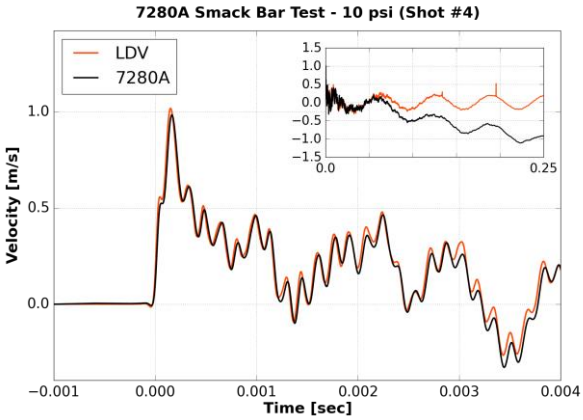
7280A Smack Bar Test - 10 psi (Shot #4)
LDV
7280A
Velocity [m/s]
Time [sec]

(b)

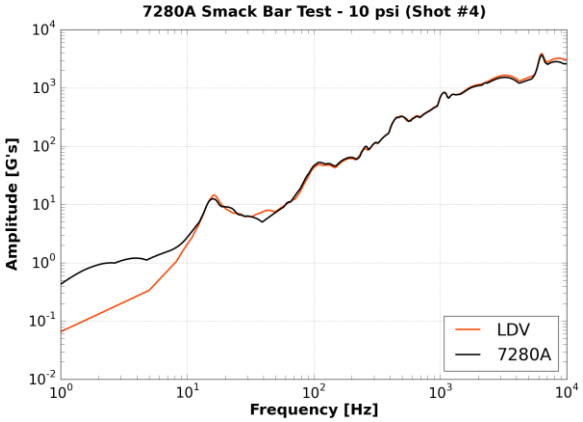
7280A Smack Bar Test - 10 psi (Shot #4)
LDV
7280A
Amplitude [G's]
Frequency [Hz]

(c)

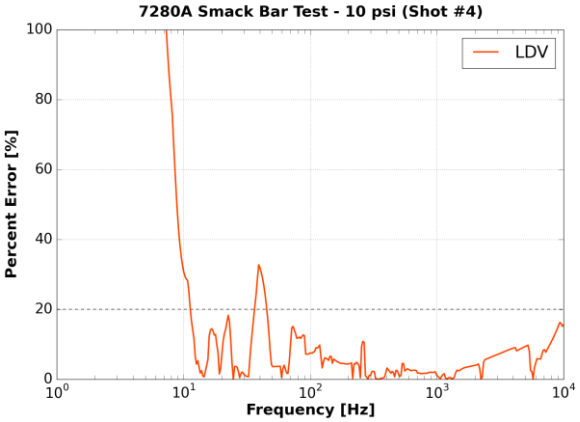
7280A Smack Bar Test - 10 psi (Shot #4)
LDV
Percent Error [%]
Frequency [Hz]

(d)

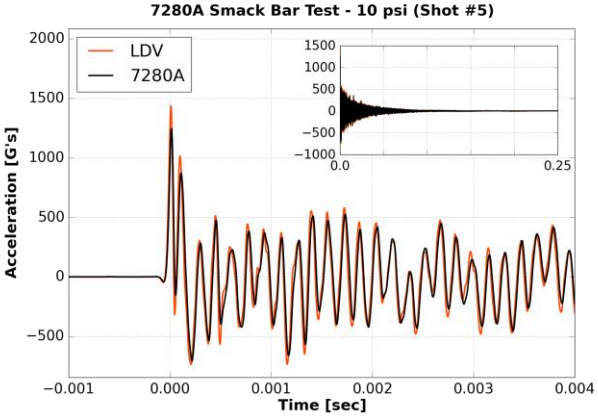
7280A Smack Bar Test - 10 psi (Shot #5)
LDV
7280A
Acceleration [G's]
Time [sec]

(a)

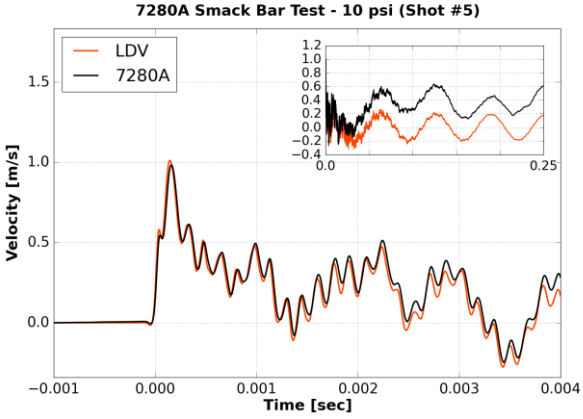
7280A Smack Bar Test - 10 psi (Shot #5)
LDV
7280A
Velocity [m/s]
Time [sec]

(b)

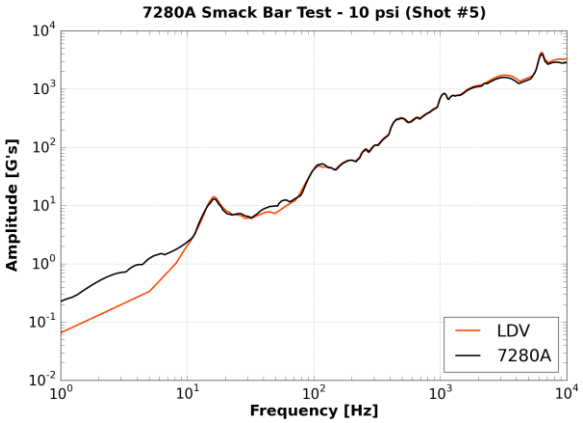
7280A Smack Bar Test - 10 psi (Shot #5)
Amplitude [G's]
Frequency [Hz]
LDV
7280A

(c)

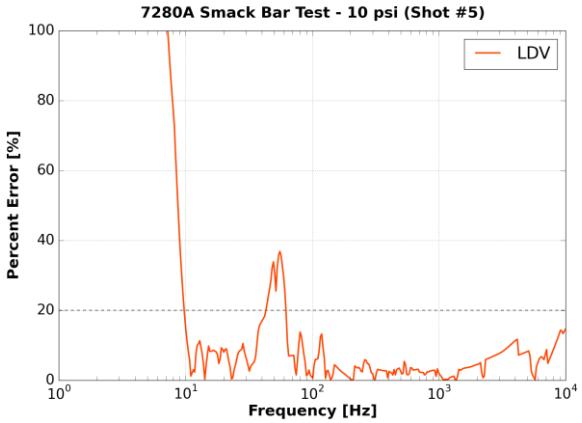
7280A Smack Bar Test - 10 psi (Shot #5)
Percent Error [%]
Frequency [Hz]
LDV

(d)

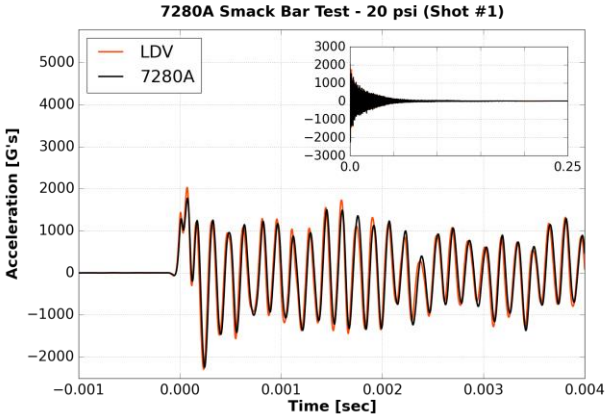
7280A Smack Bar Test - 20 psi (Shot #1)
Acceleration [G's]
Time [sec]
LDV
7280A

(a)

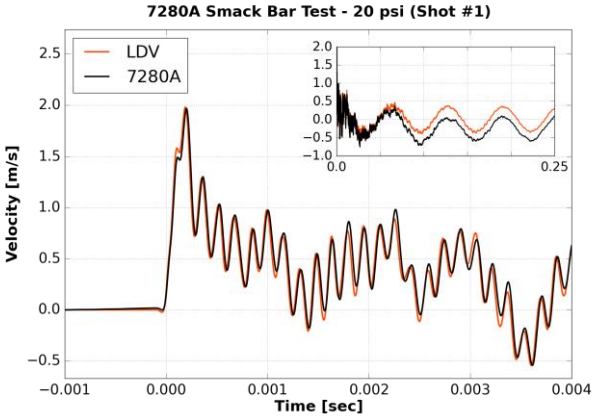
7280A Smack Bar Test - 20 psi (Shot #1)
Velocity [m/s]
Time [sec]
LDV
7280A

(b)

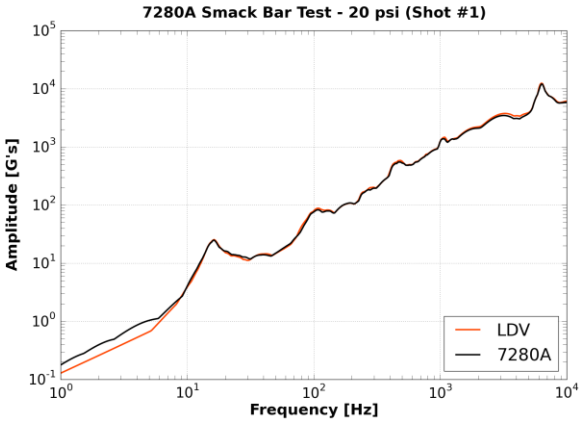
7280A Smack Bar Test - 20 psi (Shot #1)
Amplitude [G's]
Frequency [Hz]
LDV
7280A

(c)

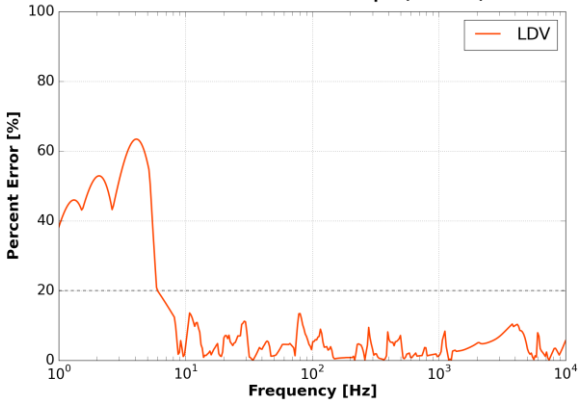
7280A Smack Bar Test - 20 psi (Shot #1)
Percent Error [%]
Frequency [Hz]
LDV

(d)

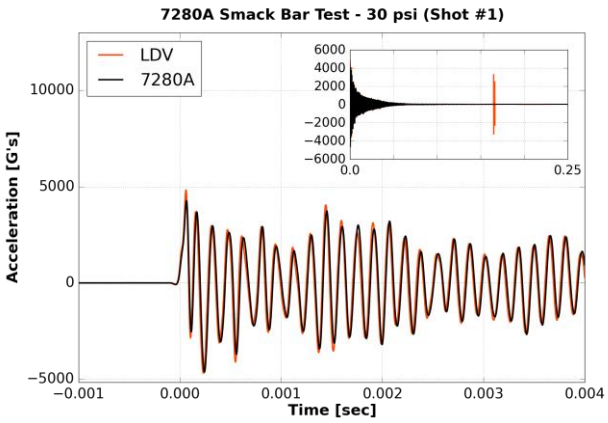
7280A Smack Bar Test - 30 psi (Shot #1)
LDV
7280A
Acceleration [G's]
Time [sec]

(a)

7280A Smack Bar Test - 30 psi (Shot #1)
LDV
7280A
Velocity [m/s]
Time [sec]

(b)

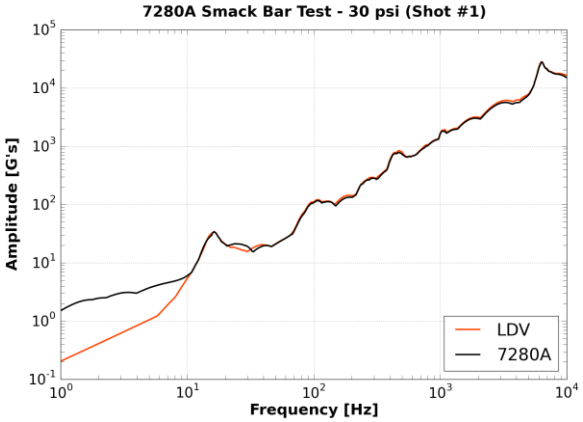
7280A Smack Bar Test - 30 psi (Shot #1)
LDV
7280A
Amplitude [G's]
Frequency [Hz]

(c)

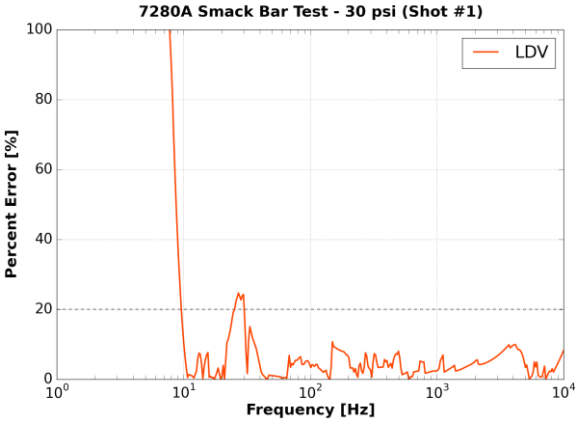
7280A Smack Bar Test - 30 psi (Shot #1)
LDV
Percent Error [%]
Frequency [Hz]

(d)

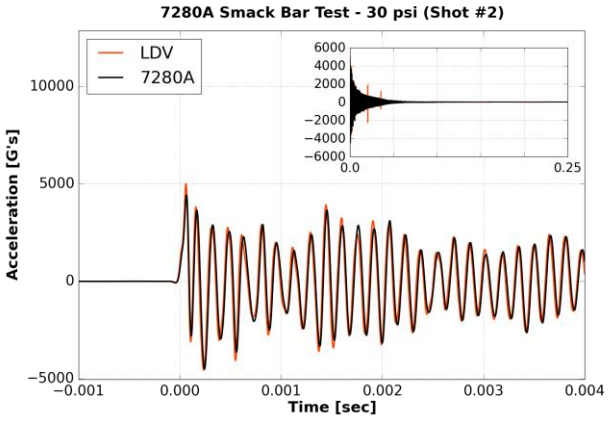
7280A Smack Bar Test - 30 psi (Shot #2)
LDV
7280A
Acceleration [G's]
Time [sec]

(a)

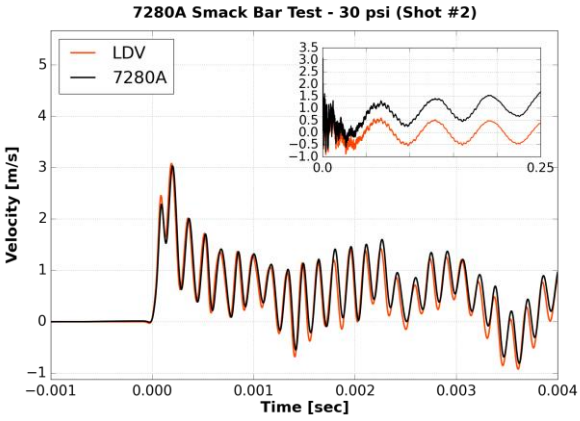
7280A Smack Bar Test - 30 psi (Shot #2)
LDV
7280A
Velocity [m/s]
Time [sec]

(b)

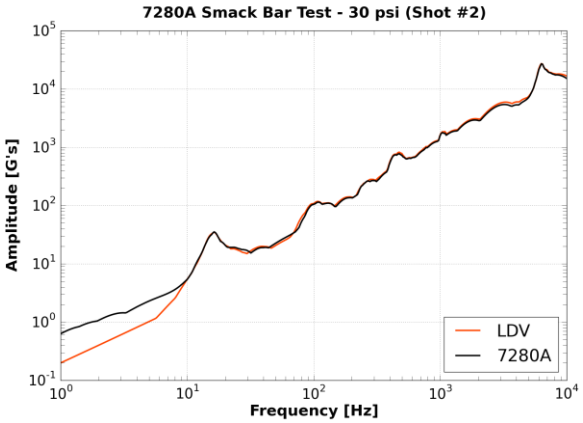
7280A Smack Bar Test - 30 psi (Shot #2)
Amplitude [G's]
Frequency [Hz]
LDV
7280A

(c)

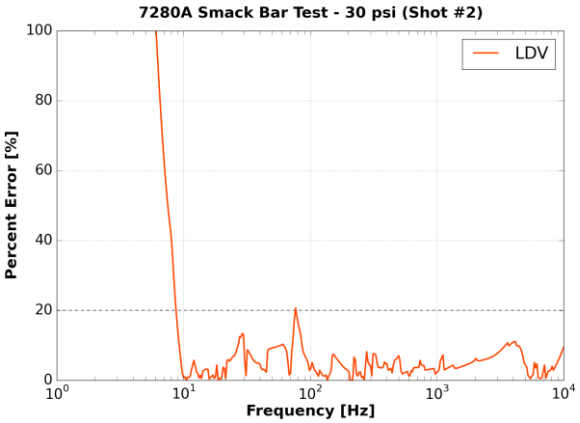
7280A Smack Bar Test - 30 psi (Shot #2)
Percent Error [%]
Frequency [Hz]
LDV

(d)

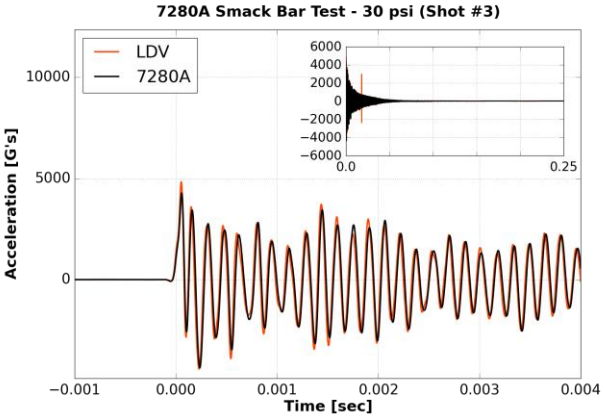
7280A Smack Bar Test - 30 psi (Shot #3)
Acceleration [G's]
Time [sec]
LDV
7280A

(a)

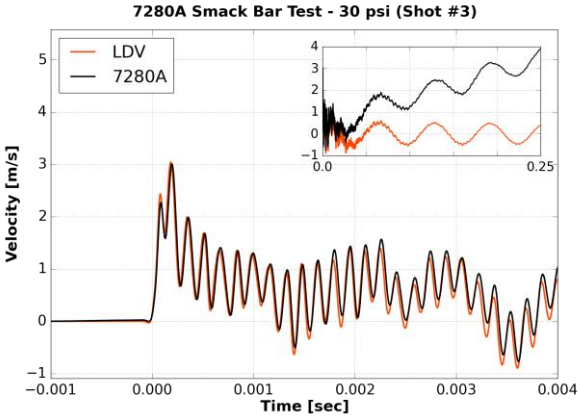
7280A Smack Bar Test - 30 psi (Shot #3)
Velocity [m/s]
Time [sec]
LDV
7280A

(b)

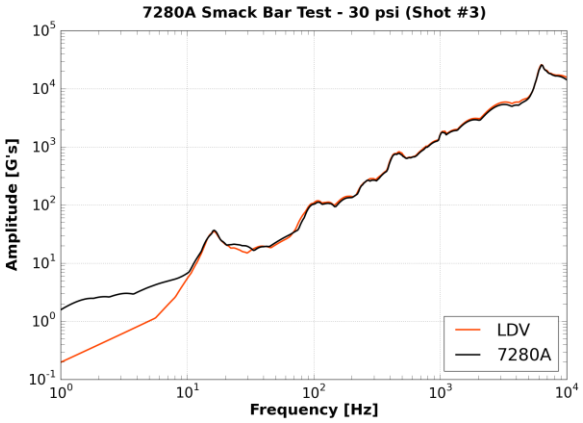
7280A Smack Bar Test - 30 psi (Shot #3)
Amplitude [G's]
Frequency [Hz]
LDV
7280A

(c)

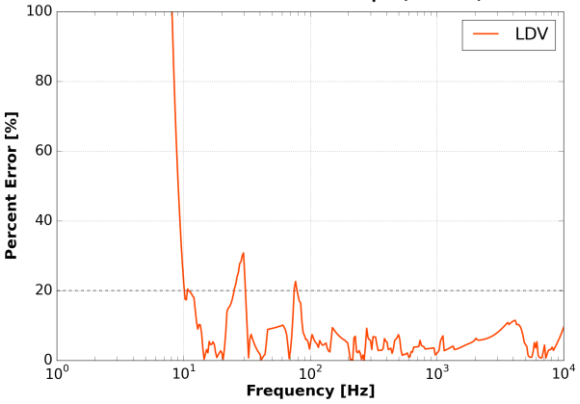
7280A Smack Bar Test - 30 psi (Shot #3)
Percent Error [%]
Frequency [Hz]
LDV

(d)

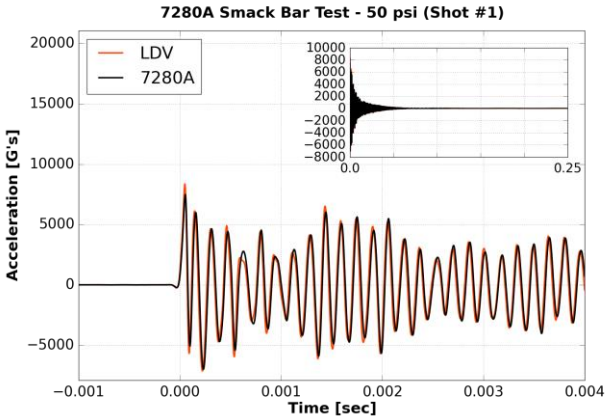
7280A Smack Bar Test - 50 psi (Shot #1)
LDV
7280A
Acceleration [G's]
Time [sec]

(a)

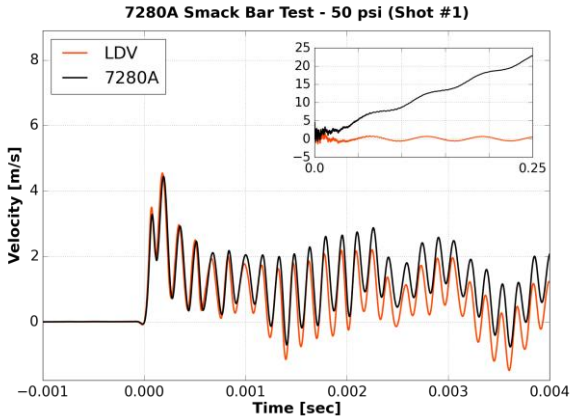
7280A Smack Bar Test - 50 psi (Shot #1)
LDV
7280A
Velocity [m/s]
Time [sec]

(b)

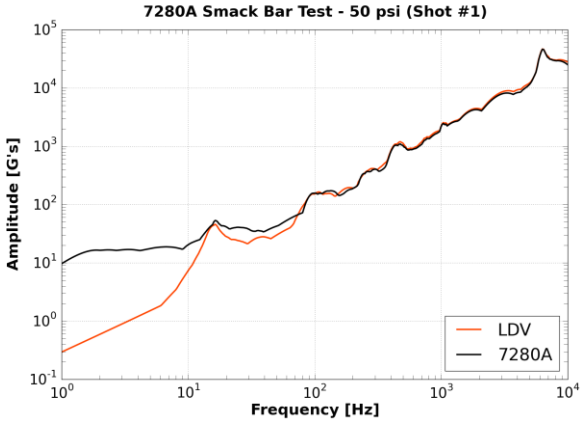
7280A Smack Bar Test - 50 psi (Shot #1)
LDV
7280A
Amplitude [G's]
Frequency [Hz]

(c)

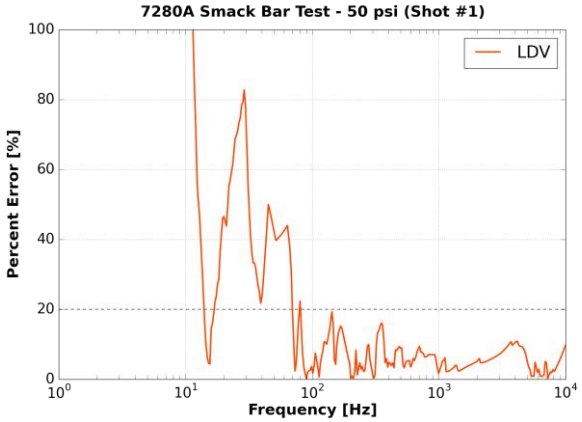
7280A Smack Bar Test - 50 psi (Shot #1)
LDV
Percent Error [%]
Frequency [Hz]

(d)

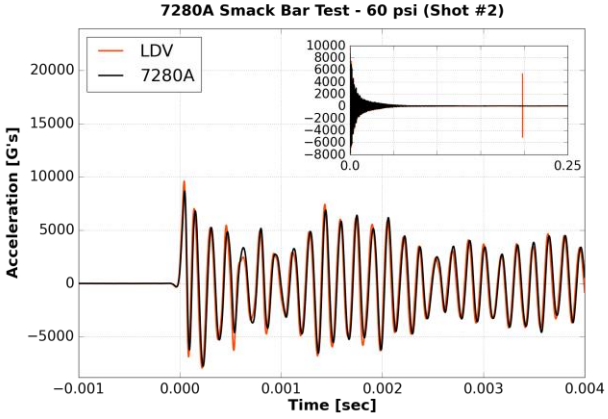
7280A Smack Bar Test - 60 psi (Shot #2)
LDV
7280A
Acceleration [G's]
Time [sec]

(a)

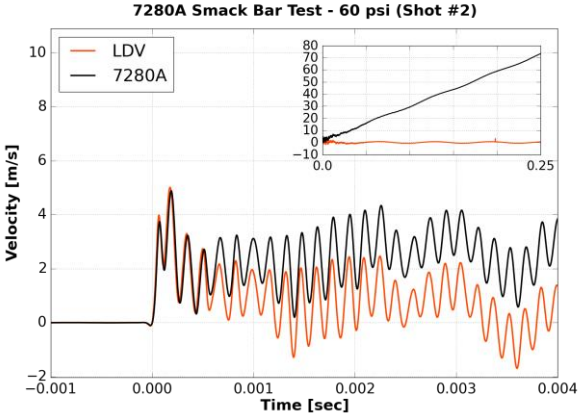
7280A Smack Bar Test - 60 psi (Shot #2)
LDV
7280A
Velocity [m/s]
Time [sec]

(b)

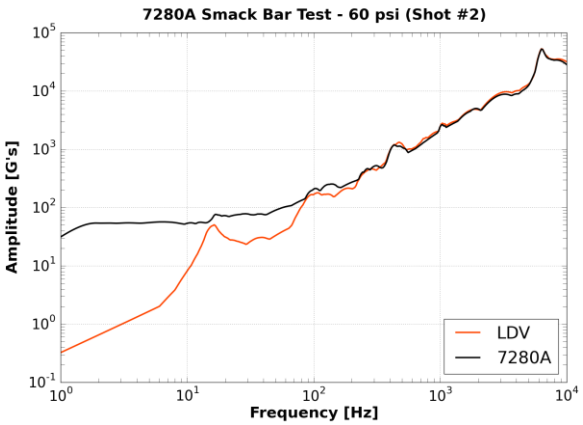
7280A Smack Bar Test - 60 psi (Shot #2)
Amplitude [G's]
Frequency [Hz]
LDV
7280A

(c)

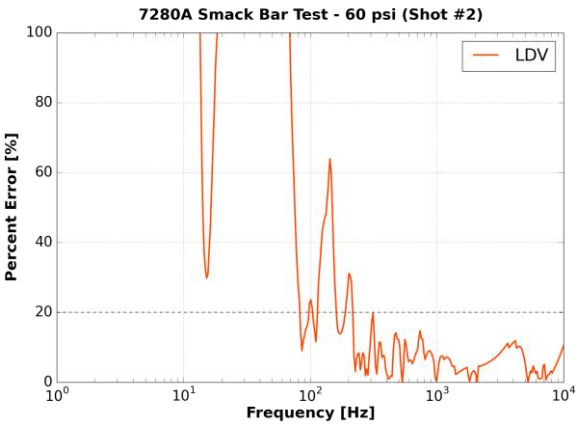
7280A Smack Bar Test - 60 psi (Shot #2)
Percent Error [%]
Frequency [Hz]
LDV

(d)

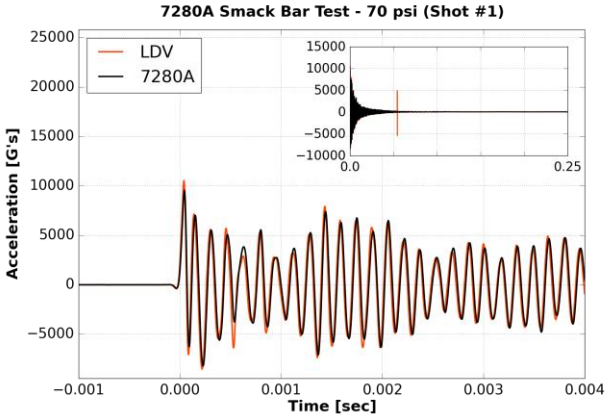
7280A Smack Bar Test - 70 psi (Shot #1)
Acceleration [G's]
Time [sec]
LDV
7280A

(a)

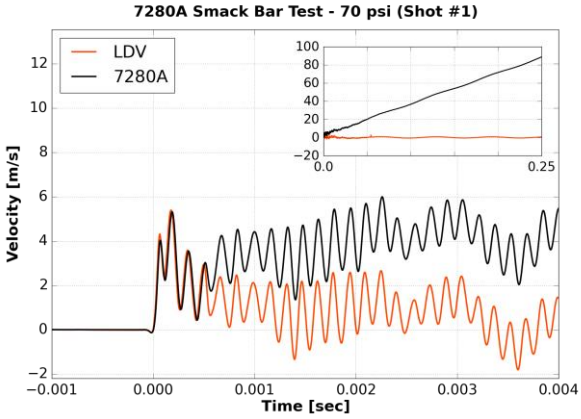
7280A Smack Bar Test - 70 psi (Shot #1)
Velocity [m/s]
Time [sec]
LDV
7280A

(b)

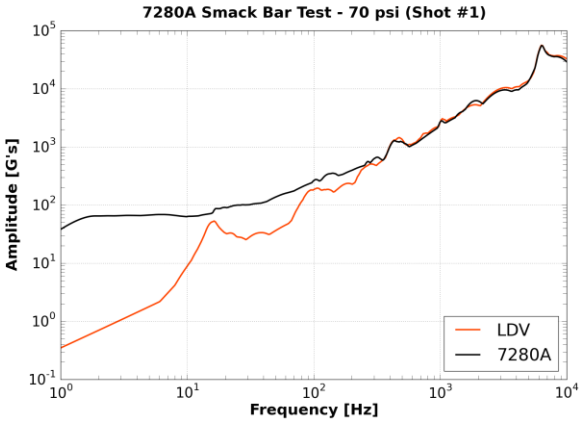
7280A Smack Bar Test - 70 psi (Shot #1)
Amplitude [G's]
Frequency [Hz]
LDV
7280A

(c)

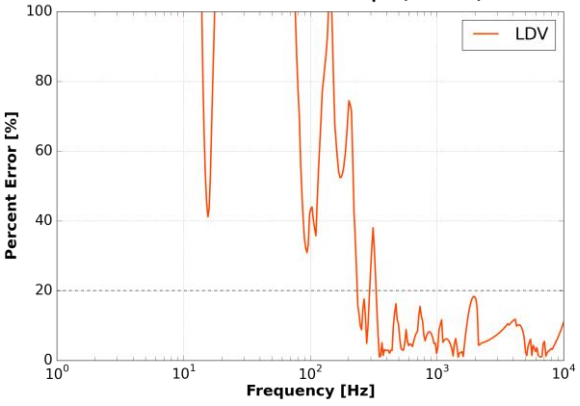
7280A Smack Bar Test - 70 psi (Shot #1)
Percent Error [%]
Frequency [Hz]
LDV

(d)

iii. Endevco 2262A

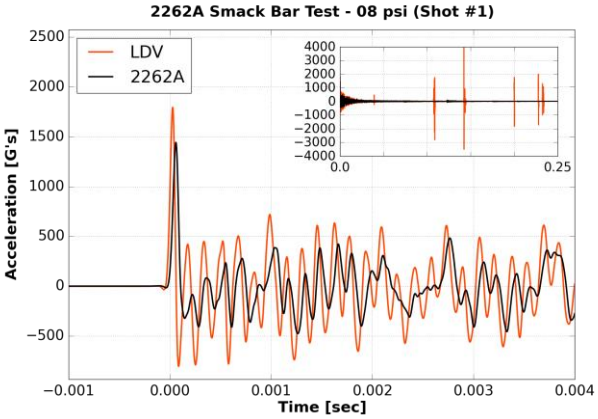

(a)

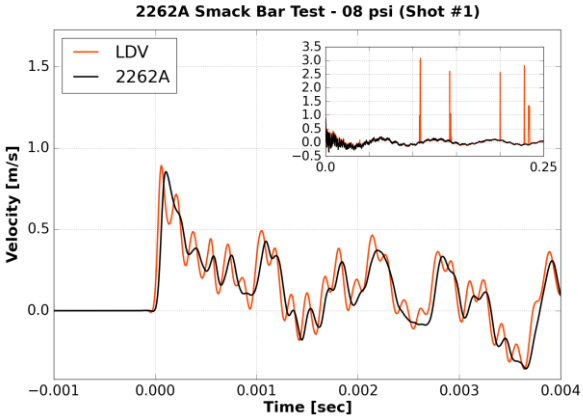

(b)

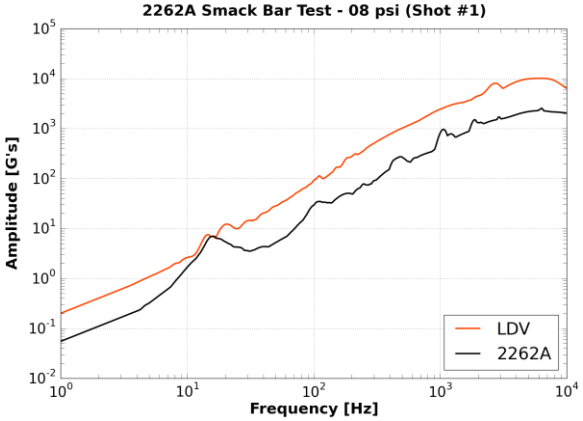

(c)

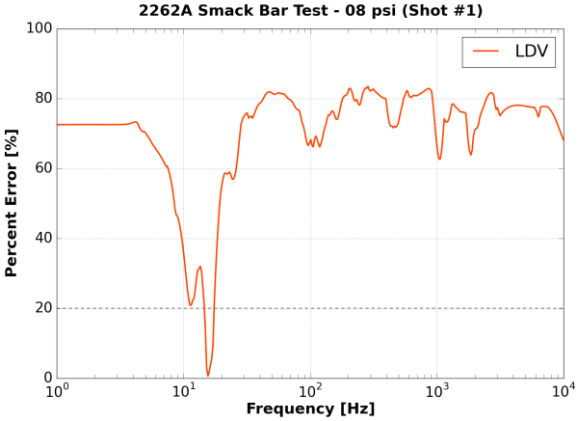

(d)

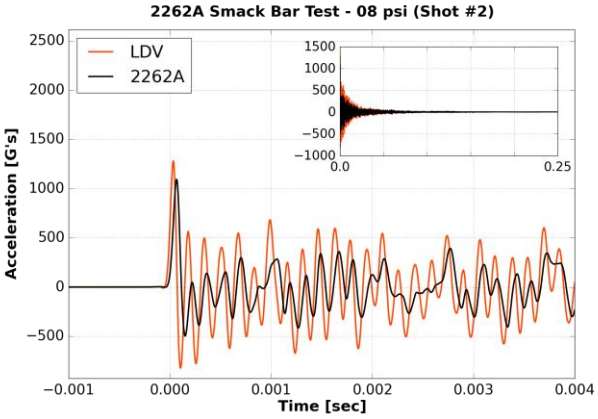

(a)

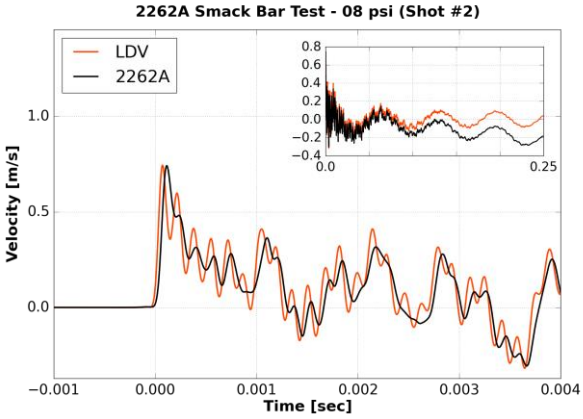

(b)

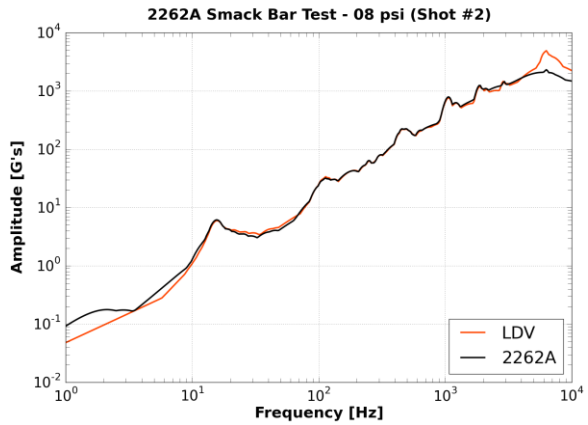
2262A Smack Bar Test - 08 psi (Shot #2)
Amplitude [G's]
Frequency [Hz]
LDV
2262A

(c)

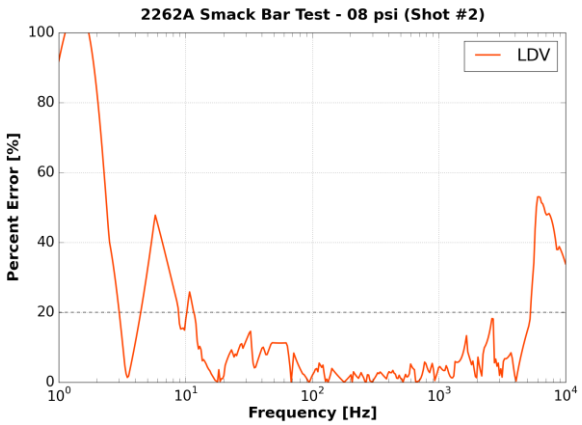
2262A Smack Bar Test - 08 psi (Shot #2)
Percent Error [%]
Frequency [Hz]
LDV

(d)

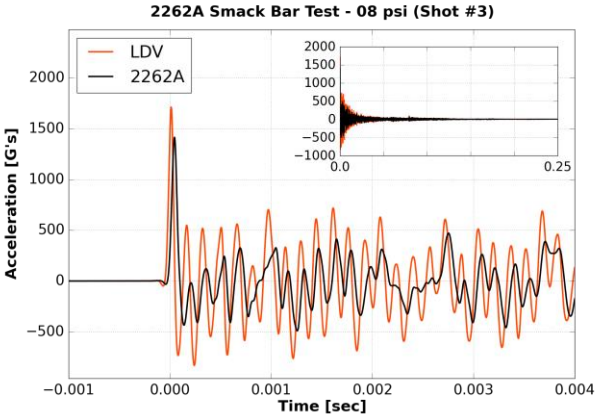
2262A Smack Bar Test - 08 psi (Shot #3)
Acceleration [G's]
Time [sec]
LDV
2262A

(a)

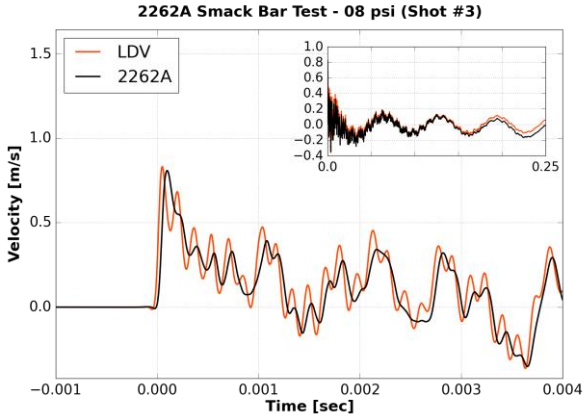
2262A Smack Bar Test - 08 psi (Shot #3)
Velocity [m/s]
Time [sec]
LDV
2262A

(b)

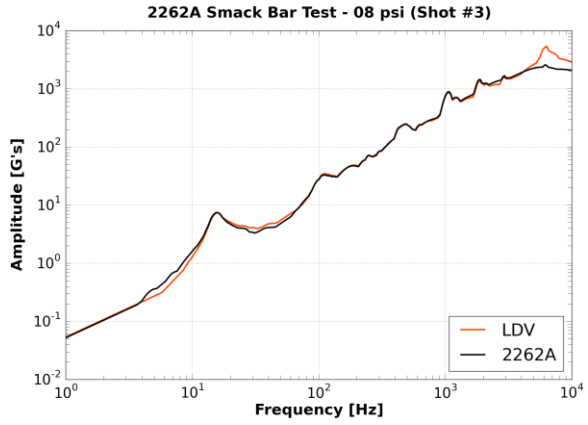
2262A Smack Bar Test - 08 psi (Shot #3)
Amplitude [G's]
Frequency [Hz]
LDV
2262A

(c)

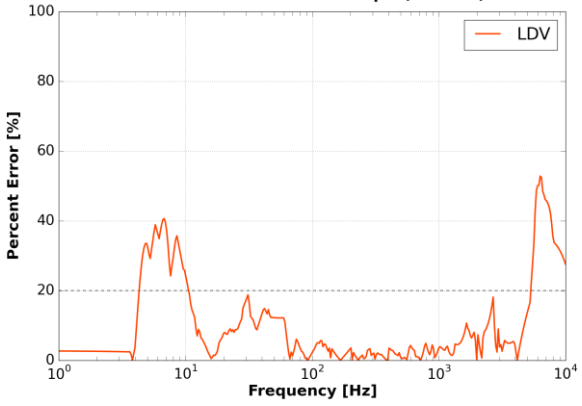
2262A Smack Bar Test - 08 psi (Shot #3)
Percent Error [%]
Frequency [Hz]
LDV

(d)

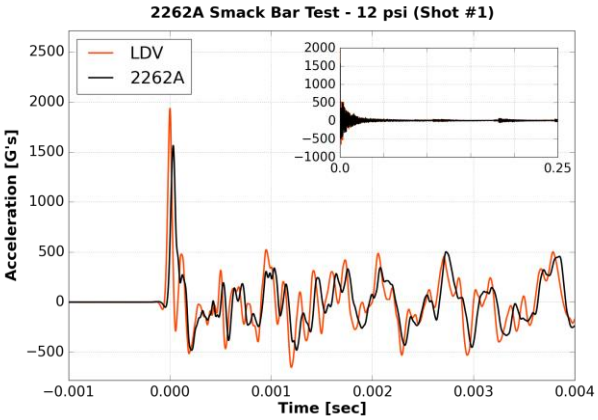
2262A Smack Bar Test - 12 psi (Shot #1)
LDV
2262A
Acceleration [G's]
Time [sec]

(a)

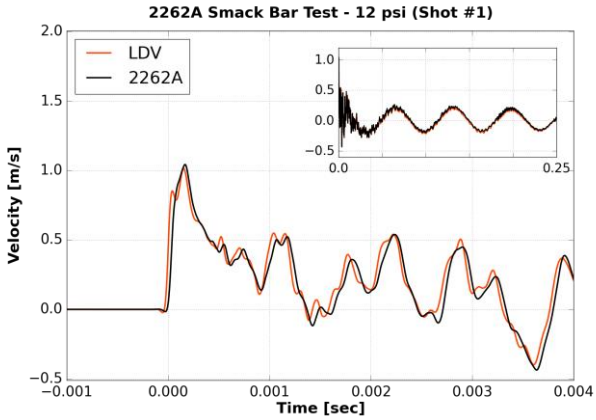
2262A Smack Bar Test - 12 psi (Shot #1)
LDV
2262A
Velocity [m/s]
Time [sec]

(b)

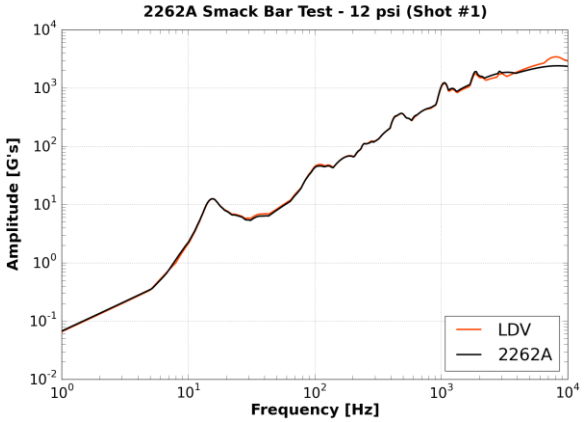
2262A Smack Bar Test - 12 psi (Shot #1)
LDV
2262A
Amplitude [G's]
Frequency [Hz]

(c)

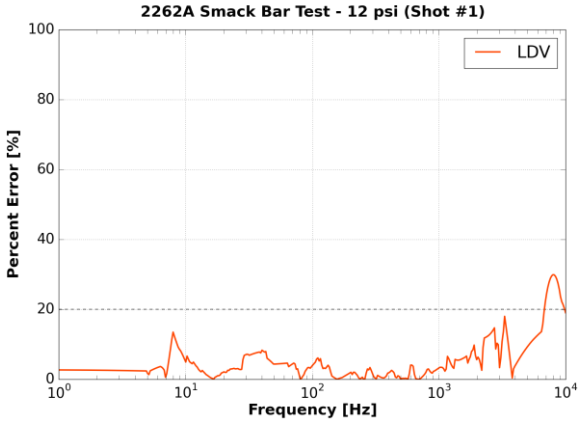
2262A Smack Bar Test - 12 psi (Shot #1)
LDV
Percent Error [%]
Frequency [Hz]

(d)

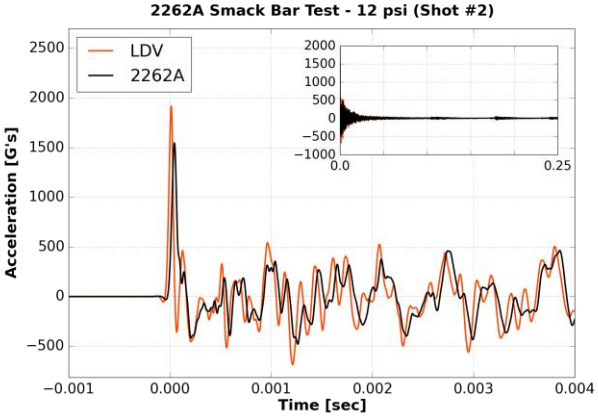
2262A Smack Bar Test - 12 psi (Shot #2)
LDV
2262A
Acceleration [G's]
Time [sec]

(a)

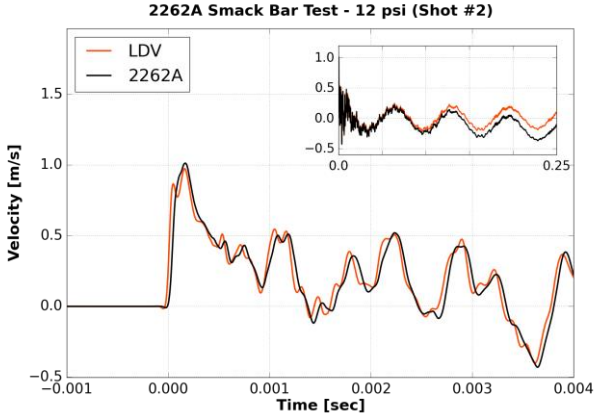
2262A Smack Bar Test - 12 psi (Shot #2)
LDV
2262A
Velocity [m/s]
Time [sec]

(b)

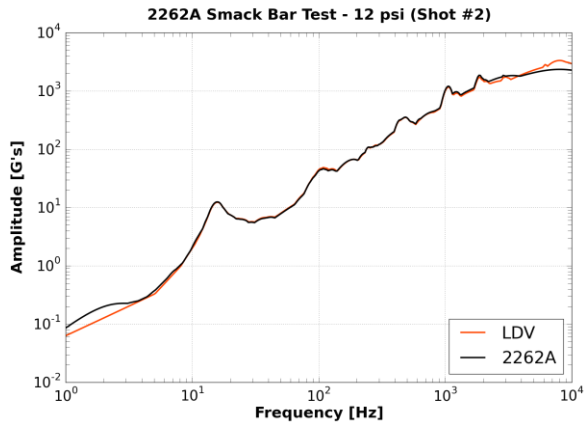
2262A Smack Bar Test - 12 psi (Shot #2)
Amplitude [G's]
Frequency [Hz]
LDV
2262A

(c)

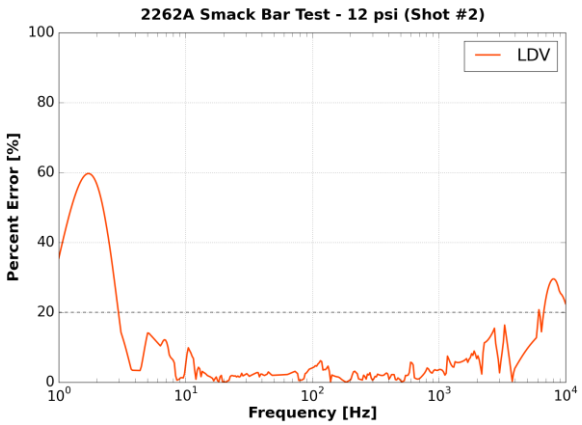
2262A Smack Bar Test - 12 psi (Shot #2)
Percent Error [%]
Frequency [Hz]
LDV

(d)

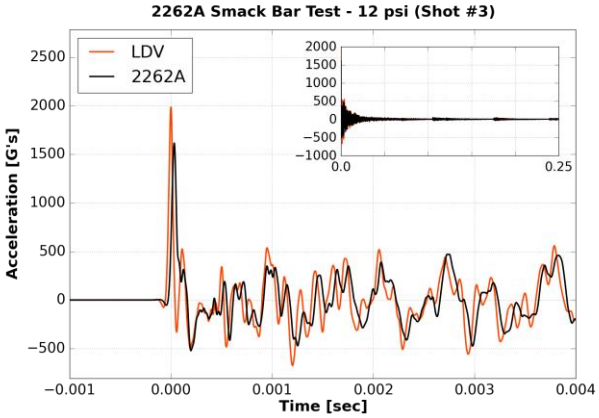
2262A Smack Bar Test - 12 psi (Shot #3)
Acceleration [G's]
Time [sec]
LDV
2262A

(a)

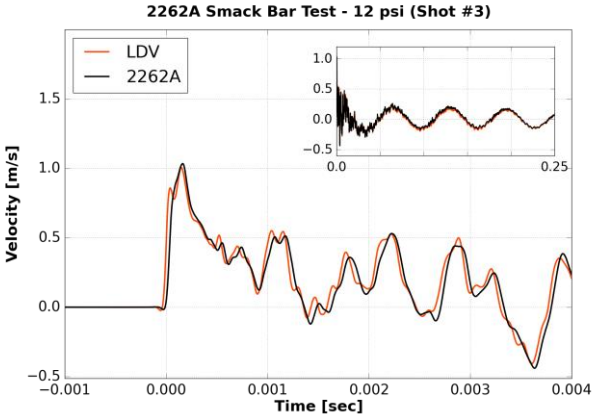
2262A Smack Bar Test - 12 psi (Shot #3)
Velocity [m/s]
Time [sec]
LDV
2262A

(b)

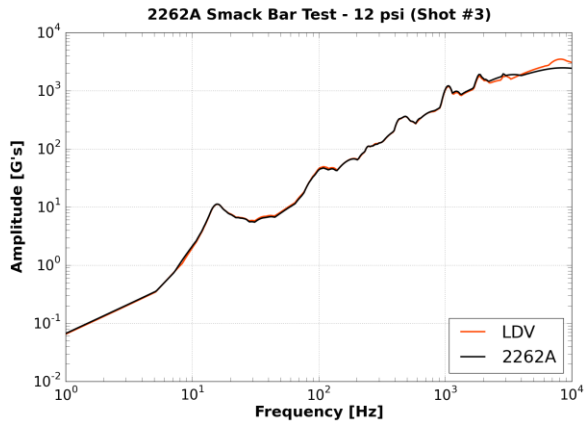
2262A Smack Bar Test - 12 psi (Shot #3)
Amplitude [G's]
Frequency [Hz]
LDV
2262A

(c)

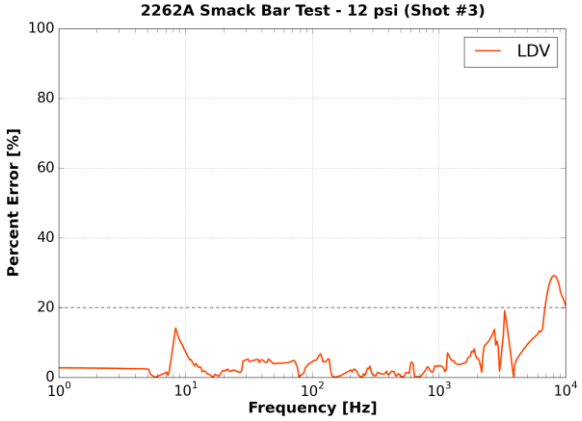
2262A Smack Bar Test - 12 psi (Shot #3)
Percent Error [%]
Frequency [Hz]
LDV

(d)

iv. Endevco 7270AM6

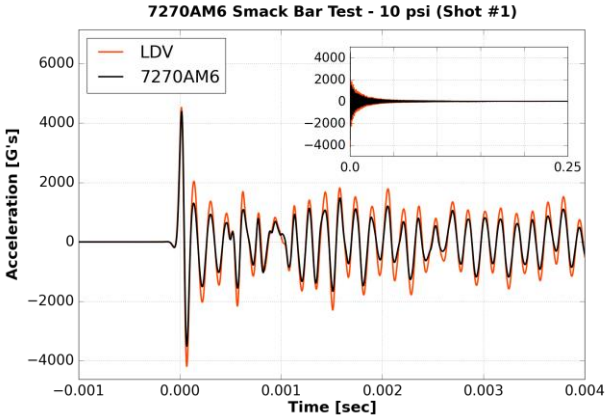

(a)

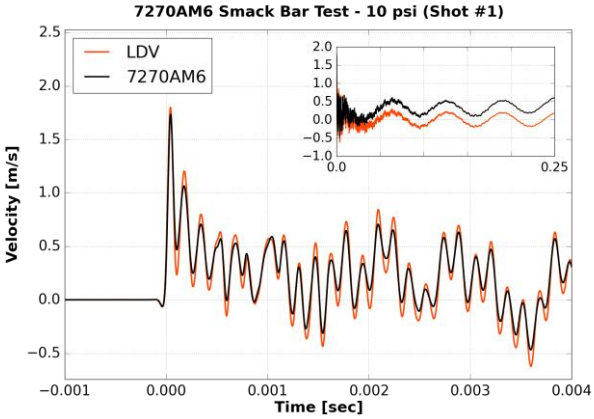

(b)

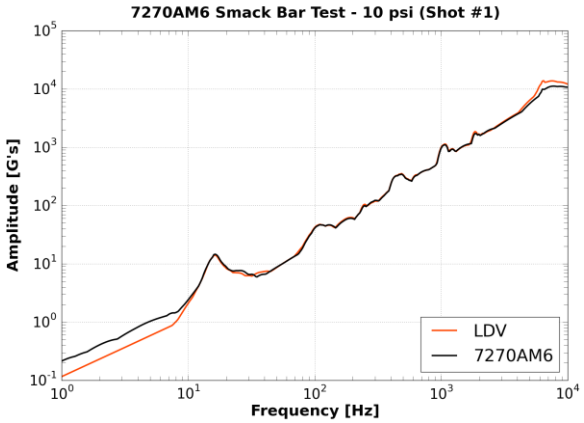

(c)

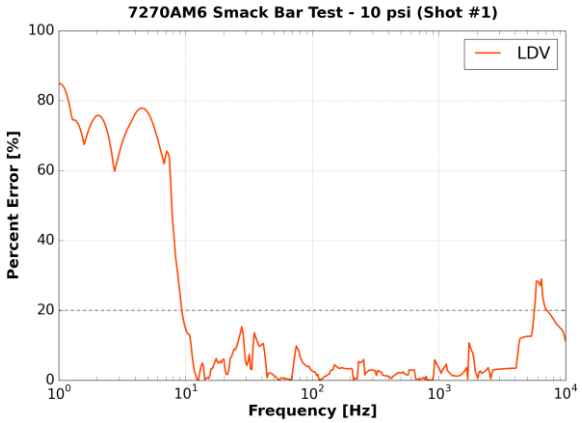

(d)

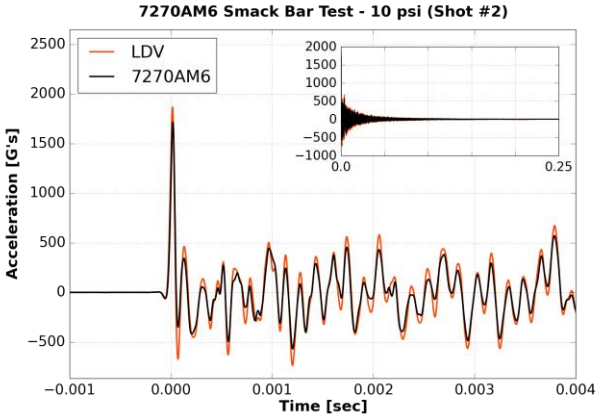

(a)

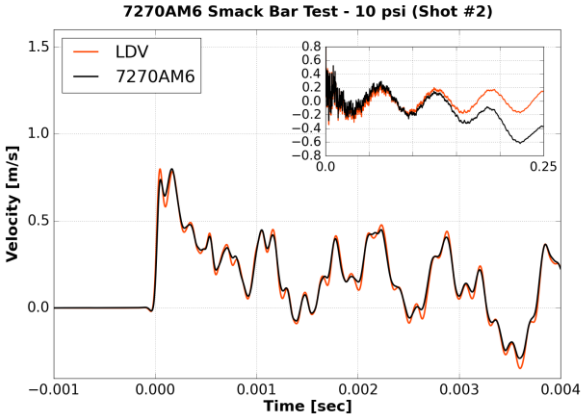

(b)

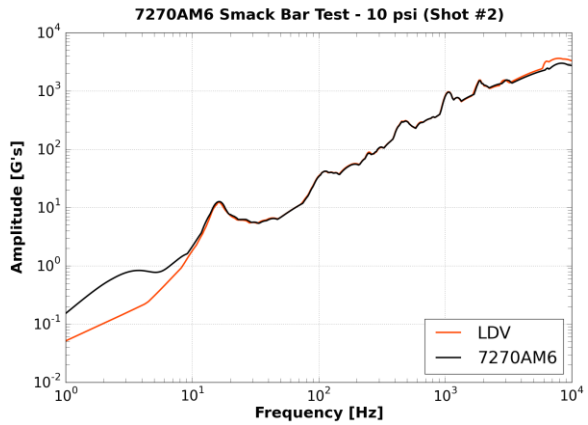
7270AM6 Smack Bar Test - 10 psi (Shot #2)
Amplitude [G's]
Frequency [Hz]
LDV
7270AM6

(c)

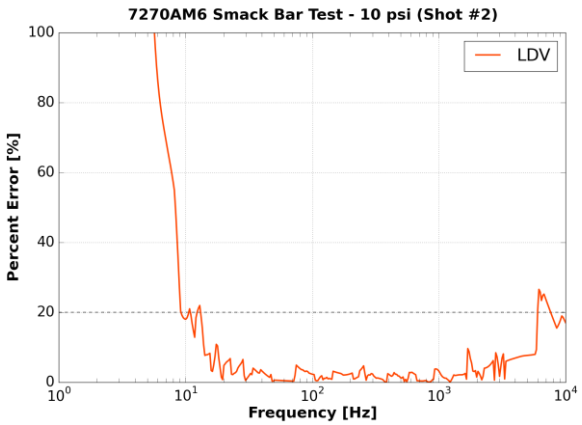
7270AM6 Smack Bar Test - 10 psi (Shot #2)
Percent Error [%]
Frequency [Hz]
LDV

(d)

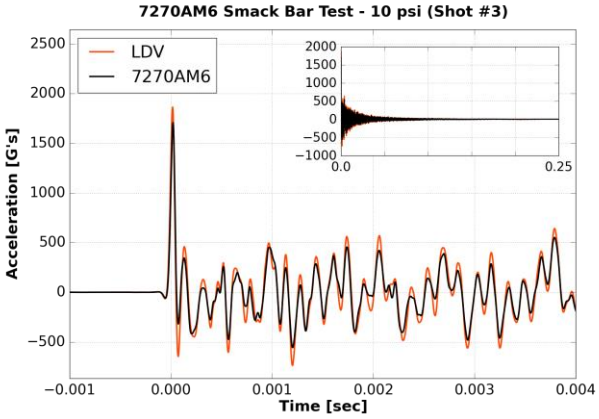
7270AM6 Smack Bar Test - 10 psi (Shot #3)
Acceleration [G's]
Time [sec]
LDV
7270AM6

(a)

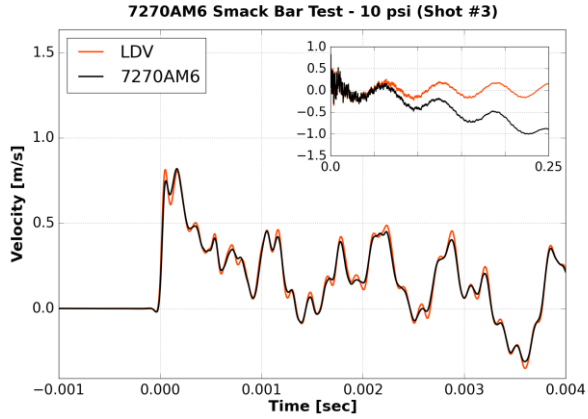
7270AM6 Smack Bar Test - 10 psi (Shot #3)
Velocity [m/s]
Time [sec]
LDV
7270AM6

(b)

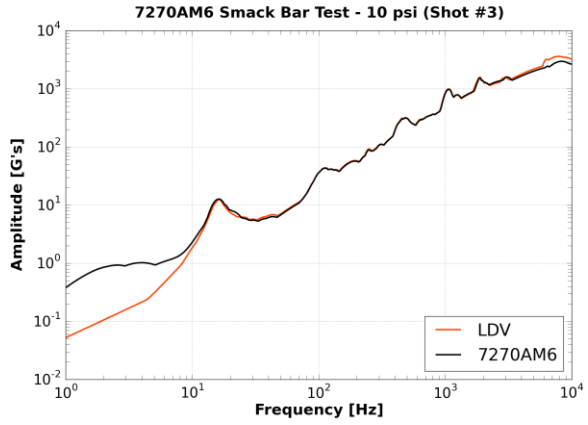
7270AM6 Smack Bar Test - 10 psi (Shot #3)
Amplitude [G's]
Frequency [Hz]
LDV
7270AM6

(c)

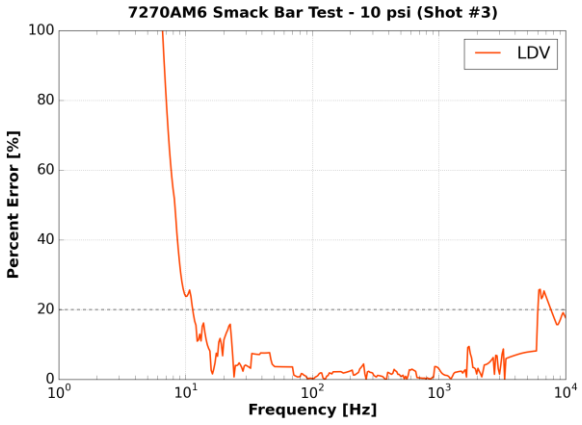
7270AM6 Smack Bar Test - 10 psi (Shot #3)
Percent Error [%]
Frequency [Hz]
LDV

(d)

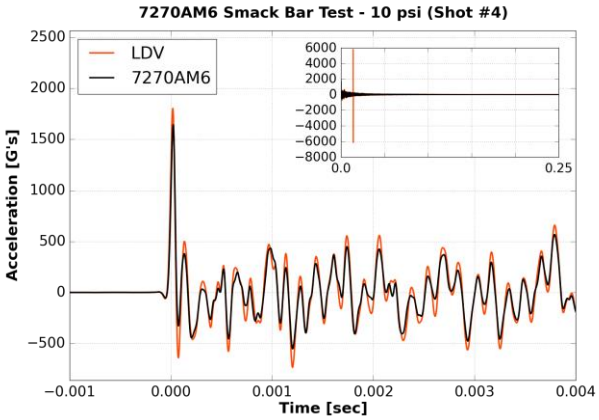
7270AM6 Smack Bar Test - 10 psi (Shot #4)
LDV
7270AM6
Acceleration [G's]
Time [sec]

(a)

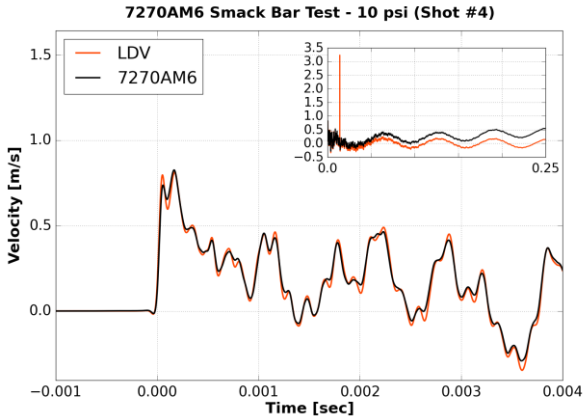
7270AM6 Smack Bar Test - 10 psi (Shot #4)
LDV
7270AM6
Velocity [m/s]
Time [sec]

(b)

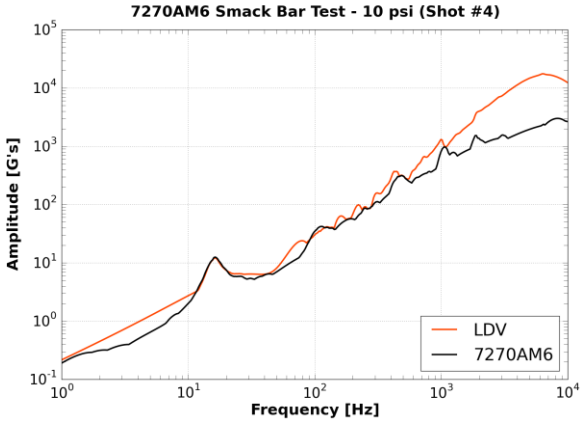
7270AM6 Smack Bar Test - 10 psi (Shot #4)
LDV
7270AM6
Amplitude [G's]
Frequency [Hz]

(c)

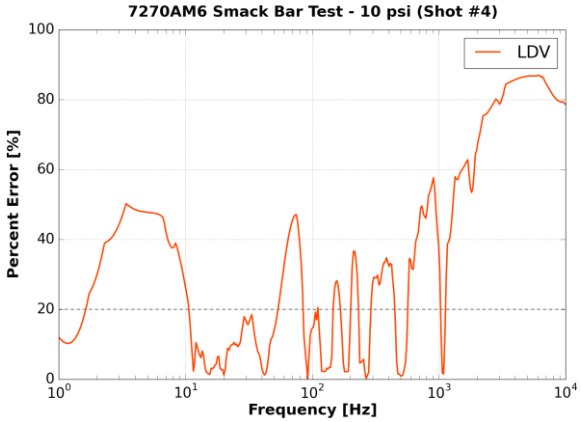
7270AM6 Smack Bar Test - 10 psi (Shot #4)
LDV
Percent Error [%]
Frequency [Hz]

(d)

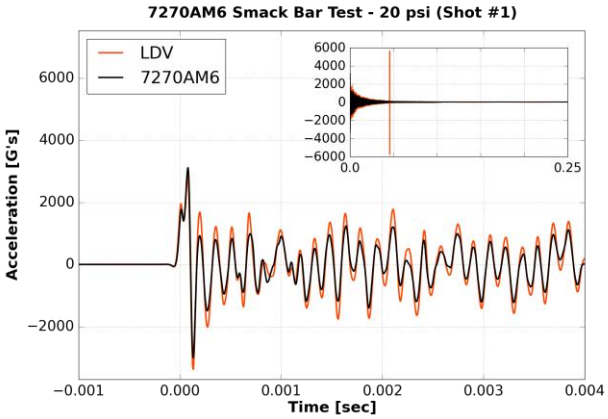
7270AM6 Smack Bar Test - 20 psi (Shot #1)
LDV
7270AM6
Acceleration [G's]
Time [sec]

(a)

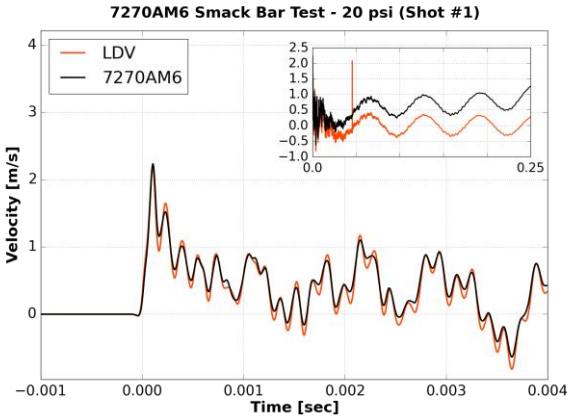
7270AM6 Smack Bar Test - 20 psi (Shot #1)
LDV
7270AM6
Velocity [m/s]
Time [sec]

(b)

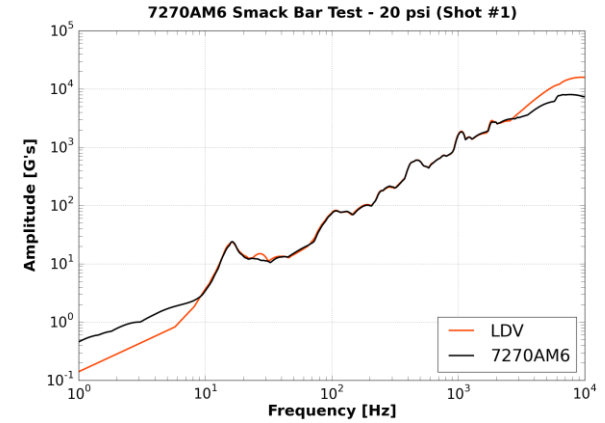
7270AM6 Smack Bar Test - 20 psi (Shot #1)
Amplitude [G's]
Frequency [Hz]
LDV
7270AM6

(c)

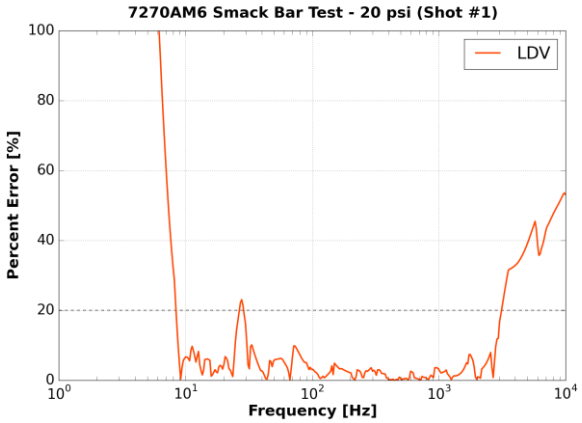
7270AM6 Smack Bar Test - 20 psi (Shot #1)
Percent Error [%]
Frequency [Hz]
LDV

(d)

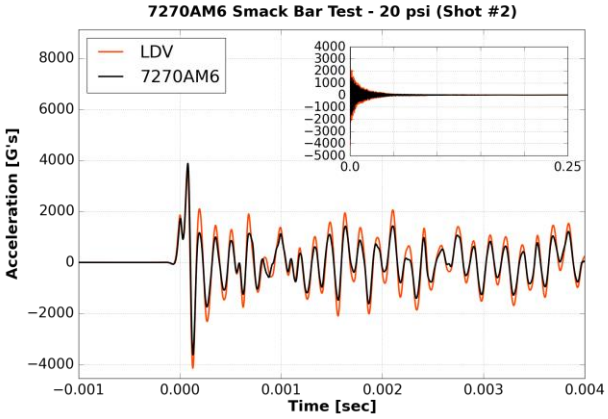
7270AM6 Smack Bar Test - 20 psi (Shot #2)
Acceleration [G's]
Time [sec]
LDV
7270AM6

(a)

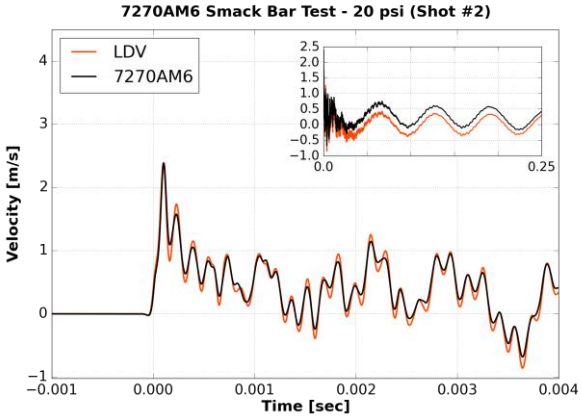
7270AM6 Smack Bar Test - 20 psi (Shot #2)
Velocity [m/s]
Time [sec]
LDV
7270AM6

(b)

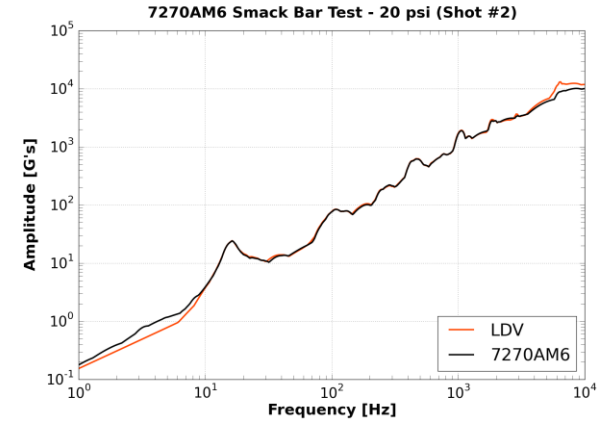
7270AM6 Smack Bar Test - 20 psi (Shot #2)
Amplitude [G's]
Frequency [Hz]
LDV
7270AM6

(c)

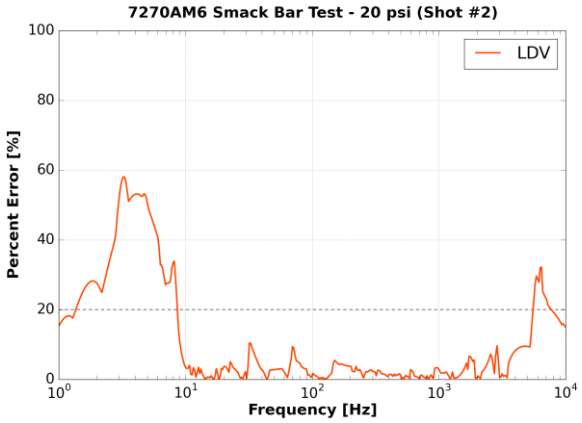
7270AM6 Smack Bar Test - 20 psi (Shot #2)
Percent Error [%]
Frequency [Hz]
LDV

(d)

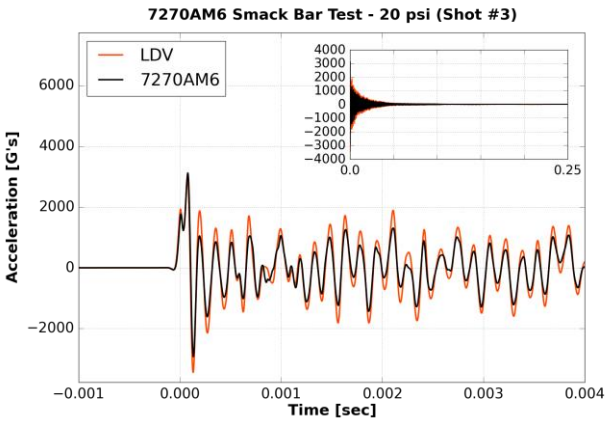
7270AM6 Smack Bar Test - 20 psi (Shot #3)
LDV
7270AM6
Acceleration [G's]
Time [sec]

(a)

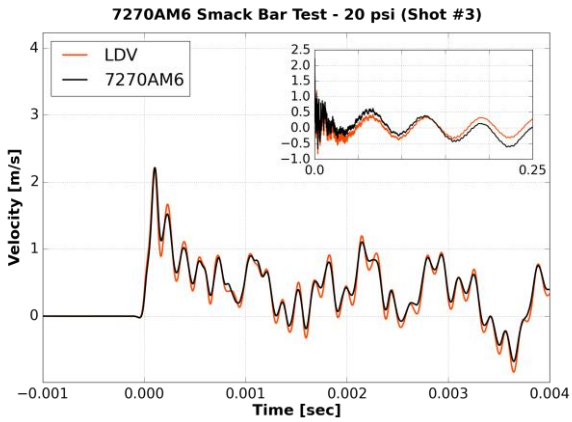
7270AM6 Smack Bar Test - 20 psi (Shot #3)
LDV
7270AM6
Velocity [m/s]
Time [sec]

(b)

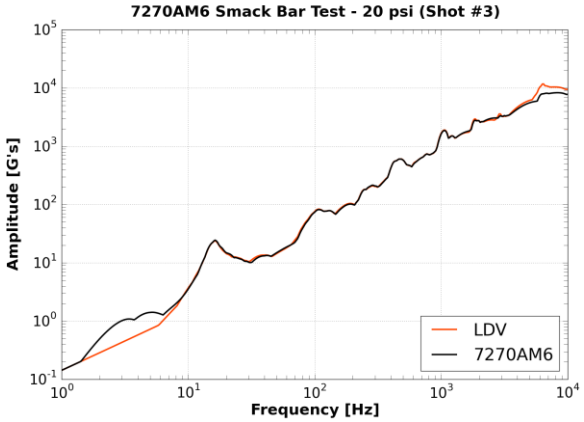
7270AM6 Smack Bar Test - 20 psi (Shot #3)
LDV
7270AM6
Amplitude [G's]
Frequency [Hz]

(c)

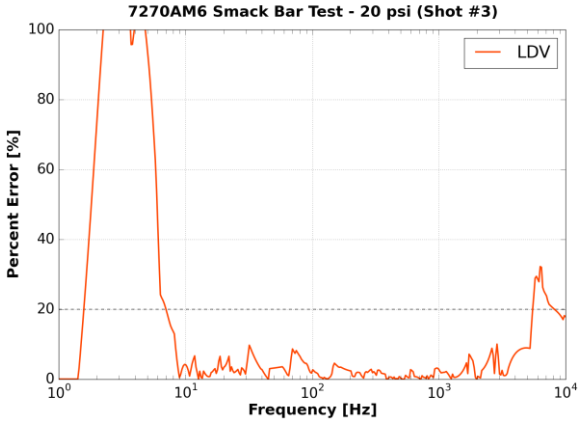
7270AM6 Smack Bar Test - 20 psi (Shot #3)
LDV
Percent Error [%]
Frequency [Hz]

(d)

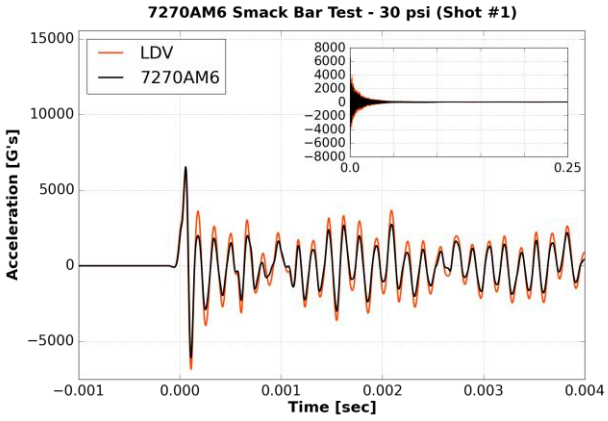
7270AM6 Smack Bar Test - 30 psi (Shot #1)
LDV
7270AM6
Acceleration [G's]
Time [sec]

(a)

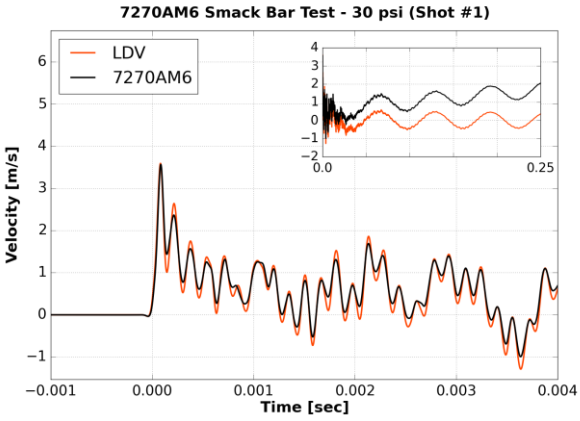
7270AM6 Smack Bar Test - 30 psi (Shot #1)
LDV
7270AM6
Velocity [m/s]
Time [sec]

(b)

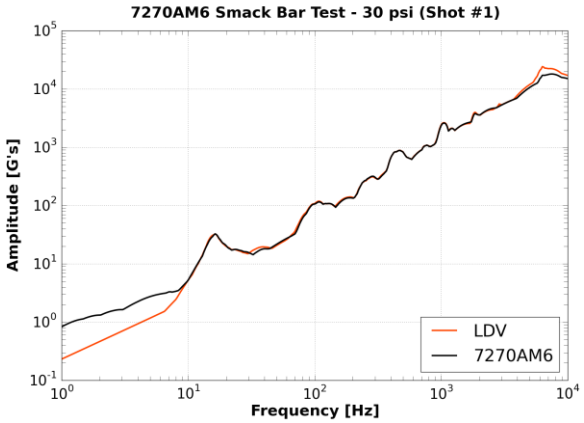
7270AM6 Smack Bar Test - 30 psi (Shot #1)
Amplitude [G's]
Frequency [Hz]
LDV
7270AM6

(c)

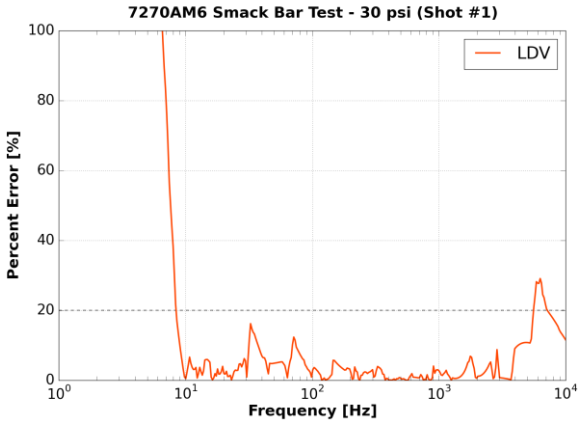
7270AM6 Smack Bar Test - 30 psi (Shot #1)
Percent Error [%]
Frequency [Hz]
LDV

(d)

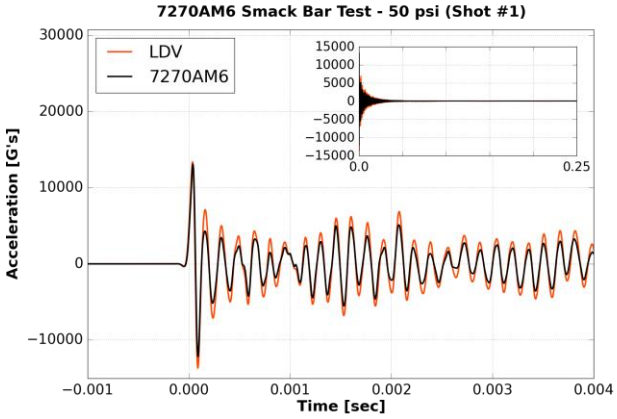
7270AM6 Smack Bar Test - 50 psi (Shot #1)
Acceleration [G's]
Time [sec]
LDV
7270AM6

(a)

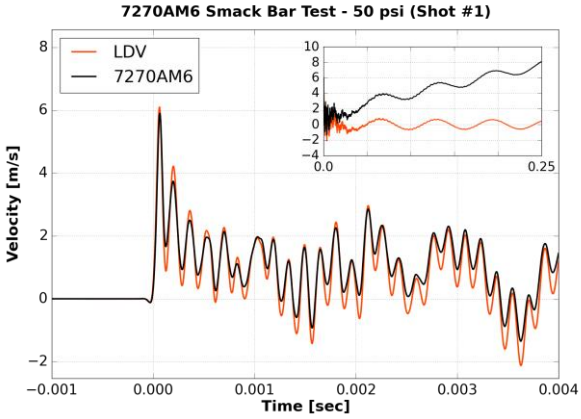
7270AM6 Smack Bar Test - 50 psi (Shot #1)
Velocity [m/s]
Time [sec]
LDV
7270AM6

(b)

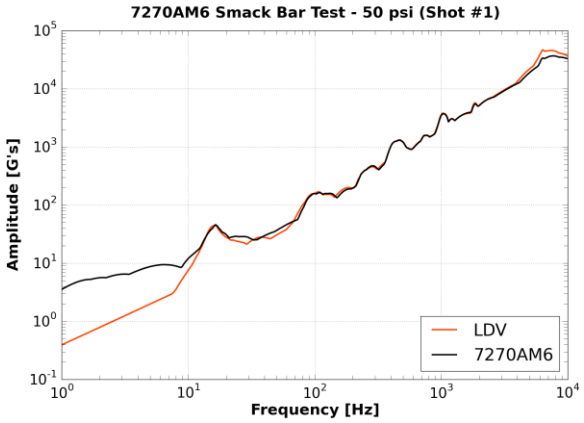
7270AM6 Smack Bar Test - 50 psi (Shot #1)
Amplitude [G's]
Frequency [Hz]
LDV
7270AM6

(c)

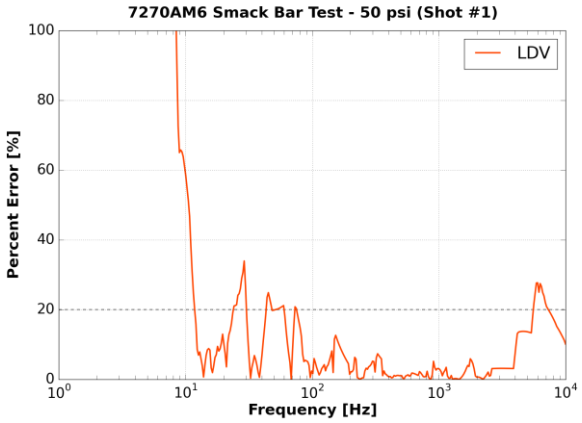
7270AM6 Smack Bar Test - 50 psi (Shot #1)
Percent Error [%]
Frequency [Hz]
LDV

(d)

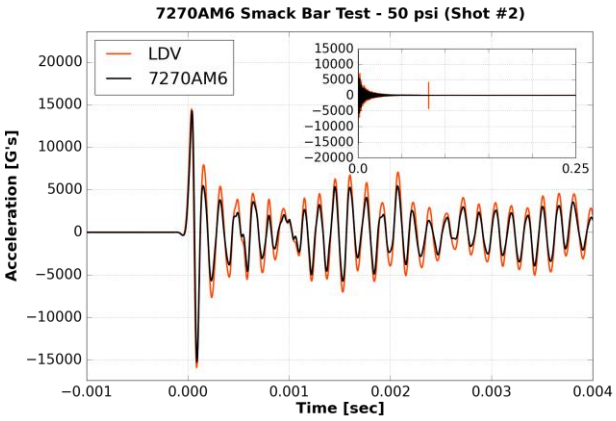
7270AM6 Smack Bar Test - 50 psi (Shot #2)
LDV
7270AM6
Acceleration [G's]
Time [sec]

(a)

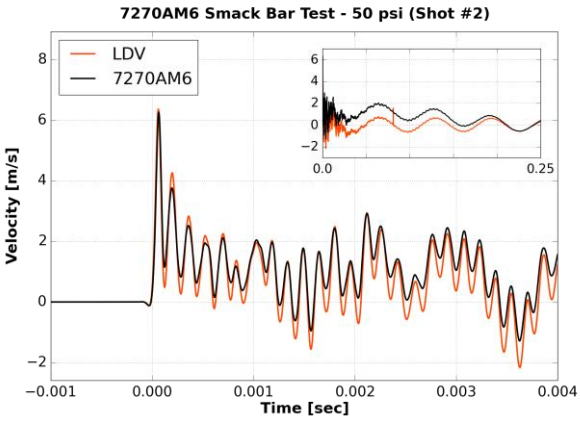
7270AM6 Smack Bar Test - 50 psi (Shot #2)
LDV
7270AM6
Velocity [m/s]
Time [sec]

(b)

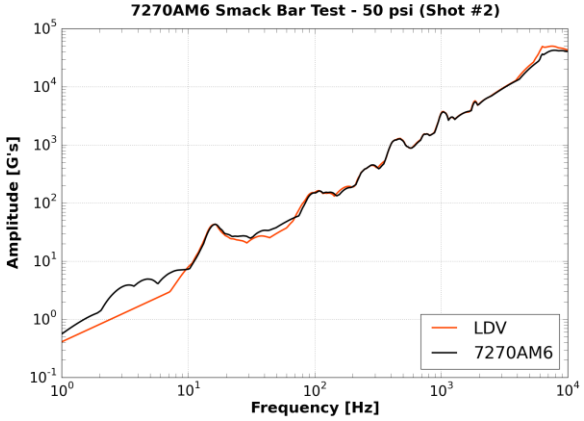
7270AM6 Smack Bar Test - 50 psi (Shot #2)
LDV
7270AM6
Amplitude [G's]
Frequency [Hz]

(c)

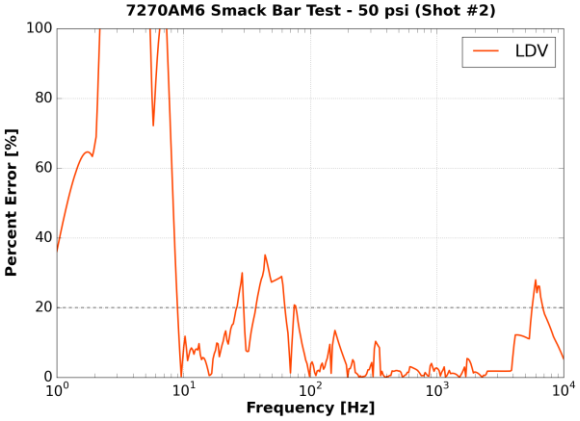
7270AM6 Smack Bar Test - 50 psi (Shot #2)
LDV
Percent Error [%]
Frequency [Hz]

(d)

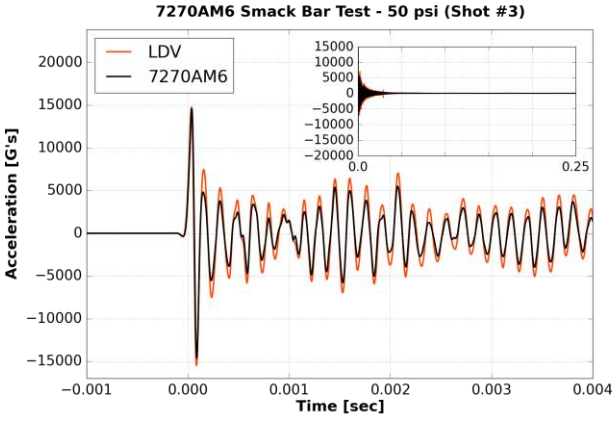
7270AM6 Smack Bar Test - 50 psi (Shot #3)
LDV
7270AM6
Acceleration [G's]
Time [sec]

(a)

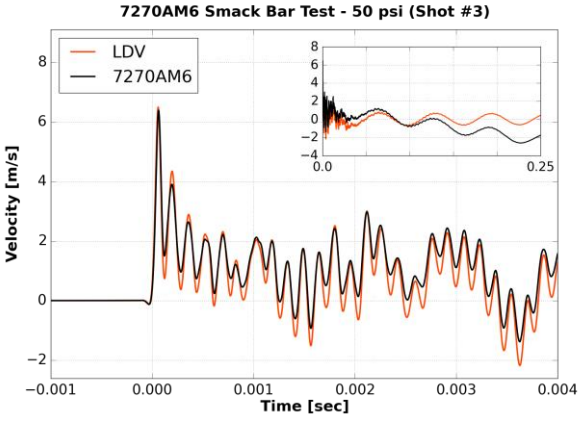
7270AM6 Smack Bar Test - 50 psi (Shot #3)
LDV
7270AM6
Velocity [m/s]
Time [sec]

(b)

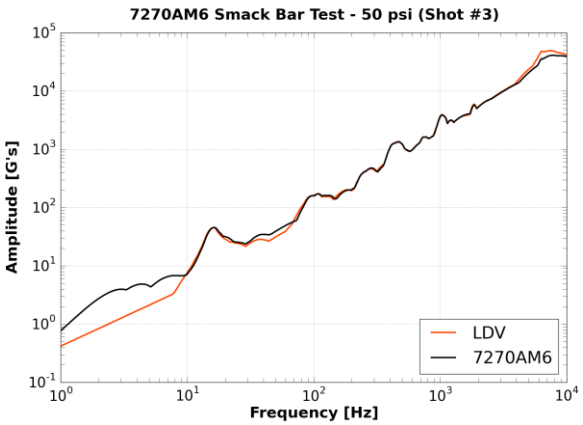
7270AM6 Smack Bar Test - 50 psi (Shot #3)
Amplitude [G's]
Frequency [Hz]
LDV
7270AM6

(c)

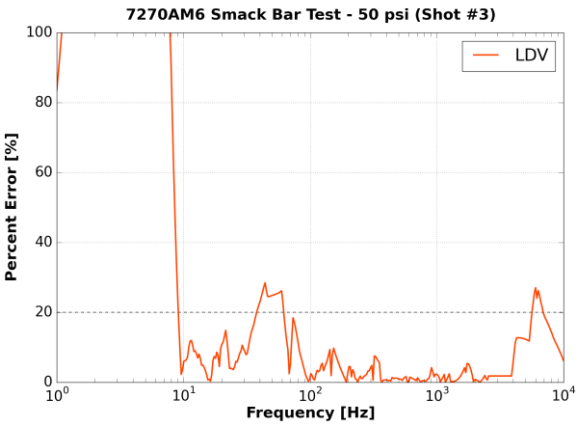
7270AM6 Smack Bar Test - 50 psi (Shot #3)
Percent Error [%]
Frequency [Hz]
LDV

(d)

v. BOBKAT

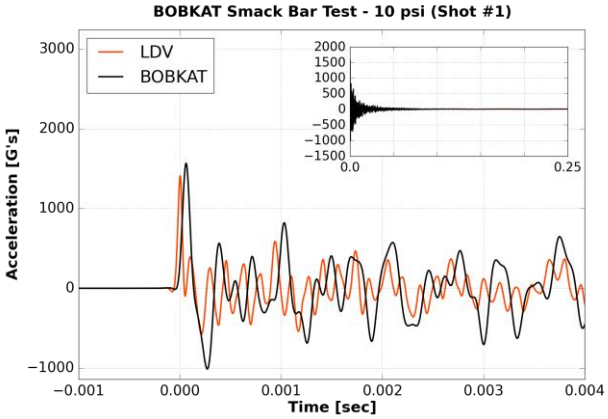

(a)

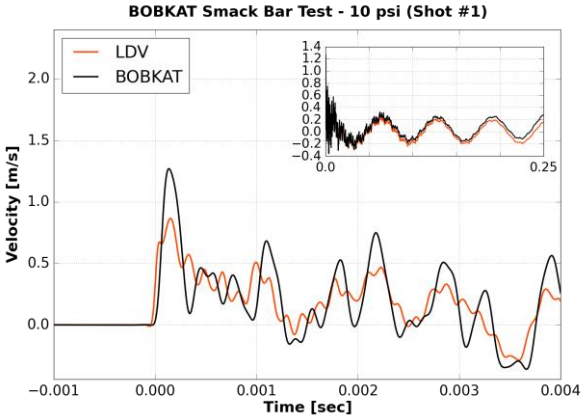

(b)

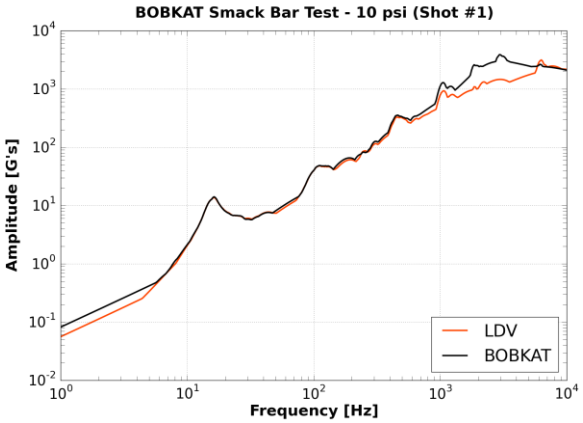

(c)

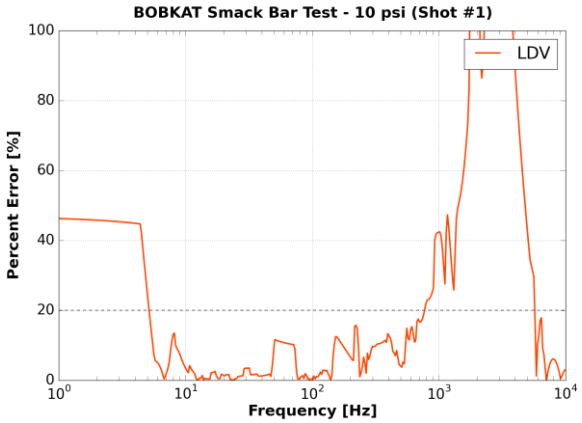

(d)

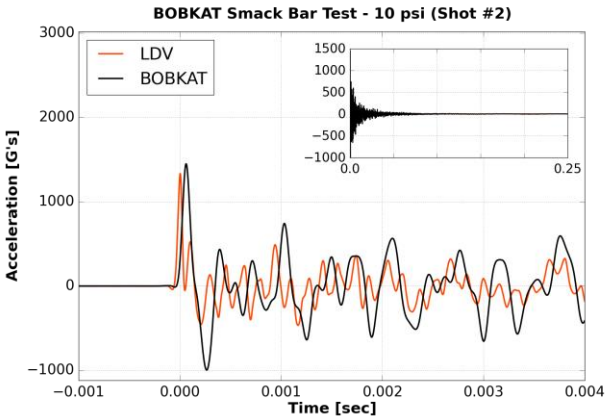

(a)

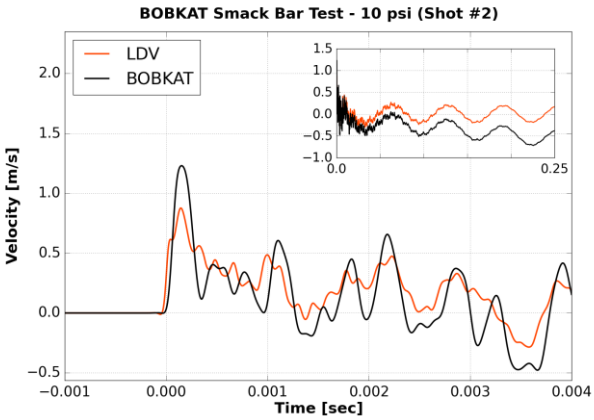

(b)

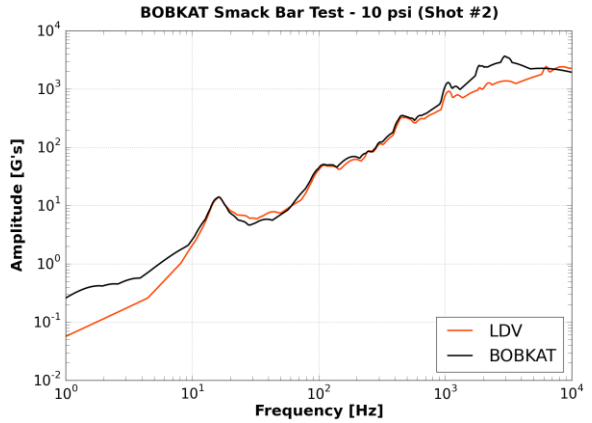
BOBKAT Smack Bar Test - 10 psi (Shot #2)
Amplitude [G's]
Frequency [Hz]
LDV
BOBKAT

(c)

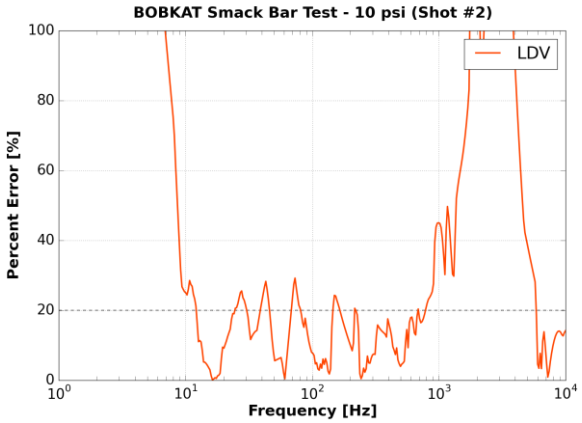
BOBKAT Smack Bar Test - 10 psi (Shot #2)
Percent Error [%]
Frequency [Hz]
LDV

(d)

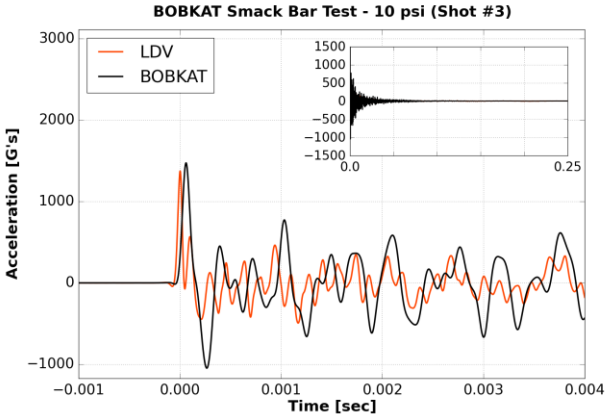
BOBKAT Smack Bar Test - 10 psi (Shot #3)
Acceleration [G's]
Time [sec]
LDV
BOBKAT

(a)

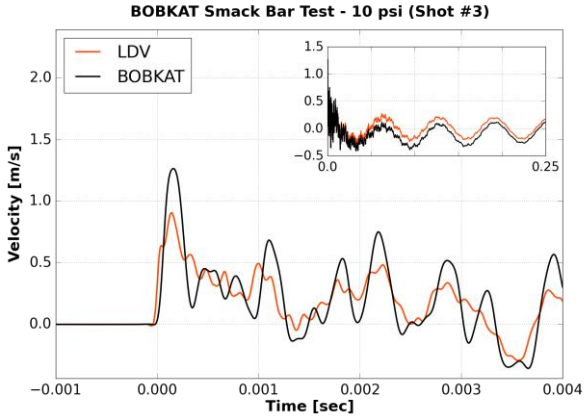
BOBKAT Smack Bar Test - 10 psi (Shot #3)
Velocity [m/s]
Time [sec]
LDV
BOBKAT

(b)

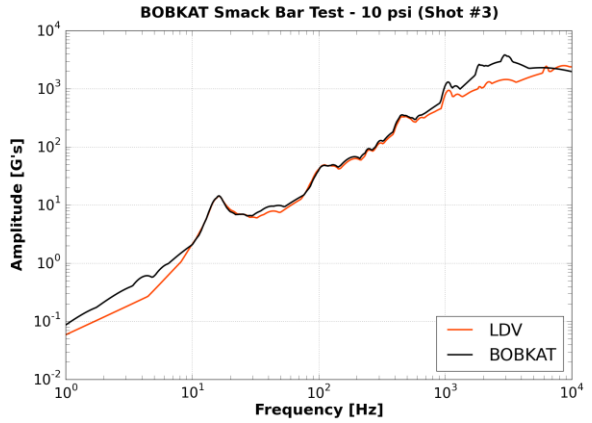
BOBKAT Smack Bar Test - 10 psi (Shot #3)
Amplitude [G's]
Frequency [Hz]
LDV
BOBKAT

(c)

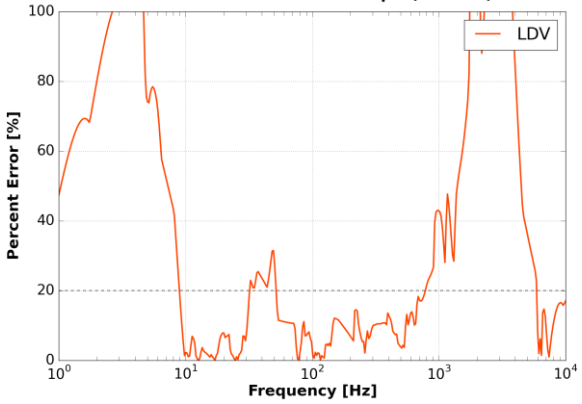
BOBKAT Smack Bar Test - 10 psi (Shot #3)
Percent Error [%]
Frequency [Hz]
LDV

(d)

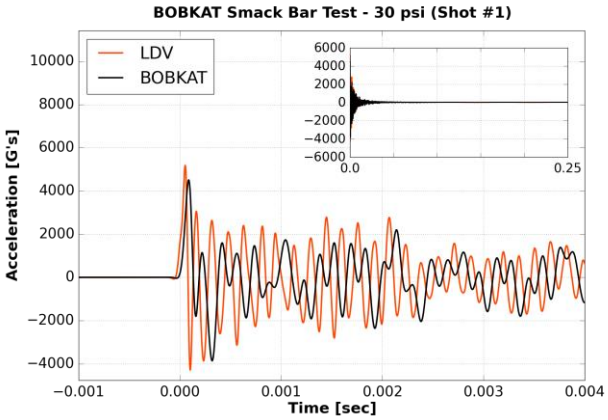
BOBKAT Smack Bar Test - 30 psi (Shot #1)
LDV
BOBKAT
Acceleration [G's]
Time [sec]

(a)

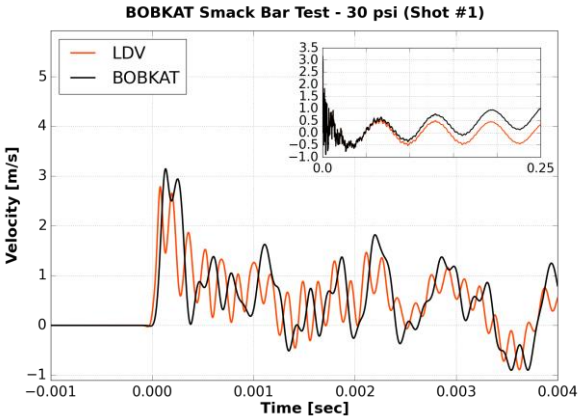
BOBKAT Smack Bar Test - 30 psi (Shot #1)
LDV
BOBKAT
Velocity [m/s]
Time [sec]

(b)

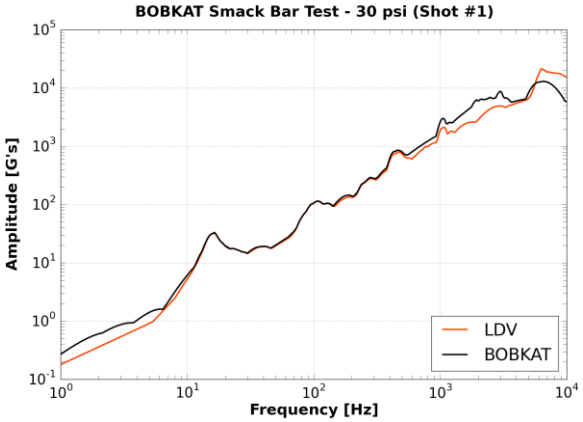
BOBKAT Smack Bar Test - 30 psi (Shot #1)
LDV
BOBKAT
Amplitude [G's]
Frequency [Hz]

(c)

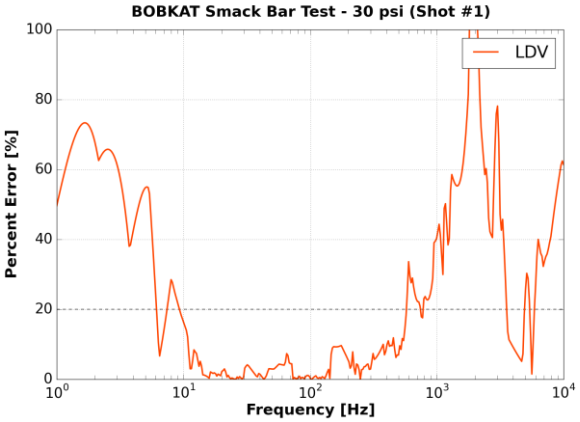
BOBKAT Smack Bar Test - 30 psi (Shot #1)
LDV
Percent Error [%]
Frequency [Hz]

(d)

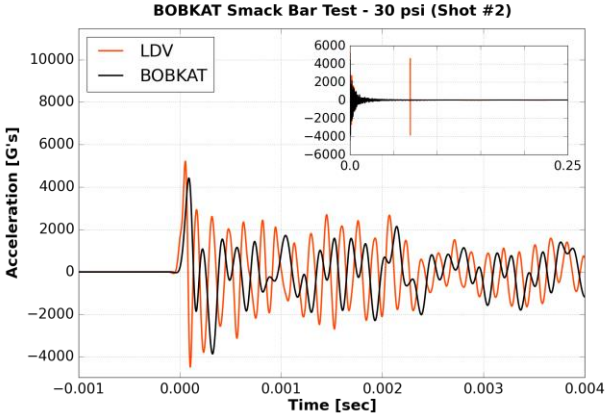
BOBKAT Smack Bar Test - 30 psi (Shot #2)
LDV
BOBKAT
Acceleration [G's]
Time [sec]

(a)

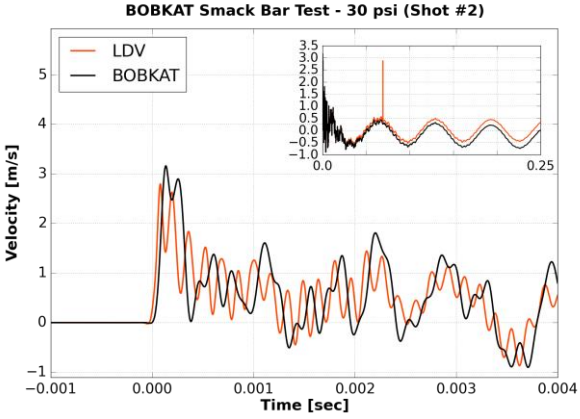
BOBKAT Smack Bar Test - 30 psi (Shot #2)
LDV
BOBKAT
Velocity [m/s]
Time [sec]

(b)

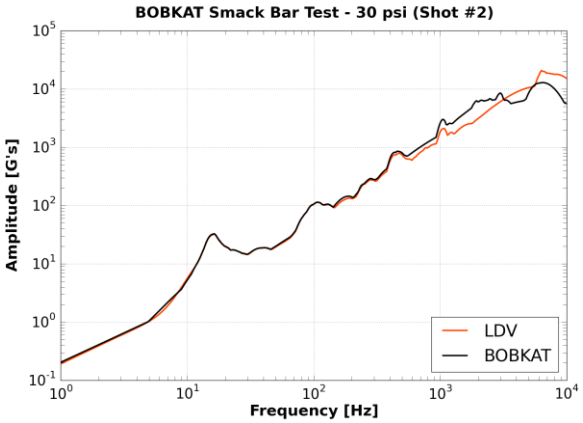
BOBKAT Smack Bar Test - 30 psi (Shot #2)
Amplitude [G's]
Frequency [Hz]
LDV
BOBKAT

(c)

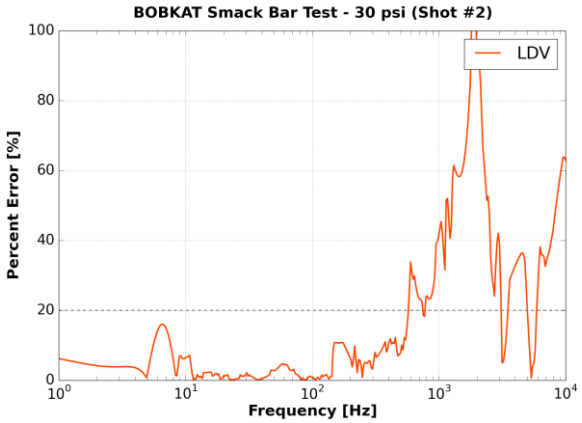
BOBKAT Smack Bar Test - 30 psi (Shot #2)
Percent Error [%]
Frequency [Hz]
LDV

(d)

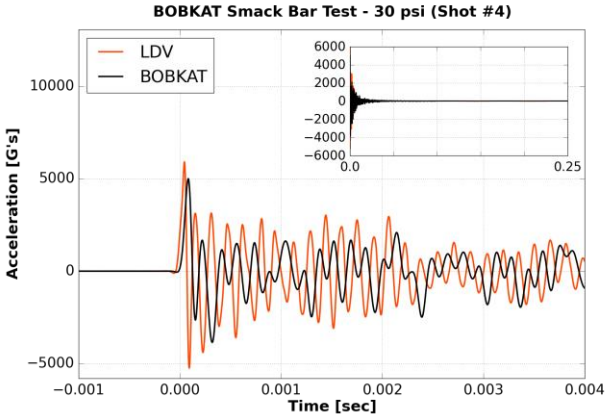
BOBKAT Smack Bar Test - 30 psi (Shot #4)
Acceleration [G's]
Time [sec]
LDV
BOBKAT

(a)

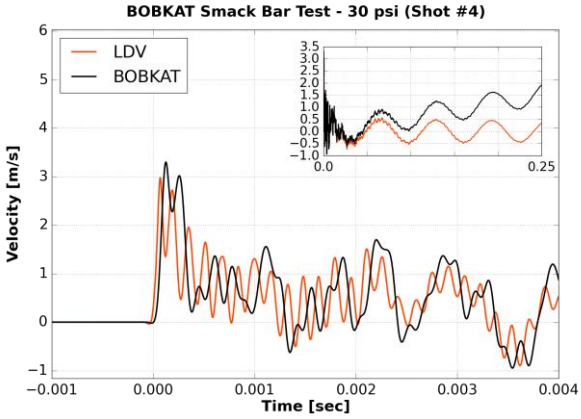
BOBKAT Smack Bar Test - 30 psi (Shot #4)
Velocity [m/s]
Time [sec]
LDV
BOBKAT

(b)

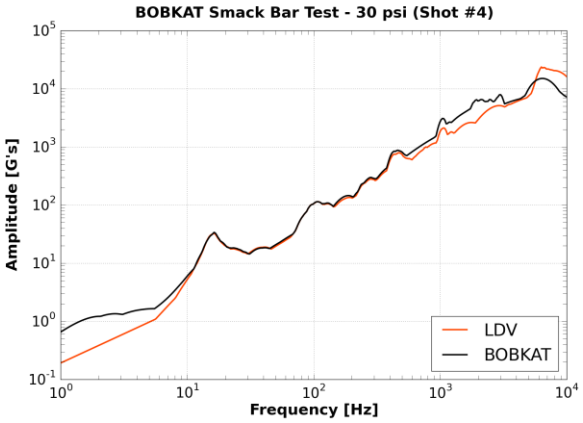
BOBKAT Smack Bar Test - 30 psi (Shot #4)
Amplitude [G's]
Frequency [Hz]
LDV
BOBKAT

(c)

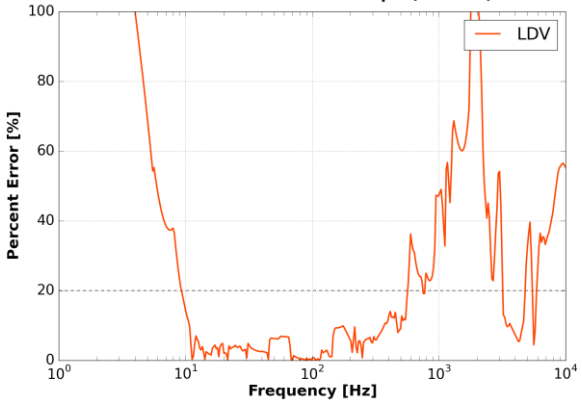
BOBKAT Smack Bar Test - 30 psi (Shot #4)
Percent Error [%]
Frequency [Hz]
LDV

(d)

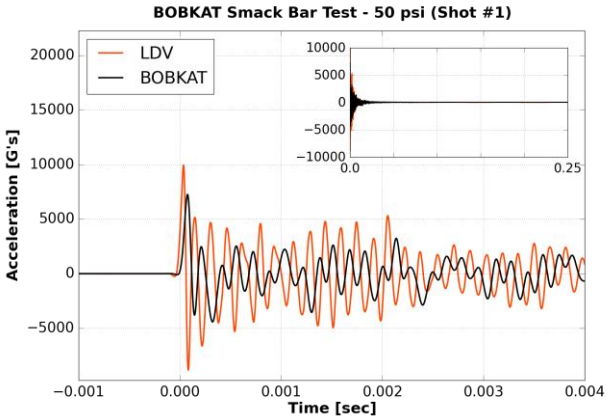
BOBKAT Smack Bar Test - 50 psi (Shot #1)
LDV
BOBKAT
Acceleration [G's]
Time [sec]

(a)

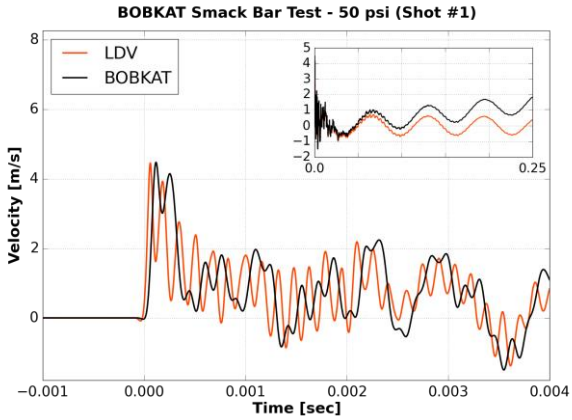
BOBKAT Smack Bar Test - 50 psi (Shot #1)
LDV
BOBKAT
Velocity [m/s]
Time [sec]

(b)

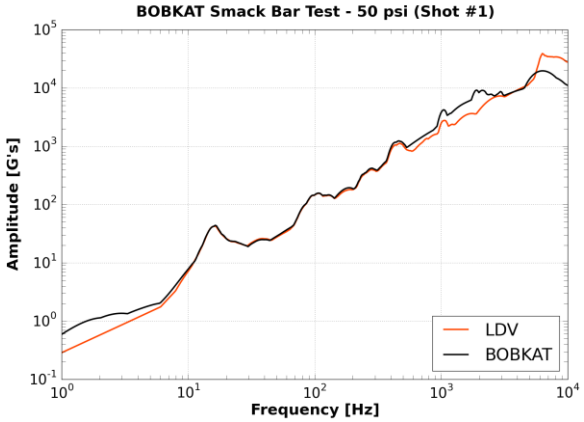
BOBKAT Smack Bar Test - 50 psi (Shot #1)
LDV
BOBKAT
Amplitude [G's]
Frequency [Hz]

(c)

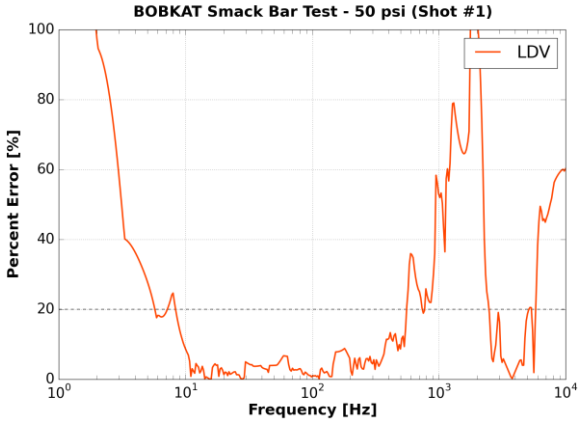
BOBKAT Smack Bar Test - 50 psi (Shot #1)
LDV
Percent Error [%]
Frequency [Hz]

(d)

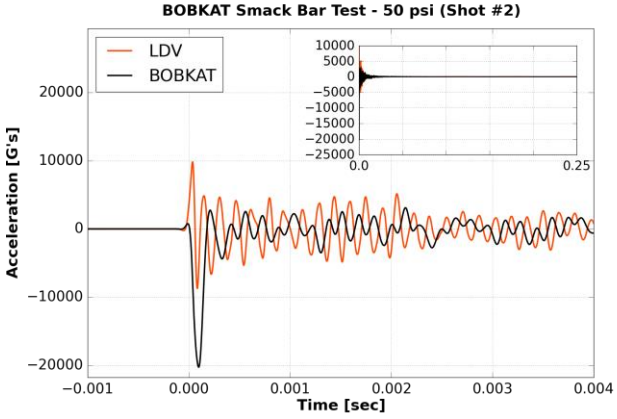
BOBKAT Smack Bar Test - 50 psi (Shot #2)
LDV
BOBKAT
Acceleration [G's]
Time [sec]

(a)

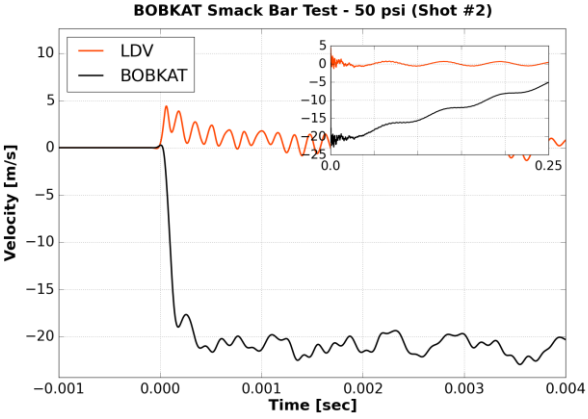
BOBKAT Smack Bar Test - 50 psi (Shot #2)
LDV
BOBKAT
Velocity [m/s]
Time [sec]

(b)

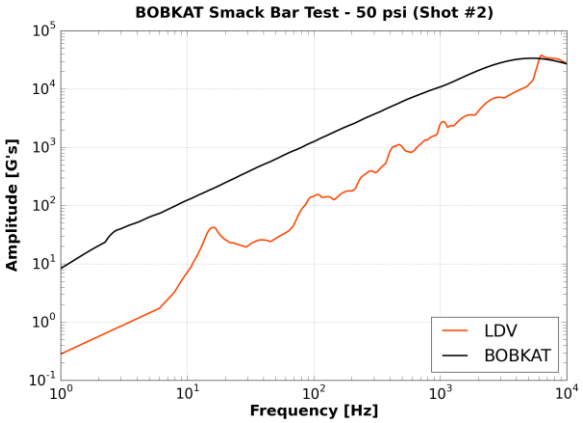
BOBKAT Smack Bar Test - 50 psi (Shot #2)
Amplitude [G's]
Frequency [Hz]
LDV
BOBKAT

(c)

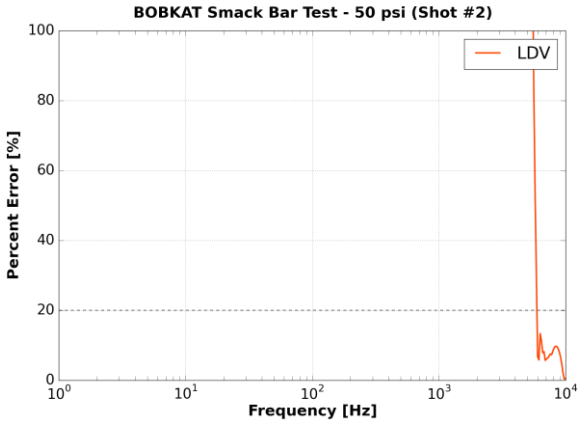
BOBKAT Smack Bar Test - 50 psi (Shot #2)
Percent Error [%]
Frequency [Hz]
LDV

(d)

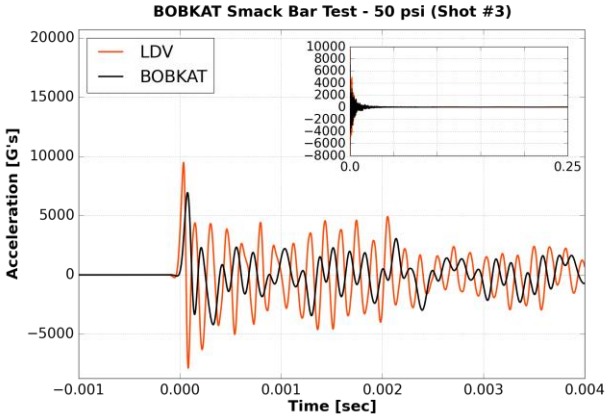
BOBKAT Smack Bar Test - 50 psi (Shot #3)
Acceleration [G's]
Time [sec]
LDV
BOBKAT

(a)

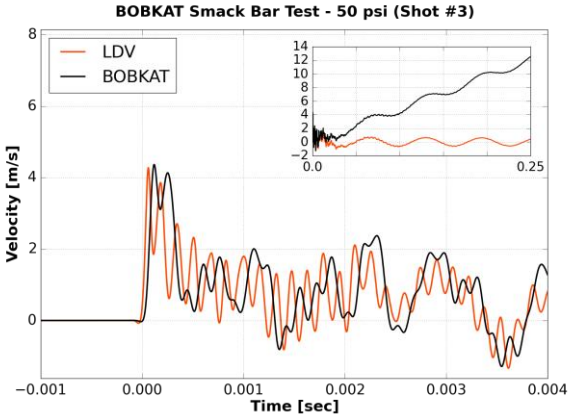
BOBKAT Smack Bar Test - 50 psi (Shot #3)
Velocity [m/s]
Time [sec]
LDV
BOBKAT

(b)

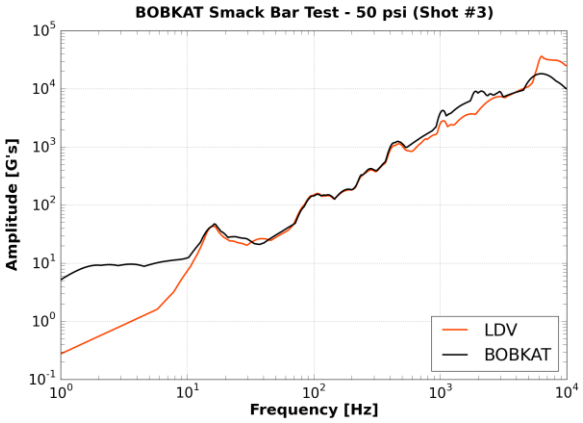
BOBKAT Smack Bar Test - 50 psi (Shot #3)
Amplitude [G's]
Frequency [Hz]
LDV
BOBKAT

(c)

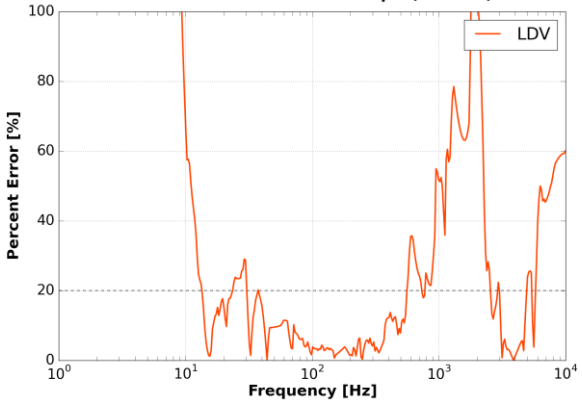
BOBKAT Smack Bar Test - 50 psi (Shot #3)
Percent Error [%]
Frequency [Hz]
LDV

(d)

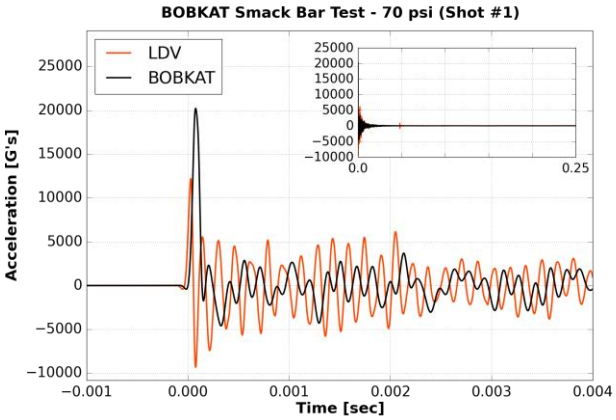
BOBKAT Smack Bar Test - 70 psi (Shot #1)
LDV
BOBKAT
Acceleration [G's]
Time [sec]

(a)

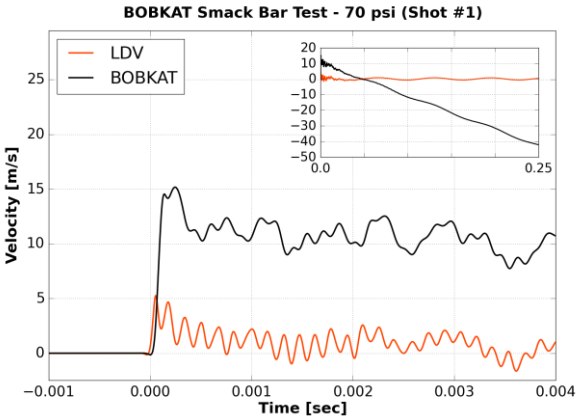
BOBKAT Smack Bar Test - 70 psi (Shot #1)
LDV
BOBKAT
Velocity [m/s]
Time [sec]

(b)

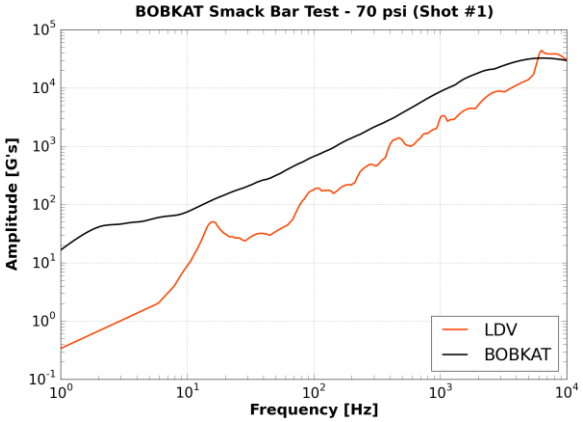
BOBKAT Smack Bar Test - 70 psi (Shot #1)
LDV
BOBKAT
Amplitude [G's]
Frequency [Hz]

(c)

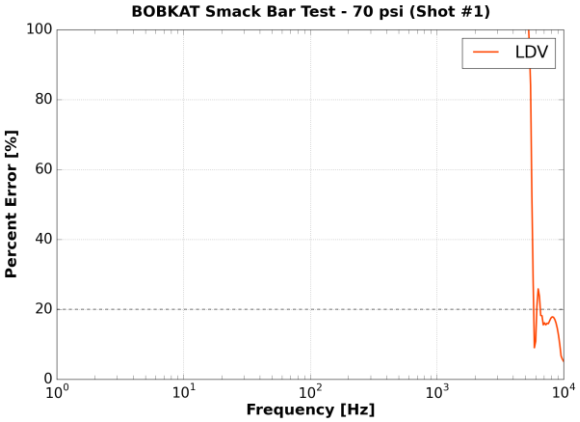
BOBKAT Smack Bar Test - 70 psi (Shot #1)
LDV
Percent Error [%]
Frequency [Hz]

(d)

vi. LOFFI

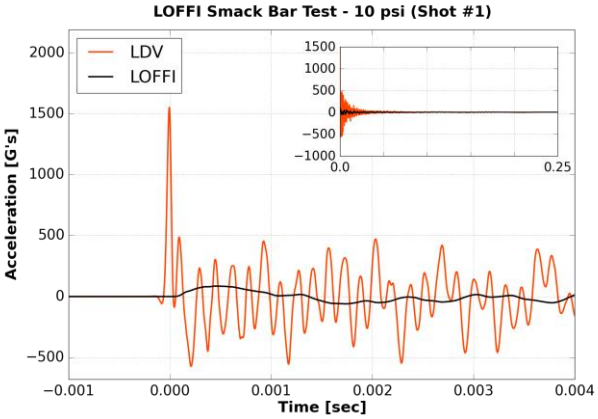

(a)

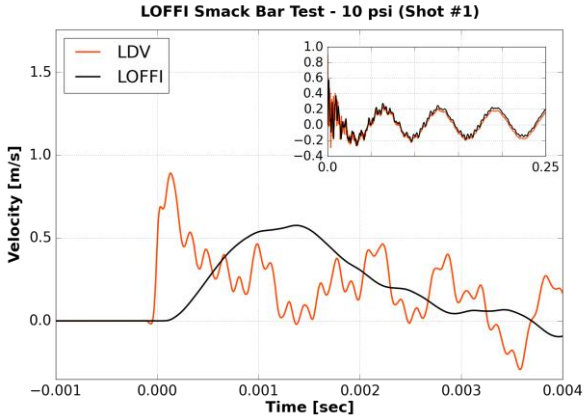

(b)

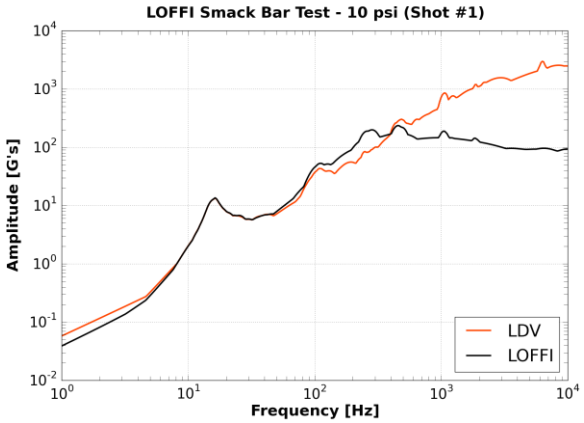

(c)

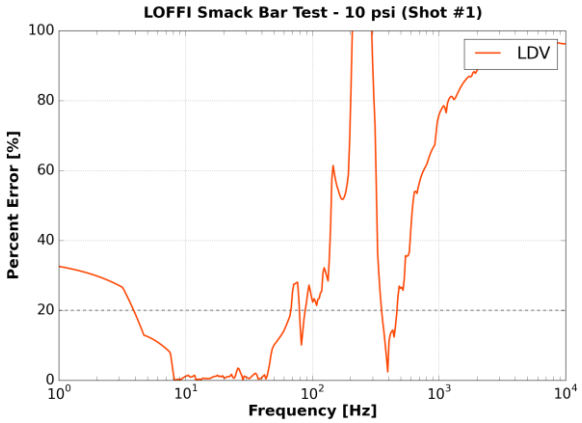

(d)

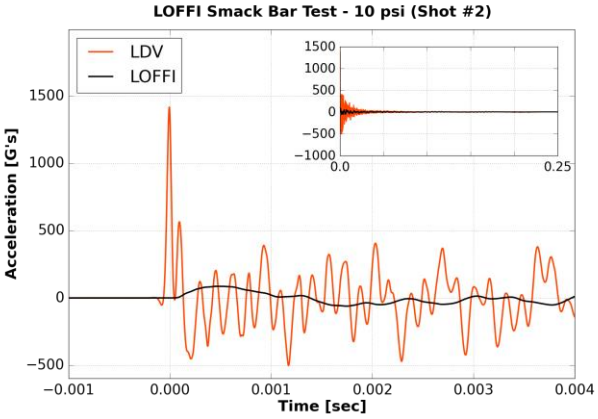

(a)

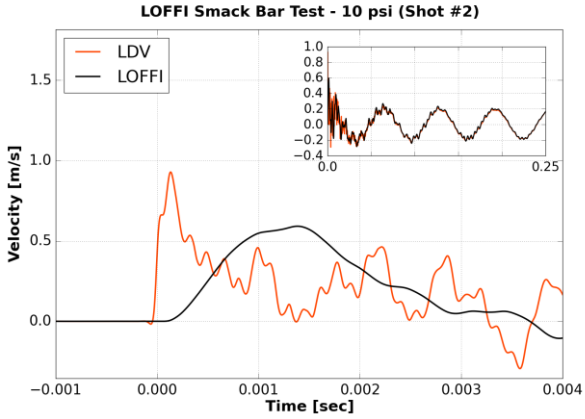

(b)

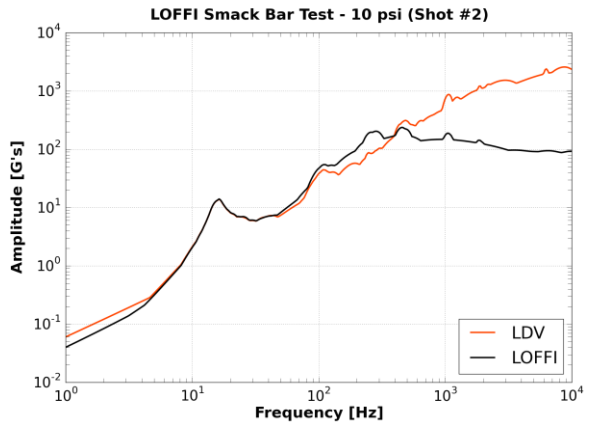
LOFFI Smack Bar Test - 10 psi (Shot #2)
Amplitude [G's]
Frequency [Hz]
LDV
LOFFI

(c)

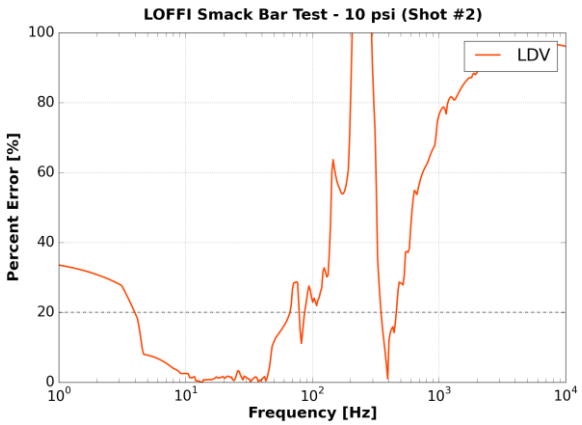
LOFFI Smack Bar Test - 10 psi (Shot #2)
Percent Error [%]
Frequency [Hz]
LDV

(d)

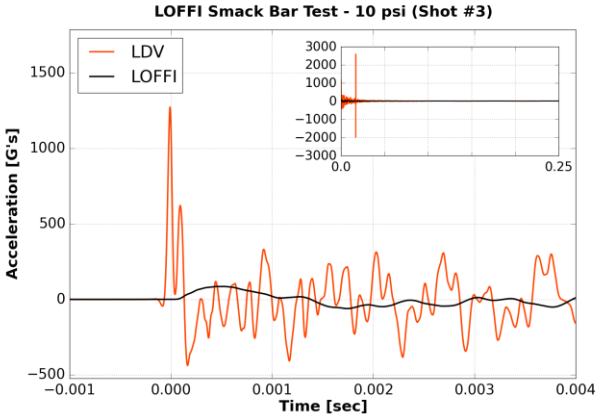
LOFFI Smack Bar Test - 10 psi (Shot #3)
Acceleration [G's]
Time [sec]
LDV
LOFFI

(a)

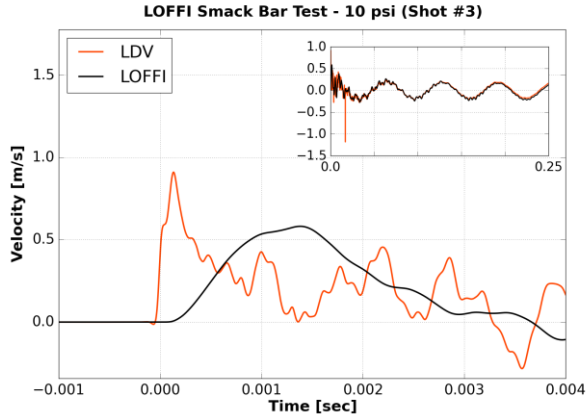
LOFFI Smack Bar Test - 10 psi (Shot #3)
Velocity [m/s]
Time [sec]
LDV
LOFFI

(b)

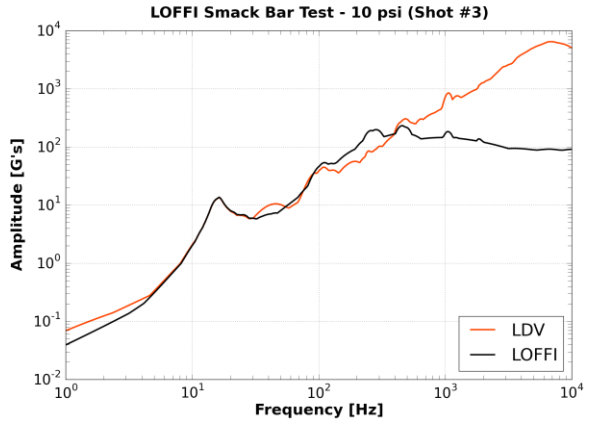
LOFFI Smack Bar Test - 10 psi (Shot #3)
Amplitude [G's]
Frequency [Hz]
LDV
LOFFI

(c)

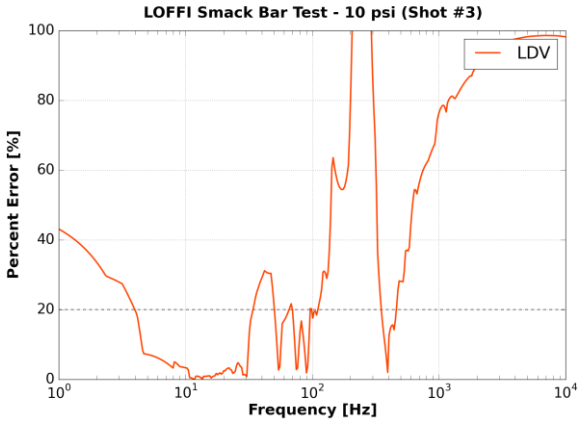
LOFFI Smack Bar Test - 10 psi (Shot #3)
Percent Error [%]
Frequency [Hz]
LDV

(d)

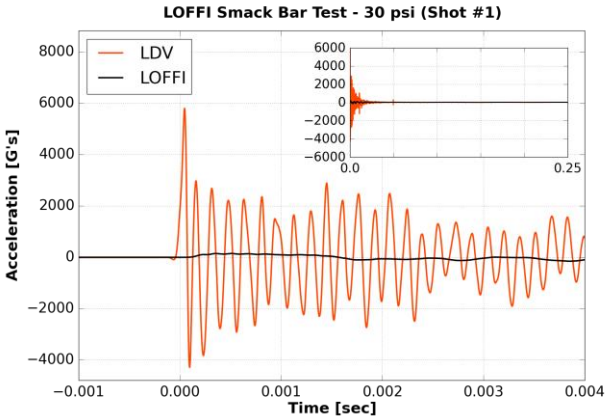
LOFFI Smack Bar Test - 30 psi (Shot #1)
LDV
LOFFI
Acceleration [G's]
Time [sec]

(a)

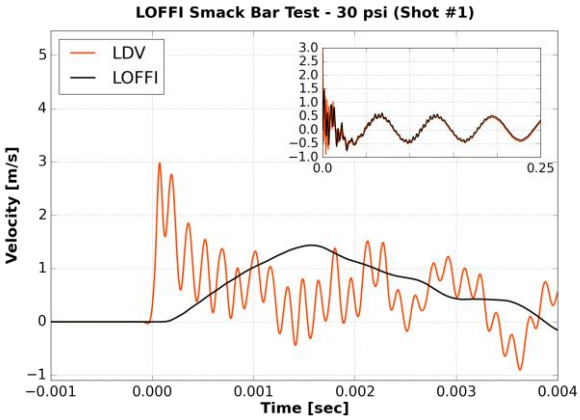
LOFFI Smack Bar Test - 30 psi (Shot #1)
LDV
LOFFI
Velocity [m/s]
Time [sec]

(b)

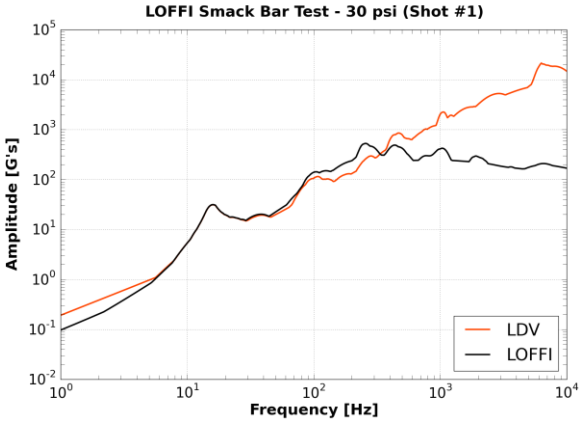
LOFFI Smack Bar Test - 30 psi (Shot #1)
LDV
LOFFI
Amplitude [G's]
Frequency [Hz]

(c)

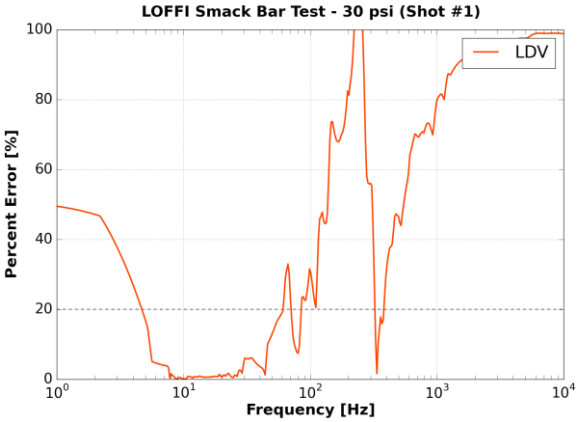
LOFFI Smack Bar Test - 30 psi (Shot #1)
LDV
Percent Error [%]
Frequency [Hz]

(d)

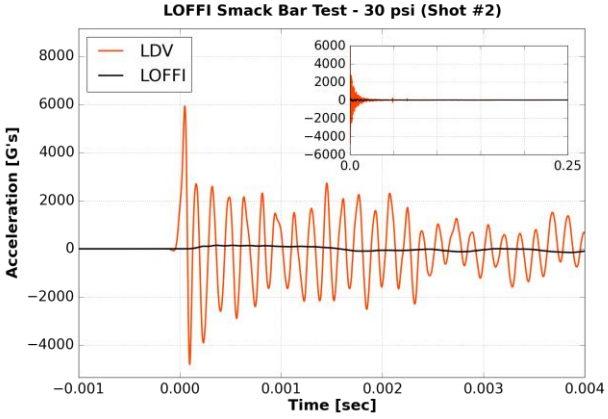
LOFFI Smack Bar Test - 30 psi (Shot #2)
LDV
LOFFI
Acceleration [G's]
Time [sec]

(a)

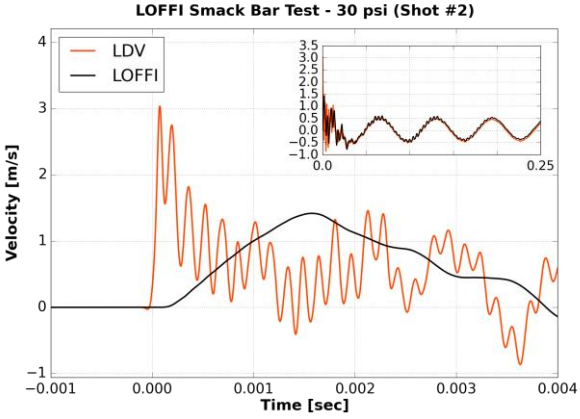
LOFFI Smack Bar Test - 30 psi (Shot #2)
LDV
LOFFI
Velocity [m/s]
Time [sec]

(b)

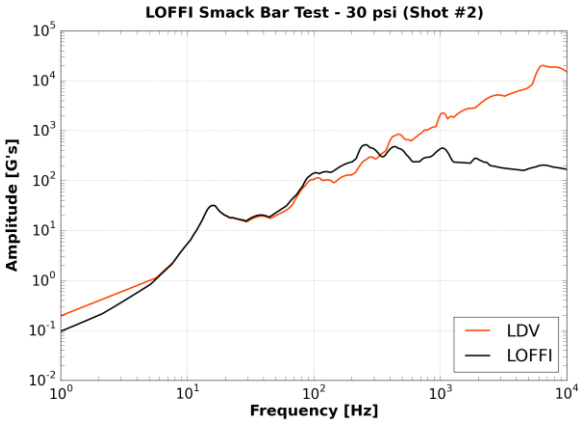
LOFFI Smack Bar Test - 30 psi (Shot #2)
Amplitude [G's]
Frequency [Hz]
LDV
LOFFI

(c)

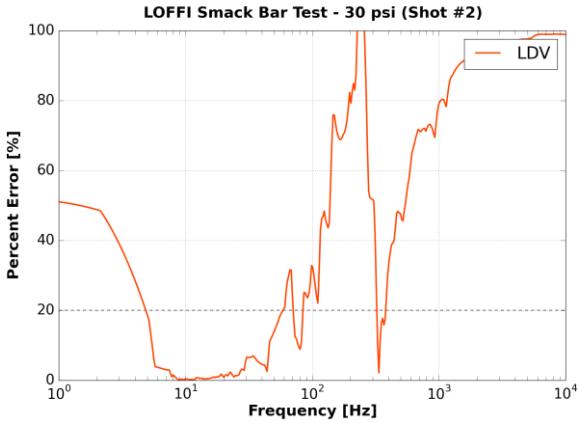
LOFFI Smack Bar Test - 30 psi (Shot #2)
Percent Error [%]
Frequency [Hz]
LDV

(d)

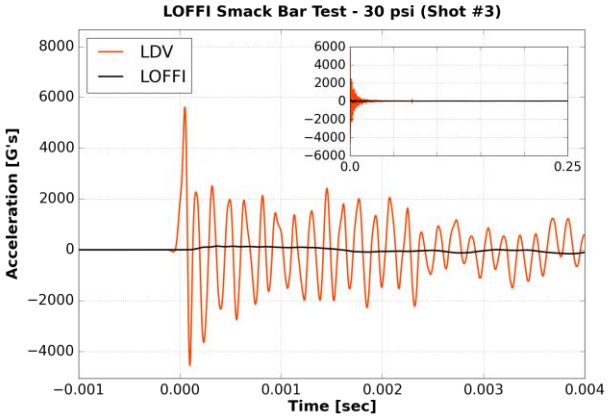
LOFFI Smack Bar Test - 30 psi (Shot #3)
Acceleration [G's]
Time [sec]
LDV
LOFFI

(a)

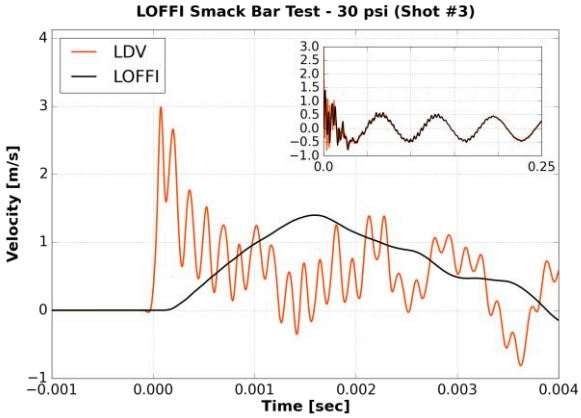
LOFFI Smack Bar Test - 30 psi (Shot #3)
Velocity [m/s]
Time [sec]
LDV
LOFFI

(b)

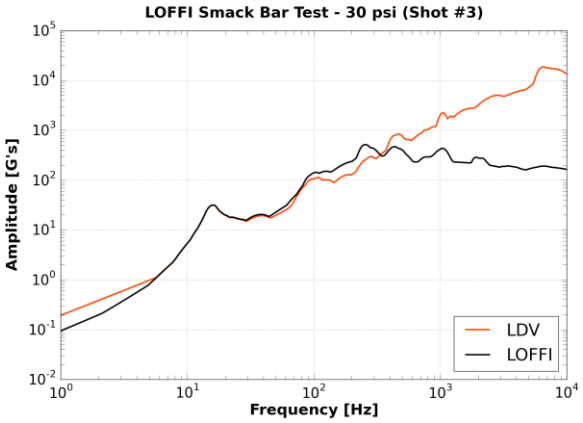
LOFFI Smack Bar Test - 30 psi (Shot #3)
Amplitude [G's]
Frequency [Hz]
LDV
LOFFI

(c)

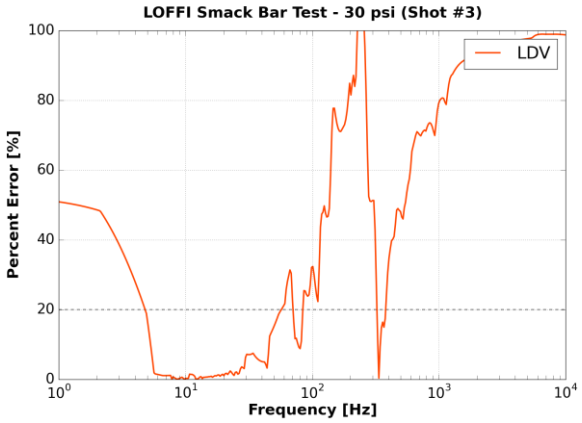
LOFFI Smack Bar Test - 30 psi (Shot #3)
Percent Error [%]
Frequency [Hz]
LDV

(d)

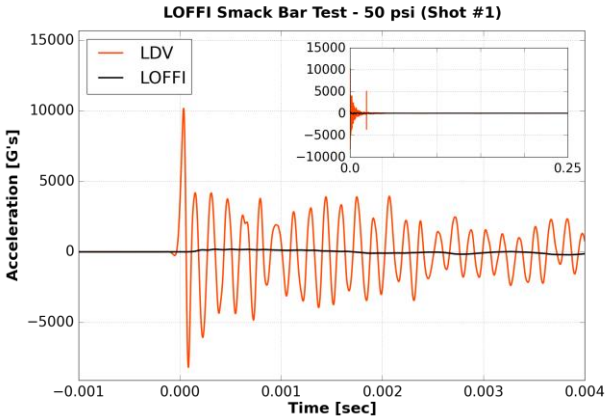
LOFFI Smack Bar Test - 50 psi (Shot #1)
LDV
LOFFI
Acceleration [G's]
Time [sec]

(a)

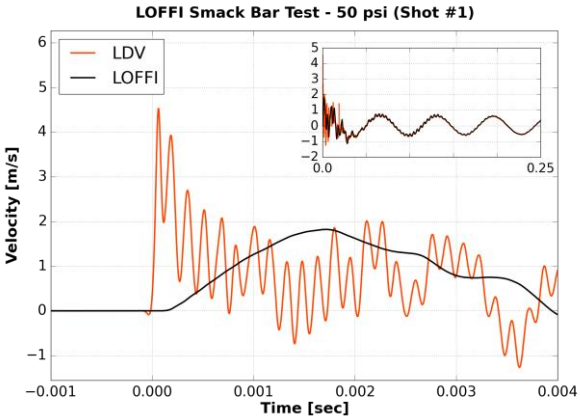
LOFFI Smack Bar Test - 50 psi (Shot #1)
LDV
LOFFI
Velocity [m/s]
Time [sec]

(b)

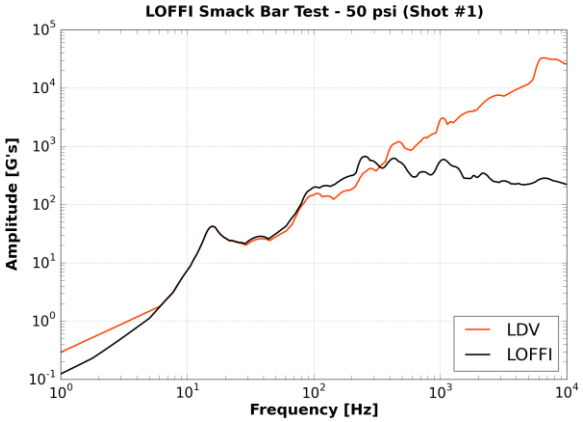
LOFFI Smack Bar Test - 50 psi (Shot #1)
LDV
LOFFI
Amplitude [G's]
Frequency [Hz]

(c)

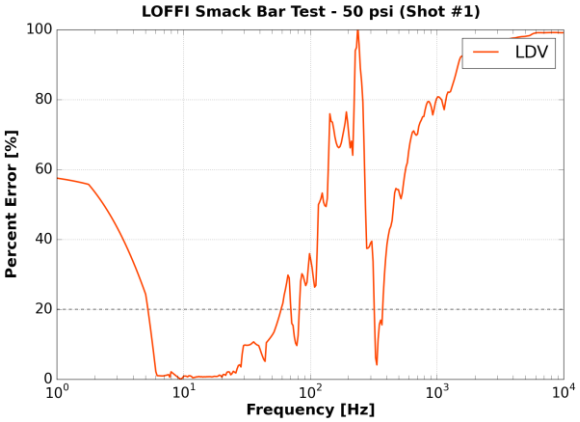
LOFFI Smack Bar Test - 50 psi (Shot #1)
LDV
Percent Error [%]
Frequency [Hz]

(d)

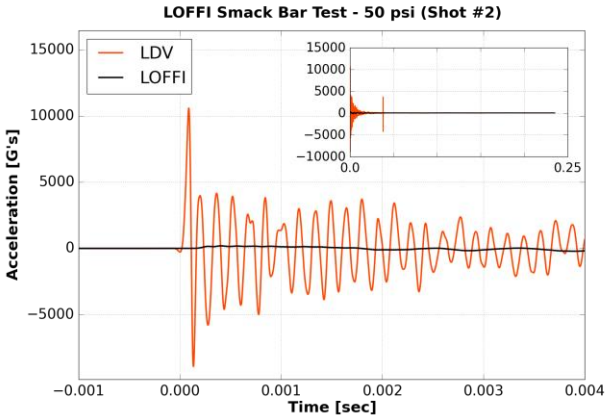
LOFFI Smack Bar Test - 50 psi (Shot #2)
LDV
LOFFI
Acceleration [G's]
Time [sec]

(a)

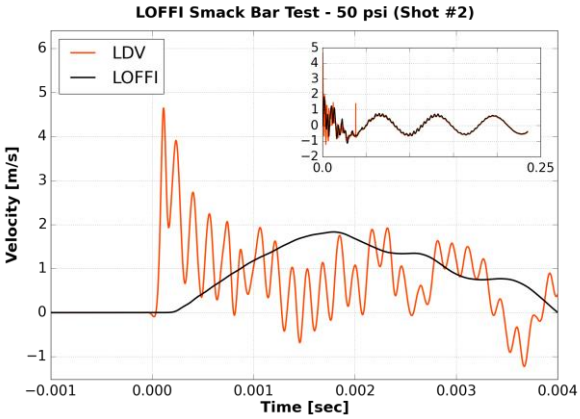
LOFFI Smack Bar Test - 50 psi (Shot #2)
LDV
LOFFI
Velocity [m/s]
Time [sec]

(b)

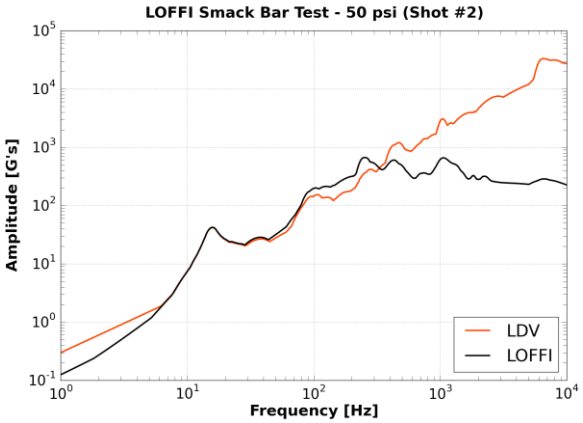
LOFFI Smack Bar Test - 50 psi (Shot #2)
Amplitude [G's]
Frequency [Hz]
LDV
LOFFI

(c)

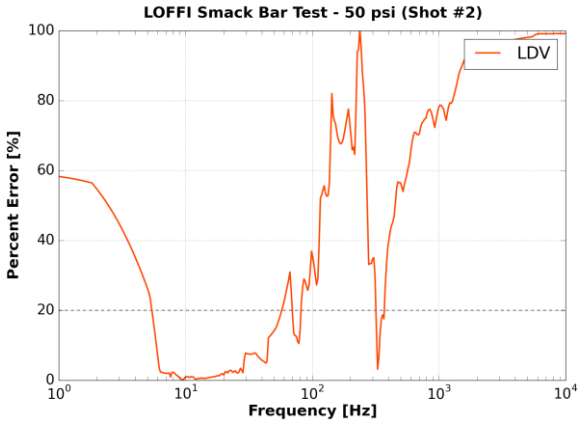
LOFFI Smack Bar Test - 50 psi (Shot #2)
Percent Error [%]
Frequency [Hz]
LDV

(d)

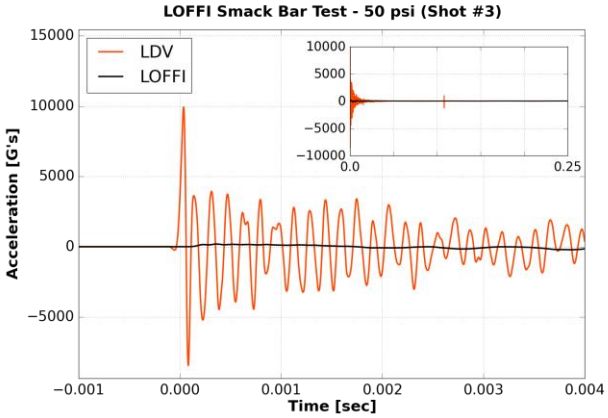
LOFFI Smack Bar Test - 50 psi (Shot #3)
Acceleration [G's]
Time [sec]
LDV
LOFFI

(a)

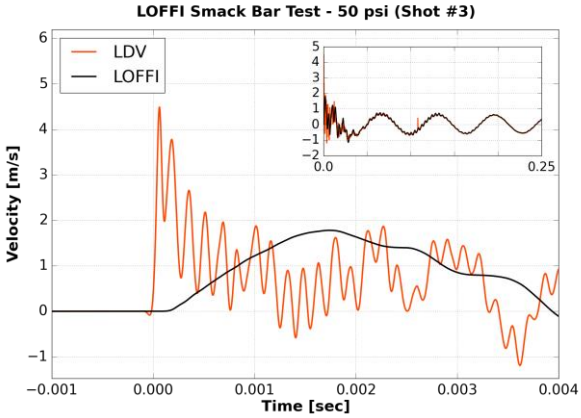
LOFFI Smack Bar Test - 50 psi (Shot #3)
Velocity [m/s]
Time [sec]
LDV
LOFFI

(b)

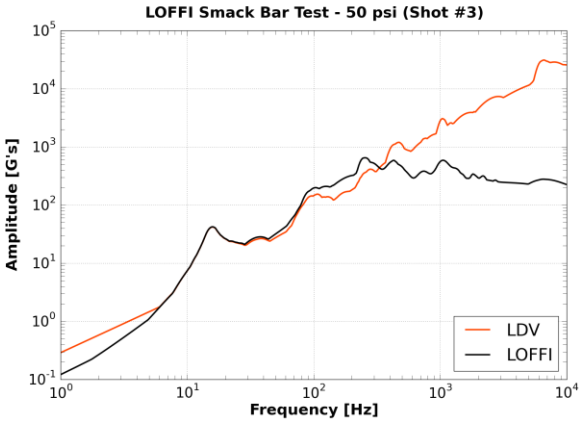
LOFFI Smack Bar Test - 50 psi (Shot #3)
Amplitude [G's]
Frequency [Hz]
LDV
LOFFI

(c)

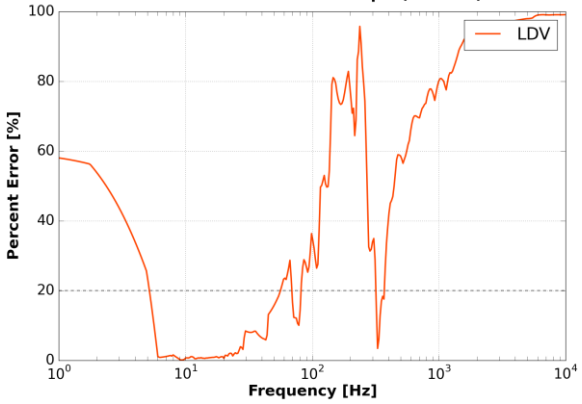
LOFFI Smack Bar Test - 50 psi (Shot #3)
Percent Error [%]
Frequency [Hz]
LDV

(d)

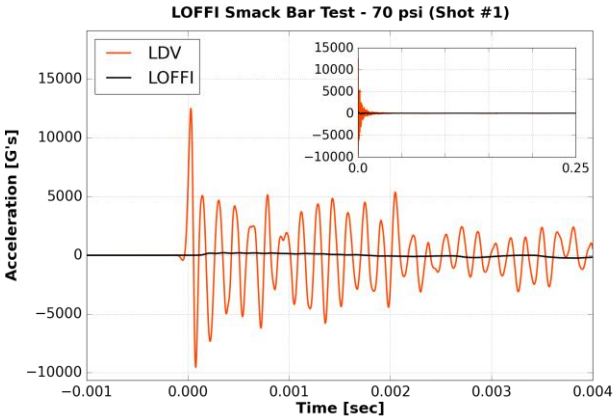
LOFFI Smack Bar Test - 70 psi (Shot #1)
LDV
LOFFI
Acceleration [G's]
Time [sec]

(a)

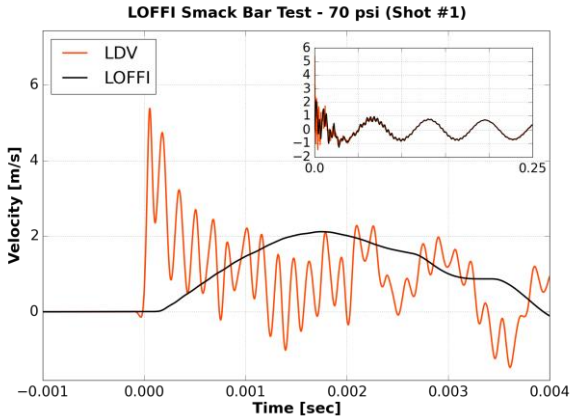
LOFFI Smack Bar Test - 70 psi (Shot #1)
LDV
LOFFI
Velocity [m/s]
Time [sec]

(b)

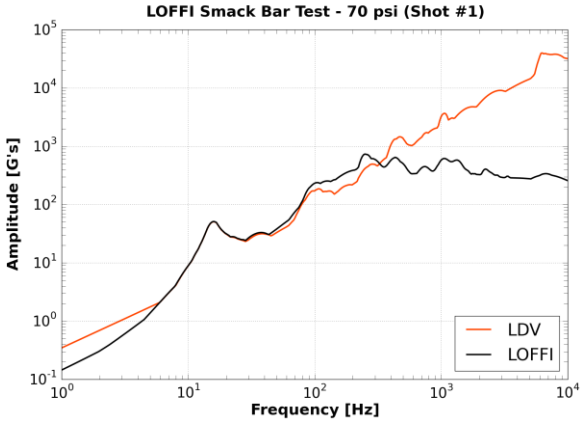
LOFFI Smack Bar Test - 70 psi (Shot #1)
LDV
LOFFI
Amplitude [G's]
Frequency [Hz]

(c)

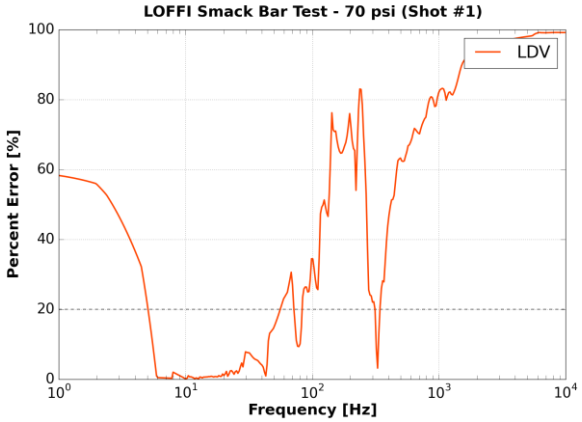
LOFFI Smack Bar Test - 70 psi (Shot #1)
LDV
Percent Error [%]
Frequency [Hz]

(d)

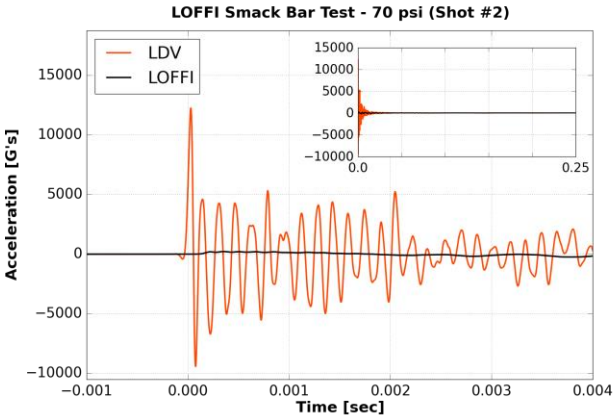
LOFFI Smack Bar Test - 70 psi (Shot #2)
LDV
LOFFI
Acceleration [G's]
Time [sec]

(a)

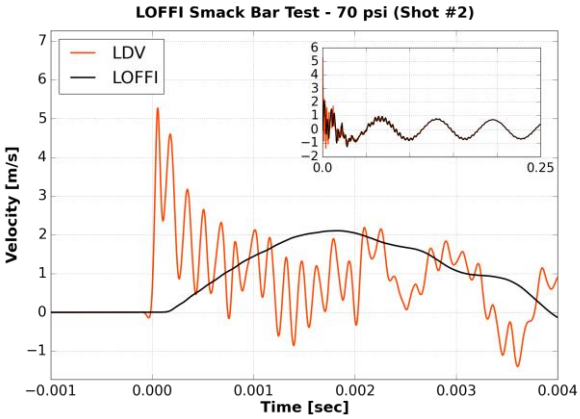
LOFFI Smack Bar Test - 70 psi (Shot #2)
LDV
LOFFI
Velocity [m/s]
Time [sec]

(b)

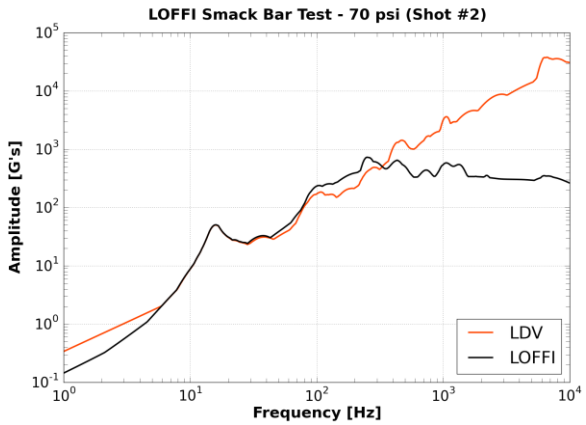
LOFFI Smack Bar Test - 70 psi (Shot #2)
Amplitude [G's]
Frequency [Hz]
LDV
LOFFI

(c)

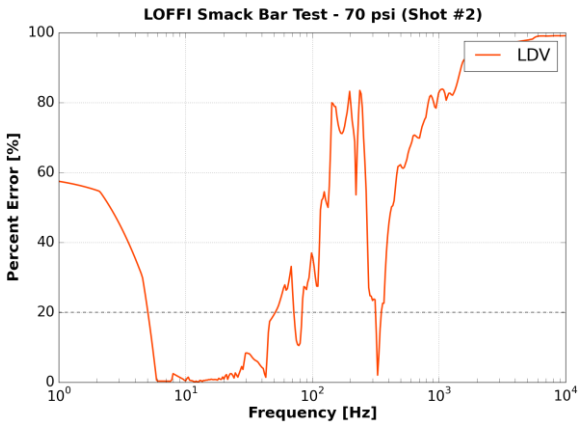
LOFFI Smack Bar Test - 70 psi (Shot #2)
Percent Error [%]
Frequency [Hz]
LDV

(d)

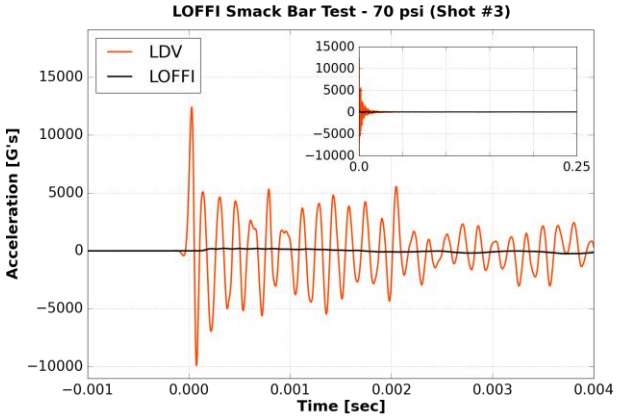
LOFFI Smack Bar Test - 70 psi (Shot #3)
Acceleration [G's]
Time [sec]
LDV
LOFFI

(a)

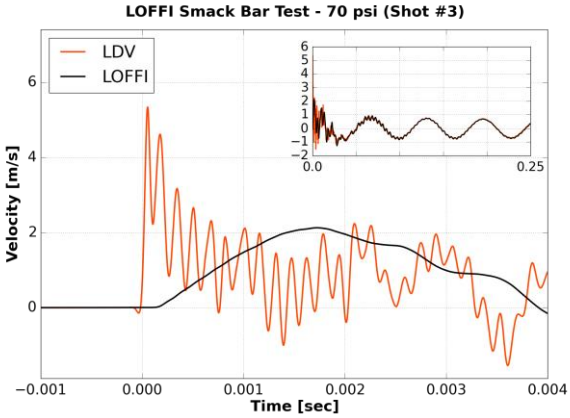
LOFFI Smack Bar Test - 70 psi (Shot #3)
Velocity [m/s]
Time [sec]
LDV
LOFFI

(b)

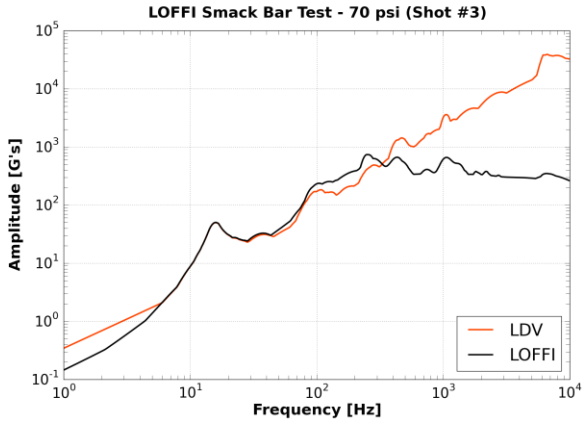
LOFFI Smack Bar Test - 70 psi (Shot #3)
Amplitude [G's]
Frequency [Hz]
LDV
LOFFI

(c)

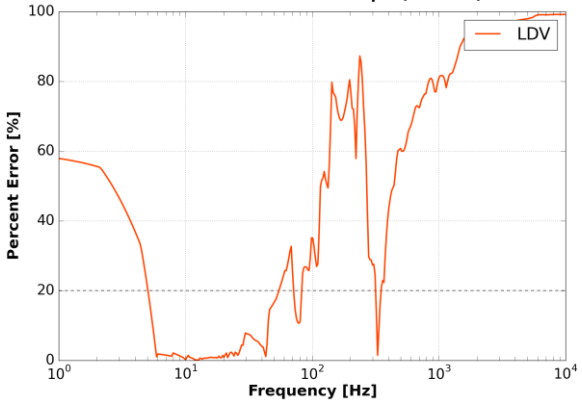
LOFFI Smack Bar Test - 70 psi (Shot #3)
Percent Error [%]
Frequency [Hz]
LDV

(d)

b. Appendix B – Flyaway Test Results

i. Endevco 7270A

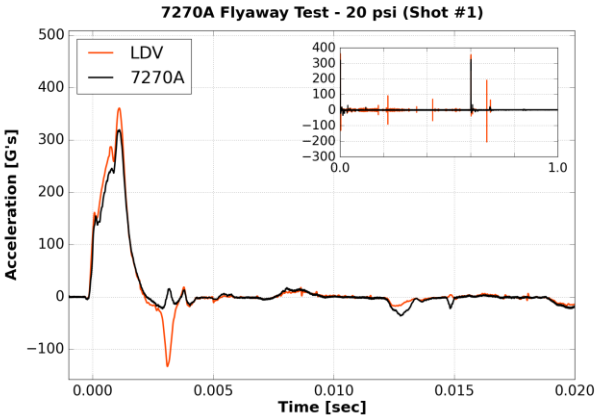

(a)

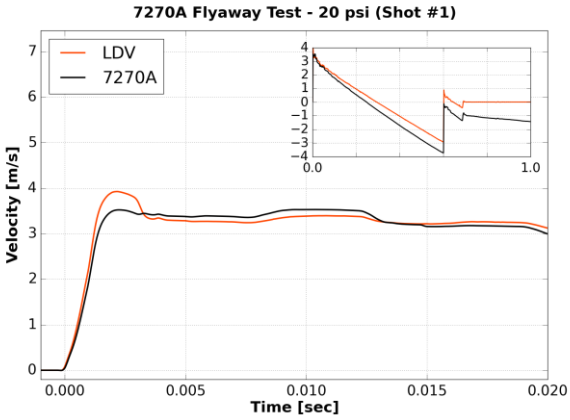

(b)

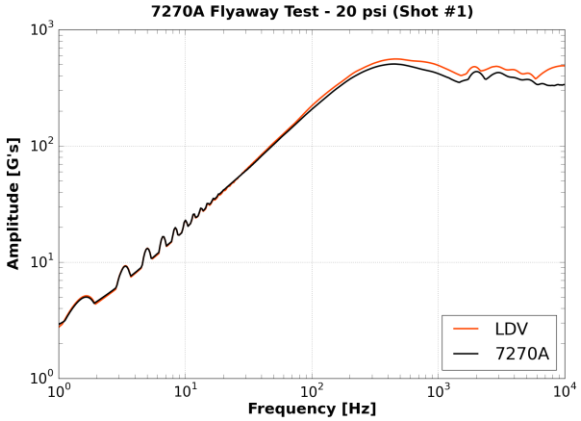

(c)

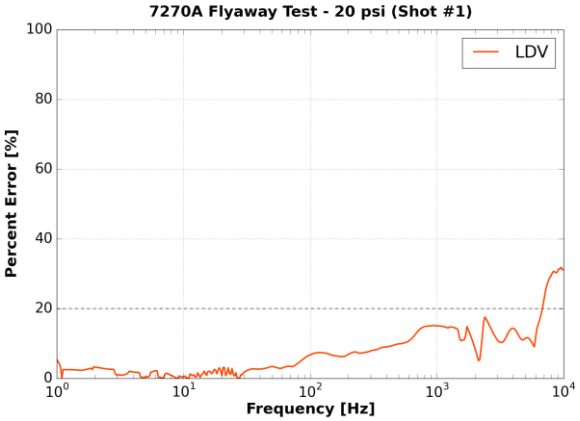

(d)

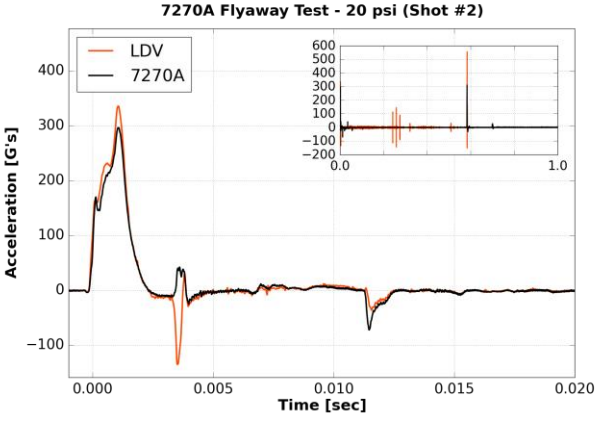

(a)

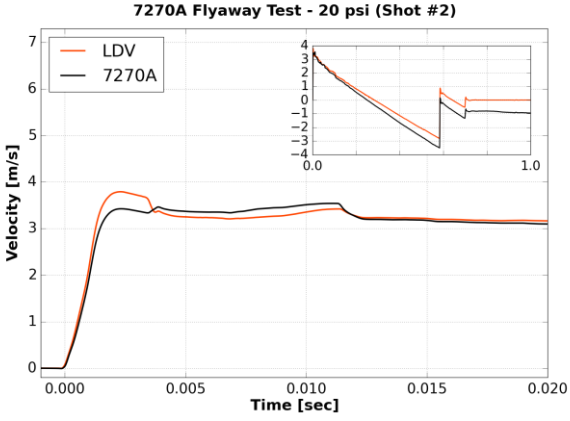

(b)

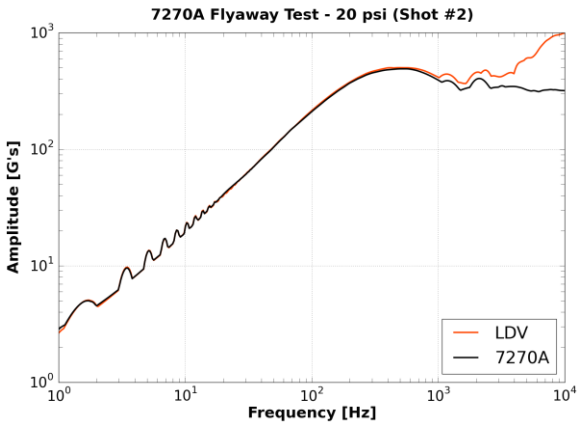
7270A Flyaway Test - 20 psi (Shot #2)
Amplitude [G's]
Frequency [Hz]
LDV
7270A

(c)

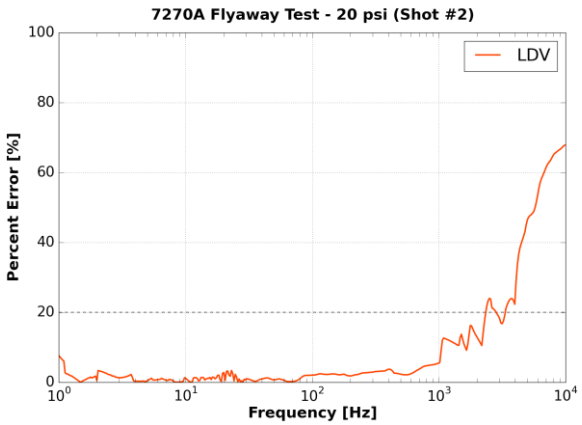
7270A Flyaway Test - 20 psi (Shot #2)
Percent Error [%]
Frequency [Hz]
LDV

(d)

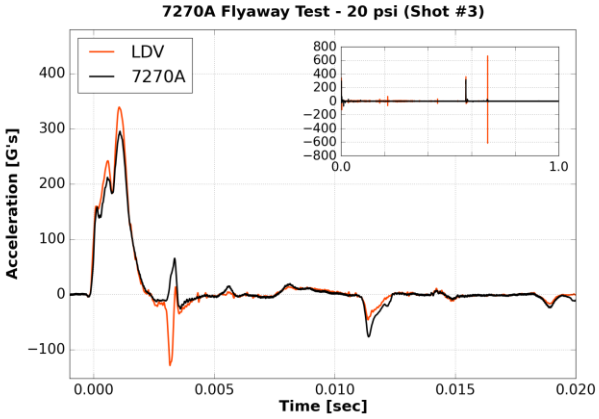
7270A Flyaway Test - 20 psi (Shot #3)
Acceleration [G's]
Time [sec]
LDV
7270A

(a)

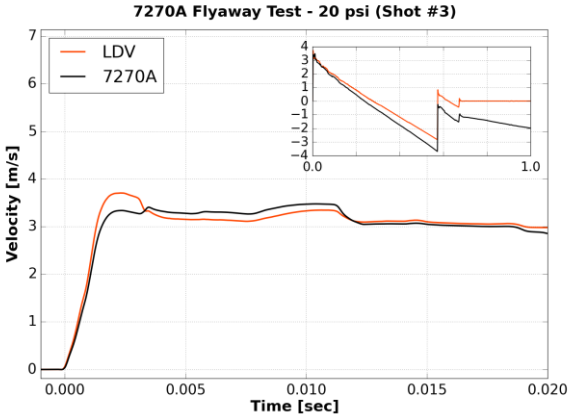
7270A Flyaway Test - 20 psi (Shot #3)
Velocity [m/s]
Time [sec]
LDV
7270A

(b)

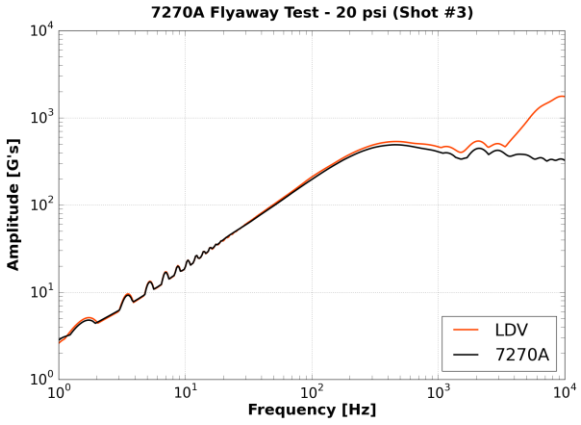
7270A Flyaway Test - 20 psi (Shot #3)
Amplitude [G's]
Frequency [Hz]
LDV
7270A

(c)

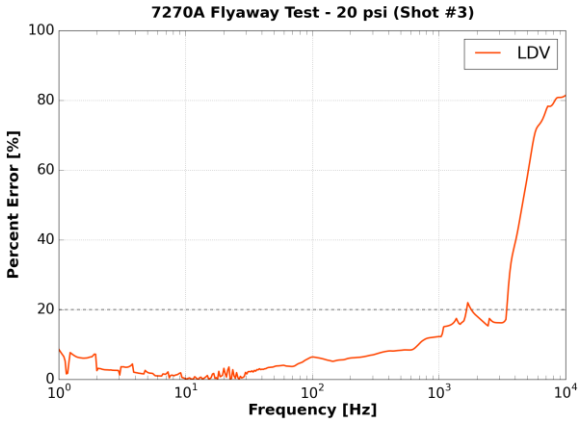
7270A Flyaway Test - 20 psi (Shot #3)
Percent Error [%]
Frequency [Hz]
LDV

(d)

ii. LOFFI

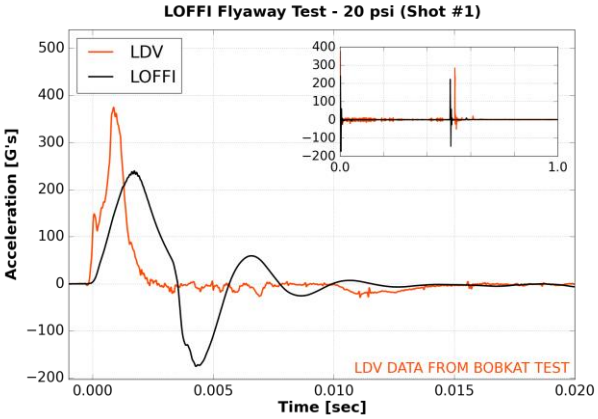

(a)

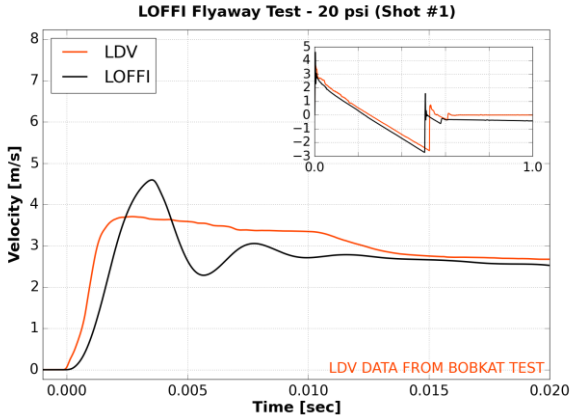

(b)

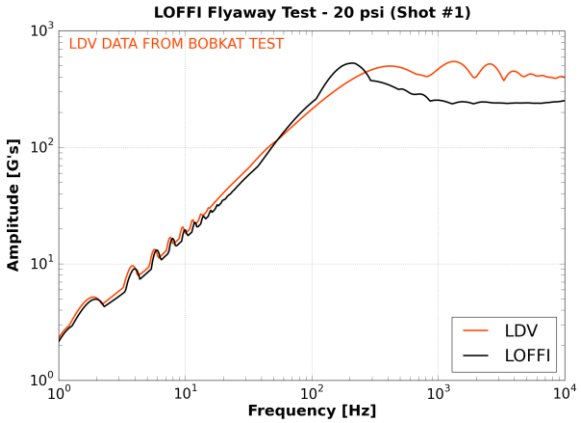

(c)

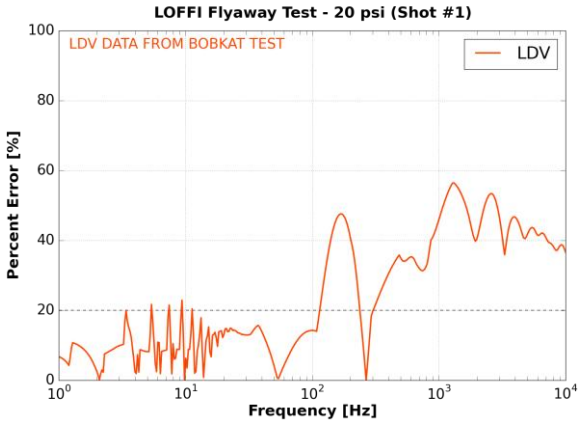

(d)

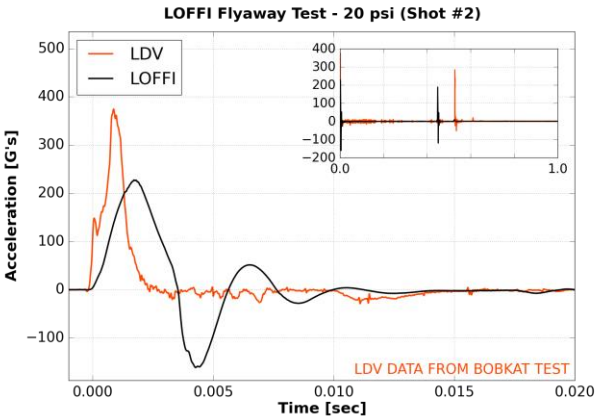

(a)

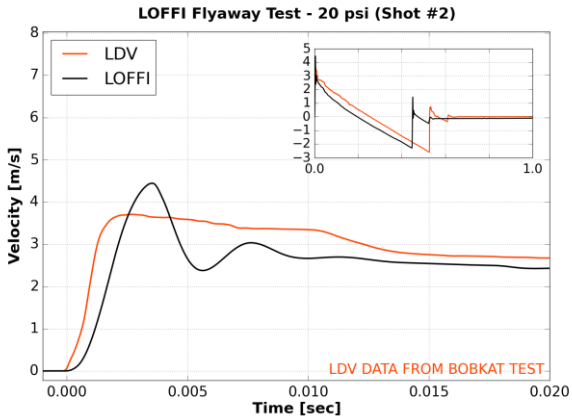

(b)

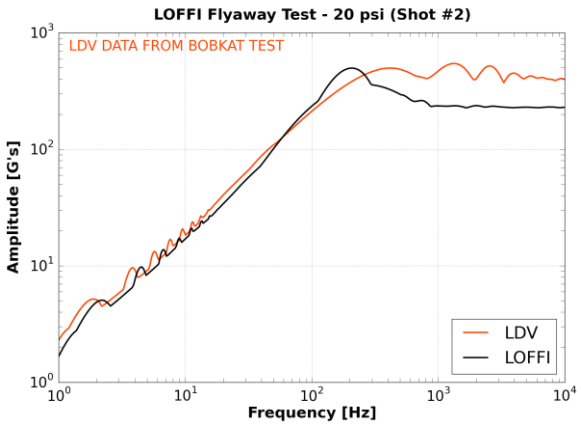
LOFFI Flyaway Test - 20 psi (Shot #2)
LDV DATA FROM BOBKAT TEST
LDV
LOFFI
Amplitude [G's]
Frequency [Hz]

(c)

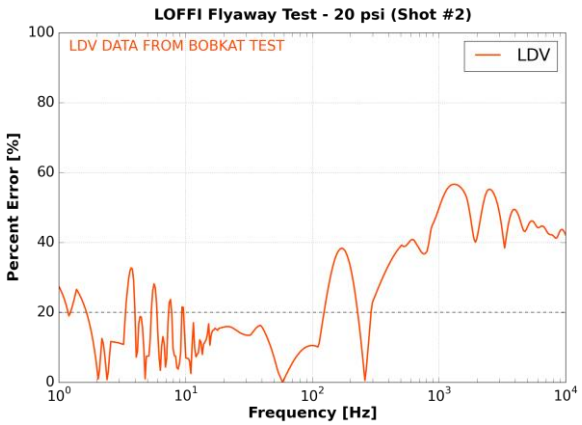
LOFFI Flyaway Test - 20 psi (Shot #2)
LDV DATA FROM BOBKAT TEST
LDV
Percent Error [%]
Frequency [Hz]

(d)

iii. Endevco 7280A

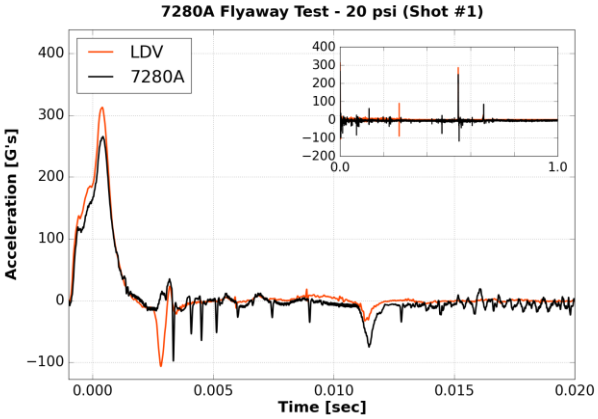

(a)

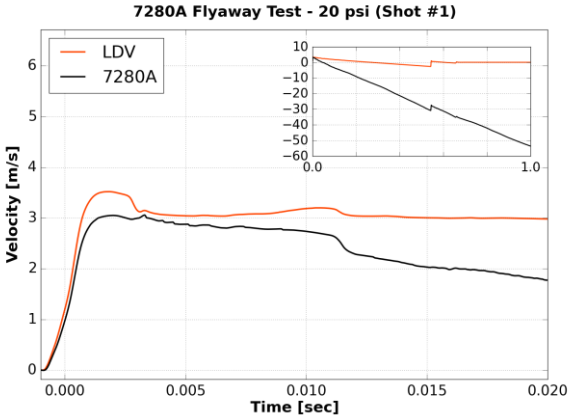

(b)

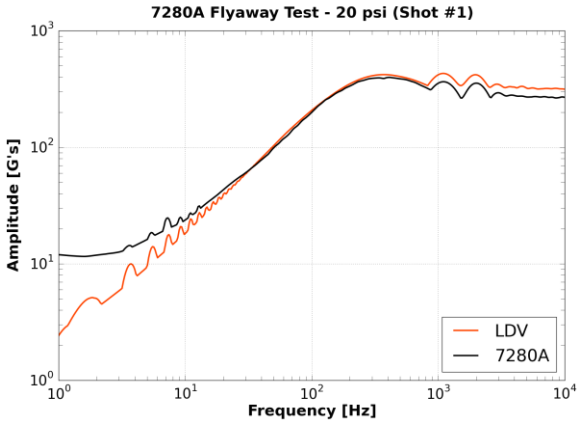

(c)

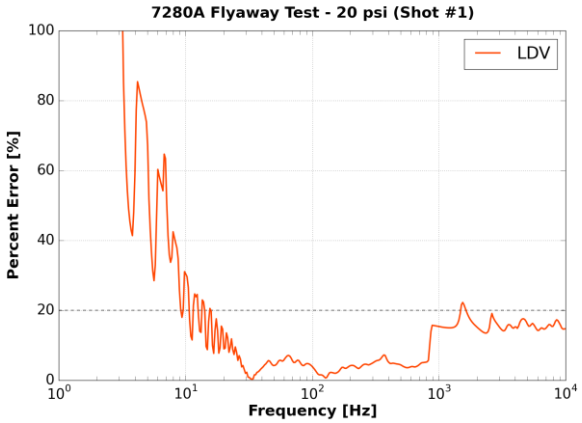

(d)

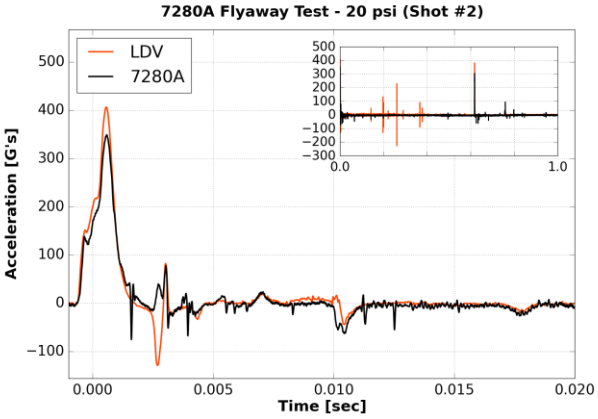

(a)

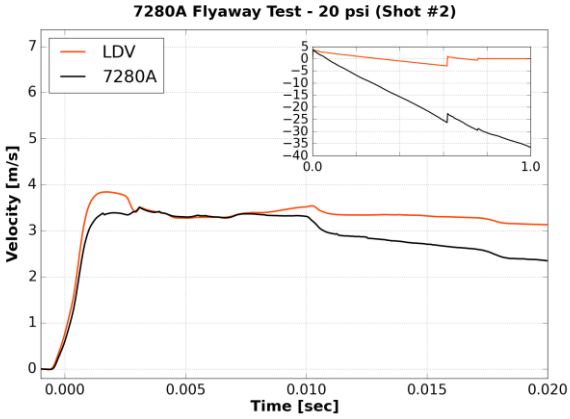

(b)

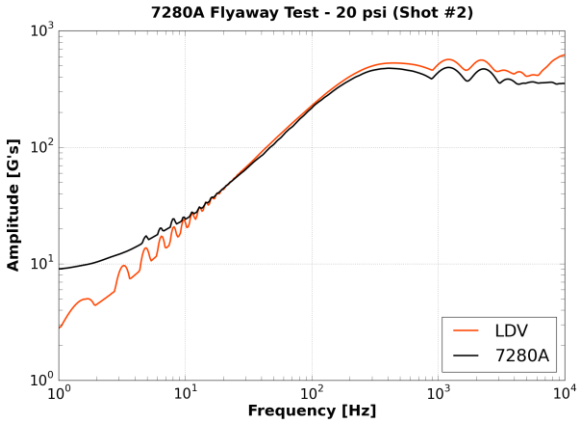
7280A Flyaway Test - 20 psi (Shot #2)
Amplitude [G's]
Frequency [Hz]
LDV
7280A

(c)

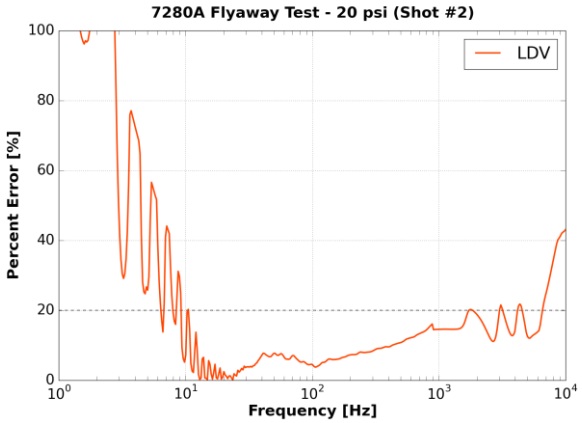
7280A Flyaway Test - 20 psi (Shot #2)
Percent Error [%]
Frequency [Hz]
LDV

(d)

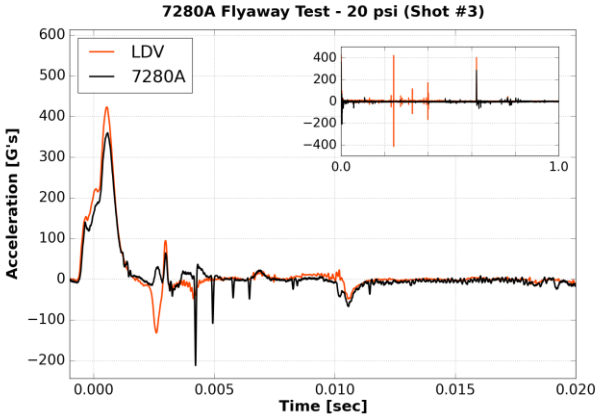
7280A Flyaway Test - 20 psi (Shot #3)
Acceleration [G's]
Time [sec]
LDV
7280A

(a)

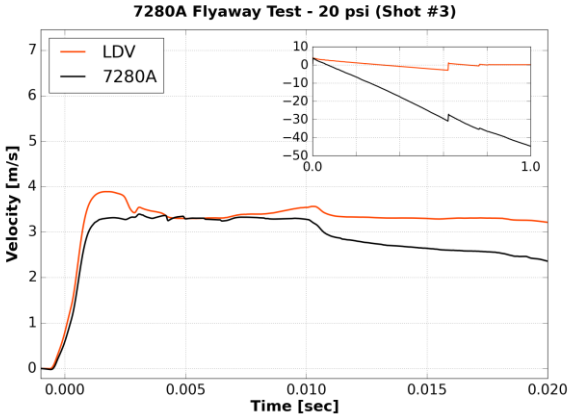
7280A Flyaway Test - 20 psi (Shot #3)
Velocity [m/s]
Time [sec]
LDV
7280A

(b)

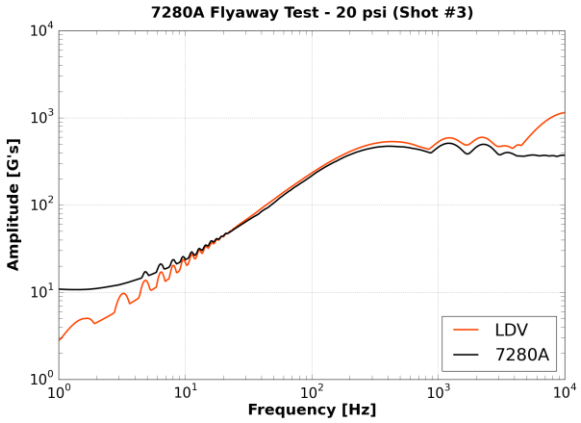
7280A Flyaway Test - 20 psi (Shot #3)
Amplitude [G's]
Frequency [Hz]
LDV
7280A

(c)

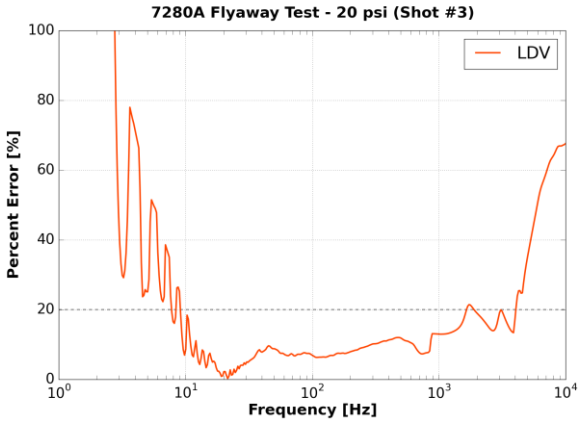
7280A Flyaway Test - 20 psi (Shot #3)
Percent Error [%]
Frequency [Hz]
LDV

(d)

iv. Endevco 2262A

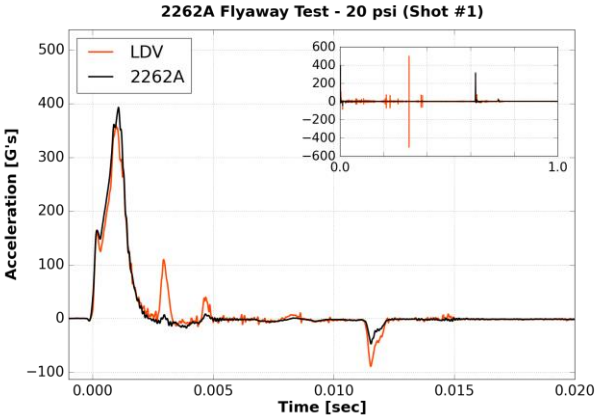

(a)

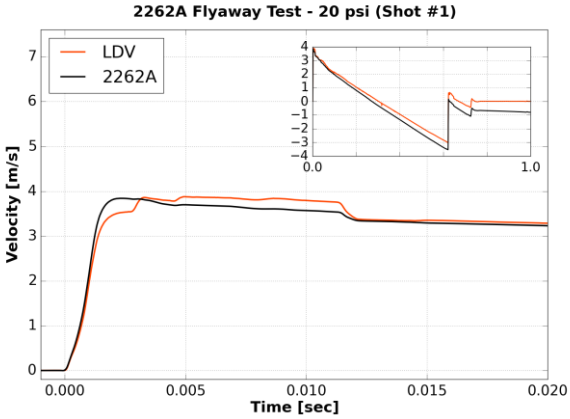

(b)

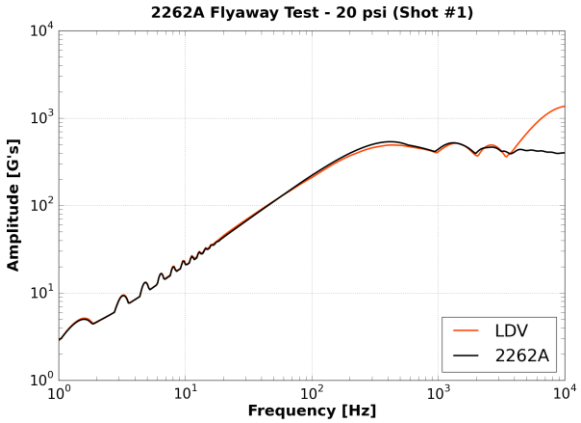

(c)

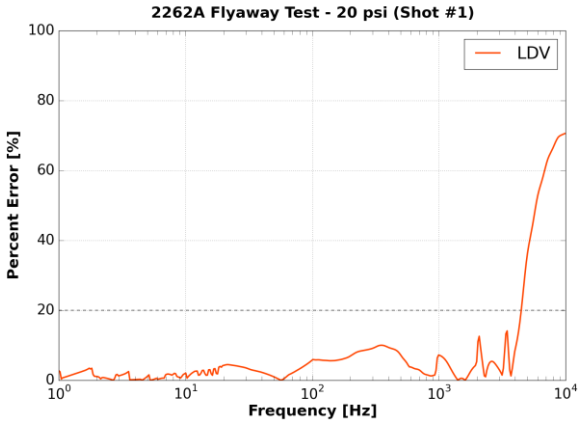

(d)

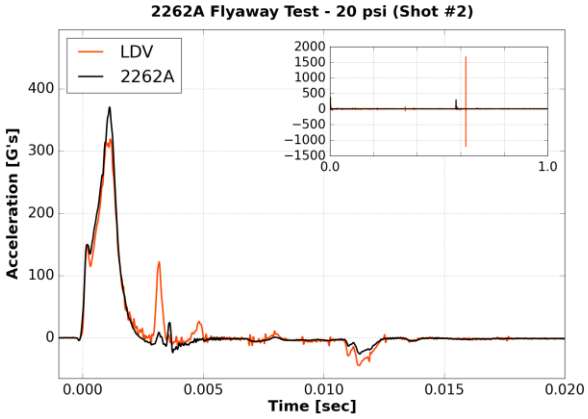

(a)

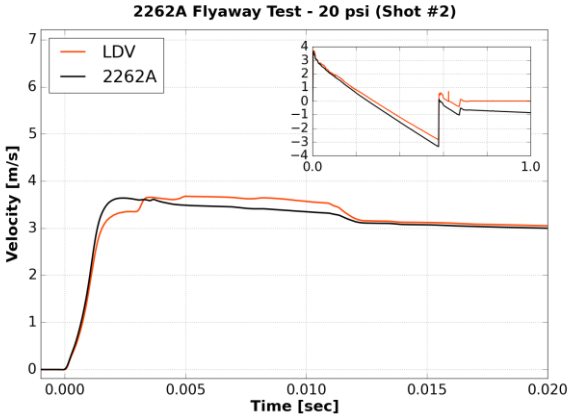

(b)

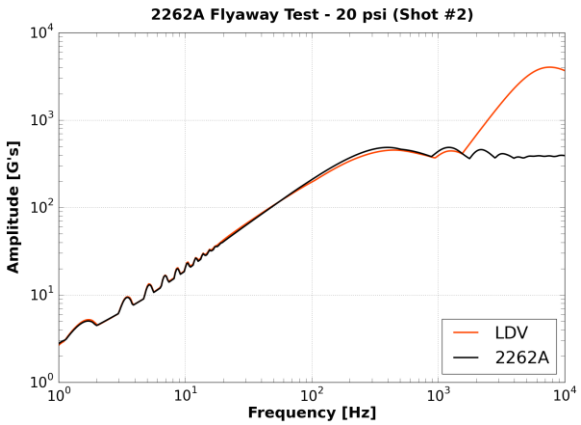
2262A Flyaway Test - 20 psi (Shot #2)
Amplitude [G's]
Frequency [Hz]
LDV
2262A

(c)

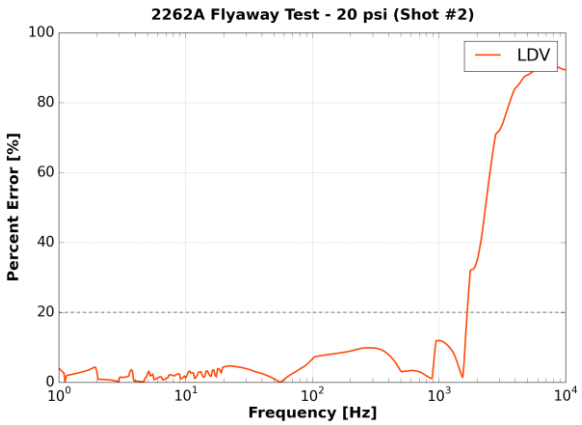
2262A Flyaway Test - 20 psi (Shot #2)
Percent Error [%]
Frequency [Hz]
LDV

(d)

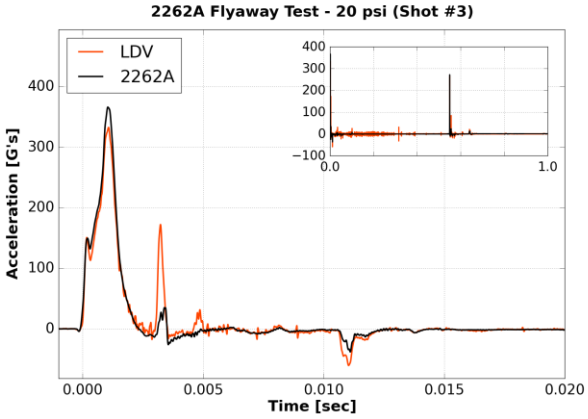
2262A Flyaway Test - 20 psi (Shot #3)
Acceleration [G's]
Time [sec]
LDV
2262A

(a)

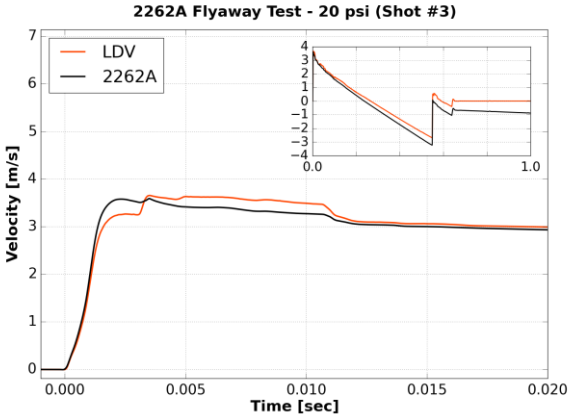
2262A Flyaway Test - 20 psi (Shot #3)
Velocity [m/s]
Time [sec]
LDV
2262A

(b)

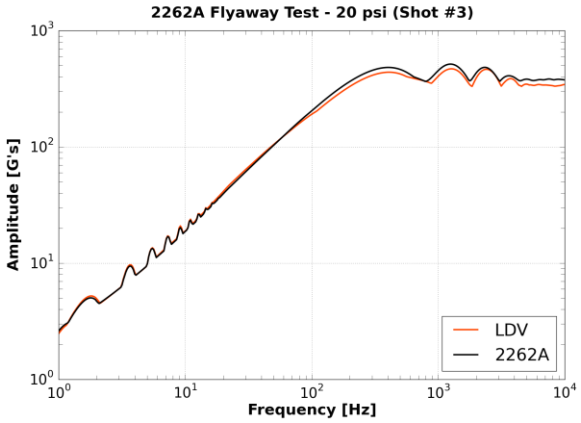
2262A Flyaway Test - 20 psi (Shot #3)
Amplitude [G's]
Frequency [Hz]
LDV
2262A

(c)

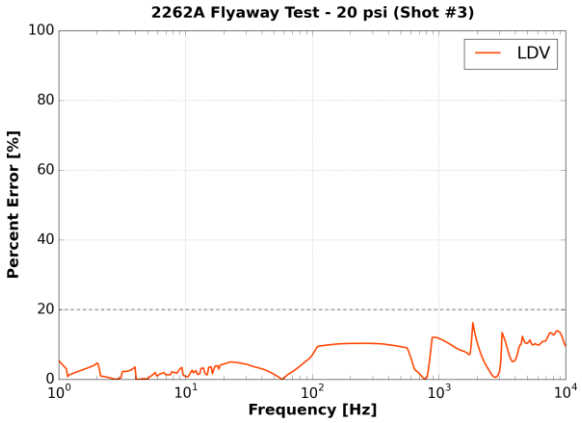
2262A Flyaway Test - 20 psi (Shot #3)
Percent Error [%]
Frequency [Hz]
LDV

(d)

v. Endevco 7270AM6

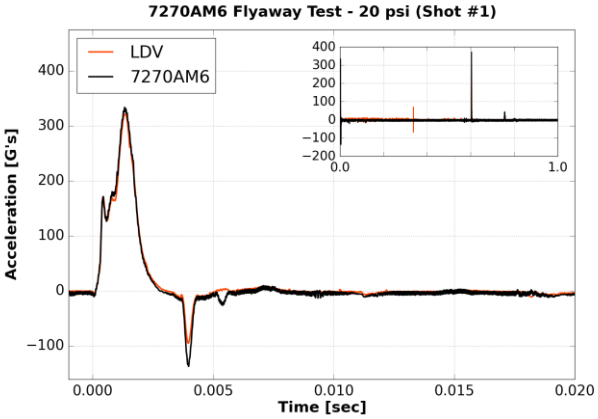

(a)

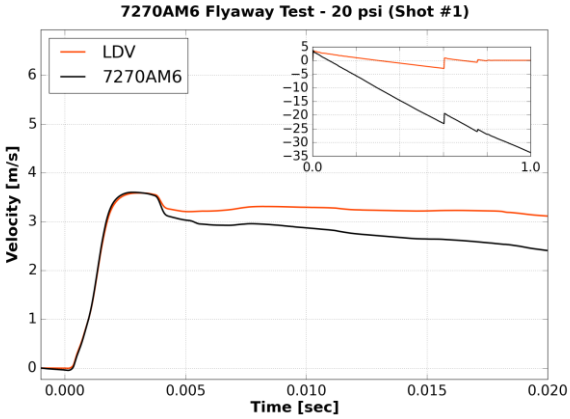

(b)

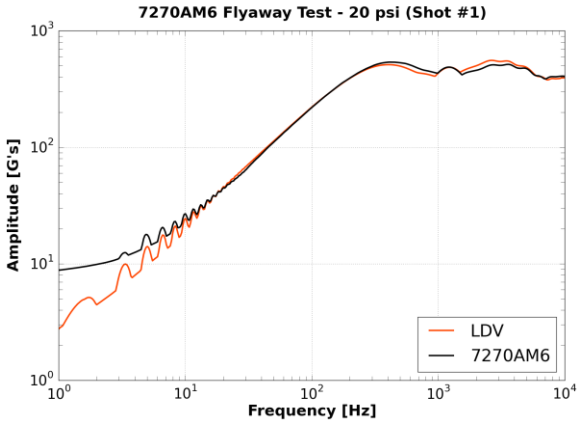

(c)

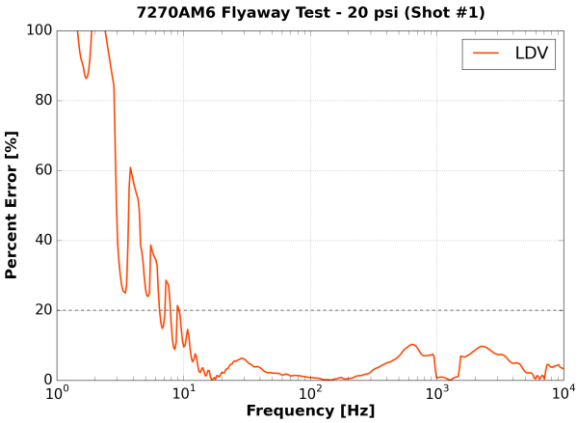

(d)

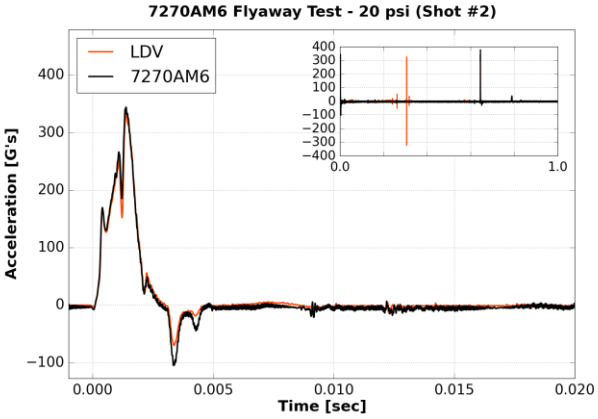

(a)

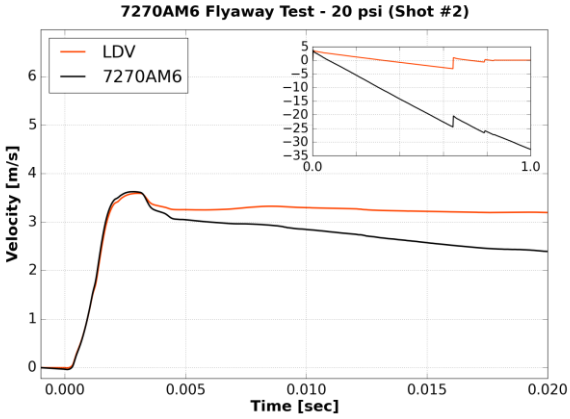

(b)

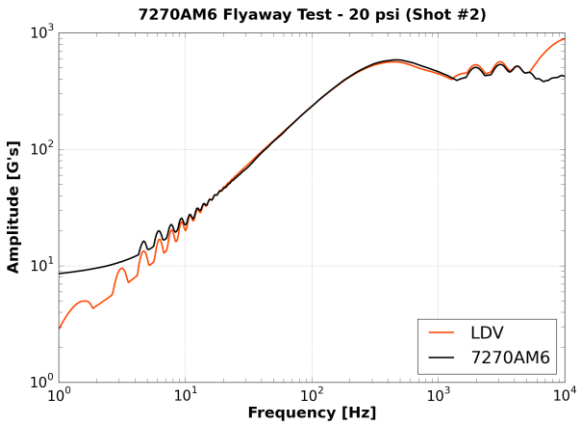
7270AM6 Flyaway Test - 20 psi (Shot #2)
Amplitude [G's]
Frequency [Hz]
LDV
7270AM6

(c)

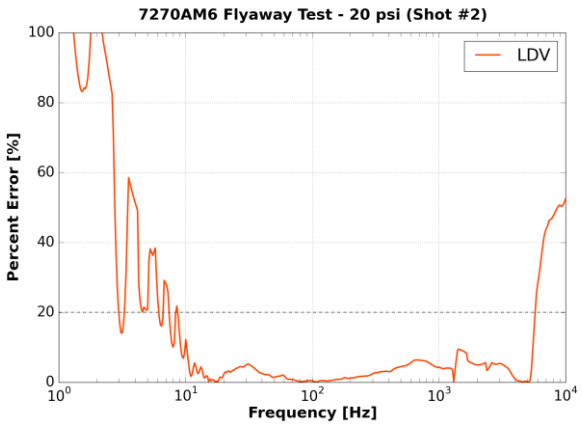
7270AM6 Flyaway Test - 20 psi (Shot #2)
Percent Error [%]
Frequency [Hz]
LDV

(d)

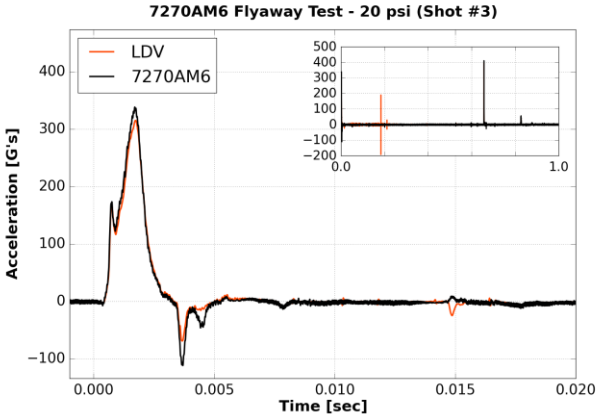
7270AM6 Flyaway Test - 20 psi (Shot #3)
Acceleration [G's]
Time [sec]
LDV
7270AM6

(a)

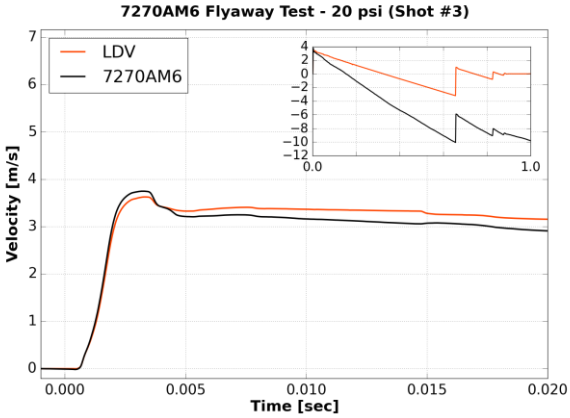
7270AM6 Flyaway Test - 20 psi (Shot #3)
Velocity [m/s]
Time [sec]
LDV
7270AM6

(b)

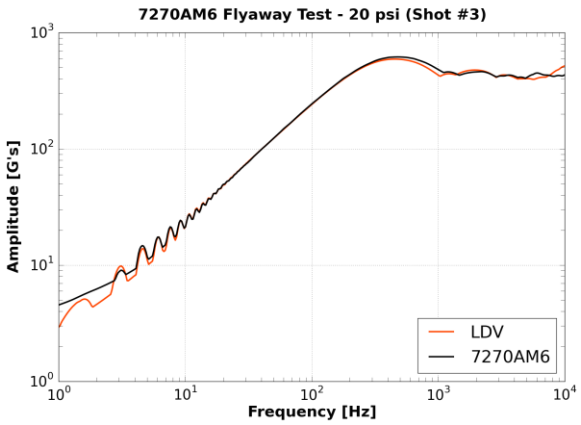
7270AM6 Flyaway Test - 20 psi (Shot #3)
Amplitude [G's]
Frequency [Hz]
LDV
7270AM6

(c)

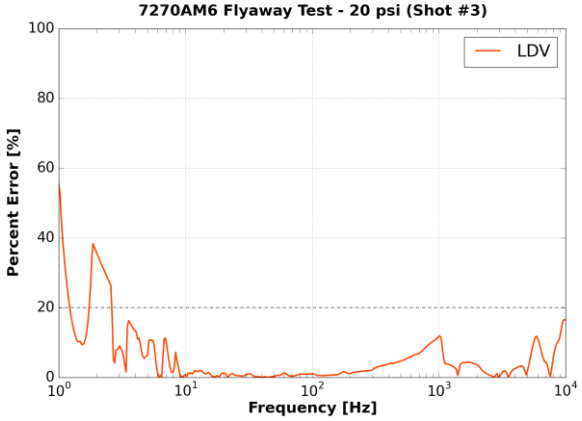
7270AM6 Flyaway Test - 20 psi (Shot #3)
Percent Error [%]
Frequency [Hz]
LDV

(d)

vi. BOBKAT

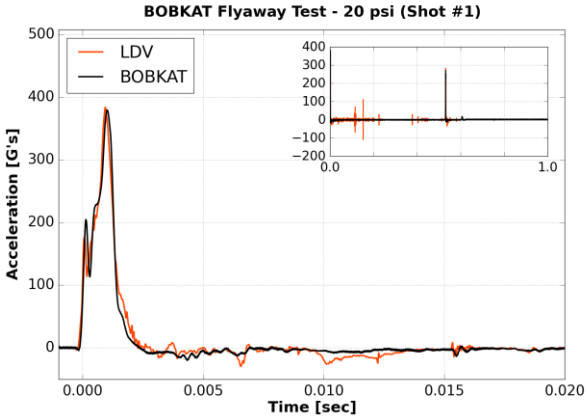

(a)

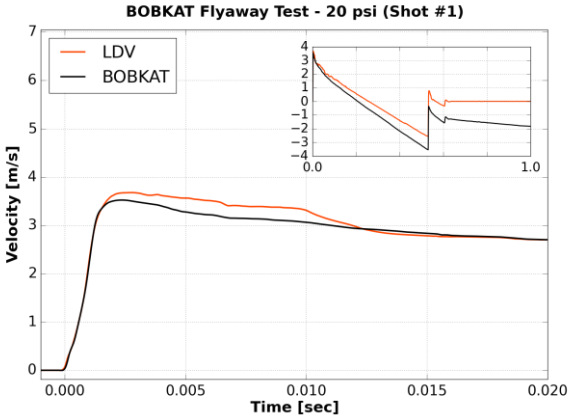

(b)

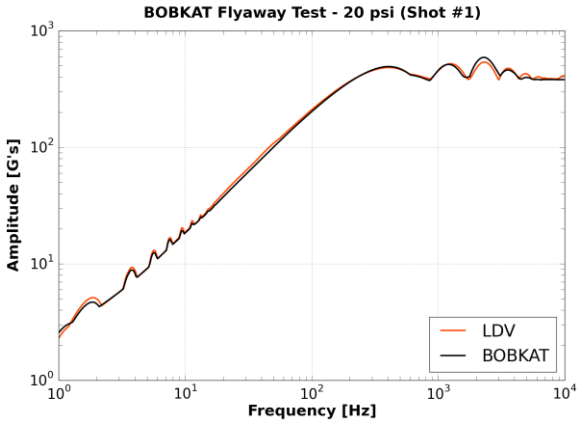

(c)

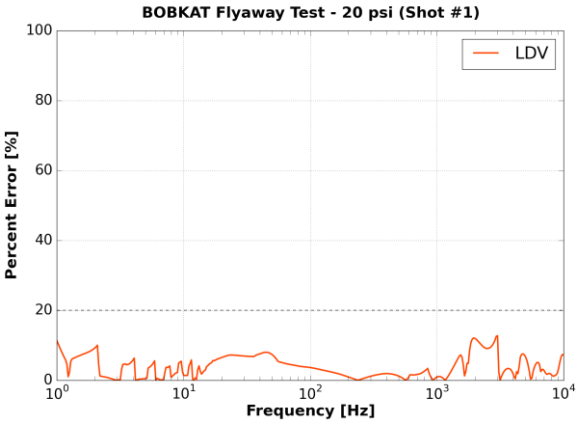

(d)

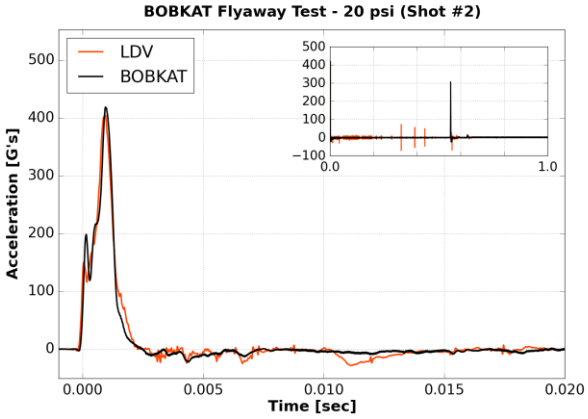

(a)

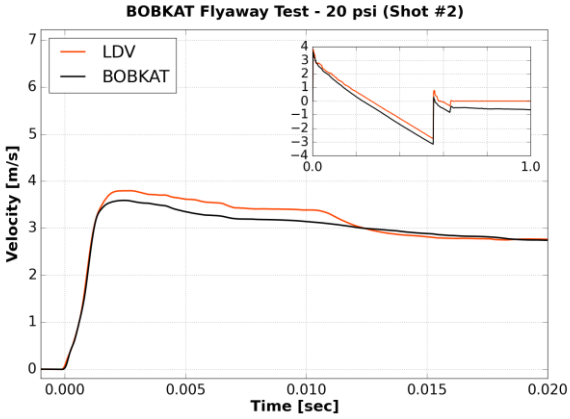

(b)

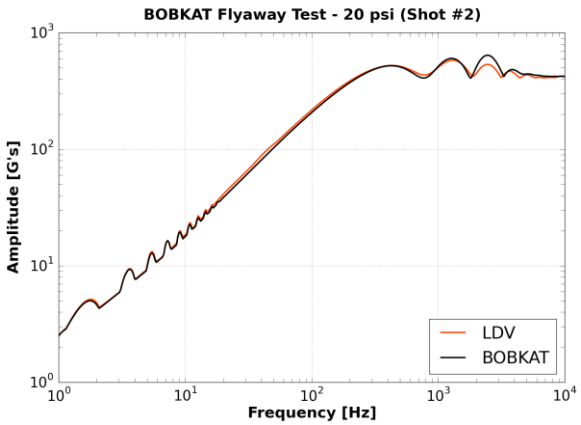
BOBKAT Flyaway Test - 20 psi (Shot #2)
Amplitude [G's]
Frequency [Hz]
LDV
BOBKAT

(c)

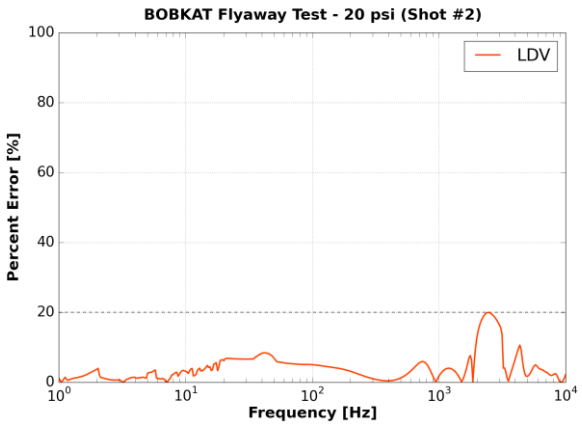
BOBKAT Flyaway Test - 20 psi (Shot #2)
Percent Error [%]
Frequency [Hz]
LDV

(d)

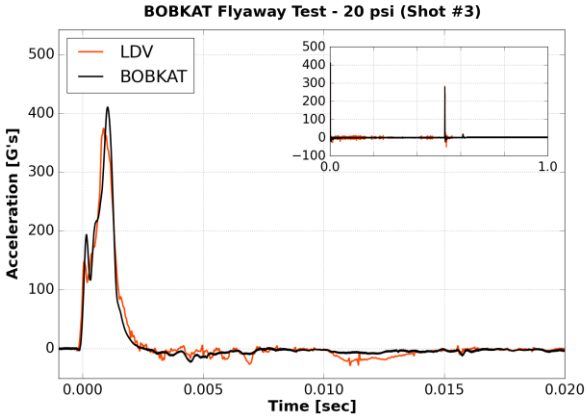
BOBKAT Flyaway Test - 20 psi (Shot #3)
Acceleration [G's]
Time [sec]
LDV
BOBKAT

(a)

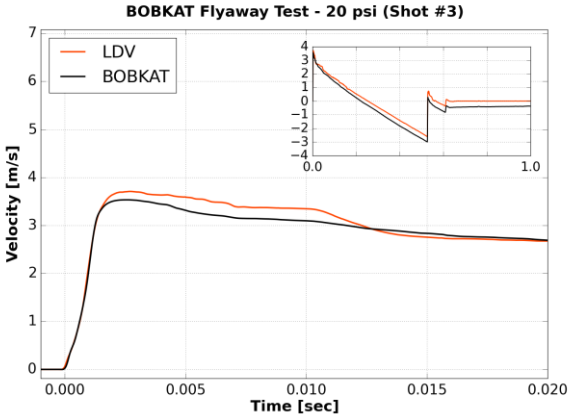
BOBKAT Flyaway Test - 20 psi (Shot #3)
Velocity [m/s]
Time [sec]
LDV
BOBKAT

(b)

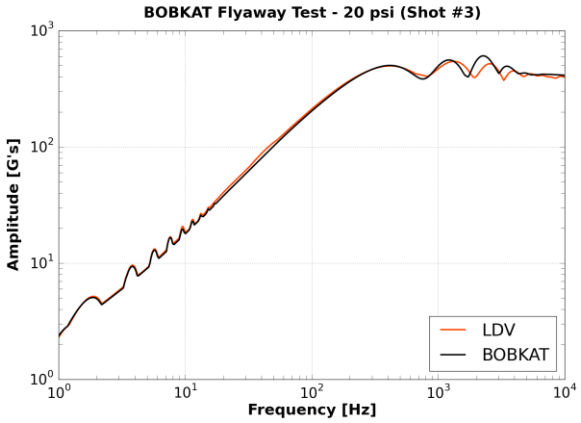
BOBKAT Flyaway Test - 20 psi (Shot #3)
Amplitude [G's]
Frequency [Hz]
LDV
BOBKAT

(c)

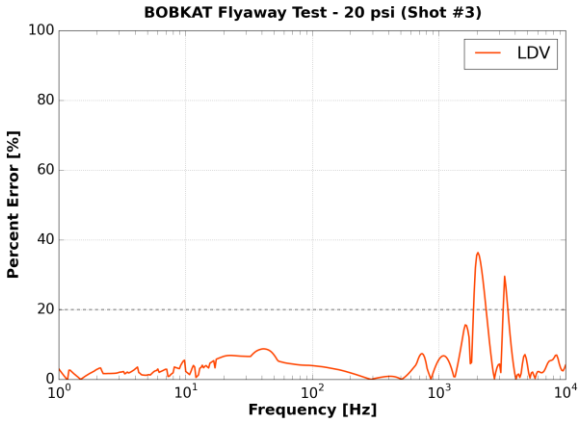
BOBKAT Flyaway Test - 20 psi (Shot #3)
Percent Error [%]
Frequency [Hz]
LDV

(d)

vii. Endevco 7264D

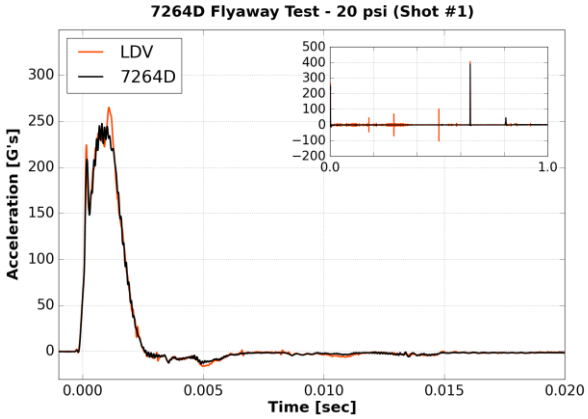

(a)

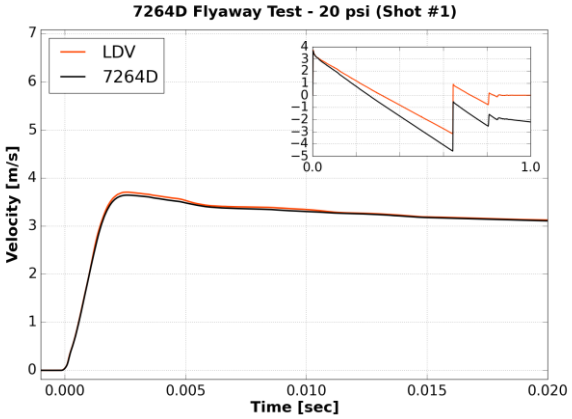

(b)

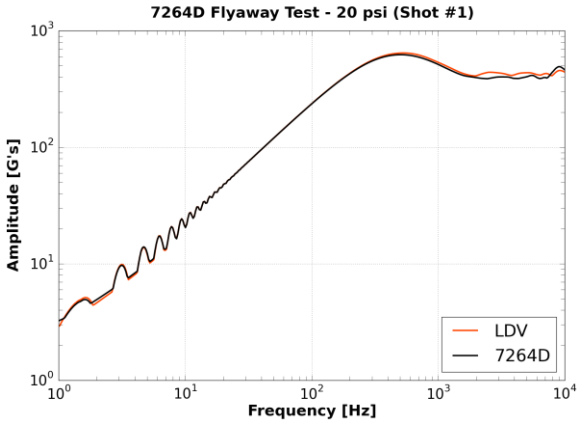

(c)

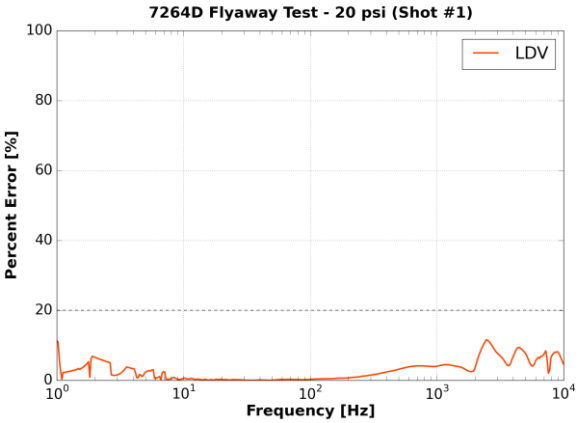

(d)

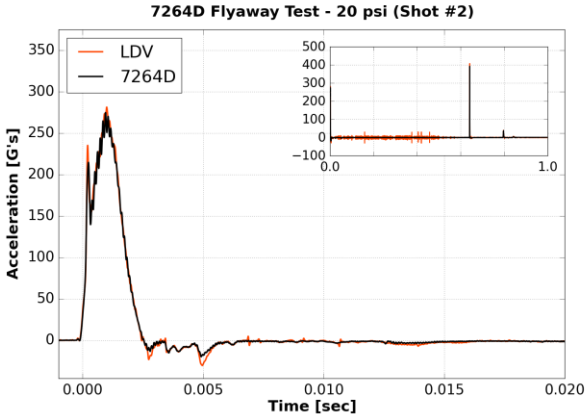

(a)

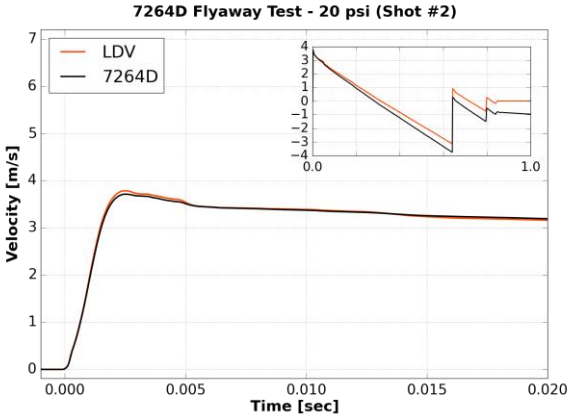

(b)

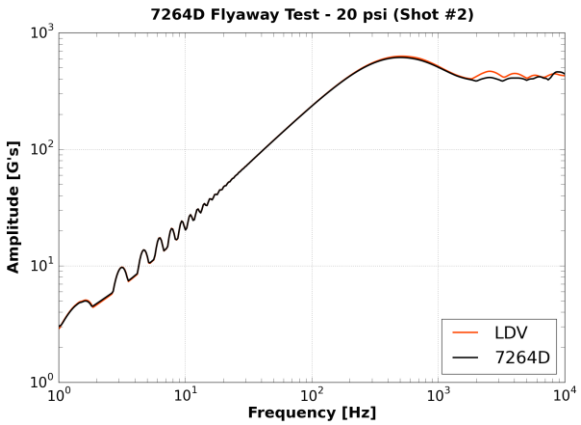
7264D Flyaway Test - 20 psi (Shot #2)
Amplitude [G's]
Frequency [Hz]
LDV
7264D

(c)

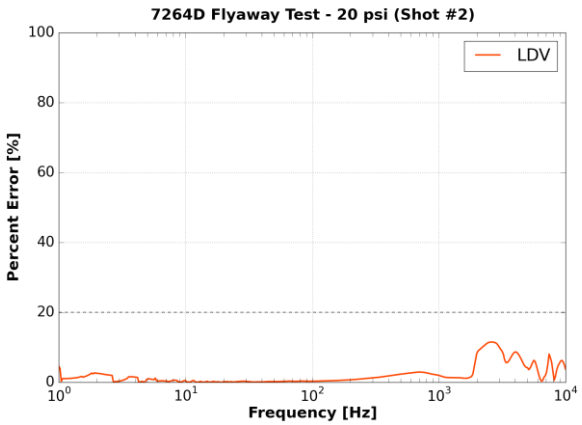
7264D Flyaway Test - 20 psi (Shot #2)
Percent Error [%]
Frequency [Hz]
LDV

(d)

c. Appendix C – Explosive Rig Test Results

i. Endevco 7270AM6

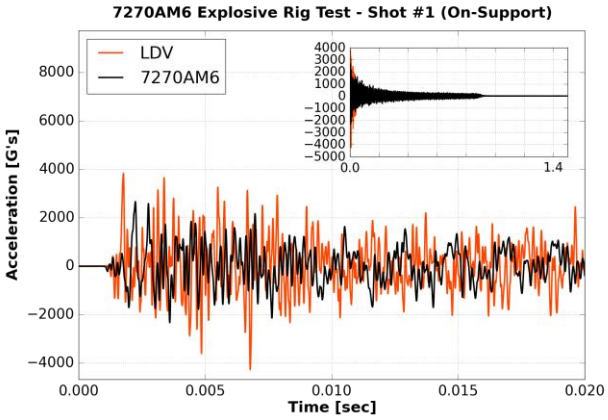

(a)

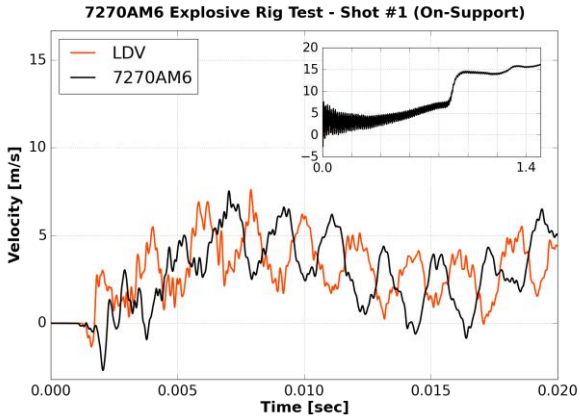

(b)

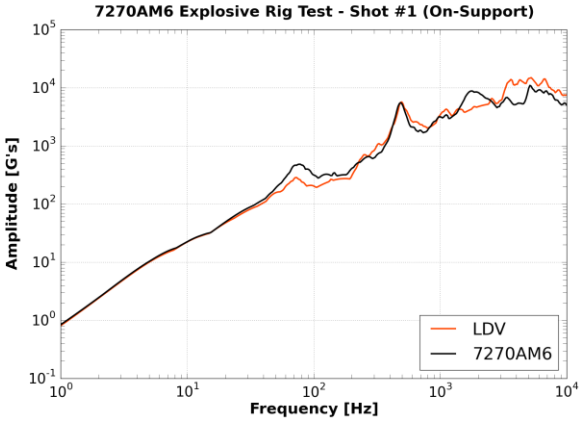

(c)

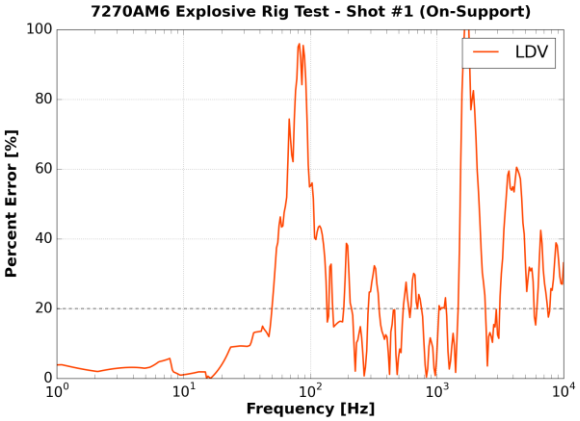

(d)

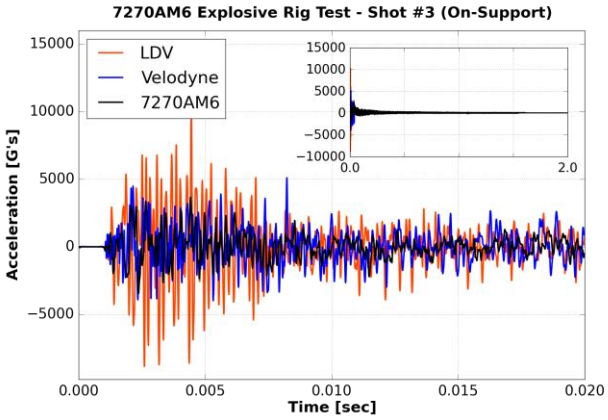

(a)

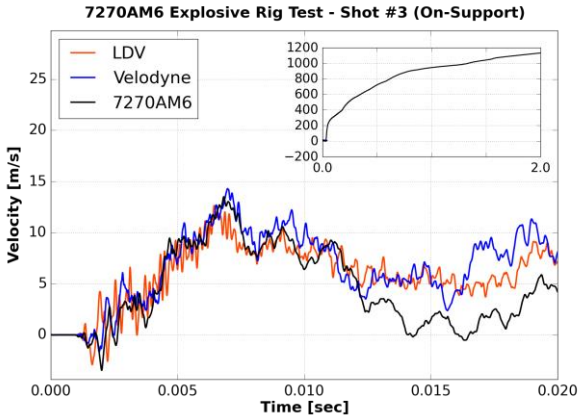

(b)

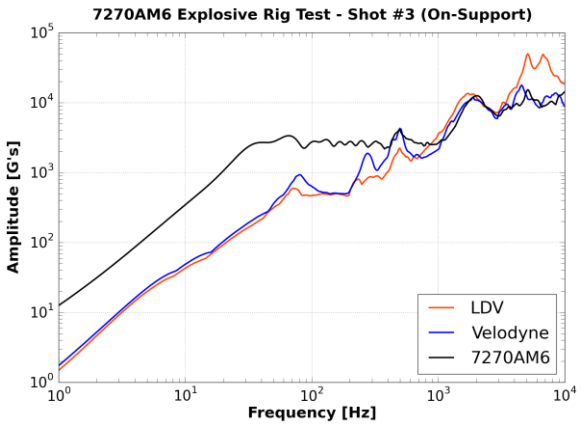
7270AM6 Explosive Rig Test - Shot #3 (On-Support)
Amplitude [G's]
Frequency [Hz]
LDV
Velodyne
7270AM6

(c)

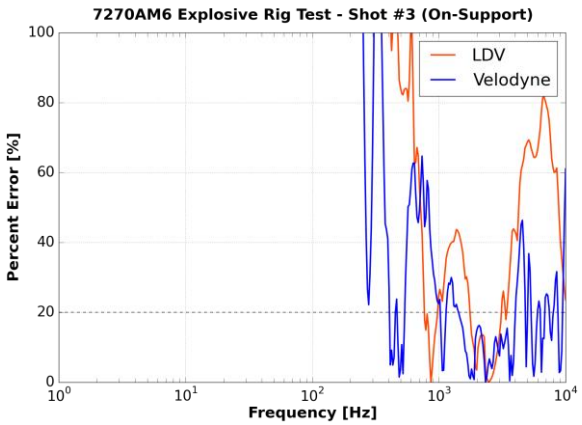
7270AM6 Explosive Rig Test - Shot #3 (On-Support)
Percent Error [%]
Frequency [Hz]
LDV
Velodyne

(d)

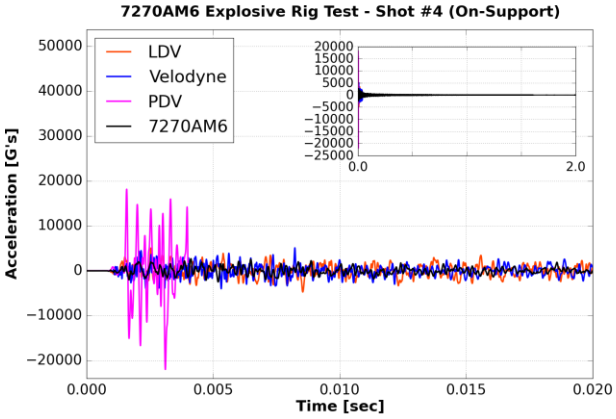
7270AM6 Explosive Rig Test - Shot #4 (On-Support)
Acceleration [G's]
Time [sec]
LDV
Velodyne
PDV
7270AM6

(a)

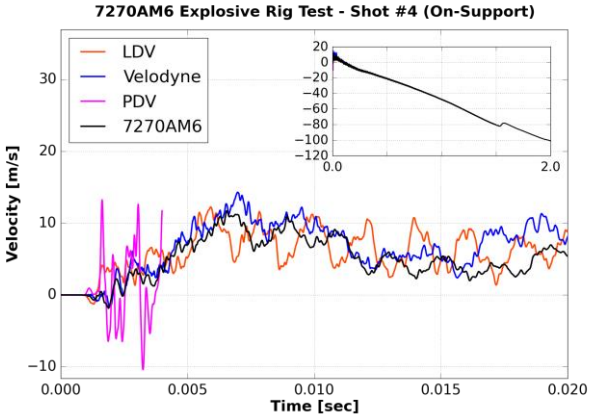
7270AM6 Explosive Rig Test - Shot #4 (On-Support)
Velocity [m/s]
Time [sec]
LDV
Velodyne
PDV
7270AM6

(b)

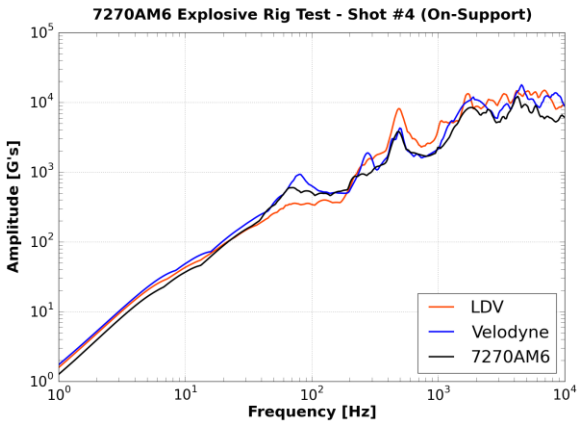
7270AM6 Explosive Rig Test - Shot #4 (On-Support)
Amplitude [G's]
Frequency [Hz]
LDV
Velodyne
7270AM6

(c)

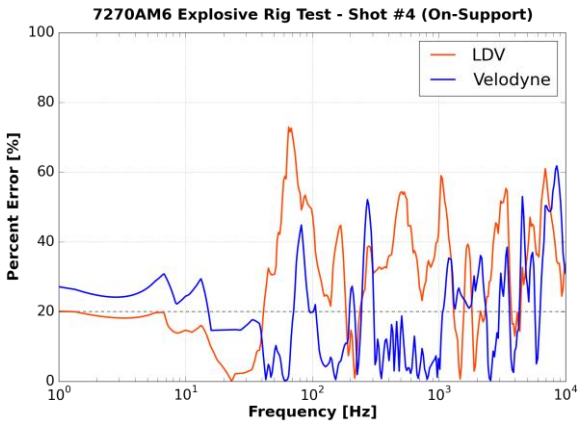
7270AM6 Explosive Rig Test - Shot #4 (On-Support)
Percent Error [%]
Frequency [Hz]
LDV
Velodyne

(d)

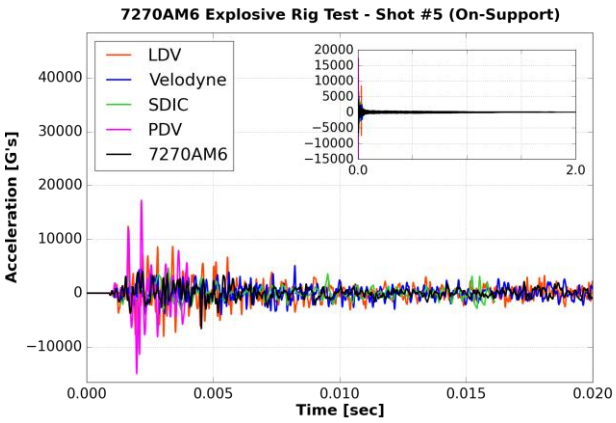
7270AM6 Explosive Rig Test - Shot #5 (On-Support)
LDV
Velodyne
SDIC
PDV
7270AM6
Acceleration [G's]
Time [sec]

(a)

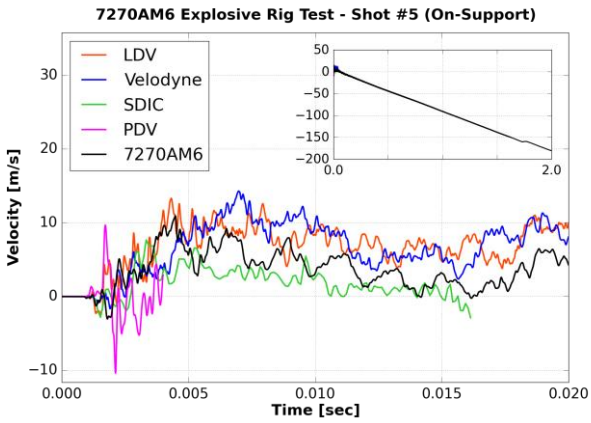
7270AM6 Explosive Rig Test - Shot #5 (On-Support)
LDV
Velodyne
SDIC
PDV
7270AM6
Velocity [m/s]
Time [sec]

(b)

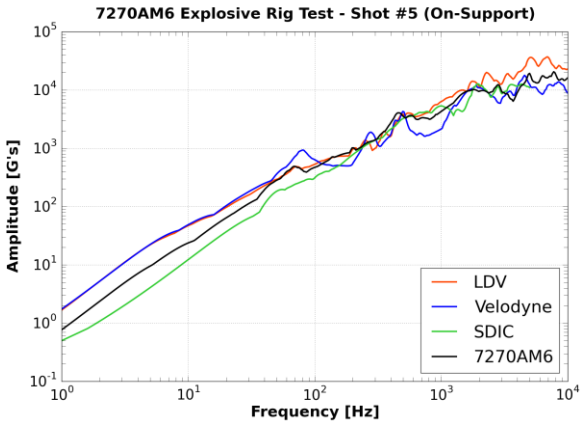
7270AM6 Explosive Rig Test - Shot #5 (On-Support)
LDV
Velodyne
SDIC
7270AM6
Amplitude [G's]
Frequency [Hz]

(c)

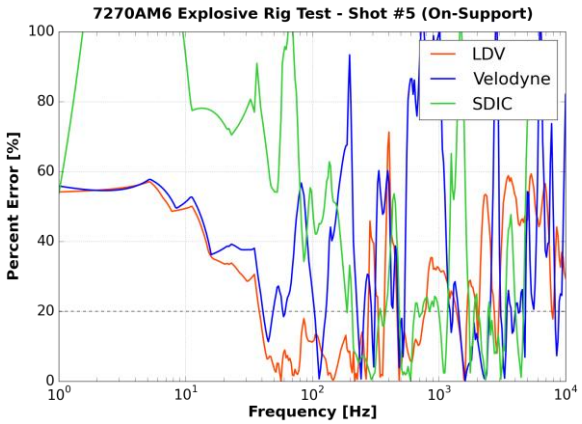
7270AM6 Explosive Rig Test - Shot #5 (On-Support)
LDV
Velodyne
SDIC
Percent Error [%]
Frequency [Hz]

(d)

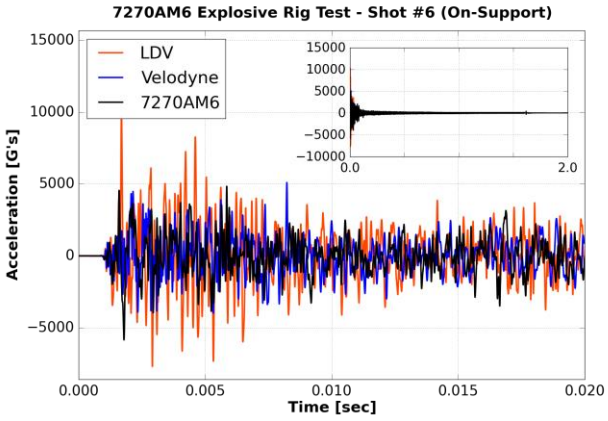
7270AM6 Explosive Rig Test - Shot #6 (On-Support)
LDV
Velodyne
7270AM6
Acceleration [G's]
Time [sec]

(a)

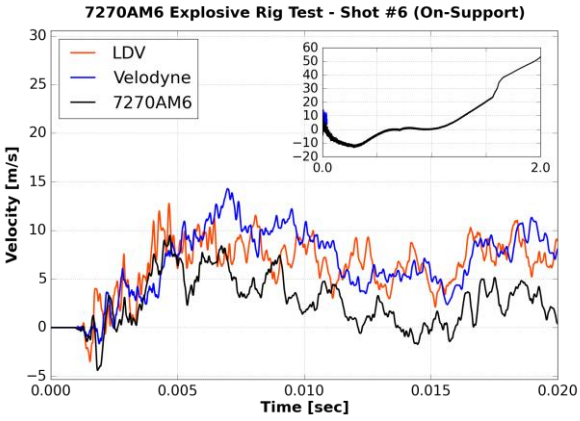
7270AM6 Explosive Rig Test - Shot #6 (On-Support)
LDV
Velodyne
7270AM6
Velocity [m/s]
Time [sec]

(b)

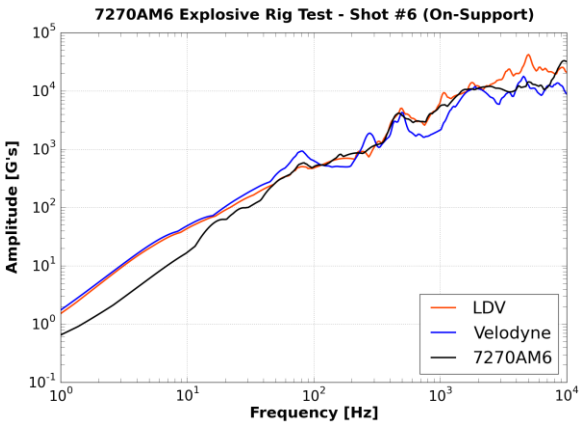
7270AM6 Explosive Rig Test - Shot #6 (On-Support)
Amplitude [G's]
Frequency [Hz]
LDV
Velodyne
7270AM6

(c)

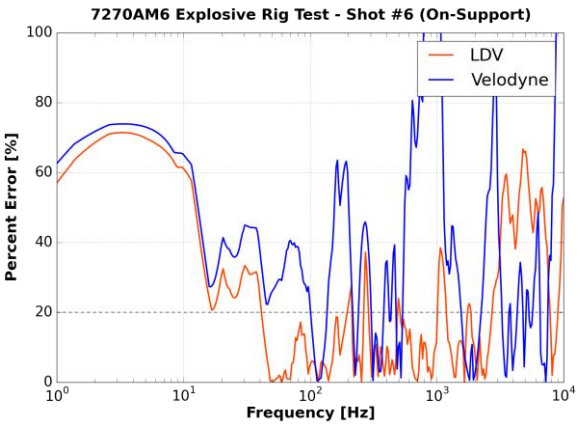
7270AM6 Explosive Rig Test - Shot #6 (On-Support)
Percent Error [%]
Frequency [Hz]
LDV
Velodyne

(d)

ii. Wave Spring

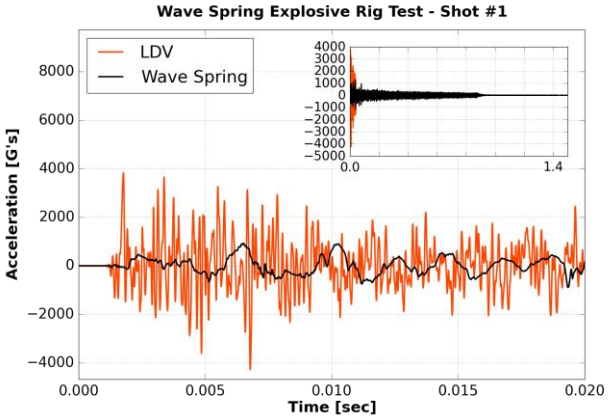

(a)

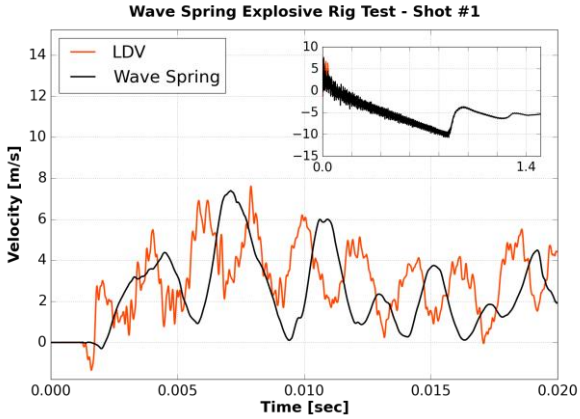

(b)

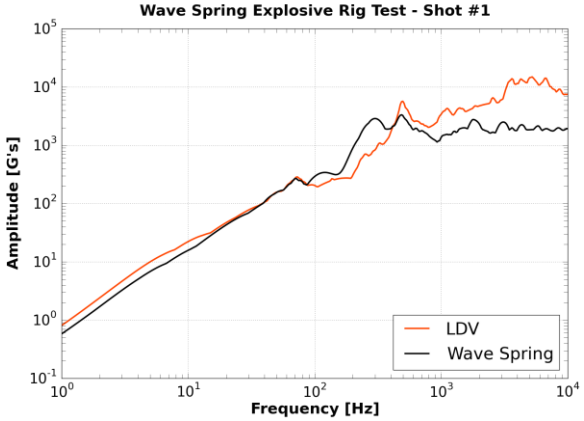

(c)

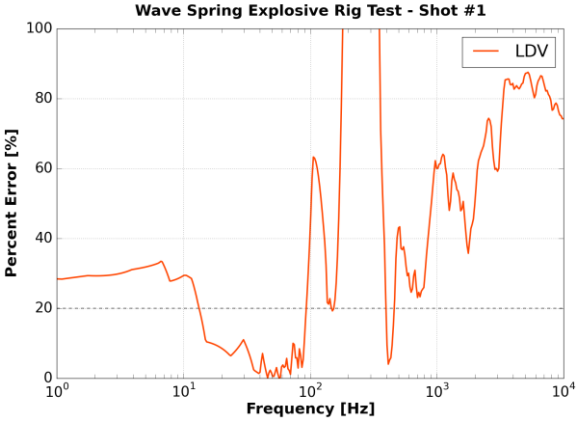

(d)

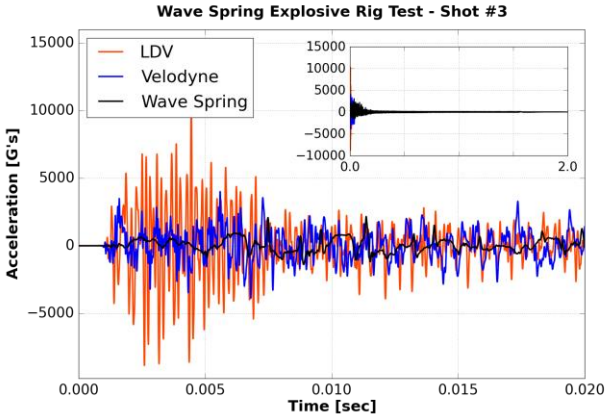

(a)

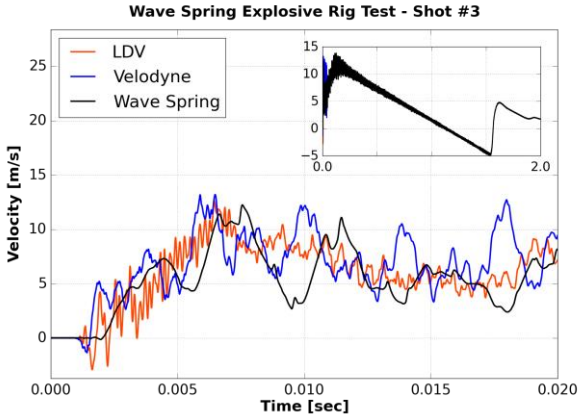

(b)

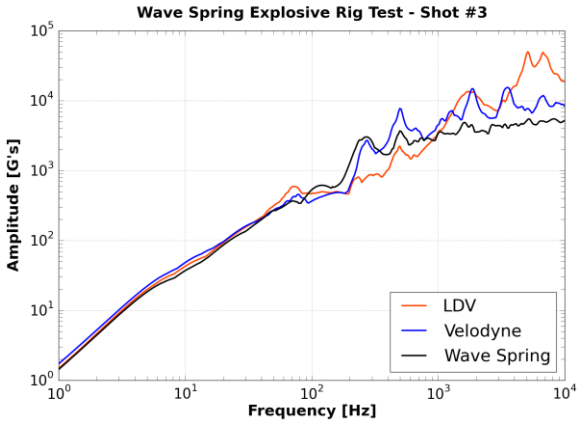
Wave Spring Explosive Rig Test - Shot #3
Amplitude [G's]
Frequency [Hz]
LDV
Velodyne
Wave Spring

(c)

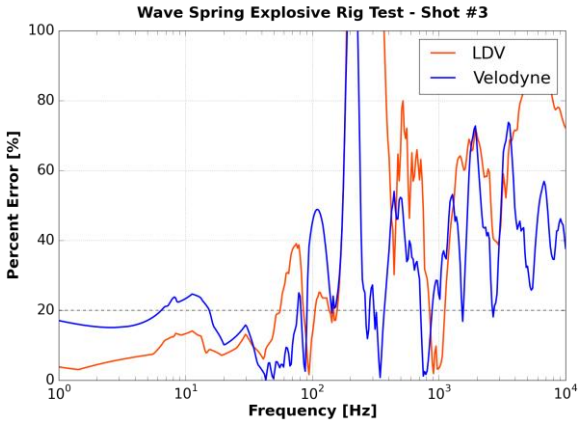
Wave Spring Explosive Rig Test - Shot #3
Percent Error [%]
Frequency [Hz]
LDV
Velodyne

(d)

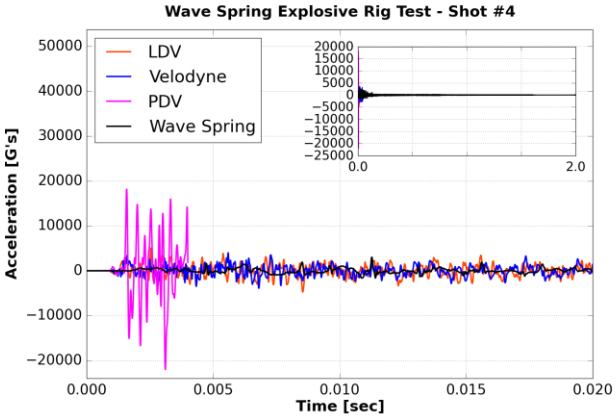
Wave Spring Explosive Rig Test - Shot #4
Acceleration [G's]
Time [sec]
LDV
Velodyne
PDV
Wave Spring

(a)

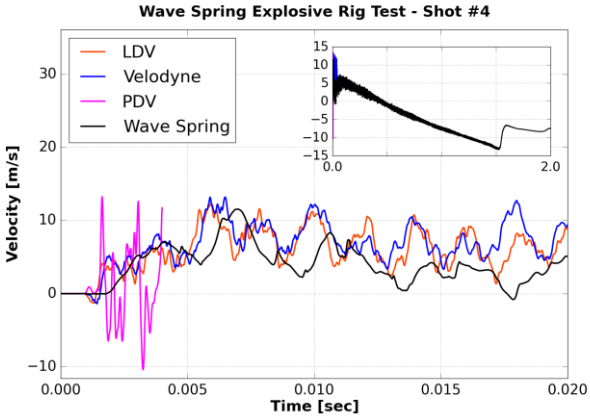
Wave Spring Explosive Rig Test - Shot #4
Velocity [m/s]
Time [sec]
LDV
Velodyne
PDV
Wave Spring

(b)

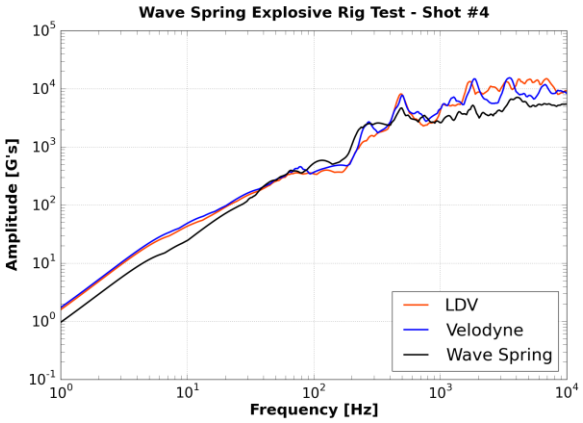
Wave Spring Explosive Rig Test - Shot #4
Amplitude [G's]
Frequency [Hz]
LDV
Velodyne
Wave Spring

(c)

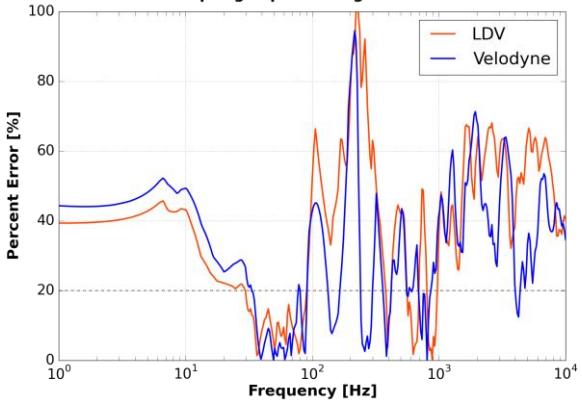
Wave Spring Explosive Rig Test - Shot #4
Percent Error [%]
Frequency [Hz]
LDV
Velodyne

(d)

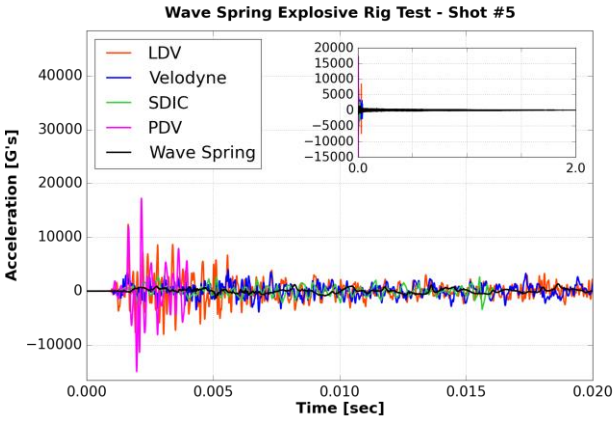
Wave Spring Explosive Rig Test - Shot #5
LDV
Velodyne
SDIC
PDV
Wave Spring
Acceleration [G's]
Time [sec]

(a)

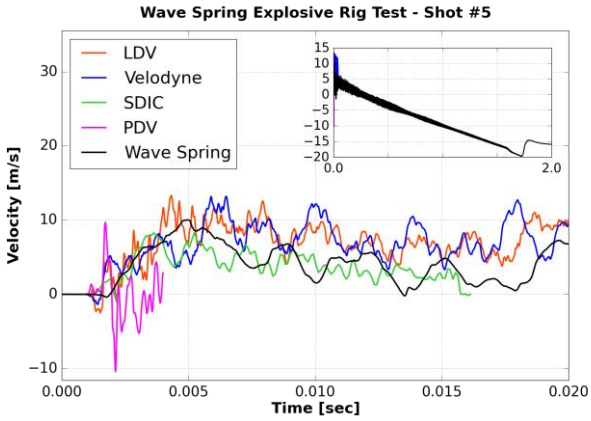
Wave Spring Explosive Rig Test - Shot #5
LDV
Velodyne
SDIC
PDV
Wave Spring
Velocity [m/s]
Time [sec]

(b)

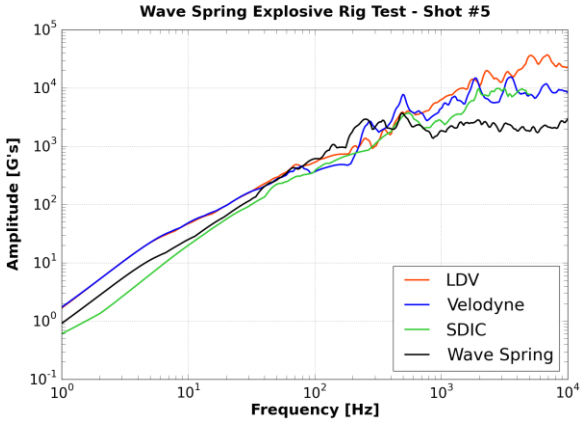
Wave Spring Explosive Rig Test - Shot #5
LDV
Velodyne
SDIC
Wave Spring
Amplitude [G's]
Frequency [Hz]

(c)

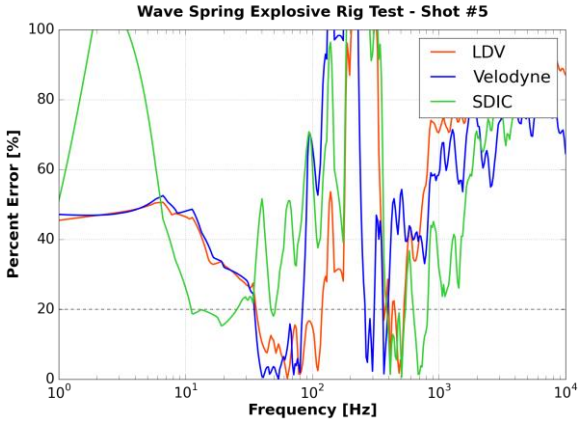
Wave Spring Explosive Rig Test - Shot #5
LDV
Velodyne
SDIC
Percent Error [%]
Frequency [Hz]

(d)

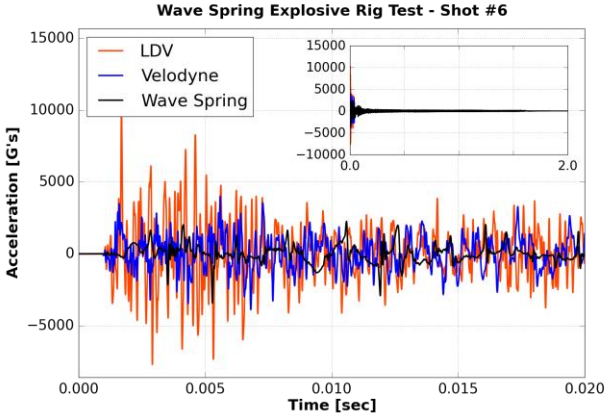
Wave Spring Explosive Rig Test - Shot #6
LDV
Velodyne
Wave Spring
Acceleration [G's]
Time [sec]

(a)

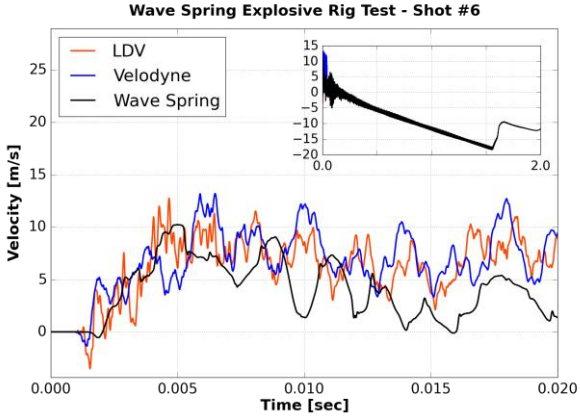
Wave Spring Explosive Rig Test - Shot #6
LDV
Velodyne
Wave Spring
Velocity [m/s]
Time [sec]

(b)

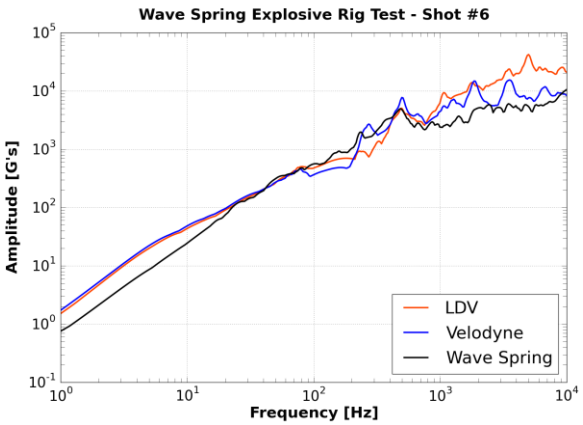
Wave Spring Explosive Rig Test - Shot #6
Amplitude [G's]
Frequency [Hz]
LDV
Velodyne
Wave Spring

(c)

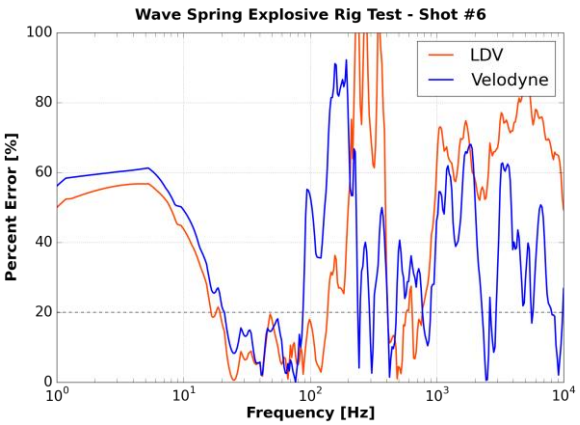
Wave Spring Explosive Rig Test - Shot #6
Percent Error [%]
Frequency [Hz]
LDV
Velodyne

(d)

iii. Base BOB

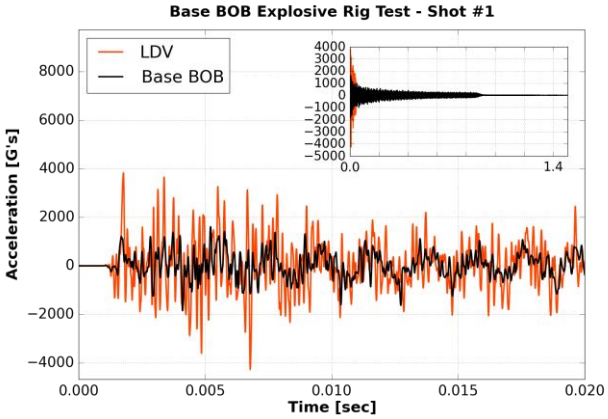

(a)

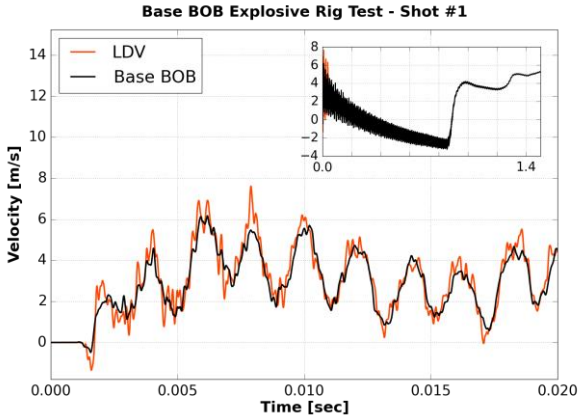

(b)

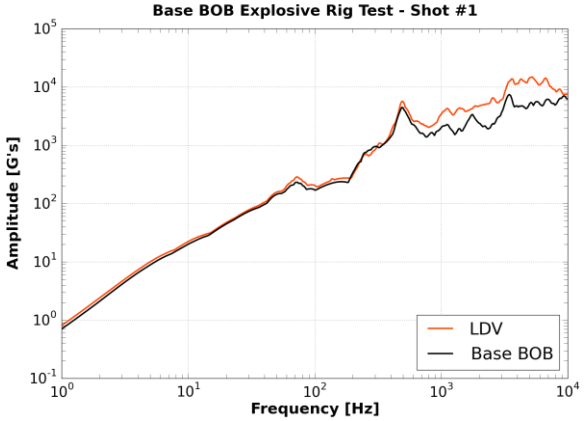

(c)

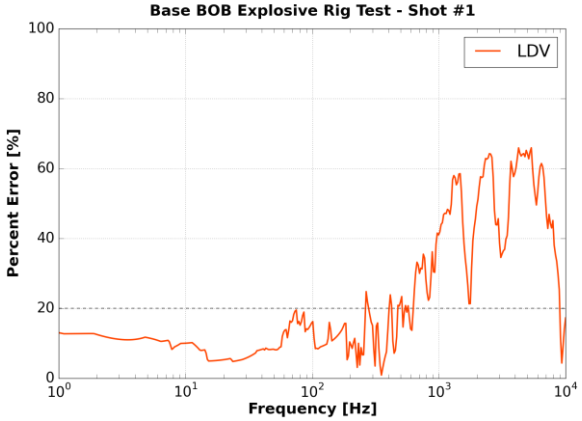

(d)

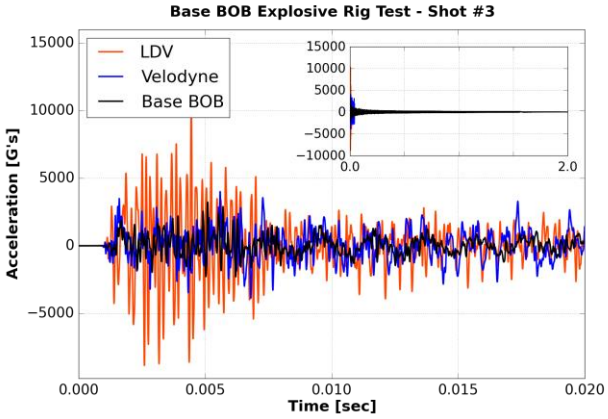

(a)

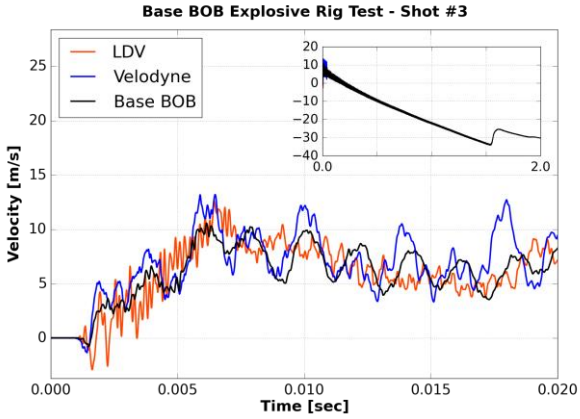

(b)

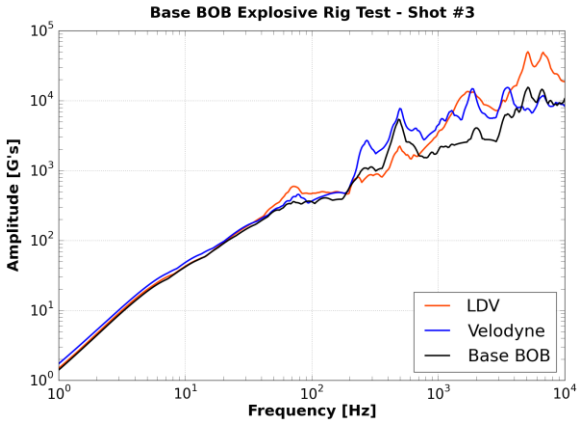
Base BOB Explosive Rig Test - Shot #3
Amplitude [G's]
Frequency [Hz]
LDV
Velodyne
Base BOB

(c)

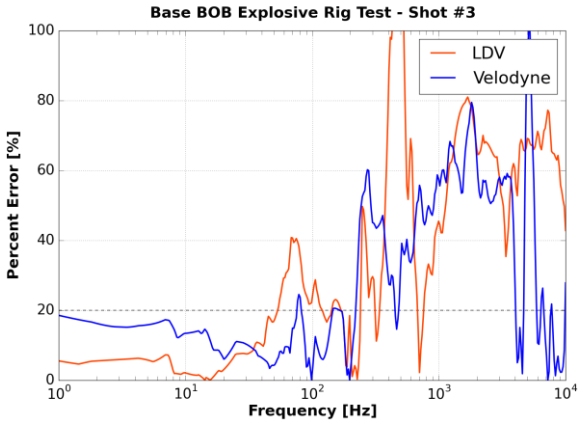
Base BOB Explosive Rig Test - Shot #3
Percent Error [%]
Frequency [Hz]
LDV
Velodyne

(d)

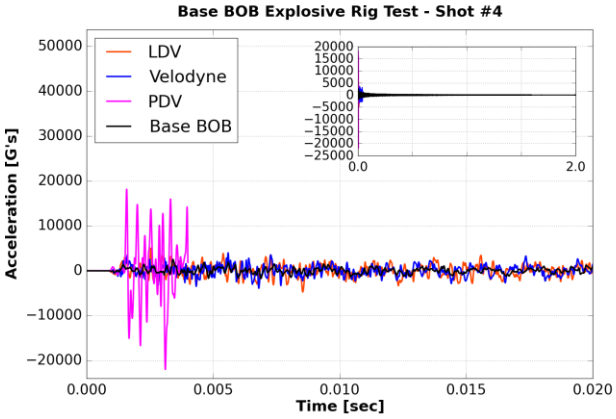
Base BOB Explosive Rig Test - Shot #4
Acceleration [G's]
Time [sec]
LDV
Velodyne
PDV
Base BOB

(a)

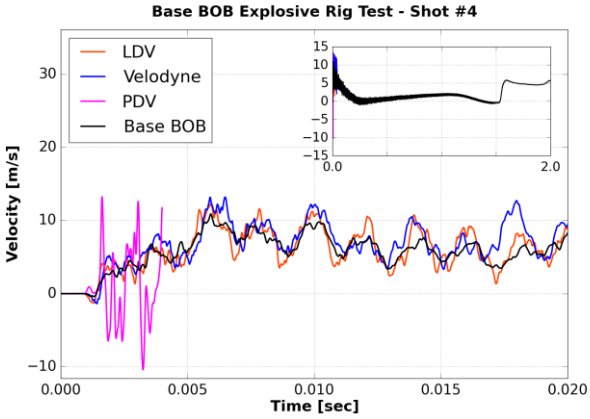
Base BOB Explosive Rig Test - Shot #4
Velocity [m/s]
Time [sec]
LDV
Velodyne
PDV
Base BOB

(b)

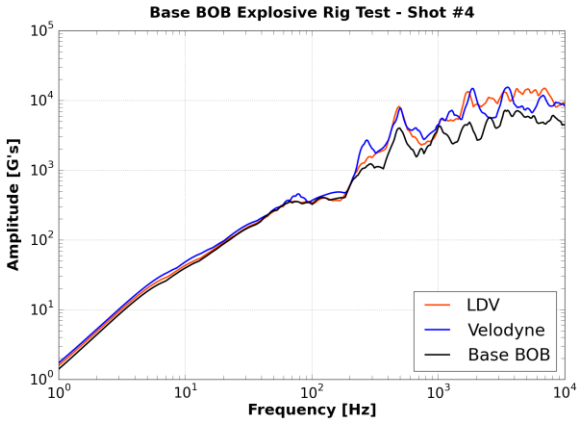
Base BOB Explosive Rig Test - Shot #4
Amplitude [G's]
Frequency [Hz]
LDV
Velodyne
Base BOB

(c)

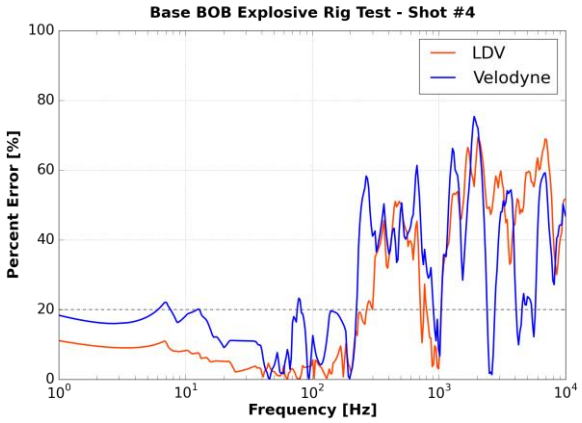
Base BOB Explosive Rig Test - Shot #4
Percent Error [%]
Frequency [Hz]
LDV
Velodyne

(d)

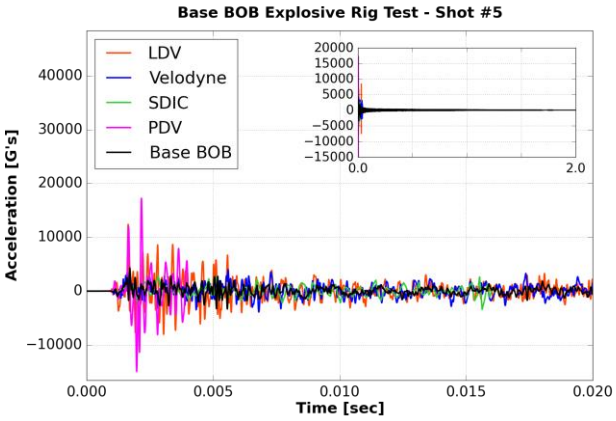
Base BOB Explosive Rig Test - Shot #5
LDV
Velodyne
SDIC
PDV
Base BOB
Acceleration [G's]
Time [sec]

(a)

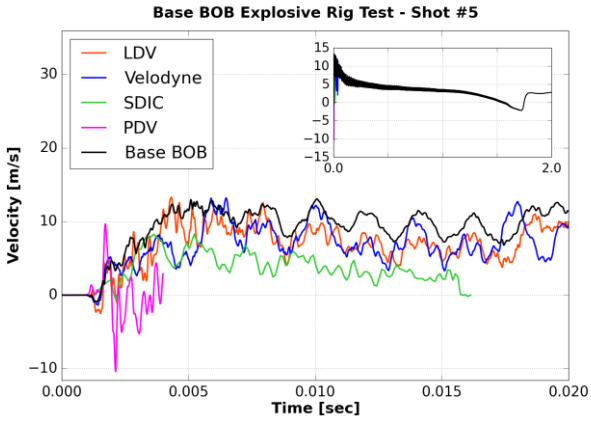
Base BOB Explosive Rig Test - Shot #5
LDV
Velodyne
SDIC
PDV
Base BOB
Velocity [m/s]
Time [sec]

(b)

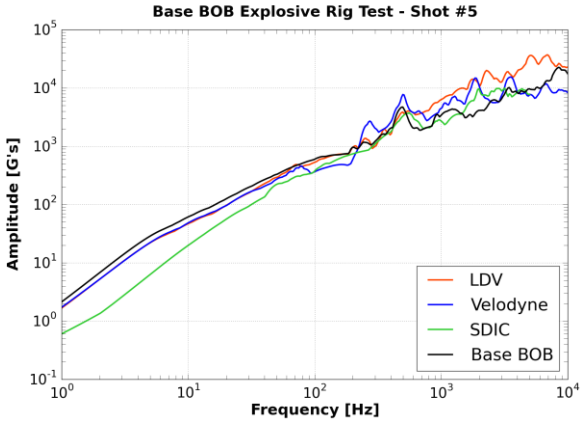
Base BOB Explosive Rig Test - Shot #5
LDV
Velodyne
SDIC
Base BOB
Amplitude [G's]
Frequency [Hz]

(c)

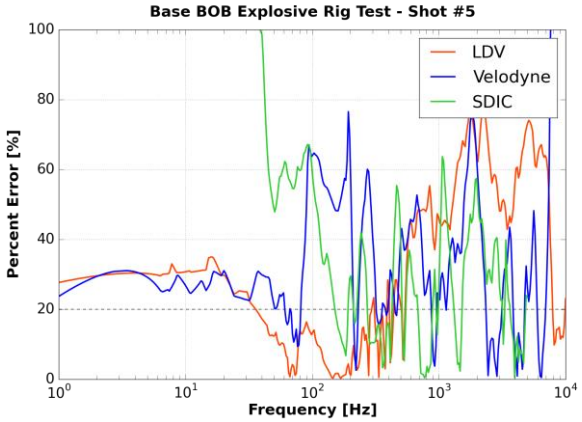
Base BOB Explosive Rig Test - Shot #5
LDV
Velodyne
SDIC
Percent Error [%]
Frequency [Hz]

(d)

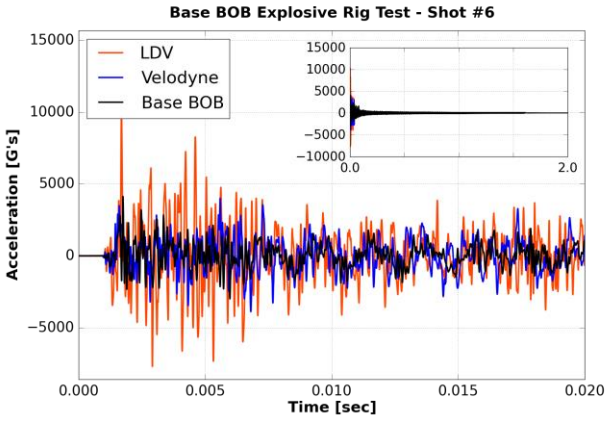
Base BOB Explosive Rig Test - Shot #6
LDV
Velodyne
Base BOB
Acceleration [G's]
Time [sec]

(a)

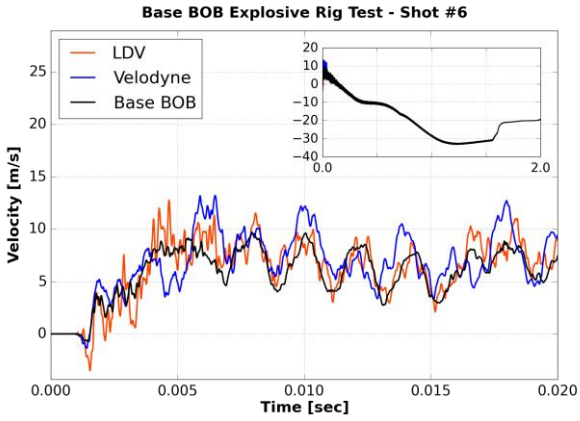
Base BOB Explosive Rig Test - Shot #6
LDV
Velodyne
Base BOB
Velocity [m/s]
Time [sec]

(b)

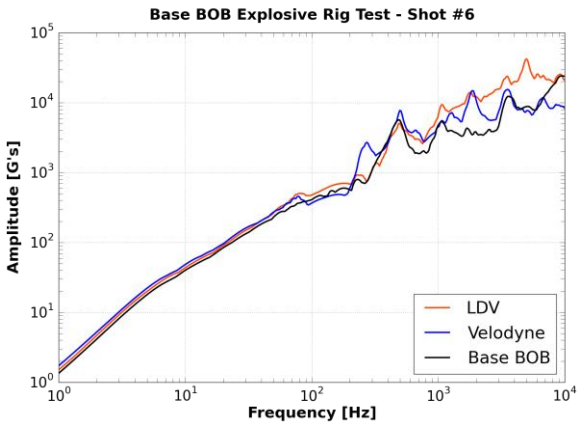
Base BOB Explosive Rig Test - Shot #6
Amplitude [G's]
Frequency [Hz]
LDV
Velodyne
Base BOB

(c)

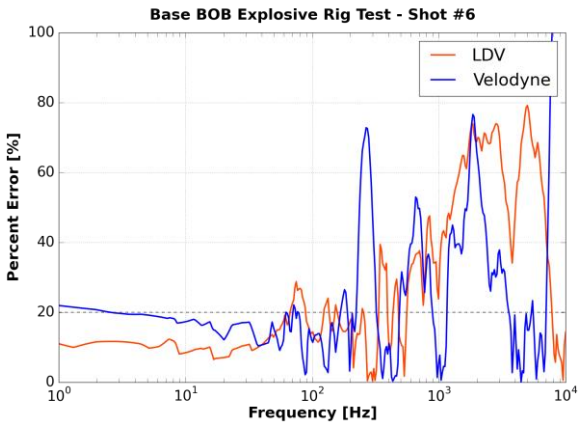
Base BOB Explosive Rig Test - Shot #6
Percent Error [%]
Frequency [Hz]
LDV
Velodyne

(d)

iv. Wheel Mount

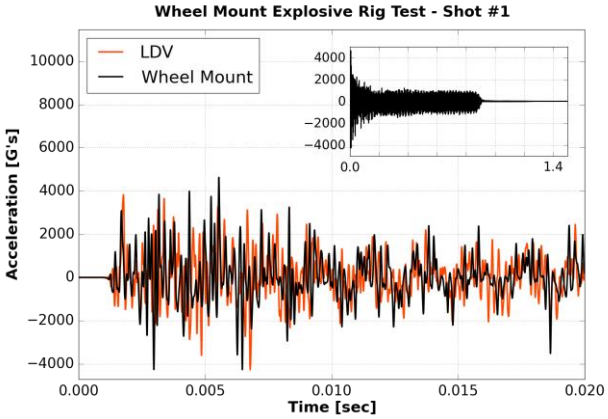

(a)

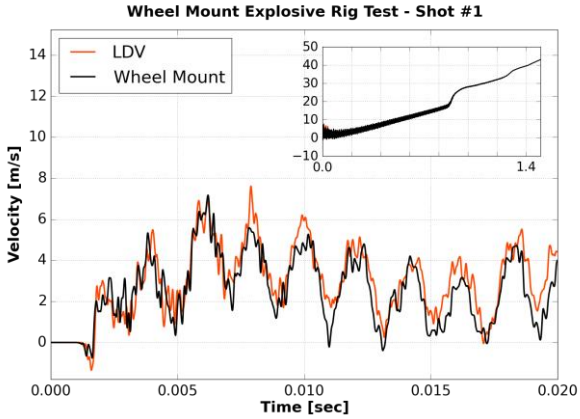

(b)

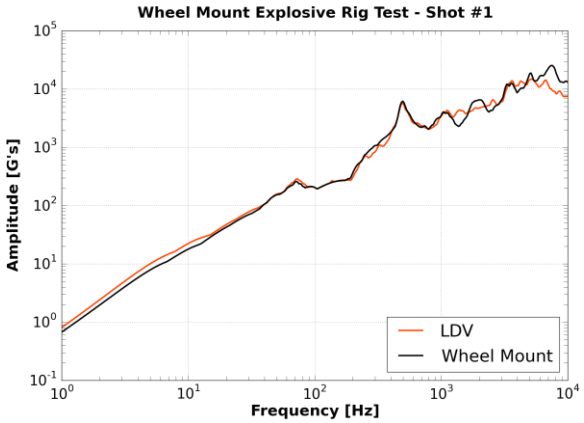

(c)

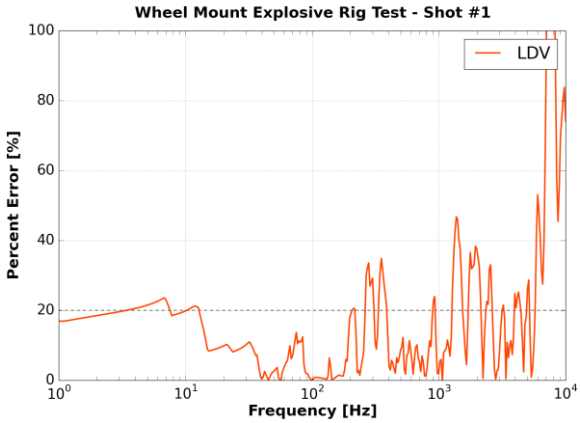

(d)

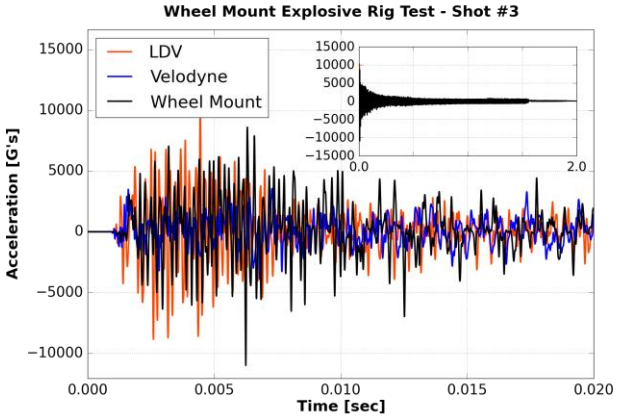

(a)

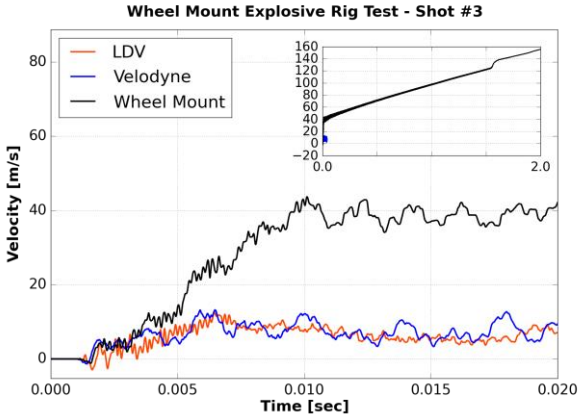

(b)

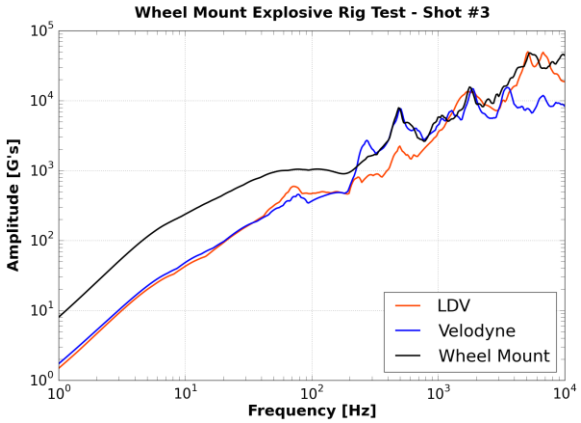
Wheel Mount Explosive Rig Test - Shot #3
Amplitude [G's]
Frequency [Hz]
LDV
Velodyne
Wheel Mount

(c)

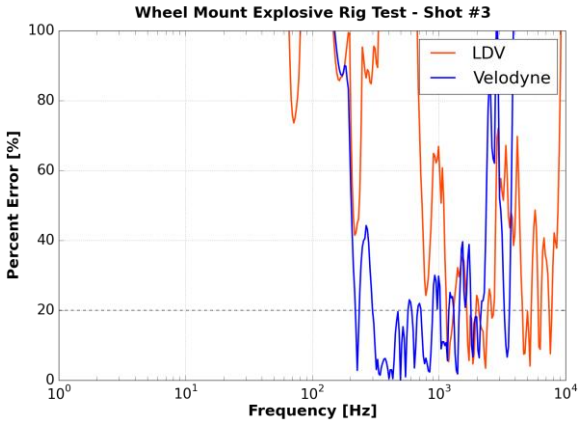
Wheel Mount Explosive Rig Test - Shot #3
Percent Error [%]
Frequency [Hz]
LDV
Velodyne

(d)

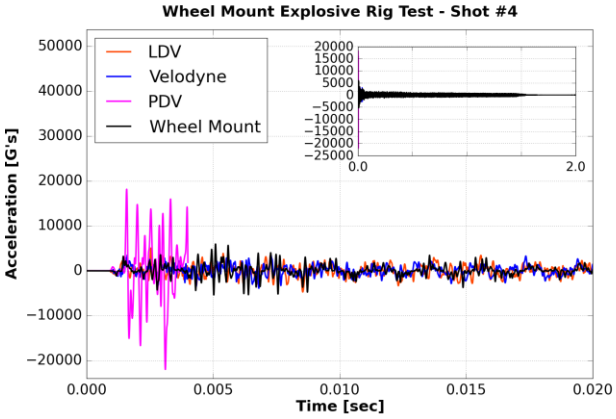
Wheel Mount Explosive Rig Test - Shot #4
Acceleration [G's]
Time [sec]
LDV
Velodyne
PDV
Wheel Mount

(a)

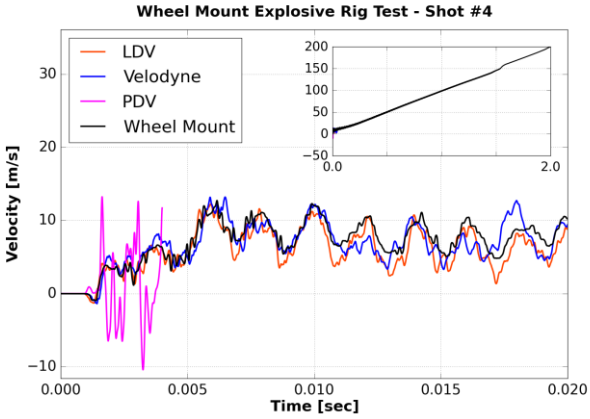
Wheel Mount Explosive Rig Test - Shot #4
Velocity [m/s]
Time [sec]
LDV
Velodyne
PDV
Wheel Mount

(b)

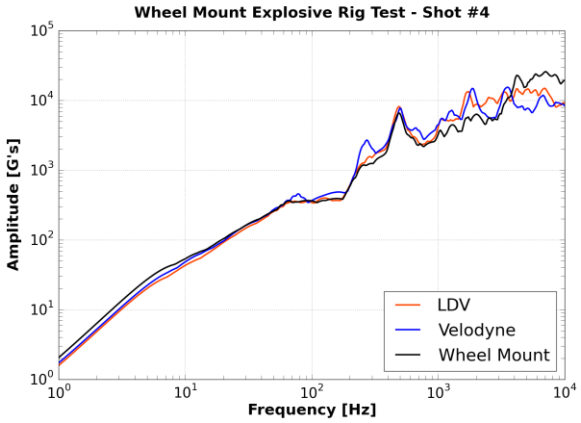
Wheel Mount Explosive Rig Test - Shot #4
Amplitude [G's]
Frequency [Hz]
LDV
Velodyne
Wheel Mount

(c)

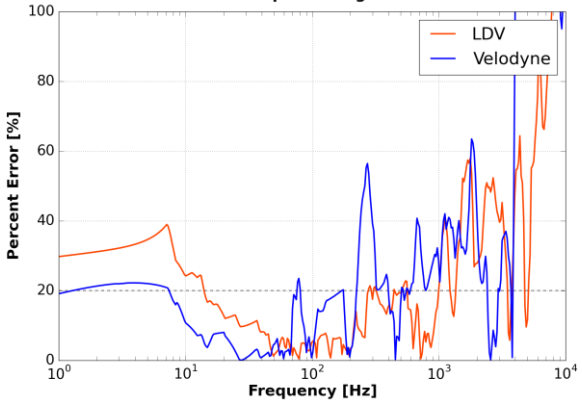
Wheel Mount Explosive Rig Test - Shot #4
Percent Error [%]
Frequency [Hz]
LDV
Velodyne

(d)

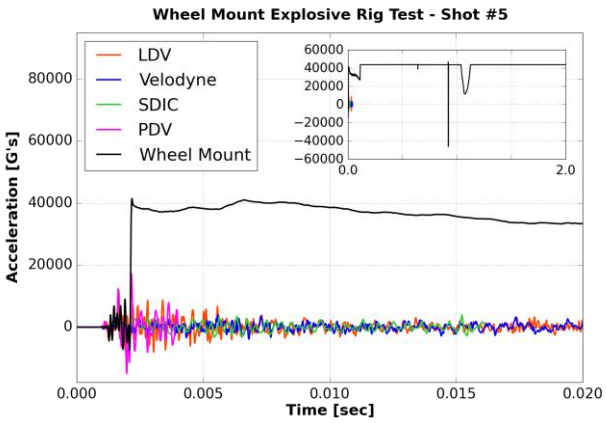
Wheel Mount Explosive Rig Test - Shot #5
LDV
Velodyne
SDIC
PDV
Wheel Mount
Acceleration [G's]
Time [sec]

(a)

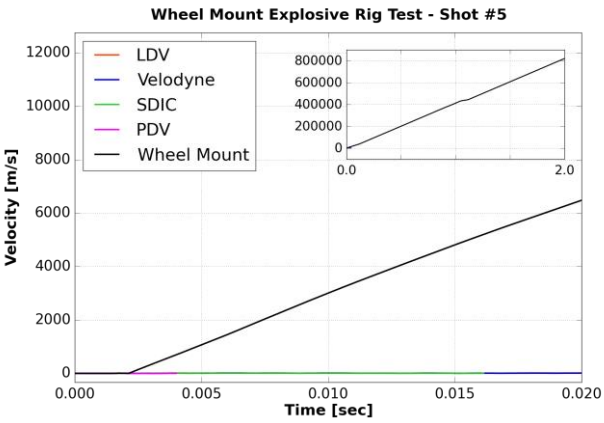
Wheel Mount Explosive Rig Test - Shot #5
LDV
Velodyne
SDIC
PDV
Wheel Mount
Velocity [m/s]
Time [sec]

(b)

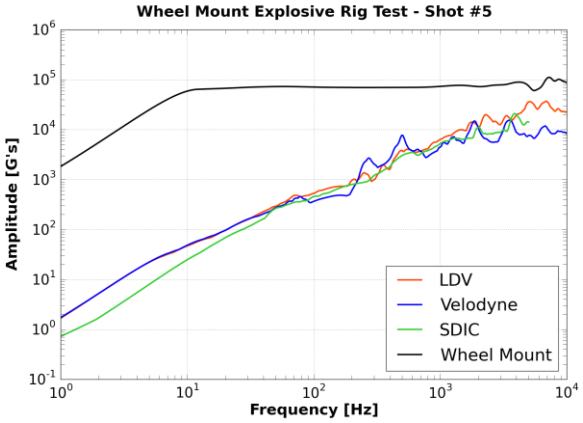
Wheel Mount Explosive Rig Test - Shot #5
LDV
Velodyne
SDIC
Wheel Mount
Amplitude [G's]
Frequency [Hz]

(c)

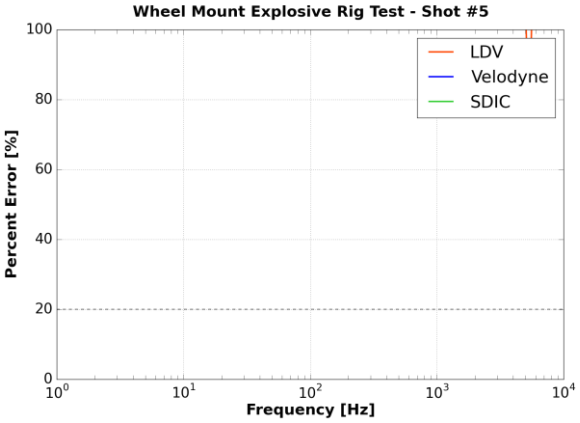
Wheel Mount Explosive Rig Test - Shot #5
LDV
Velodyne
SDIC
Percent Error [%]
Frequency [Hz]

(d)

v. AM6 Tall

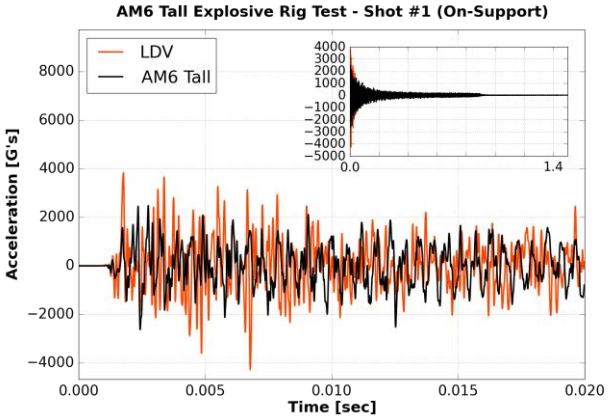

(a)

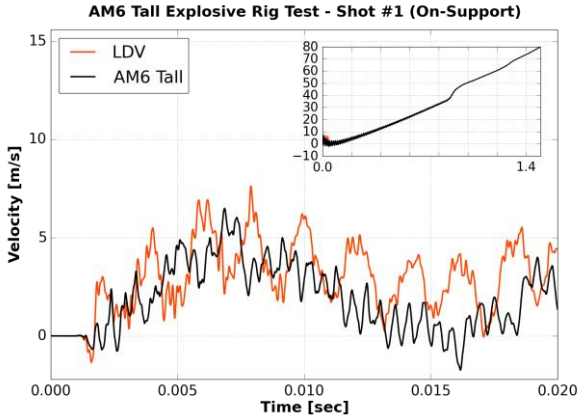

(b)

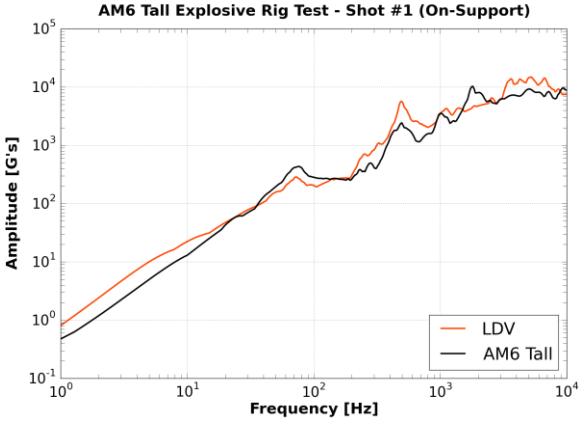

(c)

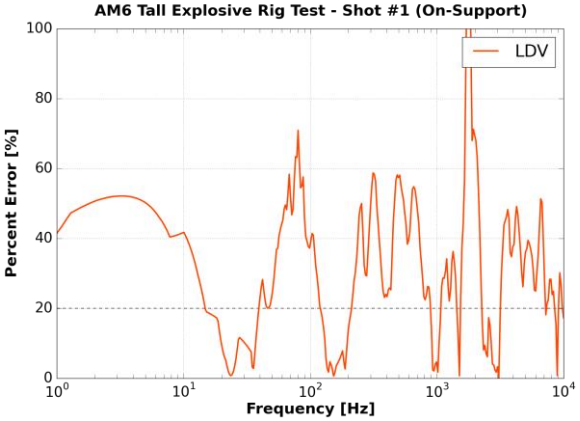

(d)

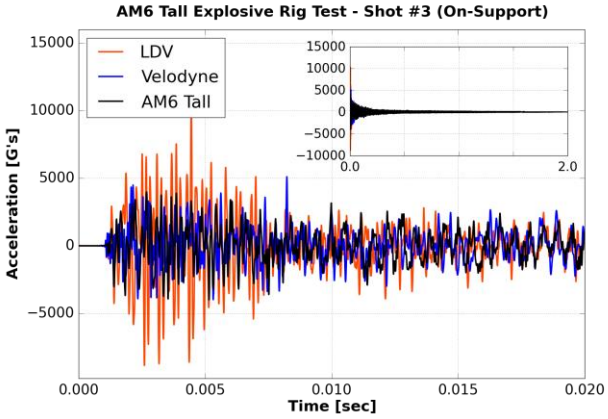

(a)

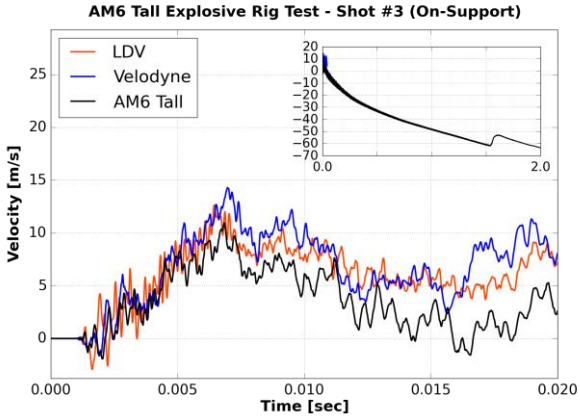

(b)

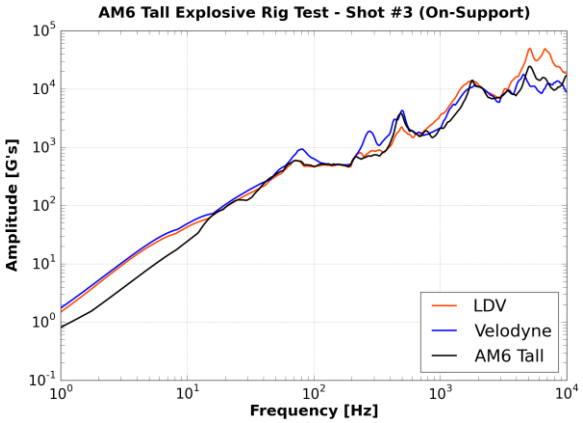
AM6 Tall Explosive Rig Test - Shot #3 (On-Support)
Amplitude [G's]
Frequency [Hz]
LDV
Velodyne
AM6 Tall

(c)

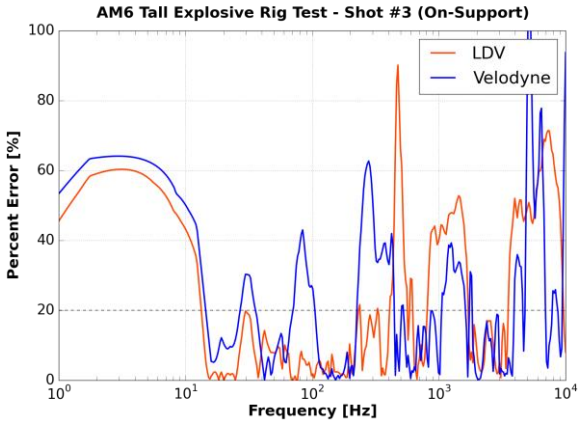
AM6 Tall Explosive Rig Test - Shot #3 (On-Support)
Percent Error [%]
Frequency [Hz]
LDV
Velodyne

(d)

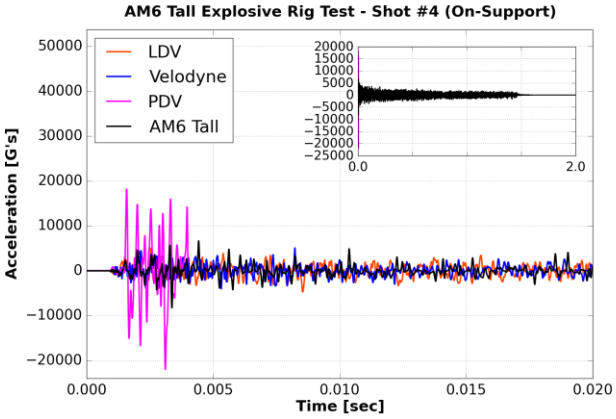
AM6 Tall Explosive Rig Test - Shot #4 (On-Support)
Acceleration [G's]
Time [sec]
LDV
Velodyne
PDV
AM6 Tall

(a)

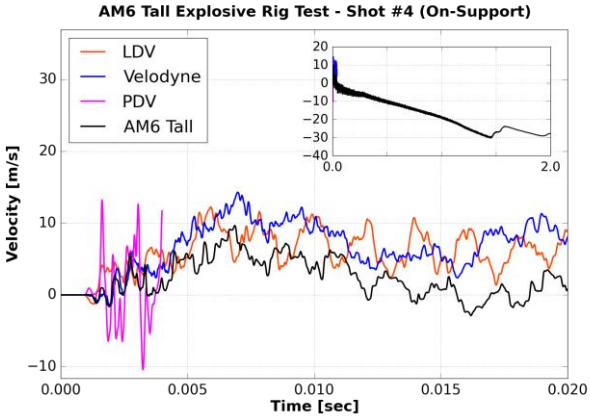
AM6 Tall Explosive Rig Test - Shot #4 (On-Support)
Velocity [m/s]
Time [sec]
LDV
Velodyne
PDV
AM6 Tall

(b)

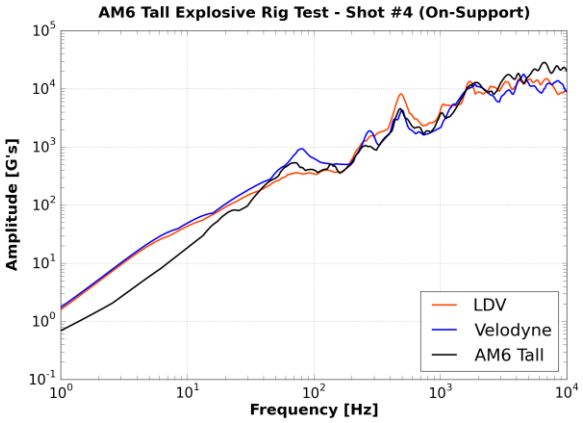
AM6 Tall Explosive Rig Test - Shot #4 (On-Support)
Amplitude [G's]
Frequency [Hz]
LDV
Velodyne
AM6 Tall

(c)

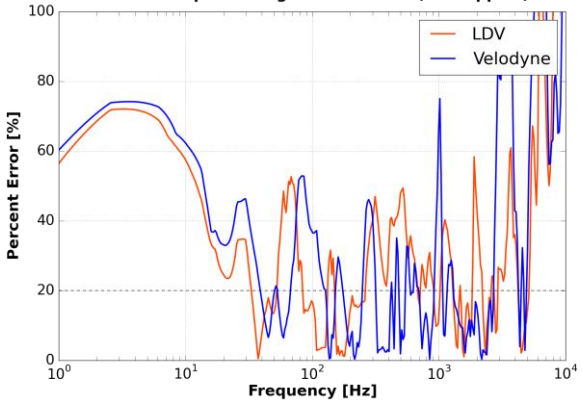
AM6 Tall Explosive Rig Test - Shot #4 (On-Support)
Percent Error [%]
Frequency [Hz]
LDV
Velodyne

(d)

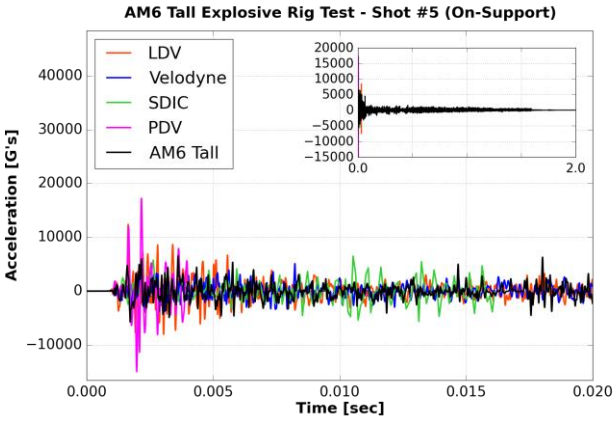
AM6 Tall Explosive Rig Test - Shot #5 (On-Support)
LDV
Velodyne
SDIC
PDV
AM6 Tall
Acceleration [G's]
Time [sec]

(a)

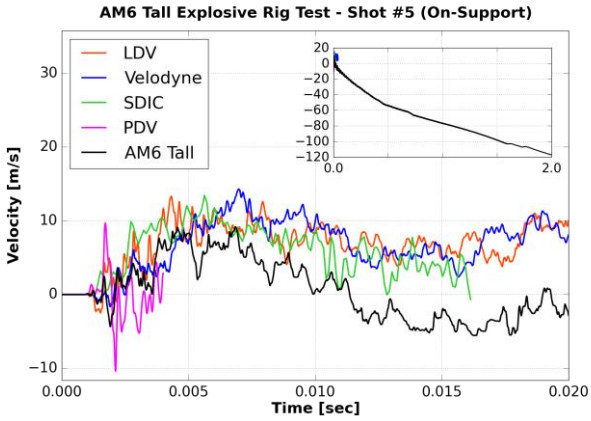
AM6 Tall Explosive Rig Test - Shot #5 (On-Support)
LDV
Velodyne
SDIC
PDV
AM6 Tall
Velocity [m/s]
Time [sec]

(b)

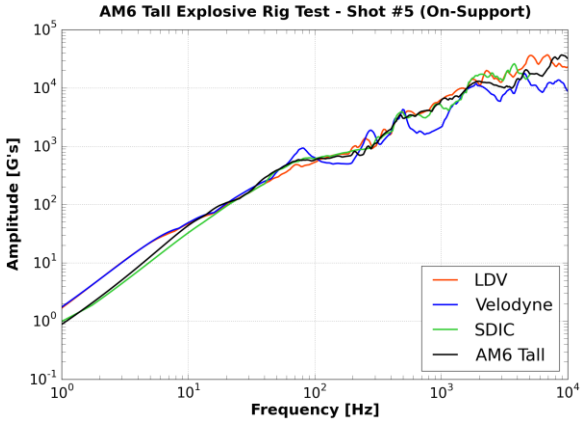
AM6 Tall Explosive Rig Test - Shot #5 (On-Support)
LDV
Velodyne
SDIC
AM6 Tall
Amplitude [G's]
Frequency [Hz]

(c)

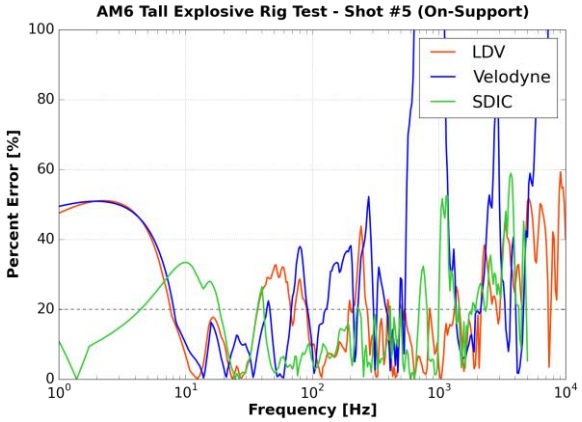
AM6 Tall Explosive Rig Test - Shot #5 (On-Support)
LDV
Velodyne
SDIC
Percent Error [%]
Frequency [Hz]

(d)

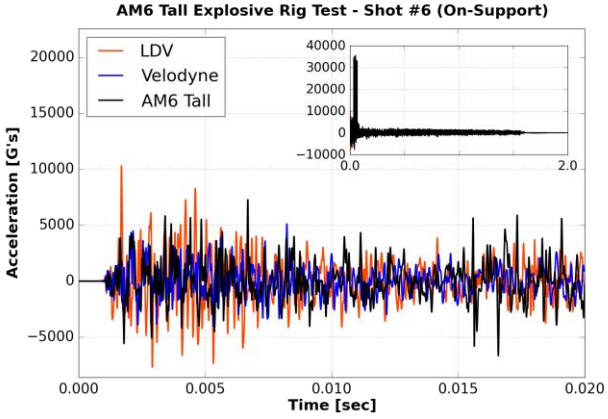
AM6 Tall Explosive Rig Test - Shot #6 (On-Support)
LDV
Velodyne
AM6 Tall
Acceleration [G's]
Time [sec]

(a)

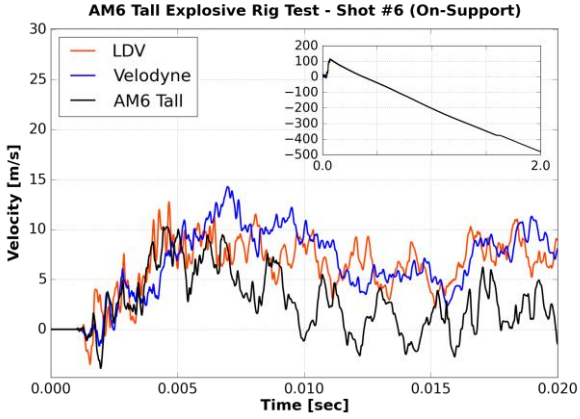
AM6 Tall Explosive Rig Test - Shot #6 (On-Support)
LDV
Velodyne
AM6 Tall
Velocity [m/s]
Time [sec]

(b)

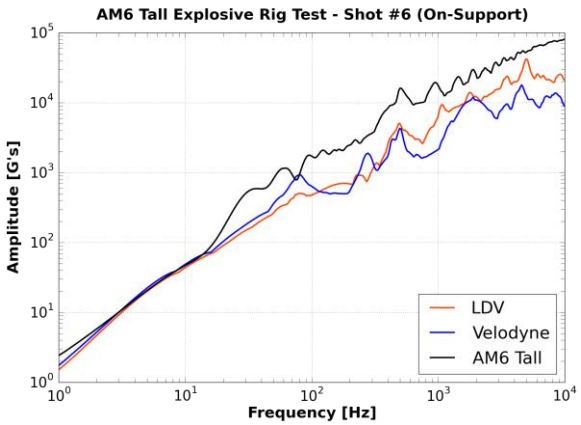
AM6 Tall Explosive Rig Test - Shot #6 (On-Support)
Amplitude [G's]
Frequency [Hz]
LDV
Velodyne
AM6 Tall

(c)

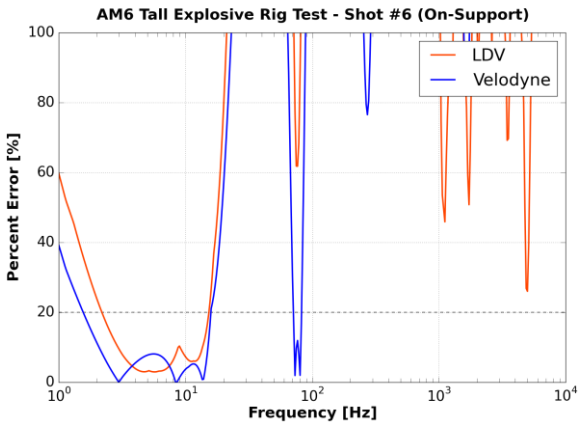
AM6 Tall Explosive Rig Test - Shot #6 (On-Support)
Percent Error [%]
Frequency [Hz]
LDV
Velodyne

(d)

vi. BOBKAT

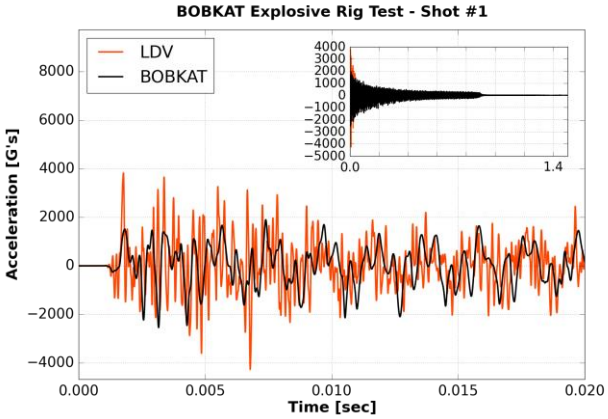

(a)

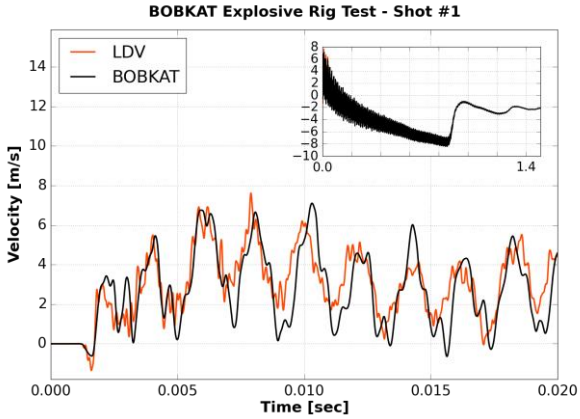

(b)

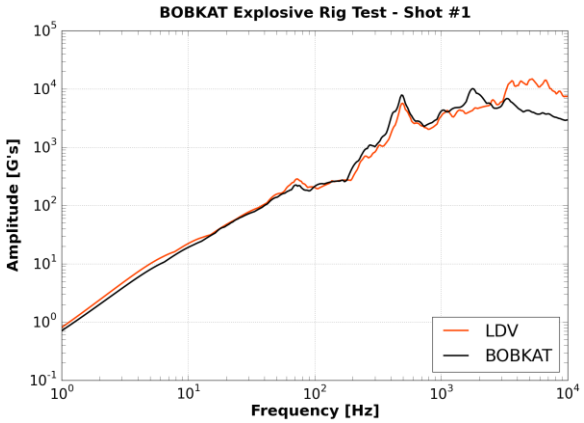

(c)

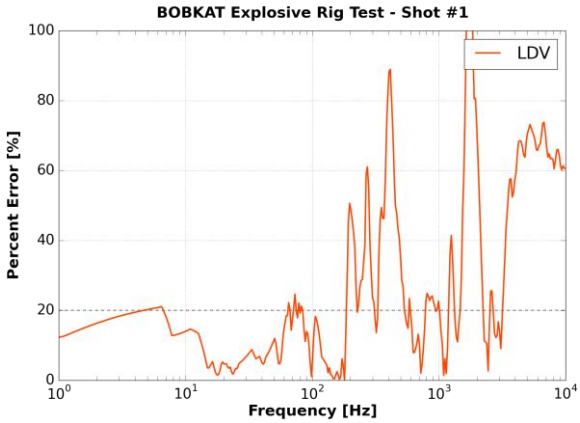

(d)

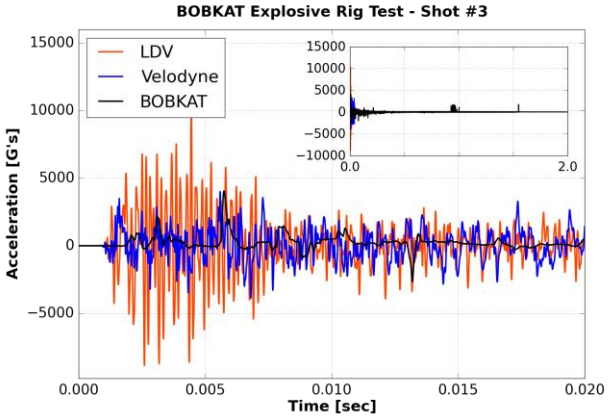

(a)

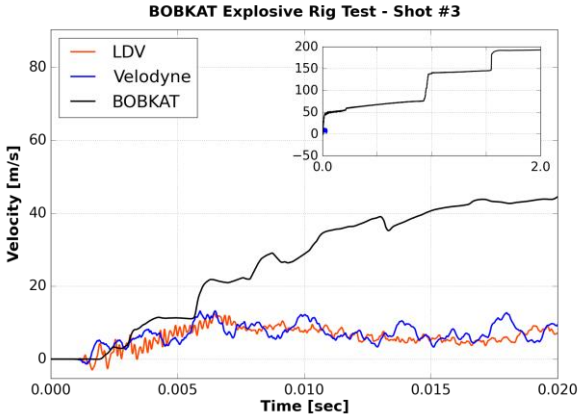

(b)

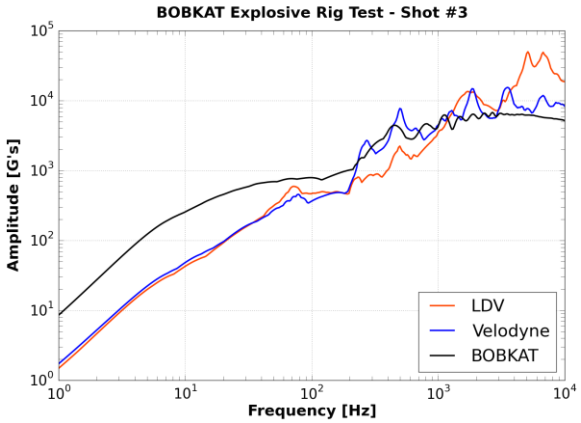
BOBKAT Explosive Rig Test - Shot #3
Amplitude [G's]
Frequency [Hz]
LDV
Velodyne
BOBKAT

(c)

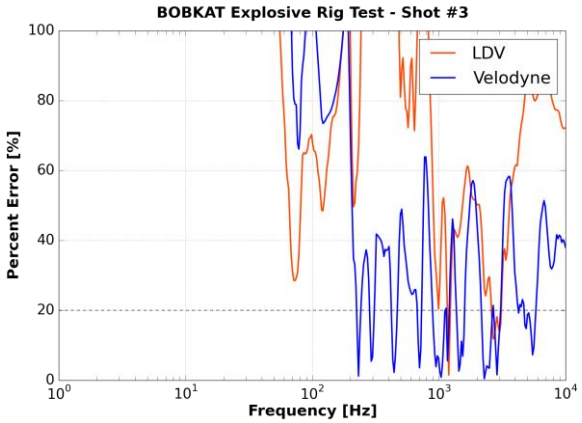
BOBKAT Explosive Rig Test - Shot #3
Percent Error [%]
Frequency [Hz]
LDV
Velodyne

(d)

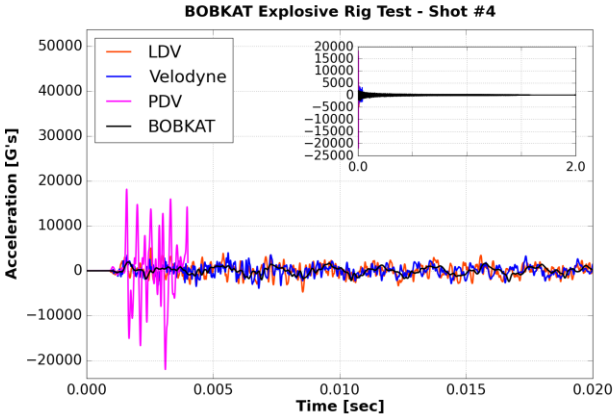
BOBKAT Explosive Rig Test - Shot #4
Acceleration [G's]
Time [sec]
LDV
Velodyne
PDV
BOBKAT

(a)

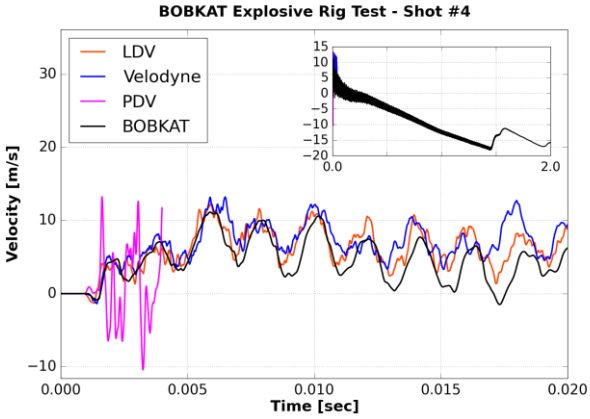
BOBKAT Explosive Rig Test - Shot #4
Velocity [m/s]
Time [sec]
LDV
Velodyne
PDV
BOBKAT

(b)

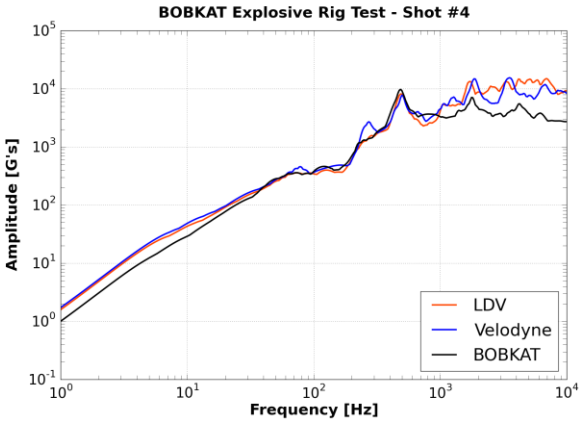
BOBKAT Explosive Rig Test - Shot #4
Amplitude [G's]
Frequency [Hz]
LDV
Velodyne
BOBKAT

(c)

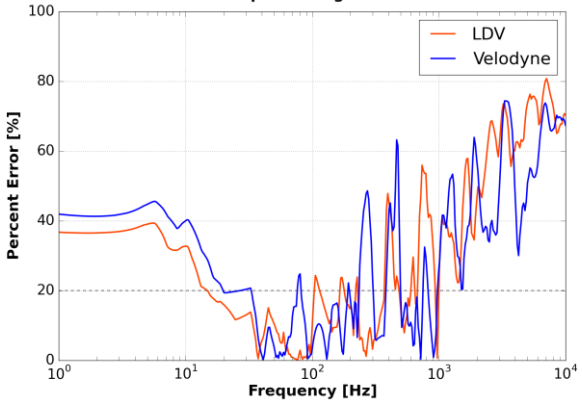
BOBKAT Explosive Rig Test - Shot #4
Percent Error [%]
Frequency [Hz]
LDV
Velodyne

(d)

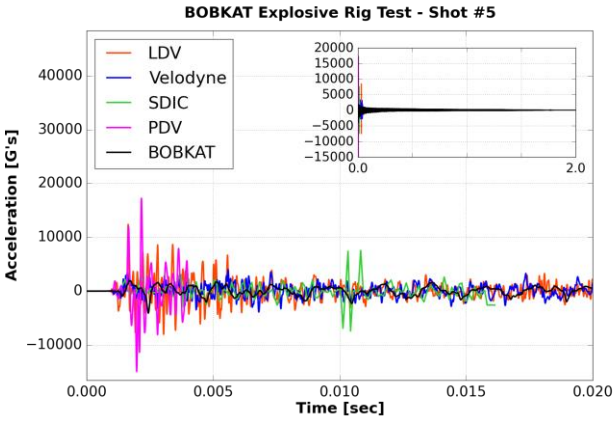
BOBKAT Explosive Rig Test - Shot #5
LDV
Velodyne
SDIC
PDV
BOBKAT
Acceleration [G's]
Time [sec]

(a)

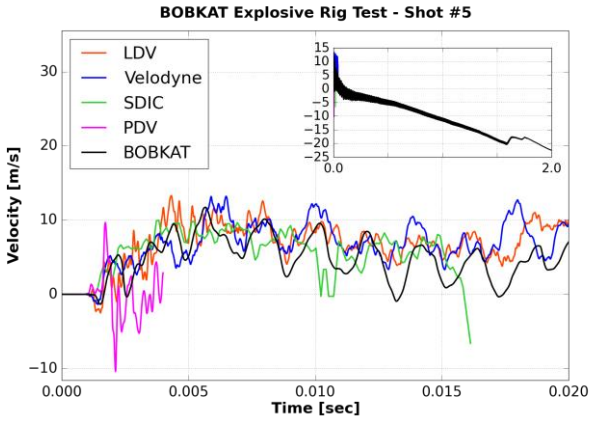
BOBKAT Explosive Rig Test - Shot #5
LDV
Velodyne
SDIC
PDV
BOBKAT
Velocity [m/s]
Time [sec]

(b)

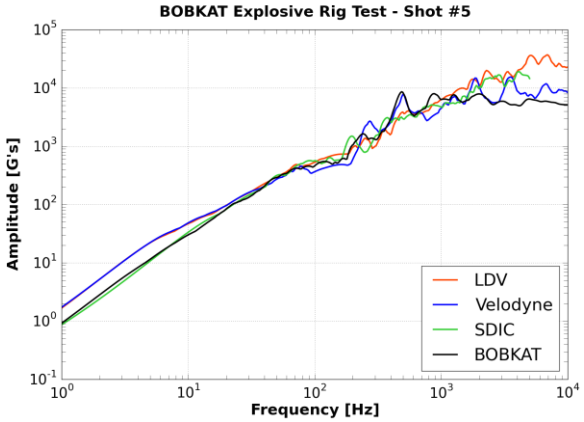
BOBKAT Explosive Rig Test - Shot #5
LDV
Velodyne
SDIC
BOBKAT
Amplitude [G's]
Frequency [Hz]

(c)

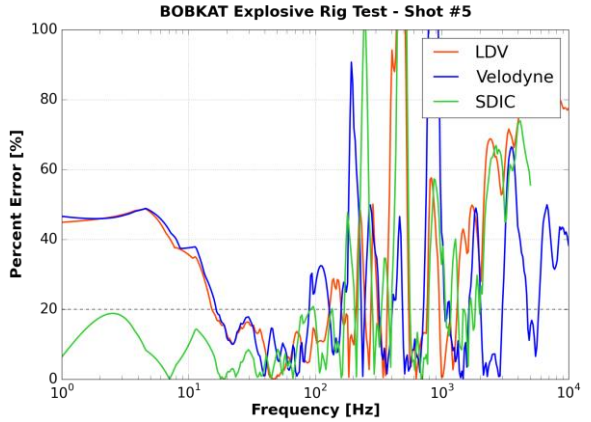
BOBKAT Explosive Rig Test - Shot #5
LDV
Velodyne
SDIC
Percent Error [%]
Frequency [Hz]

(d)

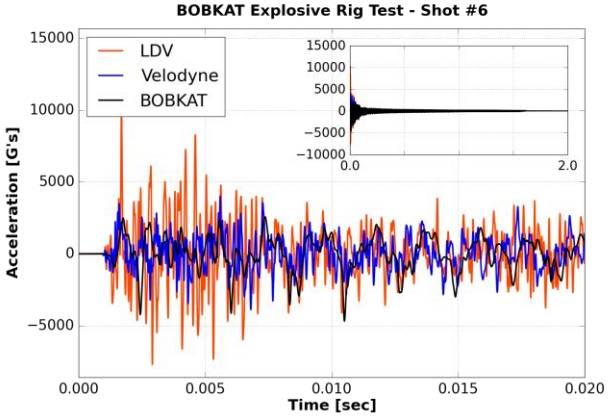
BOBKAT Explosive Rig Test - Shot #6
LDV
Velodyne
BOBKAT
Acceleration [G's]
Time [sec]

(a)

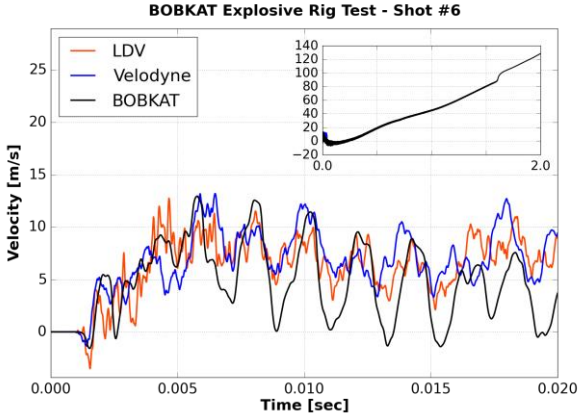
BOBKAT Explosive Rig Test - Shot #6
LDV
Velodyne
BOBKAT
Velocity [m/s]
Time [sec]

(b)

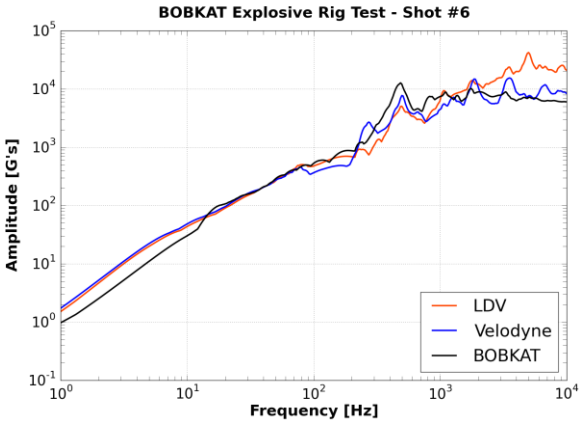
BOBKAT Explosive Rig Test - Shot #6
Amplitude [G's]
Frequency [Hz]
LDV
Velodyne
BOBKAT

(c)

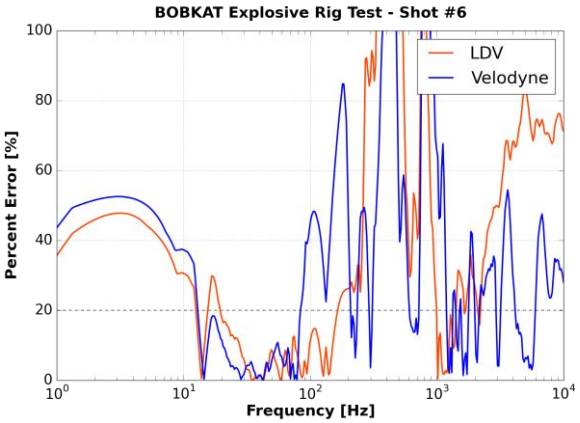
BOBKAT Explosive Rig Test - Shot #6
Percent Error [%]
Frequency [Hz]
LDV
Velodyne

(d)

vii. Mini BOB

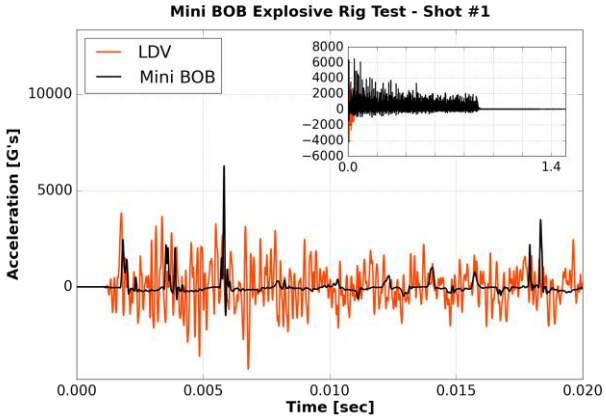

(a)

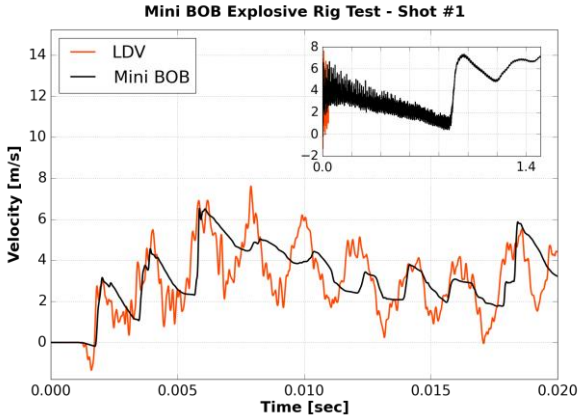

(b)

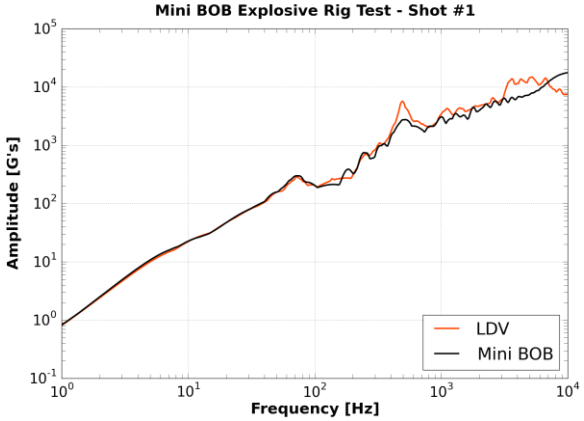

(c)

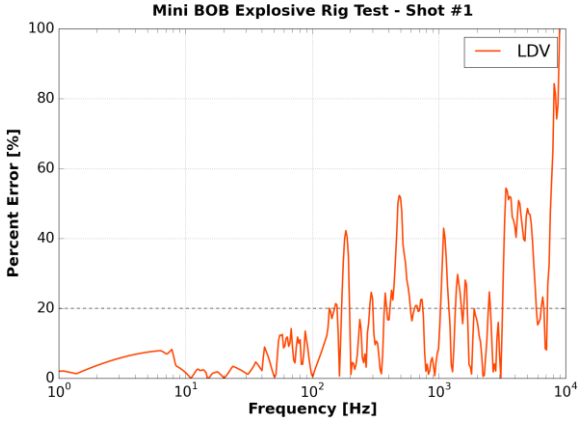

(d)

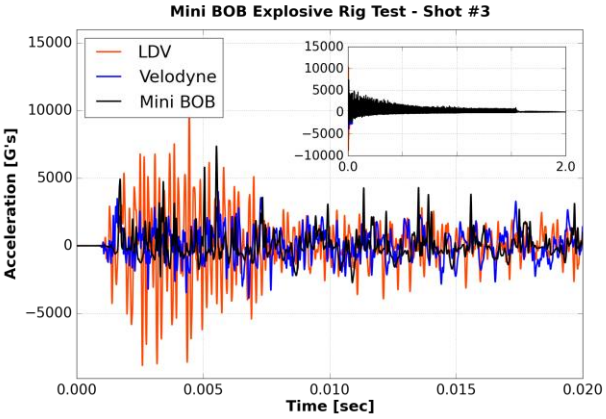

(a)

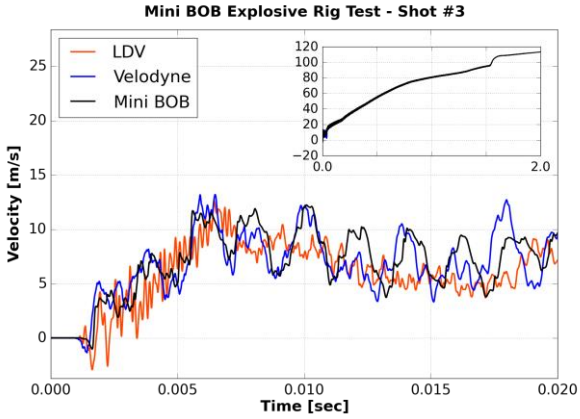

(b)

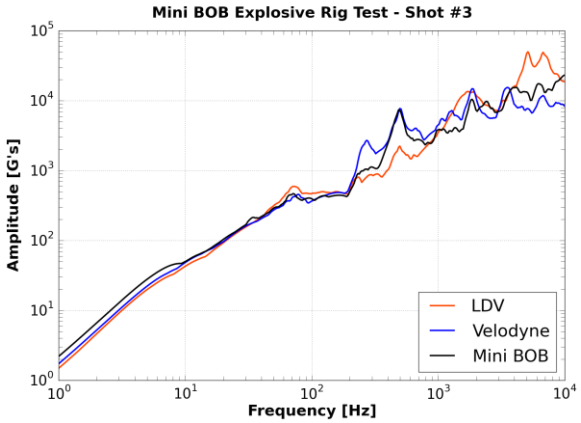
Mini BOB Explosive Rig Test - Shot #3
Amplitude [G's]
Frequency [Hz]
LDV
Velodyne
Mini BOB

(c)

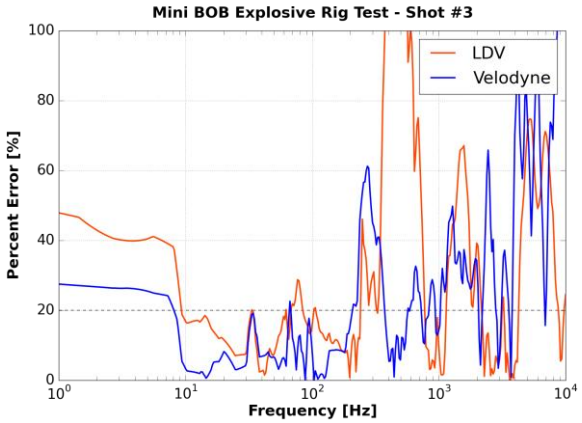
Mini BOB Explosive Rig Test - Shot #3
Percent Error [%]
Frequency [Hz]
LDV
Velodyne

(d)

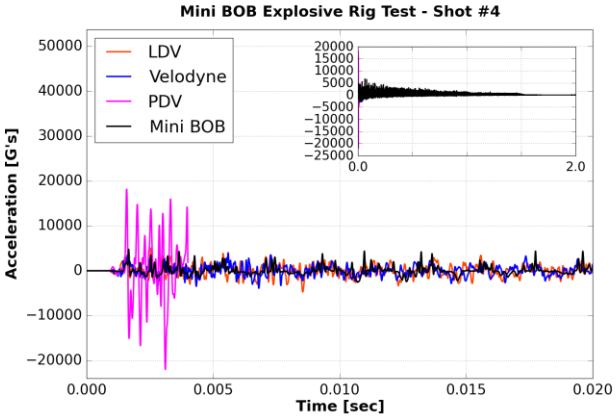
Mini BOB Explosive Rig Test - Shot #4
Acceleration [G's]
Time [sec]
LDV
Velodyne
PDV
Mini BOB

(a)

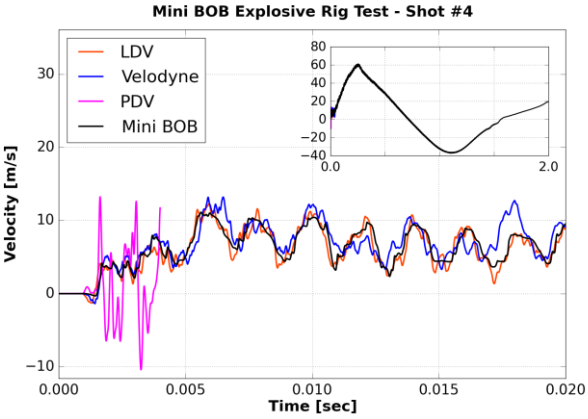
Mini BOB Explosive Rig Test - Shot #4
Velocity [m/s]
Time [sec]
LDV
Velodyne
PDV
Mini BOB

(b)

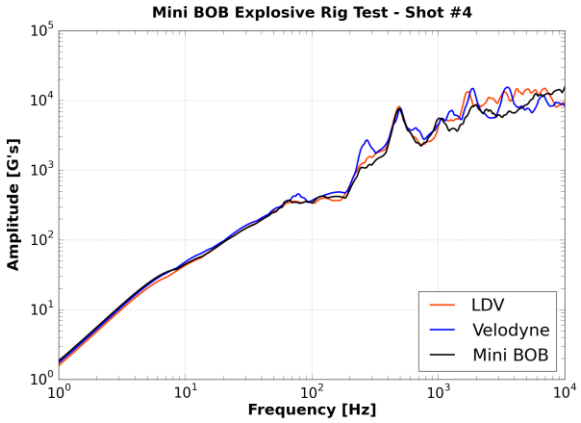
Mini BOB Explosive Rig Test - Shot #4
Amplitude [G's]
Frequency [Hz]
LDV
Velodyne
Mini BOB

(c)

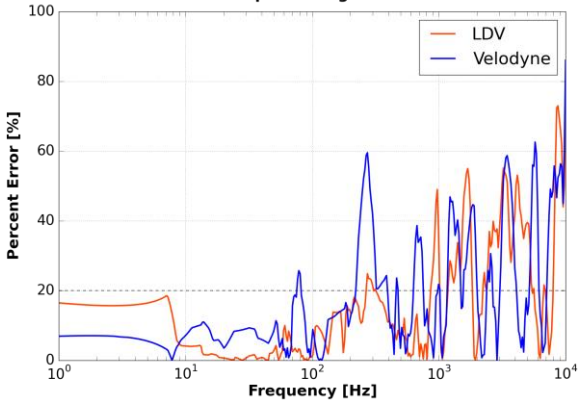
Mini BOB Explosive Rig Test - Shot #4
Percent Error [%]
Frequency [Hz]
LDV
Velodyne

(d)

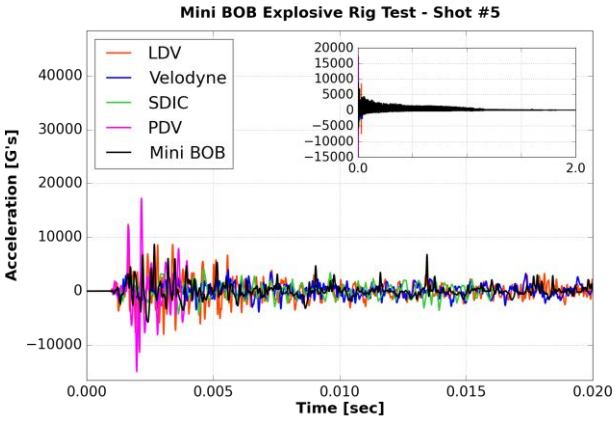
Mini BOB Explosive Rig Test - Shot #5
LDV
Velodyne
SDIC
PDV
Mini BOB
Acceleration [G's]
Time [sec]

(a)

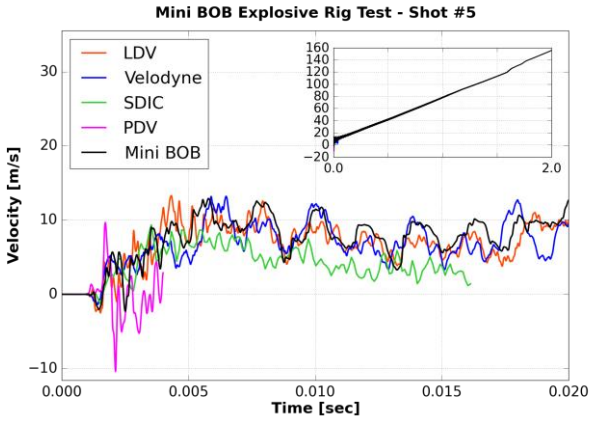
Mini BOB Explosive Rig Test - Shot #5
LDV
Velodyne
SDIC
PDV
Mini BOB
Velocity [m/s]
Time [sec]

(b)

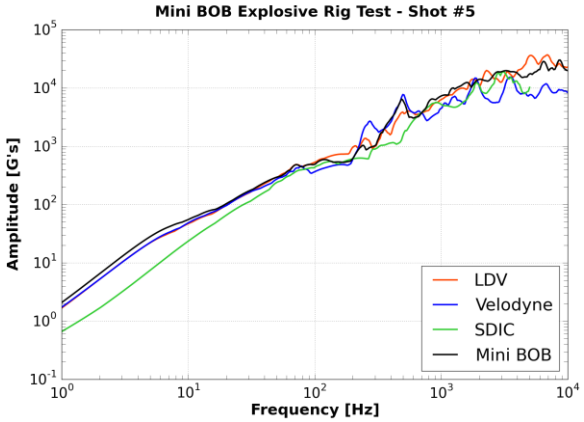
Mini BOB Explosive Rig Test - Shot #5
LDV
Velodyne
SDIC
Mini BOB
Amplitude [G's]
Frequency [Hz]

(c)

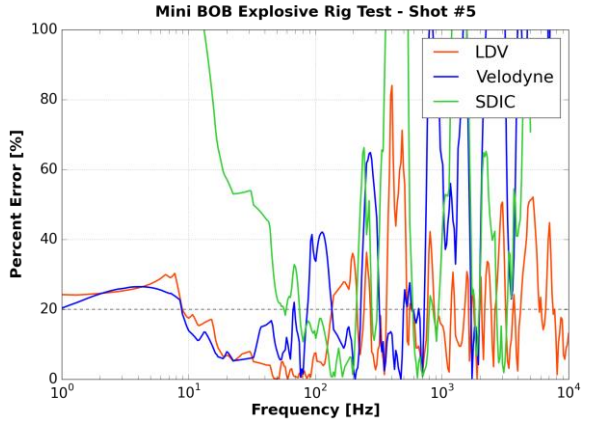
Mini BOB Explosive Rig Test - Shot #5
LDV
Velodyne
SDIC
Percent Error [%]
Frequency [Hz]

(d)

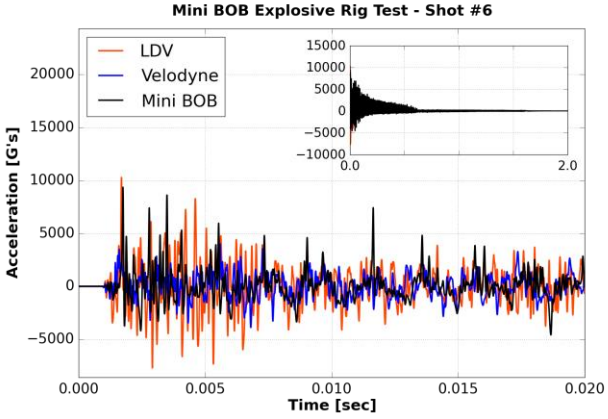
Mini BOB Explosive Rig Test - Shot #6
LDV
Velodyne
Mini BOB
Acceleration [G's]
Time [sec]

(a)

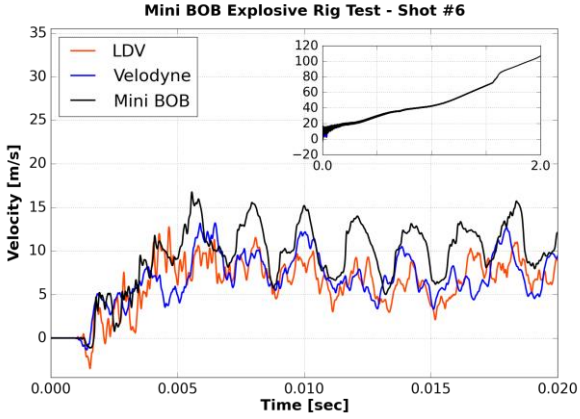
Mini BOB Explosive Rig Test - Shot #6
LDV
Velodyne
Mini BOB
Velocity [m/s]
Time [sec]

(b)

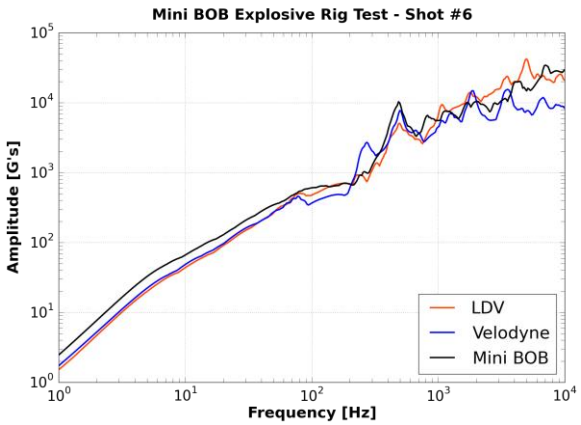
Mini BOB Explosive Rig Test - Shot #6
Amplitude [G's]
Frequency [Hz]
LDV
Velodyne
Mini BOB

(c)

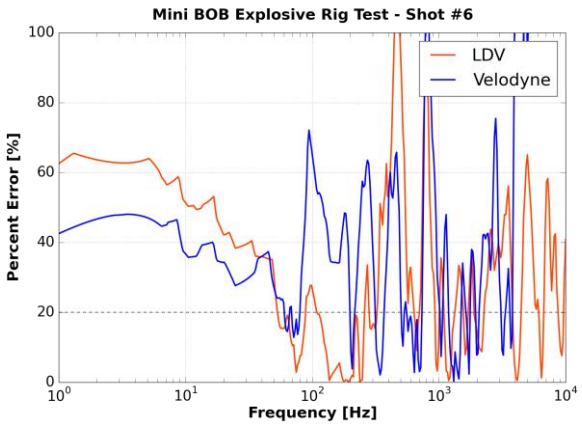
Mini BOB Explosive Rig Test - Shot #6
Percent Error [%]
Frequency [Hz]
LDV
Velodyne

(d)

viii. LOFFI

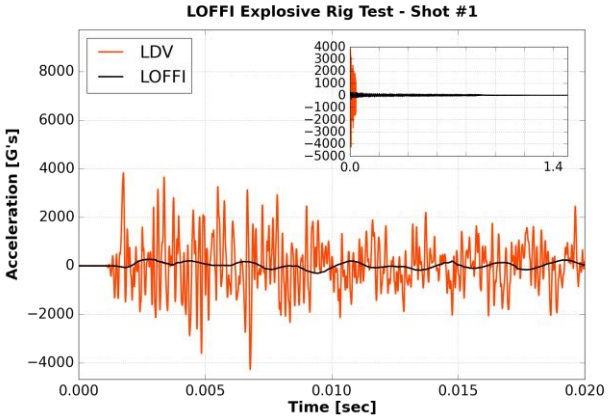

(a)

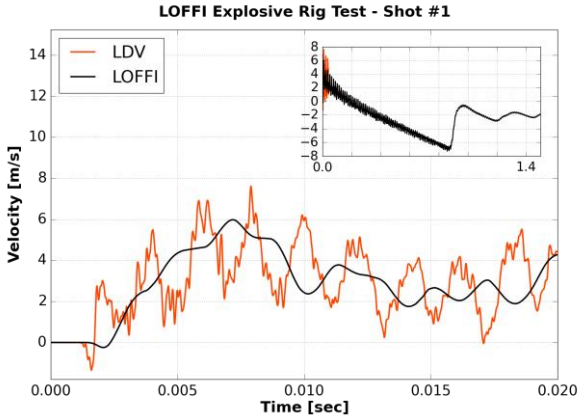

(b)

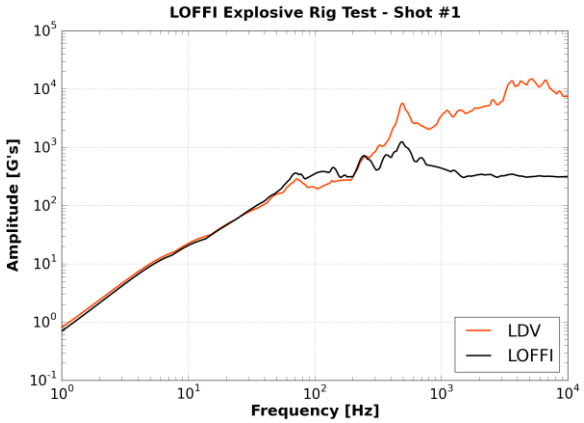

(c)

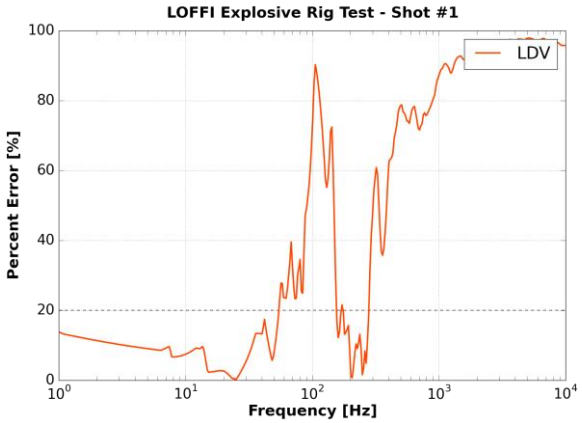

(d)

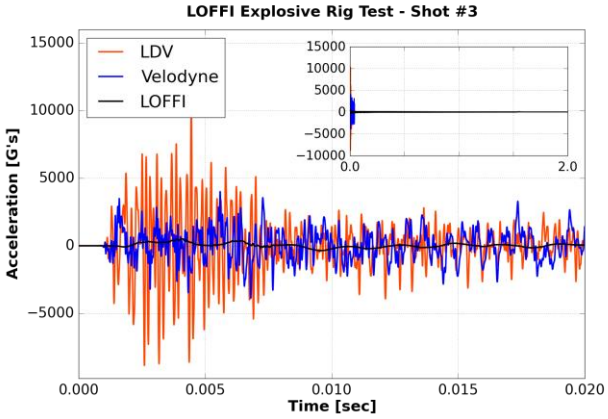

(a)

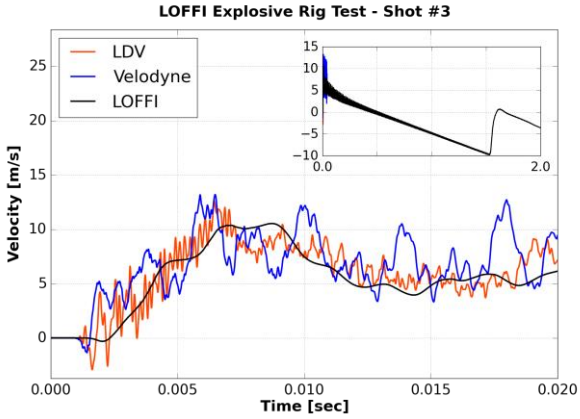

(b)

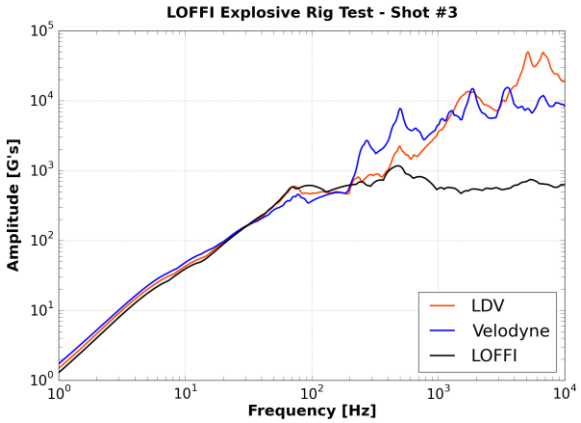
LOFFI Explosive Rig Test - Shot #3
Amplitude [G's]
Frequency [Hz]
LDV
Velodyne
LOFFI

(c)

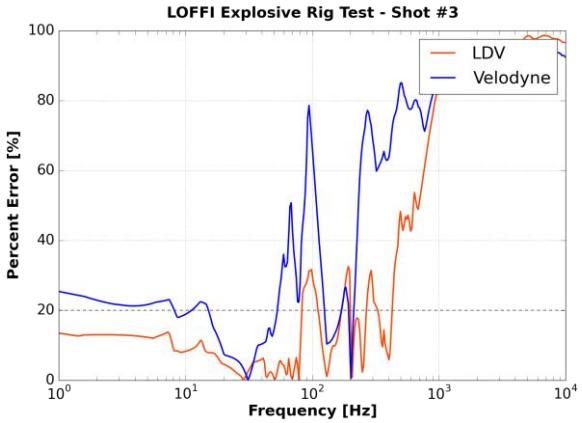
LOFFI Explosive Rig Test - Shot #3
Percent Error [%]
Frequency [Hz]
LDV
Velodyne

(d)

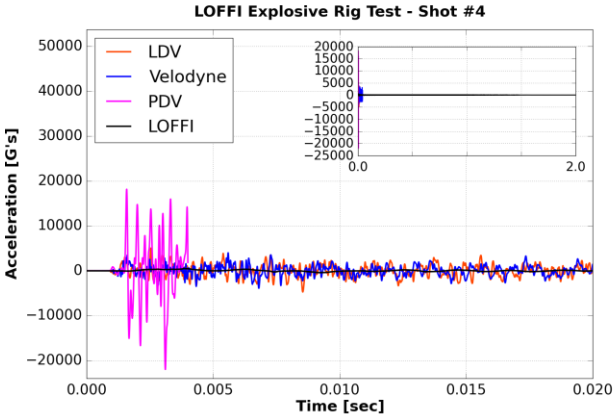
LOFFI Explosive Rig Test - Shot #4
Acceleration [G's]
Time [sec]
LDV
Velodyne
PDV
LOFFI

(a)

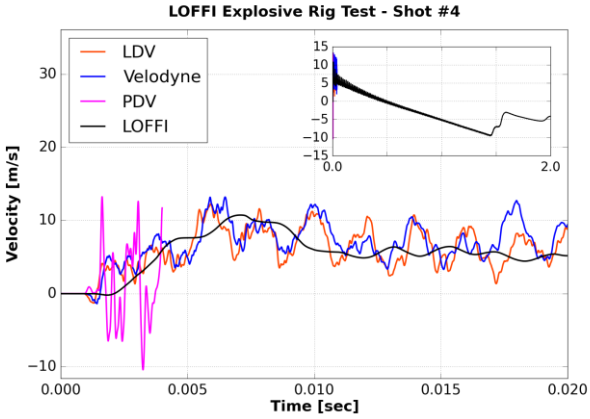
LOFFI Explosive Rig Test - Shot #4
Velocity [m/s]
Time [sec]
LDV
Velodyne
PDV
LOFFI

(b)

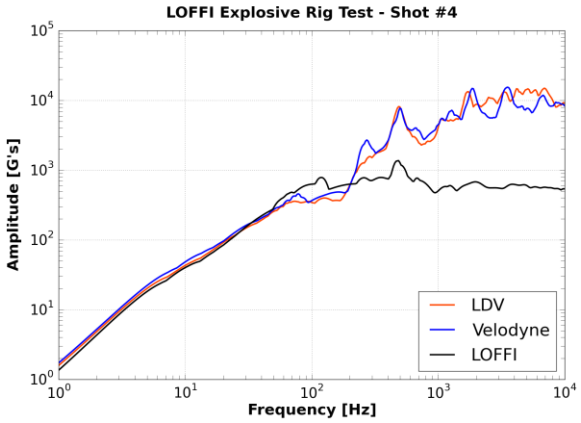
LOFFI Explosive Rig Test - Shot #4
Amplitude [G's]
Frequency [Hz]
LDV
Velodyne
LOFFI

(c)

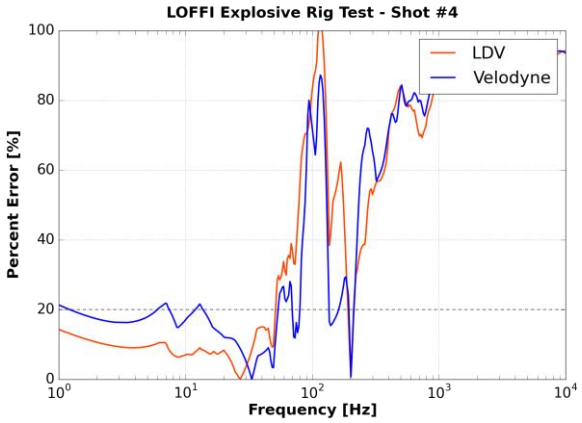
LOFFI Explosive Rig Test - Shot #4
Percent Error [%]
Frequency [Hz]
LDV
Velodyne

(d)

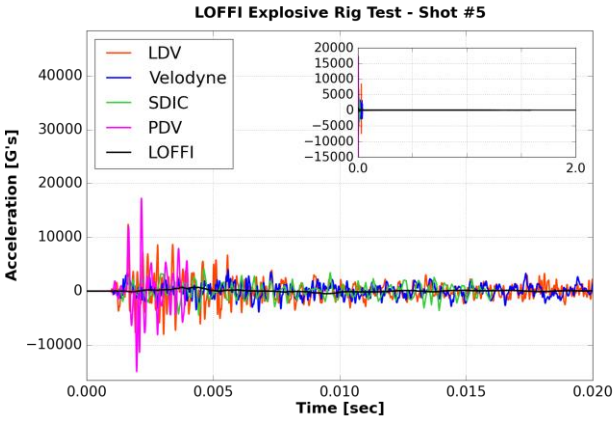
LOFFI Explosive Rig Test - Shot #5
LDV
Velodyne
SDIC
PDV
LOFFI
Acceleration [G's]
Time [sec]

(a)

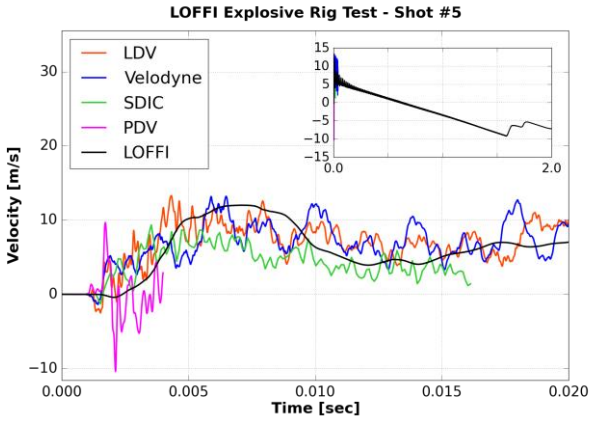
LOFFI Explosive Rig Test - Shot #5
LDV
Velodyne
SDIC
PDV
LOFFI
Velocity [m/s]
Time [sec]

(b)

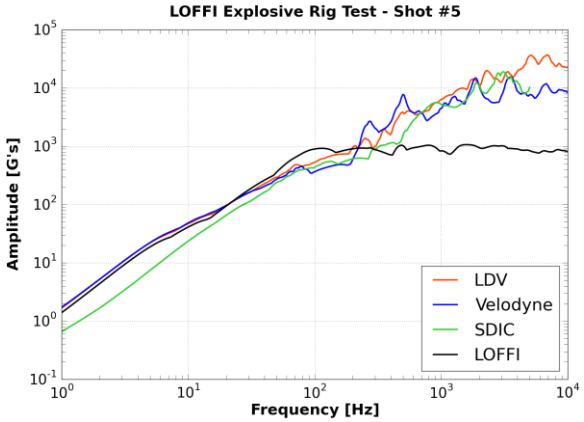
LOFFI Explosive Rig Test - Shot #5
LDV
Velodyne
SDIC
LOFFI
Amplitude [G's]
Frequency [Hz]

(c)

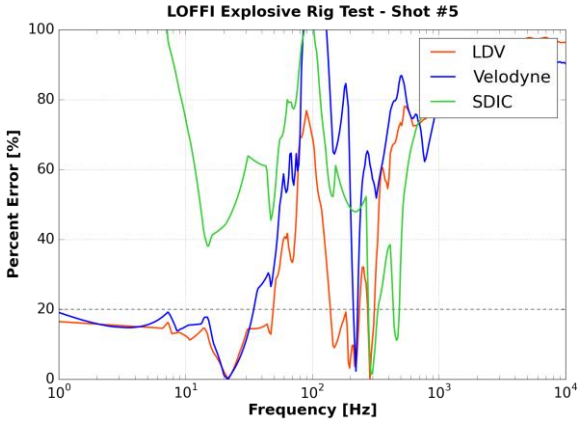
LOFFI Explosive Rig Test - Shot #5
LDV
Velodyne
SDIC
Percent Error [%]
Frequency [Hz]

(d)

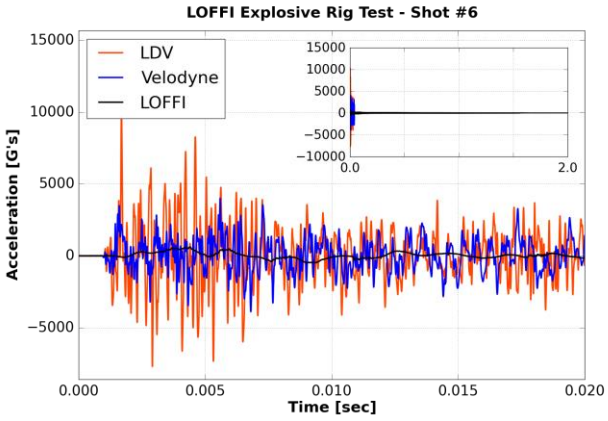
LOFFI Explosive Rig Test - Shot #6
LDV
Velodyne
LOFFI
Acceleration [G's]
Time [sec]

(a)

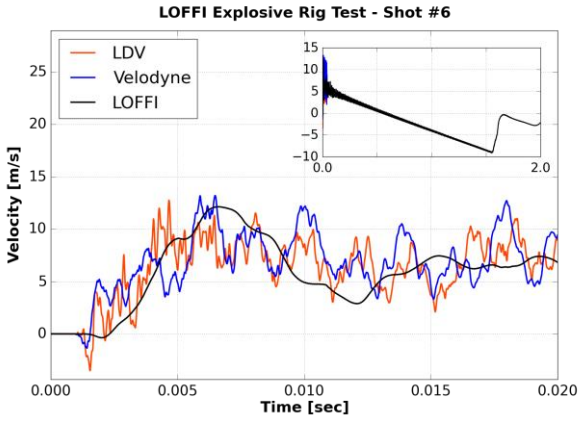
LOFFI Explosive Rig Test - Shot #6
LDV
Velodyne
LOFFI
Velocity [m/s]
Time [sec]

(b)

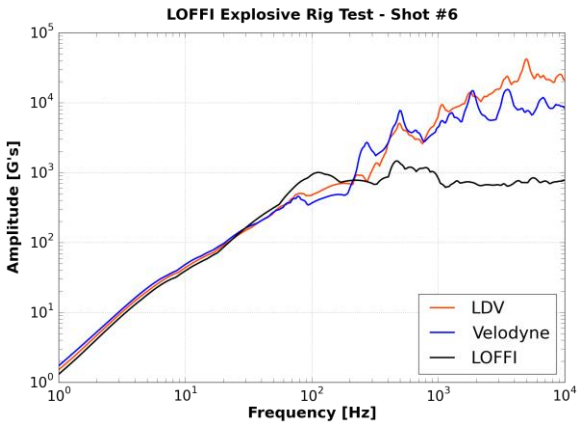
LOFFI Explosive Rig Test - Shot #6
Amplitude [G's]
Frequency [Hz]
LDV
Velodyne
LOFFI

(c)

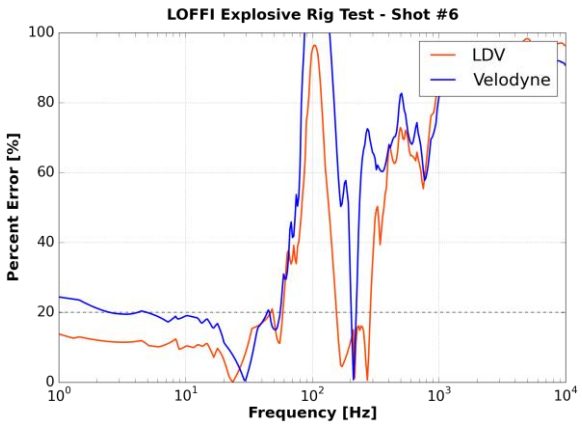
LOFFI Explosive Rig Test - Shot #6
Percent Error [%]
Frequency [Hz]
LDV
Velodyne

(d)

ix. Spring Mount

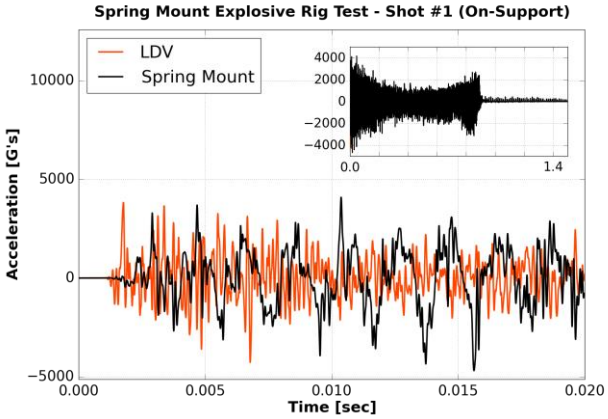

(a)

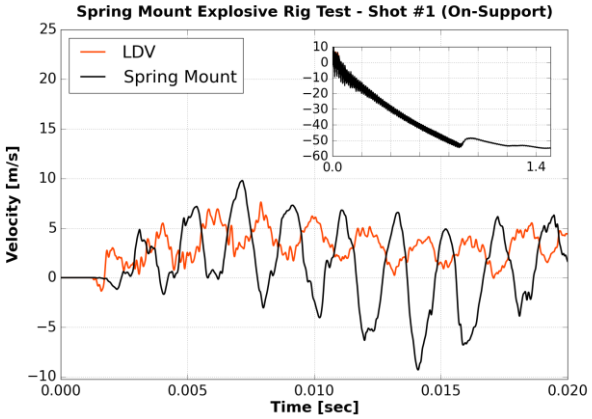

(b)

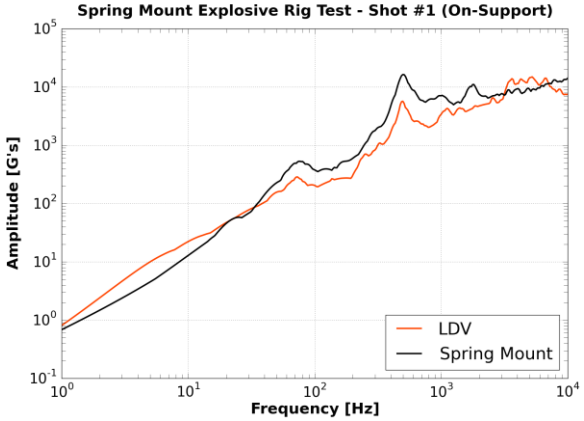

(c)

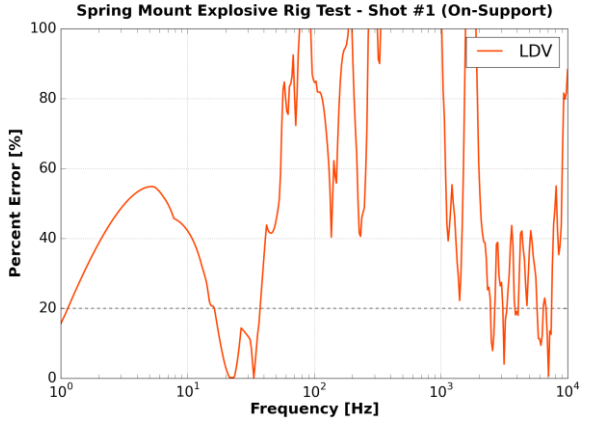

(d)

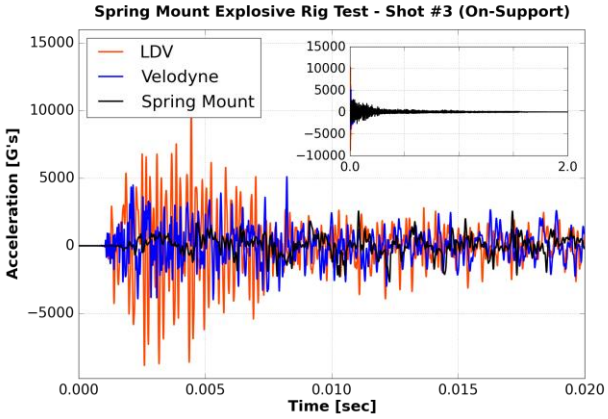

(a)

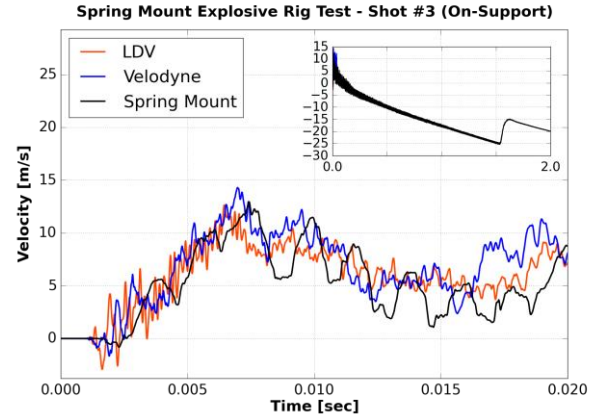

(b)

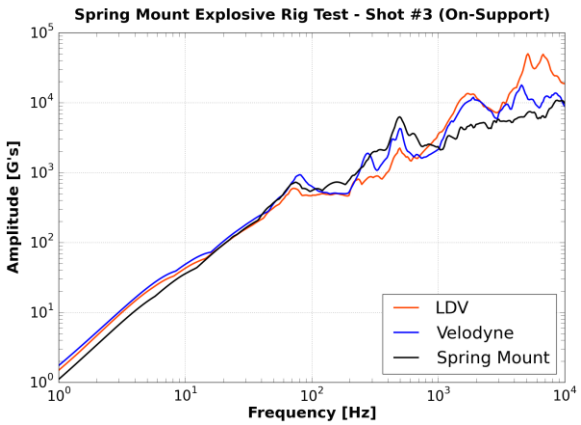
Spring Mount Explosive Rig Test - Shot #3 (On-Support)
Amplitude [G's]
Frequency [Hz]
LDV
Velodyne
Spring Mount

(c)

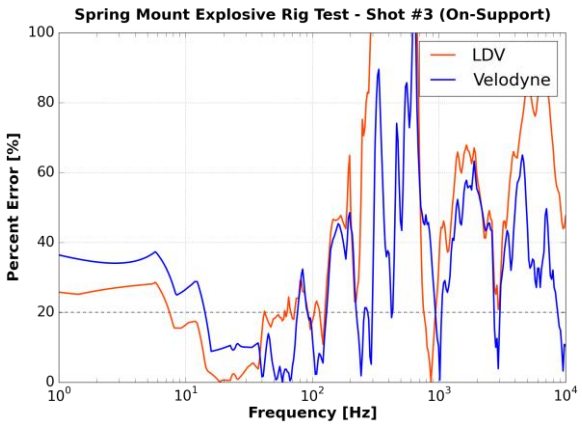
Spring Mount Explosive Rig Test - Shot #3 (On-Support)
Percent Error [%]
Frequency [Hz]
LDV
Velodyne

(d)

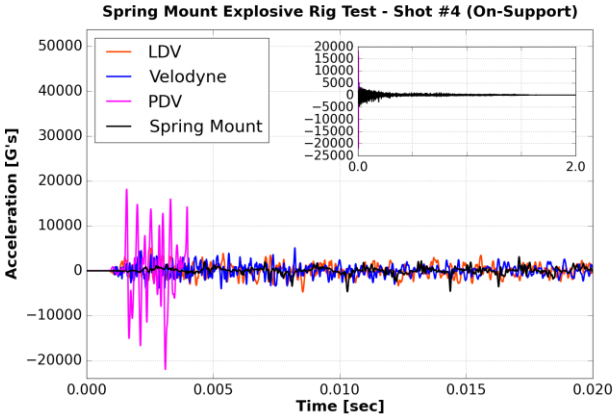
Spring Mount Explosive Rig Test - Shot #4 (On-Support)
Acceleration [G's]
Time [sec]
LDV
Velodyne
PDV
Spring Mount

(a)

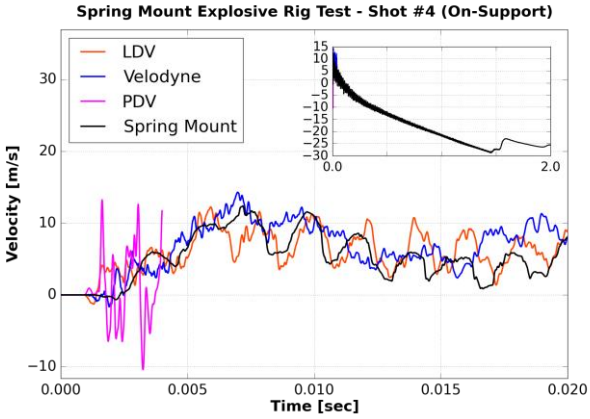
Spring Mount Explosive Rig Test - Shot #4 (On-Support)
Velocity [m/s]
Time [sec]
LDV
Velodyne
PDV
Spring Mount

(b)

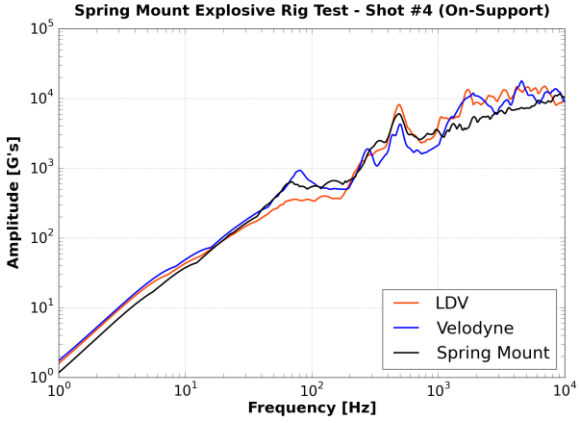
Spring Mount Explosive Rig Test - Shot #4 (On-Support)
Amplitude [G's]
Frequency [Hz]
LDV
Velodyne
Spring Mount

(c)

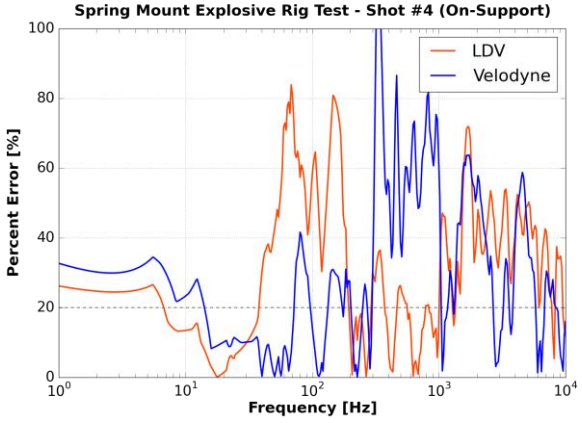
Spring Mount Explosive Rig Test - Shot #4 (On-Support)
Percent Error [%]
Frequency [Hz]
LDV
Velodyne

(d)

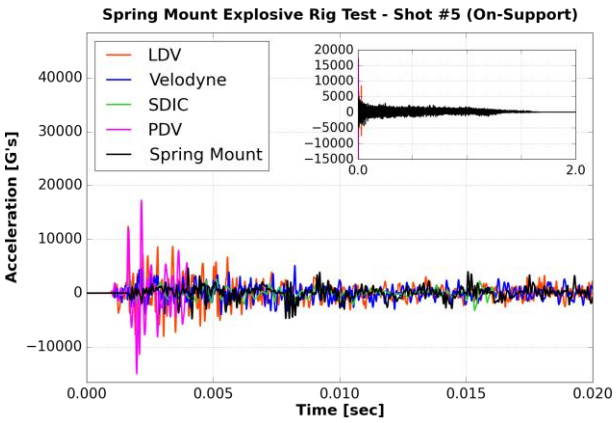
Spring Mount Explosive Rig Test - Shot #5 (On-Support)
LDV
Velodyne
SDIC
PDV
Spring Mount
Acceleration [G's]
Time [sec]

(a)

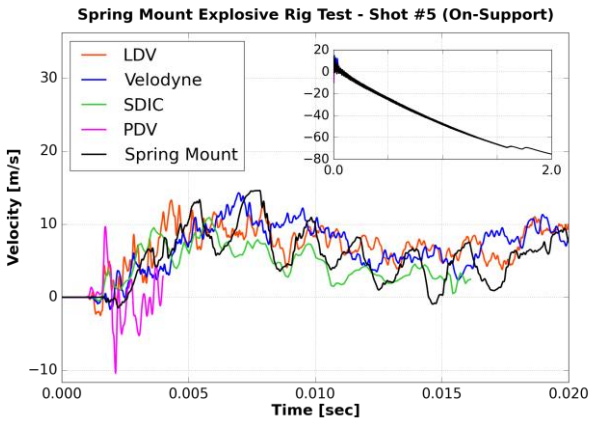
Spring Mount Explosive Rig Test - Shot #5 (On-Support)
LDV
Velodyne
SDIC
PDV
Spring Mount
Velocity [m/s]
Time [sec]

(b)

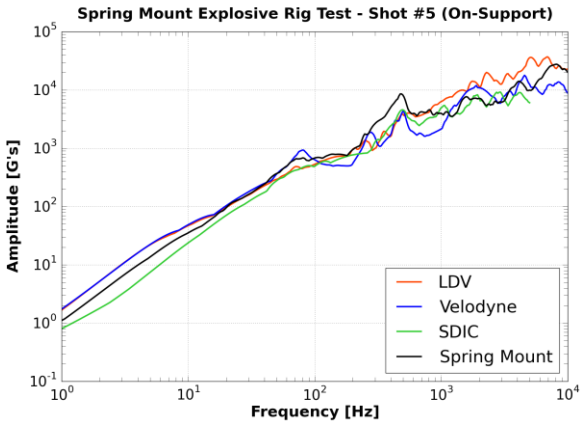
Spring Mount Explosive Rig Test - Shot #5 (On-Support)
LDV
Velodyne
SDIC
Spring Mount
Amplitude [G's]
Frequency [Hz]

(c)

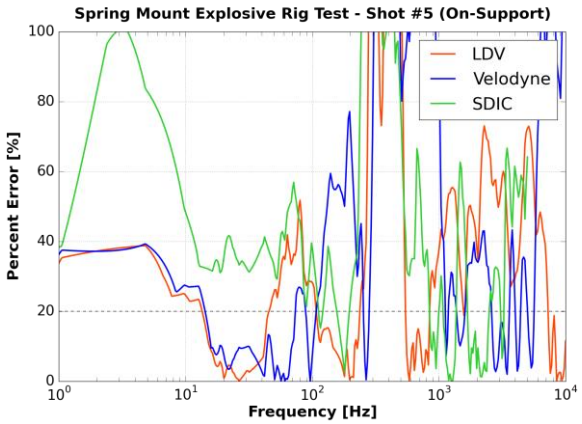
Spring Mount Explosive Rig Test - Shot #5 (On-Support)
LDV
Velodyne
SDIC
Percent Error [%]
Frequency [Hz]

(d)

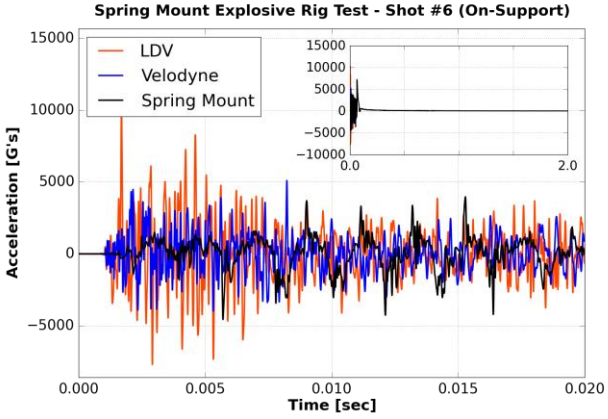
Spring Mount Explosive Rig Test - Shot #6 (On-Support)
LDV
Velodyne
Spring Mount
Acceleration [G's]
Time [sec]

(a)

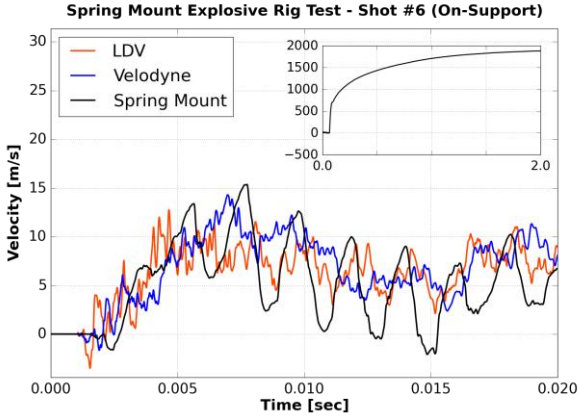
Spring Mount Explosive Rig Test - Shot #6 (On-Support)
LDV
Velodyne
Spring Mount
Velocity [m/s]
Time [sec]

(b)

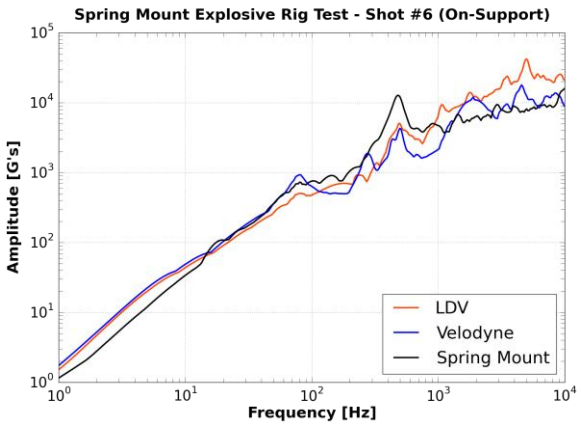
Spring Mount Explosive Rig Test - Shot #6 (On-Support)
Amplitude [G's]
Frequency [Hz]
LDV
Velodyne
Spring Mount

(c)

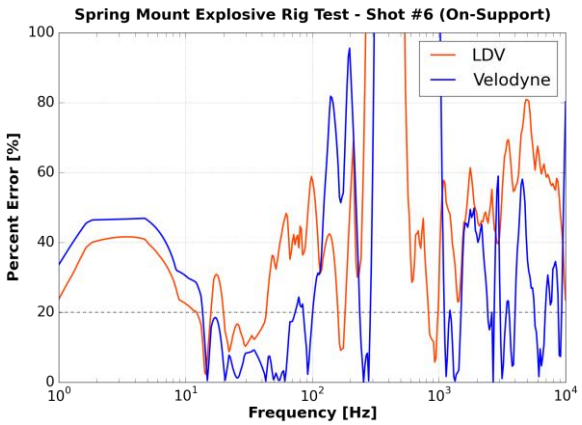
Spring Mount Explosive Rig Test - Shot #6 (On-Support)
Percent Error [%]
Frequency [Hz]
LDV
Velodyne

(d)

x. Tiny BOB

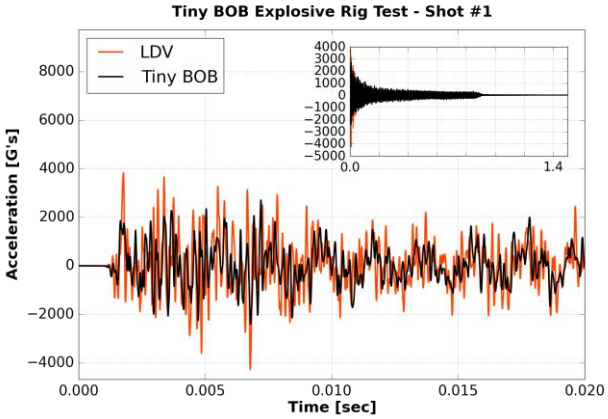

(a)

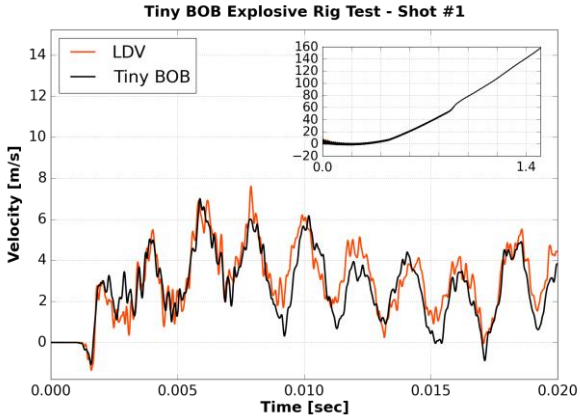

(b)

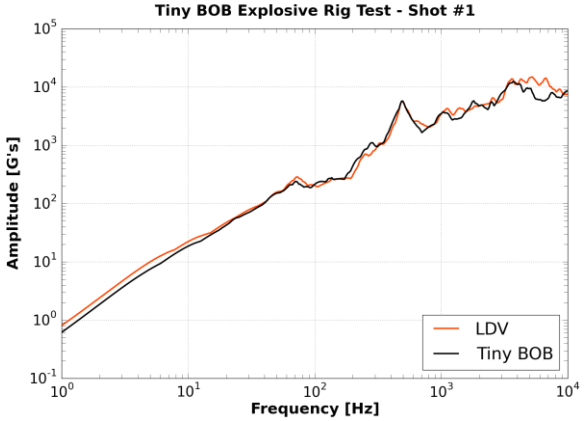

(c)

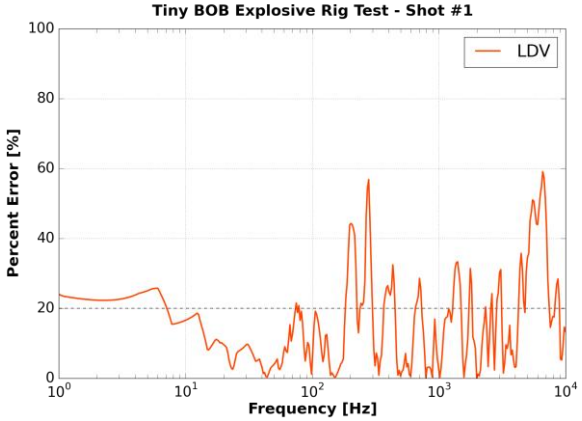

(d)

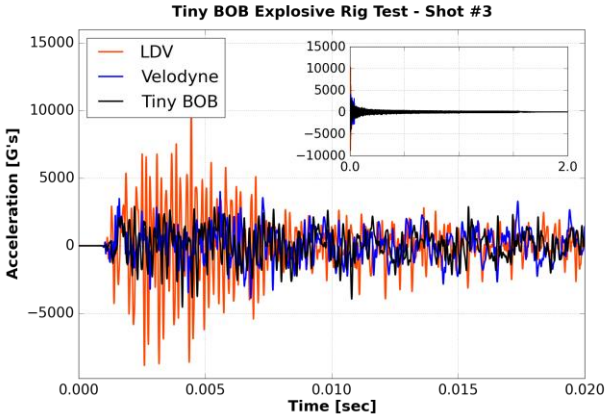

(a)

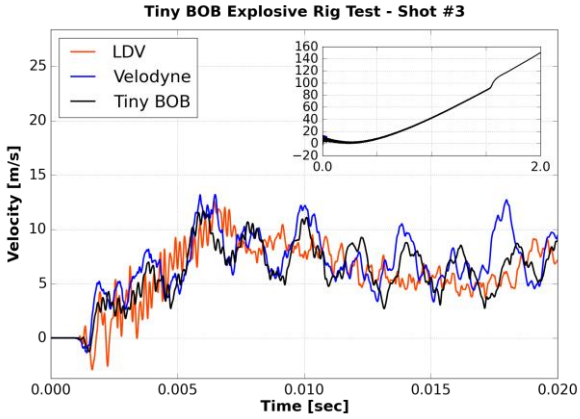

(b)

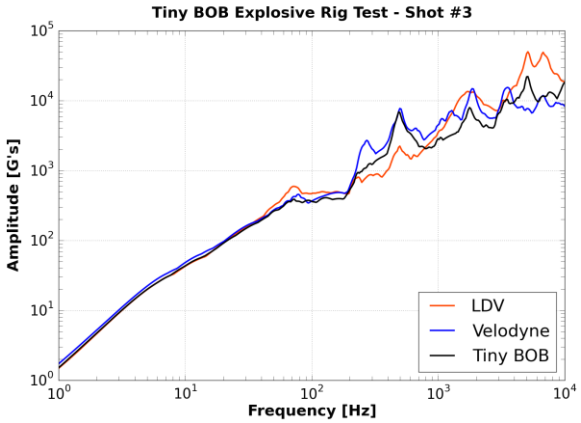
Tiny BOB Explosive Rig Test - Shot #3
Amplitude [G's]
Frequency [Hz]
LDV
Velodyne
Tiny BOB

(c)

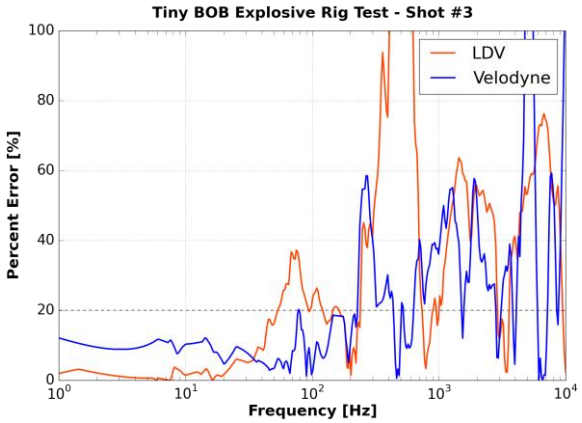
Tiny BOB Explosive Rig Test - Shot #3
Percent Error [%]
Frequency [Hz]
LDV
Velodyne

(d)

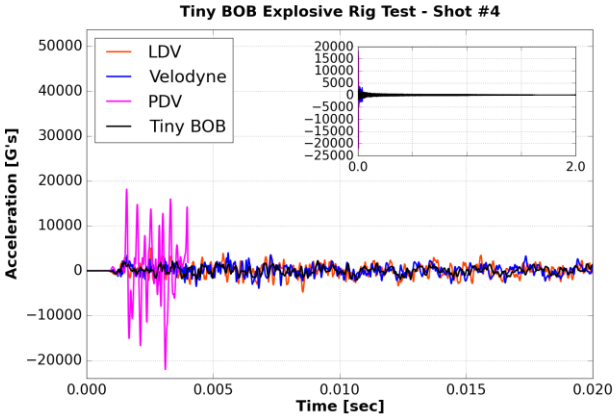
Tiny BOB Explosive Rig Test - Shot #4
Acceleration [G's]
Time [sec]
LDV
Velodyne
PDV
Tiny BOB

(a)

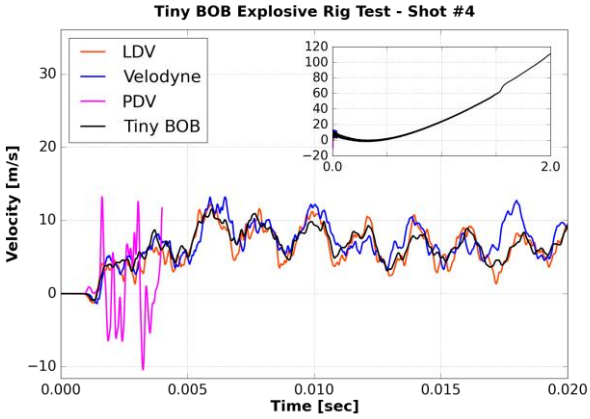
Tiny BOB Explosive Rig Test - Shot #4
Velocity [m/s]
Time [sec]
LDV
Velodyne
PDV
Tiny BOB

(b)

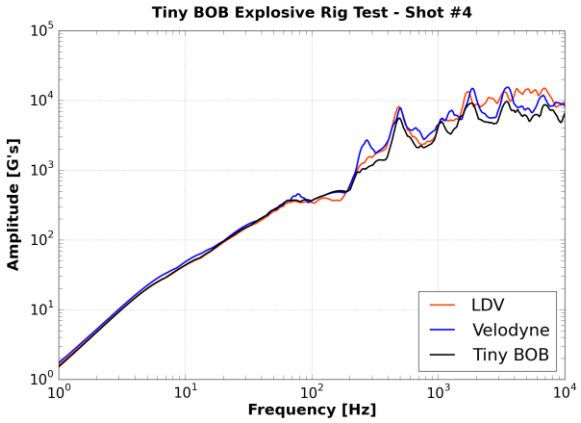
Tiny BOB Explosive Rig Test - Shot #4
Amplitude [G's]
Frequency [Hz]
LDV
Velodyne
Tiny BOB

(c)

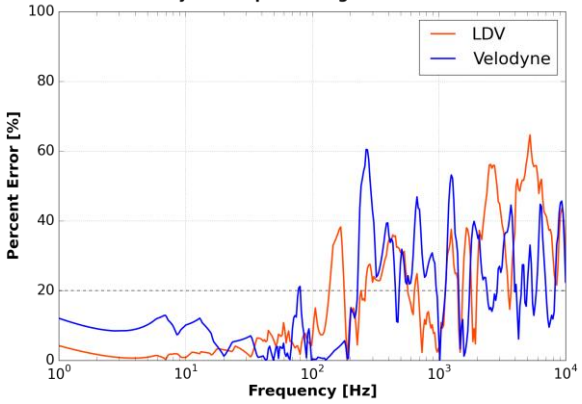
Tiny BOB Explosive Rig Test - Shot #4
Percent Error [%]
Frequency [Hz]
LDV
Velodyne

(d)

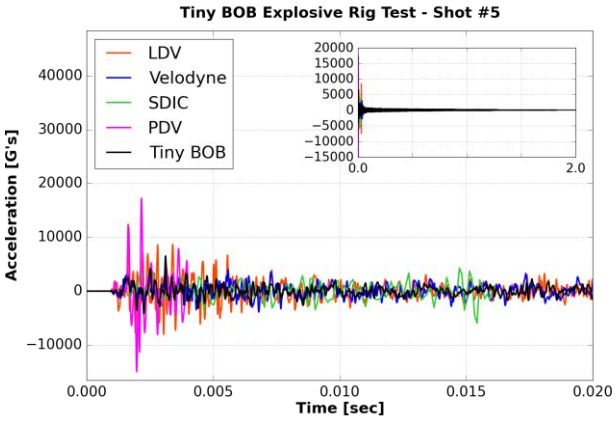
Tiny BOB Explosive Rig Test - Shot #5
LDV
Velodyne
SDIC
PDV
Tiny BOB
Acceleration [G's]
Time [sec]

(a)

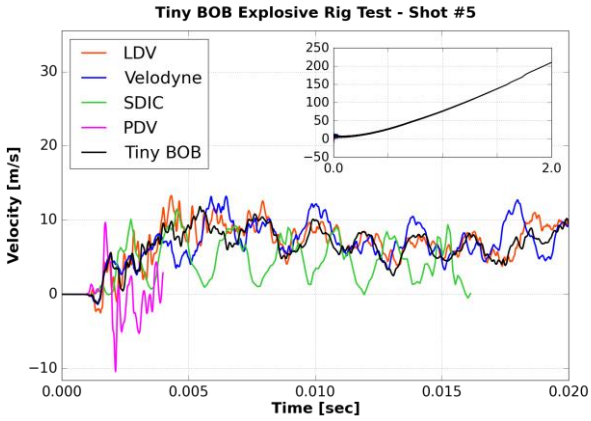
Tiny BOB Explosive Rig Test - Shot #5
LDV
Velodyne
SDIC
PDV
Tiny BOB
Velocity [m/s]
Time [sec]

(b)

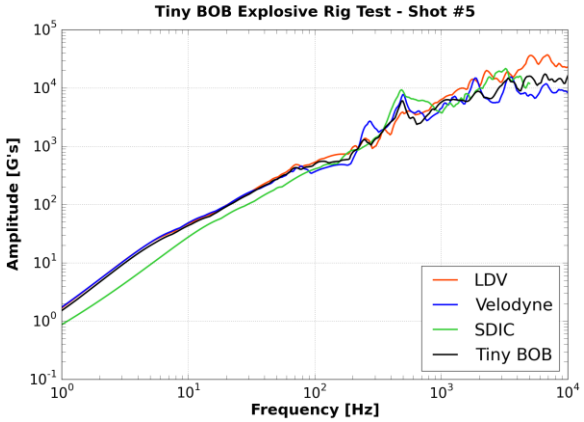
Tiny BOB Explosive Rig Test - Shot #5
LDV
Velodyne
SDIC
Tiny BOB
Amplitude [G's]
Frequency [Hz]

(c)

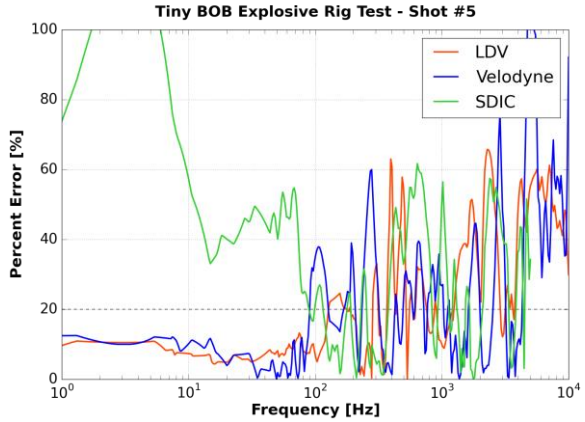
Tiny BOB Explosive Rig Test - Shot #5
LDV
Velodyne
SDIC
Percent Error [%]
Frequency [Hz]

(d)

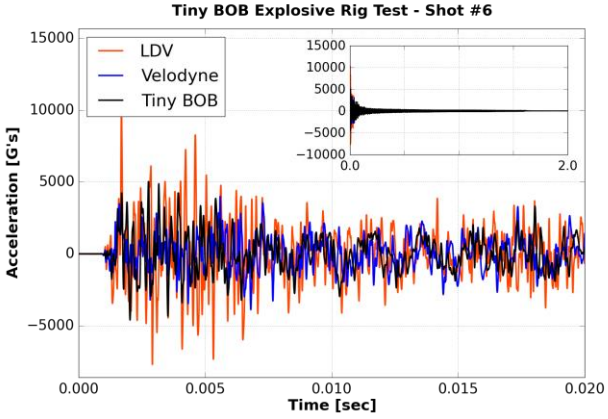
Tiny BOB Explosive Rig Test - Shot #6
LDV
Velodyne
Tiny BOB
Acceleration [G's]
Time [sec]

(a)

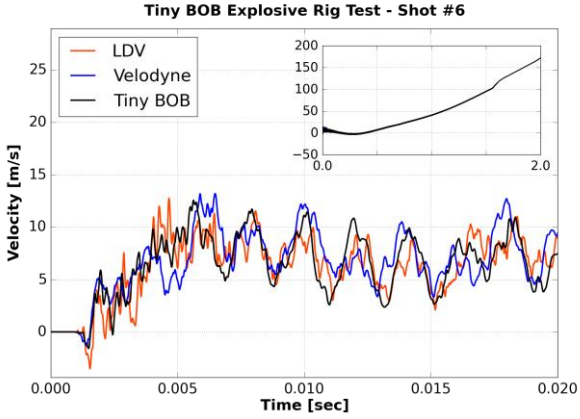
Tiny BOB Explosive Rig Test - Shot #6
LDV
Velodyne
Tiny BOB
Velocity [m/s]
Time [sec]

(b)

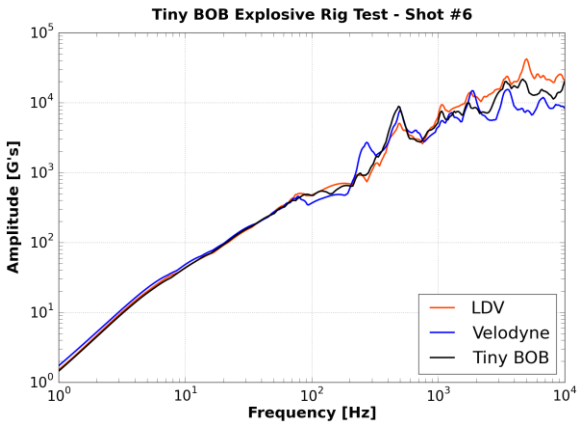
Tiny BOB Explosive Rig Test - Shot #6
Amplitude [G's]
Frequency [Hz]
LDV
Velodyne
Tiny BOB

(c)

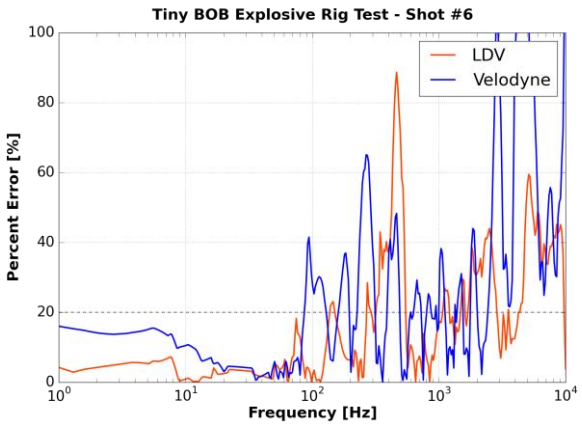
Tiny BOB Explosive Rig Test - Shot #6
Percent Error [%]
Frequency [Hz]
LDV
Velodyne

(d)

xi. Corvid Disk Mount

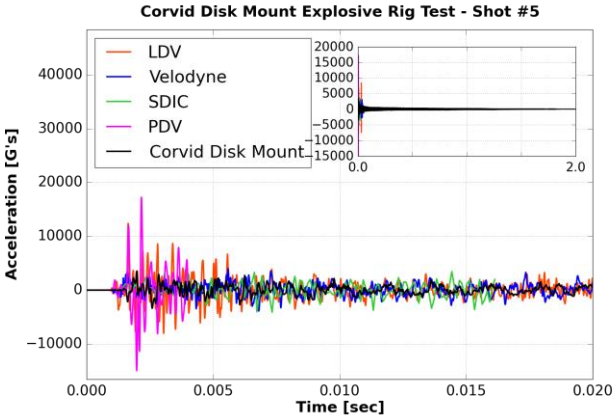

(a)

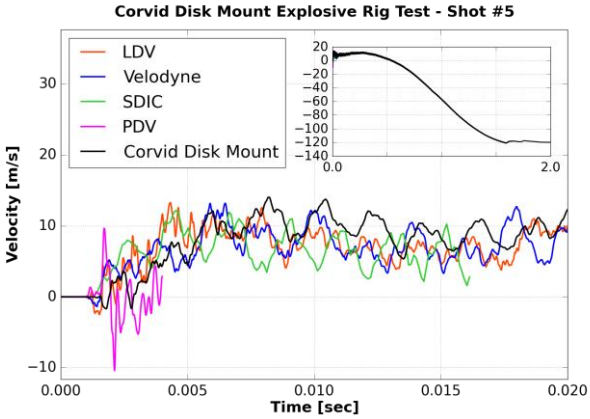

(b)

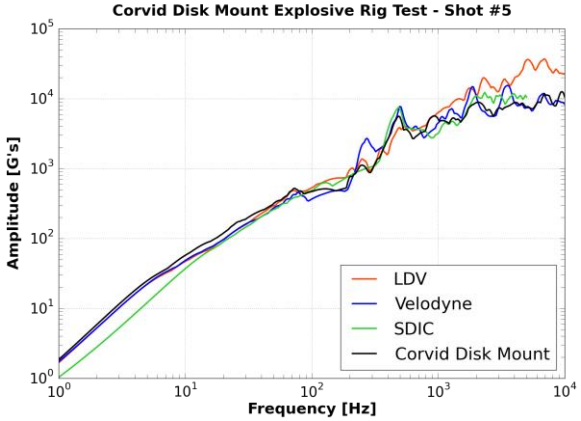

(c)

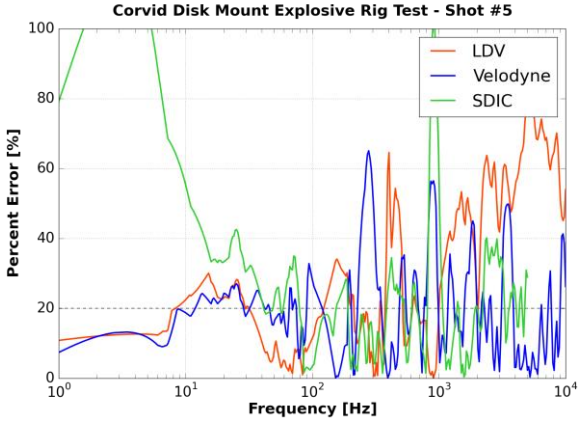

(d)

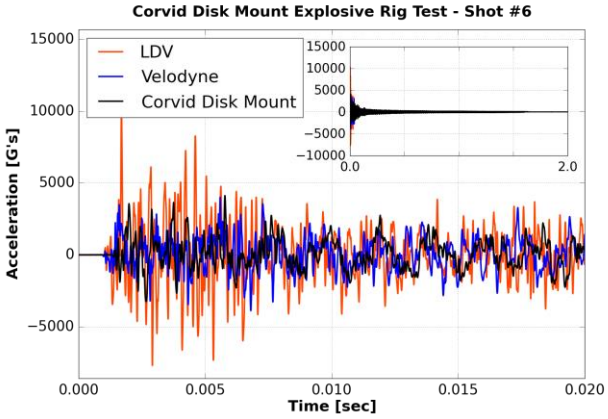

(a)

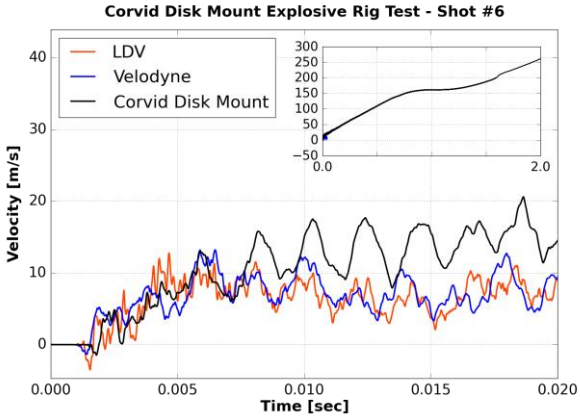

(b)

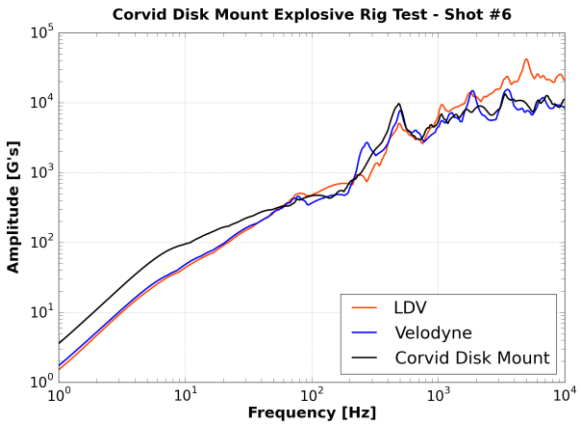
Corvid Disk Mount Explosive Rig Test - Shot #6
Amplitude [G's]
Frequency [Hz]
LDV
Velodyne
Corvid Disk Mount

(c)

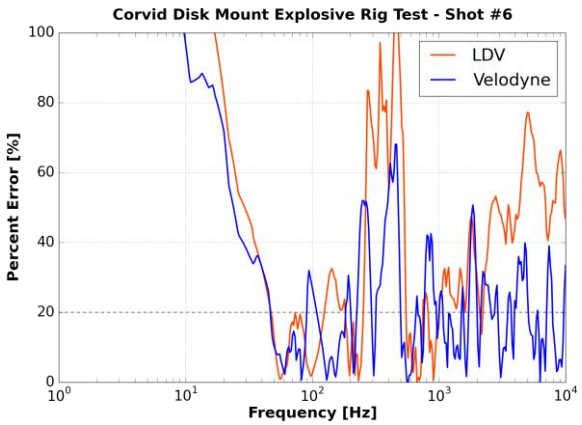
Corvid Disk Mount Explosive Rig Test - Shot #6
Percent Error [%]
Frequency [Hz]
LDV
Velodyne

(d)